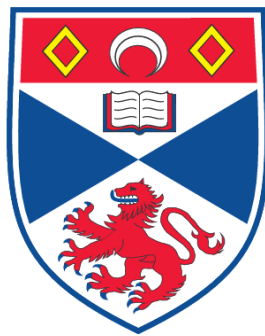


**THE APPLICATION OF QUASI-OPTICAL TECHNIQUES TO
MILLIMETRE WAVE RADAR**

Michael J. Leeson

**A Thesis Submitted for the Degree of PhD
at the
University of St. Andrews**



1993

**Full metadata for this item is available in
Research@StAndrews:FullText
at:**

<http://research-repository.st-andrews.ac.uk/>

Please use this identifier to cite or link to this item:

<http://hdl.handle.net/10023/2774>

This item is protected by original copyright

The Application of Quasi-Optical Techniques to Millimetre Wave Radar

A thesis presented by
Michael J. Leeson. B.Sc.(Hons)
to the
University of St. Andrews
in application for the degree of
Doctor of Philosophy.

August 1992.



Declaration.

I hereby certify that this thesis has been composed by myself, that it is a record of my own work, and that it has not been accepted in partial or complete fulfilment of any other degree of professional qualification.

I was admitted to the Faculty of Science of the University of St. Andrews under Ordinance General No. 12 during August 1989, and as a candidate for the degree of Ph.D. during August 1990.

In submitting this thesis to the University of St. Andrews, I understand that I am Giving permission for it to be made available for use in accordance with the regulations of the University Library for the time being in force, subject to any copyright vested in the work not being affected thereby. I also understand that the title and abstract will be published, and that a copy of the work may be made and supplied to any bona fide library or research worker.



M.J. Leeson.
1992.

Certificate.

I hereby certify that M.J. Leeson has fulfilled the conditions of the Resolution and Regulations appropriate to the degree of Ph.D.



J.C.G. Lesurf.
Research Supervisor.

Acknowledgements.

I would like to thank my supervisor Jim Lesurf, for making available his wealth of knowledge. His support, encouragement and nagging have been invaluable. His willingness to let me do my own thing, a quality rarely found and seldom appreciated, has given me much confidence in myself.

I would like to thank Graham Smith and Andy Harvey for showing me the error of my ways on many occasions, both academic and sporting. They have provided much knowledge and practical advice, from which I have received much benefit.

My other colleagues, Mike Webb, Malcolm Robertson, Darrell Smith and Duncan Robertson have each contributed to daily life in their own inimitable ways.

The practical side of this project would not have been possible without the assistance of the department's Mechanical Workshop. I would like to thank, in particular, Willie Smith for making almost everything, George Radley and Jim Clarke.

My thanks go also to Duncan Robertson and Martin Dunstan for their help during the range measurement experiments. Someone had to move the target!

I have been supported in this work by EEV, Lincoln and SERC. I would like to thank John Duff for his help beyond the call of duty.

Last but by no means least, I would like to thank my wife, Carol, and our respective parents.

Dedication.

To Carol, Laura and Jennie.

Abstract.

The application of Quasi Optical techniques has been of great benefit to the field of instrumentation for frequencies between 75GHz and several hundred GHz. The application of Quasi Optical techniques to millimetre wave radar, described in this thesis, has produced an FMCW Doppler radar capable of operation at 94GHz and 140GHz. Total polarization agility and a capability to operate over a very wide bandwidth is demonstrated. Quasi Optical circuits are proposed as solutions for many of the system requirements, and these are fully analyzed. Significant benefits of these techniques are demonstrated, and future improvements are suggested.

A new design tool, in the form of a program, for Quasi Optical circuit analysis is presented and is used for the analysis of all the optical circuits in this thesis. The program has speeded up the design process for optical circuits.

A new type of feedhorn is described and characterized. Its performance compares well with existing feedhorns, and it provides a low cost alternative to existing antenna requirements.

Chapter 1

An Introduction to Millimetre Waves and Quasi-Optical Systems.....	1
1 Abstract.....	1
1.1 Introduction to Millimetre Waves.....	1
1.2 Representing Free Space Beams.....	2
1.2.1 Properties of Gaussian Beams.....	2
1.2.1.1 Amplitude dependence.....	2
1.2.1.2 Frequency Dependence.....	5
1.2.1.3 Polarization.....	6
1.2.2 Limitations of free space beams.....	7
1.3 Applications of Millimetre Waves.....	8
1.4 Project Definition.....	9
1.4.1 Initial Design Goals.....	9
1.5 Outline of thesis.....	10

Chapter 2

An Introduction to Radar and Signal Processing Techniques.....	11
2 Abstract.....	11
2.1 Measurement techniques used in radar.....	11
2.1.1 Radial range.....	11
2.1.2 Radial Velocity.....	14
2.1.3 Angular Position.....	16
2.1.4 Target Identification.....	19
2.2 Selection of Radar Type.....	22
2.3 Range and Velocity Measurement Techniques in FMCW radar.....	23
2.3.1 Frequency Measurement Techniques.....	27
2.3.1.1 Frequency Counting.....	27
2.3.1.2 Period Timing.....	27
2.3.1.3 Phase lock loops.....	28
2.3.2 Summary of Frequency Measurement Requirements.....	31
2.4 Polarization Measurement Techniques.....	31
2.4.1 Summary of Polarization Measurement Requirements.....	32
2.5 Operation without FM.....	33
2.5.1 Summary of Measurement Requirements without FM.....	34
2.6 Combined Quasi-Optical Requirements.....	35
2.7 Quasi-Optical Design of the Receiver.....	36

Chapter 3

Gaussian Beam Theory and Quasi-Optical Component Design.	40
3 Abstract.....	40
3.1 Beam Waveguides.....	40
3.1.1 Coupling of Gaussian Beams.	40
3.1.1.1 Longitudinal Offsets.....	41
3.1.1.2 Lateral Offsets and Tilted Beams.....	42
3.1.1.3 General Case of Misaligned Beams.....	44
3.1.2 Beam Truncation.....	45
3.1.3 System Bandwidth and Frequency Response.....	47
3.2 Design of Optical Hardware.....	48
3.2.1 Half-Cube and Polarizer Design.	48
3.2.2 Lenses.....	52
3.2.3 Thermal Considerations.	52
3.2.3.1 Polarizers - First Model.	53
3.2.3.2 Polarizers - Second Model.....	59
3.2.3.4 Lenses - Second Model.	64
3.3 Oscillator and Detector Block Design.	65
3.4 A Treatment of Alignment Tolerances.	66

Chapter 4

Analysis of Quasi-Optical Circuits.	73
4 Abstract.....	73
4.1 Representation of Polarized Radiation.	73
4.1.1 Circuit Symbols and Matrices.....	73
4.2 QOCAD - A Design Tool.....	76
4.2.1 Receiver and Circulator Circuits.	79
4.3.1 Multi-Modal Signal Processing.	84
4.3.2 Passive Ranging.	86

Chapter 5

Signal Processing Electronics.	90
5 Abstract.	90
5.1 Receiver Circuitry.....	90
5.1.1 Bias Supply.	90
5.1.2 First Stage Amplification.	91
5.1.3 Further Amplification and Signal Isolation.	92

5.2 Measurement of Return Signal.....	94
5.2.1 Frequency and Phase Measurement.....	94
5.2.3 Interfacing to the Archimedes.....	99
5.3 System Master Oscillator.....	101
5.3.1 Frequency and Power Characteristics.....	101
5.4 Detection of Signals in Noise and Clutter.....	108
5.4.1 Receiver Noise Performance.....	108
5.4.2 Phase Noise and Clutter Rejection.....	115

Chapter 6

Feedhorn Design and Evaluation.....	120
6 Abstract.....	120
6.1 Dual Mode Feedhorns.....	120
6.1.1 Corrugated Feedhorns.....	120
6.1.2 Potter Horns.....	121
6.1.3 A Tunable Potter Horn.....	122
6.1.4 Antenna Measurements.....	127
6.2 Single-Mode Conical Feed Horns.....	132
6.3 An Alternative Measurement Technique.....	134

Chapter 7

Analysis of System Performance.....	137
7 Abstract.....	137
7.1 The Radar Antenna.....	137
7.2 Performance Tests.....	137
7.2.1 Loss.....	137
7.2.1.1 Insertion Loss.....	138
7.2.1.2 Coupling Losses.....	139
7.2.1.3 Absorption in Lenses and Ferrites.....	140
7.2.2 Range Measurement.....	141
7.2.3 Polarization.....	143
7.3 Conclusions.....	144
7.4 Further Work.....	145
7.4.1 Detectors.....	145
7.4.2 Feedhorns.....	145

Appendices

Appendix 1.....	146
Mathematical Derivation of a General Coupling Integral	146
Appendix 2.....	152
Horn Lens Design.....	152
Beam Lens Design.	158
Appendix 3.....	165
Wire Heating Program.....	165
Appendix 4.....	172
Matrix Representation of Misalignment Parameters.....	172
Appendix 5.....	174
QOCAD - A Design Tool.....	174
Appendix 6.....	193
Gausspat.....	193

An Introduction to Millimetre Waves and Quasi-Optical Systems

1 Abstract.

This chapter contains an introduction to millimetre waves and to the way that they are represented and manipulated. Some of the limiting factors of millimetre wave systems are discussed. A project aimed at the development of the techniques used in the millimetre wave region is defined, and initial design procedures laid out.

1.1 Introduction to Millimetre Waves

Millimetre waves occupy the region of the electro-magnetic spectrum between 30GHz and 300GHz. Around 30GHz and below, in the microwave region, waveguide techniques dominate and above 300GHz, in the submillimetre and the far infra-red regions there is a domination of optical techniques. Millimetre wave systems use a combination of these techniques.

As the physical sizes of waveguide and waveguide components are scaled down with wavelength, so as to restrict all but the fundamental mode, losses increase and a great strain is placed on dimensional tolerances and surface finishes. It becomes increasingly advantageous to launch the signal into a free space beam. The wavelength, however, is too large to validate the use of ray optics in most practical sized systems, and requires the use of Gaussian beam techniques. Although not the same as ray optics there are stark similarities : Gaussian beam lenses look like optical lenses; Gaussian beam systems use mirrors, polarizers and other components that are common in optical systems, so much so that these techniques have become known as *quasi* optics. The submillimetre region is also a transitional region : from Gaussian optics to ray optics. It would often be more convenient if the four regions : microwave, millimetre and submillimetre waves and the far infra-red were instead divided into waveguide, quasi optic and ray optic regions.

1.2 Representing Free Space Beams

The transverse field of the free space beam can be described by the sum of an infinite set of orthogonal spatial modes. There are several different sets of modes that can be used to describe the fields any of which can be chosen to suit the situation. Spherical waves and angular spectra of plane waves have unique physical interpretations, whereas Gauss-Laguerre and Gauss-Hermite modes are representations of the same modes in different co-ordinate systems. In cartesian co-ordinates the modes are in terms of Gauss-Hermite polynomials, which form an orthogonal set. The fundamental mode is most commonly used as it is easy to generate and has the smallest transverse size which helps to minimize the physical size of systems. The amplitude of this mode has a Gaussian distribution with radial distance, hence the term Gaussian beams. Higher order modes are so infrequently used that the terms *free-space* beams, *Gaussian* beams and *quasi-optical* beams are synonymous and refer to the fundamental mode. Figure 1.1 shows qualitatively this Gaussian nature. The variation with axial distance z , also shown, is discussed more in the following section.

1.2.1 Properties of Gaussian Beams.

1.2.1.1 Amplitude dependence.

As mentioned above, the transverse field of a free-space beam can be described by an infinite set of orthogonal spatial modes. The \mathbf{E} -field for the fundamental mode, in cartesian co-ordinates, is given by

$$E_x = E_{0,x} \sqrt{\frac{2}{\pi\omega^2}} \exp\left\{\frac{-r^2}{\omega^2} - \frac{jkr^2}{2R} - j\phi\right\} \exp j\{kz - 2\pi ft\} \quad 1.1$$

with a similar expression for E_y . The method of derivation is commonplace¹ and isn't presented here but it involves the solution of a scalar wave equation and the use of a paraxial approximation. This latter point should be borne in mind when measuring the angular extent of a Gaussian beam². The terms in the first exponent describe respectively the Gaussian profile of the amplitude, the spherical nature of the phase fronts and the phase slippage relative to a plane wave at the same frequency. The square root term normalizes the field pattern to have power of $|E_{0,x}|^2$ when integrated over a transverse plane. The parameter ω , is the half width at $1/e$ field and is known as

¹ J. A. Arnaud. "Beam and Fiber Optics" London: Academic Press 1976.

² Refer to chapter 6, on feedhorn characterization.

the beamwidth parameter or simply the beamwidth. The parameter R , is the radius of curvature for a given phase front. Figure 1.1 shows qualitatively the variation of ω and R along the propagation axis. The beamwidth, ω , reaches a minimum value ω_0 , as shown, which is known as the beam waist. Defining this position as $z=0$ the variation of ω , R and ϕ with z is given by

$$\omega^2 = \omega_0^2 \left\{ 1 + \left[\frac{z\lambda}{\pi\omega_0^2} \right]^2 \right\} \quad 1.2$$

$$R = z \left\{ 1 + \left[\frac{\pi\omega_0^2}{z\lambda} \right]^2 \right\} \quad 1.3$$

$$\phi = \arctan \left\{ \frac{z\lambda}{\pi\omega_0^2} \right\} \quad 1.4$$

These expressions are produced as part of the derivation of equation 1.1 and are not derived here. The Rayleigh range, z_r , is defined by

$$z_r = \frac{\pi\omega_0^2}{\lambda} \quad 1.5$$

This marks the transition from near field to far field. In practice the far field is usually considered to be several Rayleigh ranges from the beamwaist position. In the far field the above expressions reduce to

$$w \approx \frac{z\lambda}{\pi\omega_0} \quad 1.6$$

$$R \approx z \quad 1.7$$

$$\phi \approx \pm \frac{\pi}{2} \quad 1.8$$

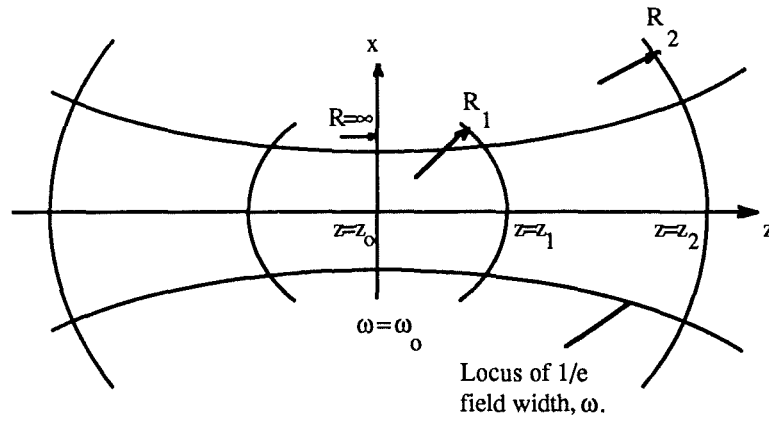


Figure 1.1a Variation of phase front curvature and beamsize with z

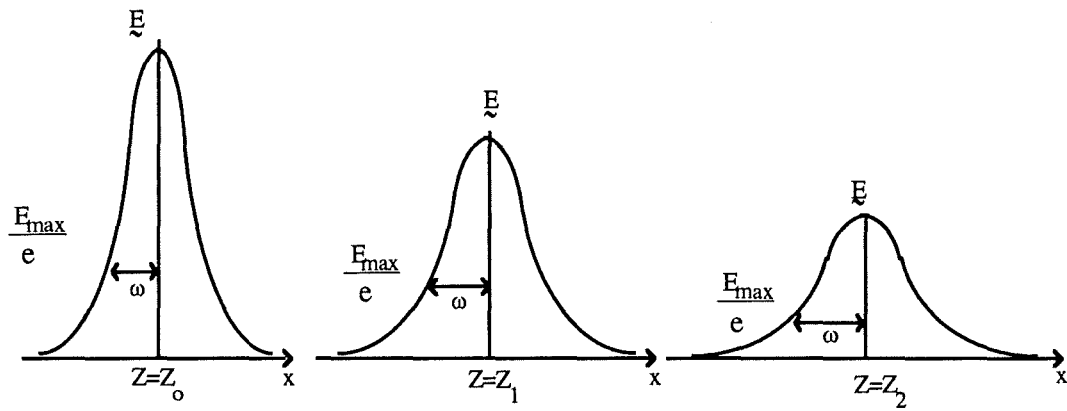


Figure 1.1b Variation of Gaussian field profile with Z

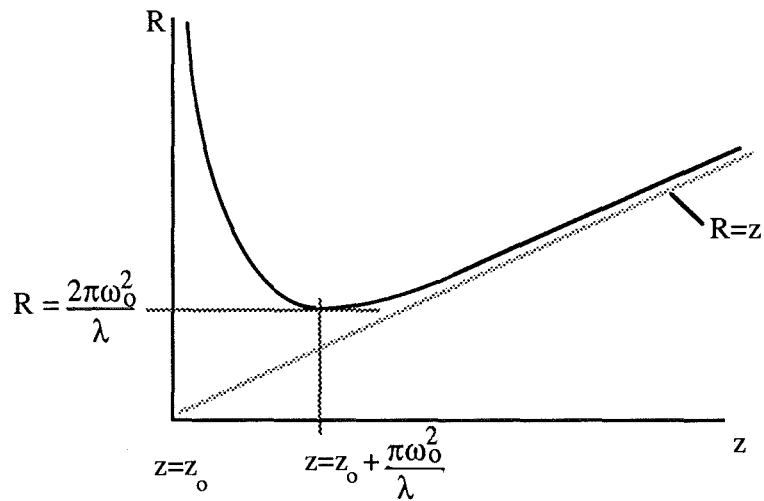


Figure 1.1c Variation of Radius of Curvature with z

The size of beamwaist that can be produced depends on the initial beam and the focussing optics but it can be seen from equation 1.2 that divergence is more rapid from a small beamwaist and the rate of change of phase front curvature and slippage with distance is larger. Equation 1.2 can be expanded and rewritten as a quadratic in ω_0^2 from which the roots can be written as

$$\omega_0^2 = \frac{\omega^2}{2} \pm \frac{\sqrt{\omega^4 - \left[\frac{2z\lambda}{\pi}\right]^2}}{2} \quad 1.9$$

This shows that for a given set of λ , z and ω it is possible to form two different sized beamwaists depending on focussing optics. More importantly, though, it shows that there is no arbitrary choice of λ , z and ω since the square root term must be real.

This is most often written as

$$z \leq \frac{\pi\omega^2}{2\lambda} = z_{\max} \quad 1.10$$

where z is the distance between the beam waist and the position at which the beamsize is ω . At $z = z_{\max}$ the two solutions to equation 1.9 are identical and only one waist is formed. This distance is known as the maximum throw and is an important parameter for determining the size of optical components within a system. For values of z less than the maximum throw the two beamwaists, one larger and one smaller than the waist at maximum throw, are known as parallel and focussed waists respectively. It is not possible to form a waist at values of z greater than the maximum throw.

1.2.1.2 Frequency Dependence.

There are no cut-off frequencies for free space modes because there are no boundaries to constrain the beam, indeed there is no frequency dependence to the wave impedance (within limits) and all beams of all frequencies in the millimetre wave region propagate at the same velocity, c . Strictly speaking there is frequency dependence in the phase slippage relative to a plane wave, as well as dispersion between different modes. For the majority of situations there are no problems with dispersion and this allows signals to be time division multiplexed and/or wavelength and frequency division multiplexed. There is, however, an effective cut-off frequency governed by the transverse size of the beam. Fundamental beams, as mentioned above, can be generated easily and efficiently, but from the Gaussian nature of the beam some truncation is inevitable. The effect of this can be limited and is often negligible¹ but can become a

¹ R. J. Wilde. "Millimetre-wave Gaussian beam-mode optics and corrugated feed horns"
Proc. IEE, Vol 131, Pt. H, No. 4 Aug. 1984 p258

problem when the size of any aperture is too small compared with the beam's width. The width of the beam is a function of frequency and increases with increasing wavelength, all else being equal. There is, therefore, a low-frequency limit where, for a given size of system (or aperture) the degree of truncation becomes unacceptable. This is somewhat flexible in that it depends on the choice of 'acceptable' but does provide some guidelines. The effect of truncation and the choice of acceptable limits are discussed in detail in chapter 3.

1.2.1.3 Polarization.

The two components E_x and E_y of a beam are orthogonal and may therefore be processed independently. This provides an extra capacity for carrying information. The two channels may carry signals at different frequencies which are easily separable by linear polarizers, or they may carry signals of the same frequency that differ only in amplitude and phase. The polarization state of a beam describes the behaviour of the resultant E -vector.

All of the information, and hence interest, in a particular polarization state lies in the relative amplitudes and phases of the two components. When the amplitudes and phases are both different the E -vector traces an ellipse, the shape of which depends on the relative amplitudes and phases. In certain cases the ellipse becomes a circle or a line and these states are named circular and linear respectively. In most cases, however, it is more intuitive to describe the polarization state by the relative phase and the ratio of the amplitudes than it is to describe the shape of the ellipse.

In the above discussion the orthogonal states described were linear. It is equally valid to resolve the resultant E -vector into a pair of circular states, rotating in opposite directions. In some cases it is more useful to do this. In the case of propagation through magnetized ferrite, for example, the natural modes of propagation are orthogonal circularly polarized beams¹.

Manipulation of the polarization state is a very common method of signal processing in quasi-optics, primarily because it is both easy and efficient : near perfect polarizers can be made by winding fine pitched wire grids with small diameter wire. Perhaps the most efficient property of signal processing using the polarization state is when two beams are interfered. If the two beams are combined using a polarizer, the two beams will occupy the orthogonal states of the resultant beam, and relative phase differences between the beams will serve only to alter the resultant polarization state. In the case where the two beams have equal amplitudes the polarization will change from linear, through circular to the orthogonal linear state as the relative phase varies from zero, through 90° to 180° . An analyzing polarizer or polarization sensitive detector is

¹ M. R. Webb. PhD Thesis. University of St. Andrews. 1992.

therefore required to detect the resulting amplitude modulation. Even at a null the signal power is not lost but appears in the orthogonal polarization state where it may be used further.

1.2.2 Limitations of free space beams.

The ability of a quasi-optical circuit to perform its required task can be split into two areas. The first is its ability to manipulate the polarization state of the input beams correctly to produce the required output states. The second is its ability to transmit sufficient signal power through the system to be detected. The first point is addressed with the aid of quasi-optical circuit theory that enables the polarization state of a beam to be traced through a system as it is manipulated by each component. This technique is based on a matrix representation for each component and a vector description of the polarization state. This technique is explained further in chapter 4, where it is incorporated into a CAD program running on an Acorn Archimedes. The second point is addressed with the aid of Gaussian beam theory. This technique uses the E-field representation of equation 1.1, to determine coupling between beams, the effects of focussing elements and the limits imposed by truncation. This technique is discussed further in chapter 3, where the requirements for quasi-optical components are determined and the components designed. In practice both techniques are required to produce a solution to a given problem. Quasi-optic theory is used first to derive an optical circuit and to produce a schematic circuit diagram containing the required components. Gaussian beam theory is then applied to determine beamsizes and the position of focussing elements and their focussing requirements.

1.3 Applications of Millimetre Waves.

Much of the drive for the development of quasi optics has come from the desire to exploit those properties of millimetre waves that are absent from the microwave and far infra-red regions. This is particularly so in radar, where moving up in frequency from microwaves provides greater bandwidth, resolution and directionality and where moving down in frequency from the far infra-red results in lower attenuation. The attenuation of a free space beam, figure 1.2, shows the increase in attenuation in the infra-red and the absorption minima at 35GHz, 94GHz, 140GHz and 220GHz, most used by millimetre wave radar. The full width of the millimetre wave region is used by a variety of other applications including plasma heating¹, plasma diagnostics², astronomy and as intermediate frequencies for the processing of optical and infra-red signals³.

dB/km

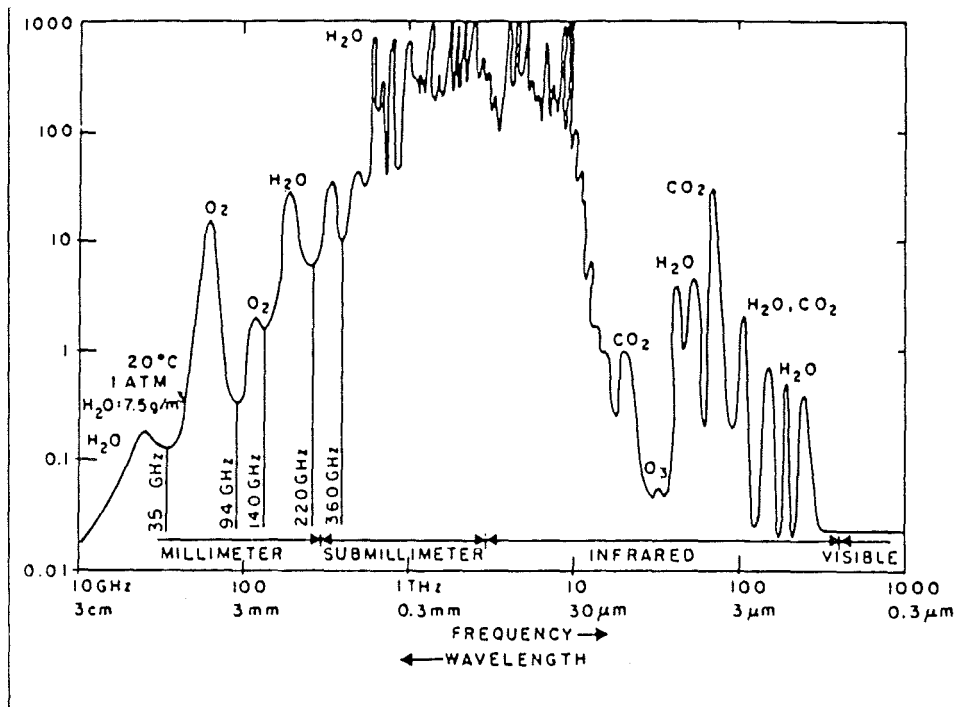


Figure 1.2 One Way Attenuation of a Free Space Beam

- ¹ Joint European Torus. Private communication with R. Smith, D. Bartlett.
- ² Joint European Torus. Private communications with R. Smith, A Harvey, J. Lesurf.
- ³ Private communications with P. Sutton, W. Dawber.

1.4 Project Definition.

It has been mentioned in the preceding sections that the field of radar is a prime candidate for exploiting the properties of the millimetre and submillimetre wave regions. For this reason, and from consideration of the interests of the sponsoring company EEV, the development of a millimetre wave radar provides an excellent vehicle for the implementation of existing quasi-optical techniques and for the development of novel quasi-optical circuits as solutions to the ensuing problems.

The project target was chosen, after consultation with EEV and Dr. J. Lesurf, to be the design, construction and operation of a full and working radar involving the implementation of quasi-optical techniques.

1.4.1 Initial Design Goals.

There are many different types of radar and within each type the degree of complexity can vary considerably, as will become apparent in the next chapter. It is therefore necessary to define the project more rigidly, to divide it into a number of sub-sections and to outline the methods by which the problems in each section are to be addressed.

Firstly, the choice needs to be made on the type of radar. This involves a detailed study of different types of radar and of the methods used to extract the required information from the return beam and process it into a more useable form.

Secondly, having decided on a specific type of radar using the results of the above study, the project needs to be divided into a number of sub-sections. Those sub-sections that can be realized using quasi-optical techniques are identified.

Thirdly, having identified the sub-sections that are to be realized optically, the degree of sophistication of the remaining sub-sections needs to be defined. This includes areas such as the handling and display of data extracted from returning signals.

The choice of operating frequency for the system alternated between 94GHz and 140GHz. Each frequency has its relative merits : 94GHz being favoured for the relatively high powers available and 140GHz being favoured for its smaller wavelength (and consequent system size) and because it marks a trend toward higher frequencies and the regions where quasi-optics will dominate. As the project evolved it became apparent that proof of concept could be obtained at 140GHz, though with the lack of a suitable source at this frequency the majority of the tasks performed by the radar would be at 94GHz.

1.5 Outline of thesis.

The thesis describes the processes involved in producing a quasi-optical radar. After an initial study of radar types the choice of radar is made. The subsequent chapters describe the design and construction of each section of the radar. The sections are divided into Optical Hardware; Electronic Hardware; Software Design Aids and Feedhorn Design and Evaluation. There then follows a concluding chapter on the evaluation of the system. Computer listings and full circuit diagrams are contained in the appendices for completeness and clarity. Lengthy mathematical treatments that would clutter the description of a part of a chapter are also included in the appendices.

An Introduction to Radar and Signal Processing Techniques

2 Abstract.

In this chapter there is a discussion of some of the many types of radar and of the methods used to extract the information in the returning signal. Based on the findings of this study, the choice of radar for this project is made and justified. A preliminary quasi-optical design is presented for the receiver, and other areas suited to the application of quasi-optical techniques are identified.

2.1 Measurement techniques used in radar.

Although initially used for 'detection and ranging', radar is currently used in a multitude of remote sensing, detection and identification areas. Despite the apparent diversity, common to all radar systems is the requirement to extract information from the returning signal and process it into a usable form. When approached from this signal processing point of view, the many types of radar appear more similar.

An echo from a distant target can be analyzed in terms of its amplitude, frequency, phase and polarization. If a timing mark is imposed on the transmitted signal the round trip time of the signal can also be measured. The variation of amplitude and phase across the width of the beam also provides information on the nature of the target and this technique of analyzing the mode content of a beam is especially useful and easy to implement at millimetre wave frequencies using optical techniques¹. These techniques are to be discussed more fully later.

Consider initially the target's radial range, radial velocity and angular position. Each of these quantities are determined to a greater accuracy in some radars than in others, but the principles of measurement are broadly the same.

2.1.1 Radial range.

Radial range may be determined by measuring the round trip time of a signal. This requires the imposition of some sort of timing mark on the transmitted signal that can be identified in the return. The simplest form of marking the time is to pulse the

¹ M.R. Webb. PhD Thesis, University of St. Andrews 1992.

transmitter. By measuring the time elapsed between sending and receiving the pulse, τ , the range can be determined from

$$R = \frac{c\tau}{2} \quad 2.1$$

This uses only the amplitude information from the return signal. The range resolution and maximum range are determined by the duration of the pulse and the pulse repetition frequency respectively although clearly the two are not independent. The round trip time can only be determined to within the temporal width of a pulse. The width of the pulse translates to a spread of ranges and hence a minimum range resolution. The pulse width can be reduced to improve this resolution but the bandwidth of the transmitted signal increases as a result and the receiver bandwidth must be correspondingly increased. Shorter pulses give a radar the advantage of better range resolution and range accuracy and, by the reduction in the size of the resolution cell, reduces the levels of clutter and interference. A short pulse radar has the disadvantage, however, of low levels of target illumination. This requires such a radar to use high power pulses and/or highly sensitive receivers to be able to detect remote or small targets.

To maintain the advantages of short pulses whilst using only moderate pulse power requires the use of pulse compression techniques. One way of looking at pulse compression is to consider first a method of encoding timing information in a continuous signal by frequency or phase modulation of the source. Each section of the waveform, viewed as a function of time, has a different frequency and this distinguishes it from other sections. This is shown schematically in figure 2.1.

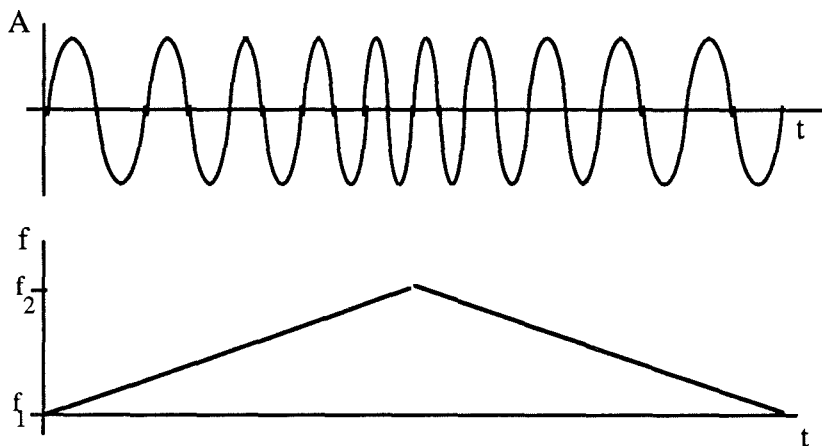


Figure 2.1 Schematic of Linear Frequency Modulation.

If the modulation is linear, the difference in frequency between the received signal and the transmitted signal, obtained by mixing the return signal with a portion of the transmitted signal, is directly proportional to the range.

Frequency or phase modulation causes an increase in the bandwidth of the transmitted signal. The larger the required range resolution, the larger the range of modulation and consequently the receiver bandwidth.

Using frequency modulation on a continuous source gives, in many situations, adequate range resolution and accuracy. When this type of modulation is applied within the duration of a pulse, timing marks are imposed throughout the pulse and the timing resolution, range resolution and range accuracy are improved. This enables long pulses to be used to give good illumination of the target, without losing the resolution of a shorter pulse. The long pulses have become, to all intent and purpose, compressed. The term 'pulse compression'¹ is also applied to the method by which modulated pulses are decoded. The return signal, in the case of linear frequency modulated pulses, is passed to a dispersive filter through which the propagation time is frequency dependent. If the frequency dependence is arranged such that the higher frequencies propagate more quickly, the tail end of the pulse, which is at a higher frequency, will catch up with the front end resulting in a narrower or compressed pulse at the filter output.

There are other ways of encoding the pulse, such as phase coded pulse compression which involves encoding the pulse with a binary word by modulating the phase by 0 radians (a zero) or π radians (a one) at regular intervals throughout the pulse. If the modulation tends toward random, the pulse takes on noise-like properties. This is advantageous because the correlation of two unrelated pseudo-random signals is very low, but the correlation of a signal with its replica (i.e. when $\tau=0$) is high since correlation is given by

$$C_{AB}(\tau) = \int_{t=-\infty}^{t=+\infty} A[t].B[t-\tau].dt \quad 2.2$$

Cross correlation of an unknown return pulse and the expected return pulse (or transmitted pulse) can be achieved in either a cross-correlation filter or a matched filter.

A matched filter has a frequency response that is tailored, from the knowledge of the transmitted spectrum, to give a maximum signal to noise ratio at the output when the input is the expected return pulse. The return pulse is therefore correlated with the image of the transmitted pulse built into the filter's frequency response. This is used widely where the transmitted signal has a known and constant frequency spectrum that can be encoded into the matched filter.

¹ M.I. Skolnik "Introduction to Radar Systems" 2nd Ed. McGraw-Hill 1980.

A cross correlation filter performs the operation of correlation by multiplying or mixing the return signal with a copy or delayed version of the transmitted signal, and integrating the result. This is shown in figure 2.2.

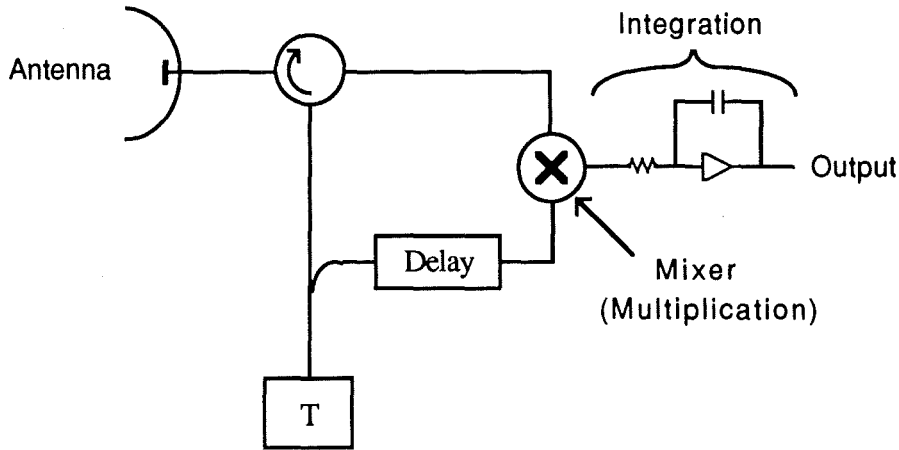


Figure 2.2 A Cross Correlation Filter

This type of filter enables the transmitter to be modulated in any way so long as a copy is kept for comparing with the return. This opens the way for modulating with a narrow band of 'noise' or pseudo-random modulation. The problems associated with how best to retain a copy of a signal or to delay a portion are currently of great interest as is the use of deterministic chaos for signal encoding¹.

2.1.2 Radial Velocity.

Radial velocity is determined by analyzing the temporal variation of the radial range. For slowly varying radial positions the target can be tracked from pulse to pulse, or at periods of the pulse repetition frequency for a CW radar, and the velocity calculated from

$$v_r = \frac{\Delta R}{\Delta t} \quad 2.3$$

The accuracy is limited since ΔR can only be measured to an accuracy determined by the pulse width and Δt is fixed as the pulse repetition period. The measured velocity will be an average value over one pulse which limits the resolution of the velocity measurement. Integration over several pulses will increase the accuracy to which the average velocity is known, but will reduce the ability to resolve small changes in the velocity. To obtain a better measure of the radial velocity it is necessary to measure variations of the range within the duration of the pulse. These variations

¹ Private communications with J.C.G. Lesurf and P. Sutton.

manifest themselves as Doppler frequency shifts of the return frequency. At a range, R , and a signal wavelength, λ , the phase length of a round trip is ϕ , where

$$\phi = 2\pi \cdot \frac{2R}{\lambda} \quad 2.4$$

and the return signal is of the form

$$A = A_0 \cos \{ \omega_0 t + \phi \} \quad 2.5$$

Any temporal variations of R , produce a time varying phase $\phi[t]$ such that

$$\phi[t] = \frac{4\pi}{\lambda} R[t] \quad 2.6$$

and hence

$$\frac{d\phi}{dt} = \frac{4\pi}{\lambda} \frac{dR}{dt} = \frac{4\pi}{\lambda} v_r \quad 2.7$$

When $v_r \ll c$, the rate of change of phase due to v_r is much smaller than the signal's rate of change of phase $2\pi f_0$. Thus $\frac{d\phi}{dt}$ can be regarded as constant over many cycles at $2\pi f_0$. This enables $\phi(t)$ to be written in the form

$$\phi[t] = \frac{d\phi}{dt} t = \omega_d t \quad 2.8$$

The received signal is now of the form

$$A = A_0 \cos \{ [\omega_0 + \omega_d] t \} \quad 2.9$$

By convention R increases radially from the transmitter and so a decreasing range produces an increase in the return frequency. The Doppler shift is therefore written as

$$f_d = - \frac{2v_r}{\lambda} \quad 2.10$$

At 140GHz, $f_d \approx 1\text{kHz}$ per m/s which demonstrates a further advantage of moving to higher frequencies.

The existence of Doppler shifted components in a return pulse often complicates the process of extracting range information. The imposition of a timing mark on a signal produces a characteristic spectrum which contains all of the information on the shape of the pulse or on the nature of the timing mark. A moving target produces a unique Doppler shift on each component. This alters both the bandwidth and the centre frequency of the spectrum thereby altering the shape and/or nature of the timing mark. Excessive Doppler shifts may move the return spectrum outside of the receiving filter's

bandwidth, especially when gating has been employed to reduce unwanted signals. If the receiver contains a filter bank, the Doppler shifts may result in erroneous range data as the Doppler components shift the return frequency to adjacent filters. To reduce such losses of signal, Doppler tolerant waveforms and receiving filters are required.

2.1.3 Angular Position.

The angular position of a target is defined by its azimuthal and elevation angles which are determined to a first order from the direction that the antenna is pointing. Radar antennas are usually highly directional, a quality reflected by the antennas gain parameters.

The directive gain is determined by the antenna pattern. An antenna producing a beam of solid angle Ω has a directive gain G_d given by

$$G_d = \frac{4\pi}{\Omega} \quad 2.11$$

This is the gain required to bring the power density of an isotropic antenna, with the same total radiated power, up to the level of the measured antenna in a given direction on the main lobe axis.

The power gain is similar to the directive gain but incorporates the power losses within the antenna. The power gain G_p is the gain required to bring the power density of a lossless isotropic antenna up to the level of the measured antenna that is fed with the same power. The total power fed to a real antenna will always be greater than the total power transmitted to the antenna and hence G_p is always less than G_d . The two gains are often very similar and are related by a radiation efficiency factor η_r such that

$$G_p = \eta_r \cdot G_d \quad 2.12$$

These two gain parameters determine the angular width of the beam. Using the antenna direction as the measure of angular position is therefore only accurate to within the width of the beam. Typical beam widths of a few degrees give a field of view of the order of 10m in diameter at 1km. This degree of angular resolution may be satisfactory for many applications but in, for example, tracking radar higher resolution is required. The angular resolution can be improved, in a way analogous to improving range resolution by pulse compression, by modulating the angular extent of the beam.

Consider a beam with an angular direction that is switched between two states. These two states are separated by an angle much smaller than the beamwidth so that a target visible to one state will always be visible to the other state as shown in figure 2.3.

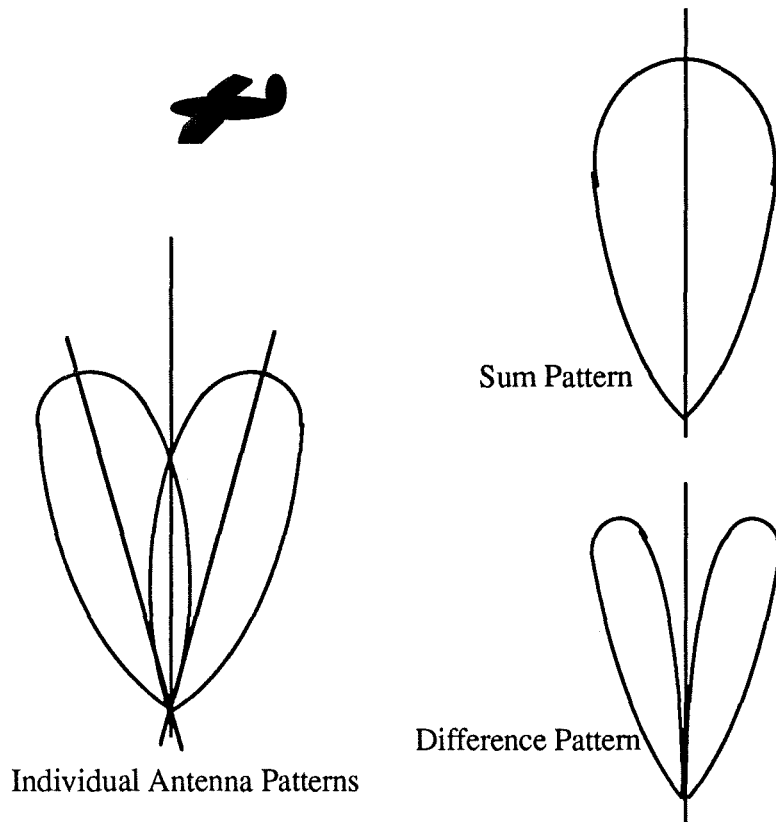


Figure 2.3 The use of Two Beams in Monopulse Radar

A target lying to the left of the centre line will produce a bigger response in the receiver when in the left state than in the right. The difference in sensitivity can be exploited by alternately measuring the return power at each position of the antenna. The relative power levels can then be used to calculate the angular offset of the target from the centre line. To reduce the effects of unknown side lobe levels and artefacts of the switching process it is common to move the mean position, or centre line, of the antenna to equalize the received powers thereby tracking the target. Taking the difference of the received powers produces a control voltage to automate the nulling and tracking mechanisms. The sum of the two signal powers is also taken to ensure that a target is still present when the difference becomes zero. The drawbacks with this method are the reliance on the amplitude information and the need to measure at least two pulses, four if both elevation and azimuth angles are required. Amplitude modulation from pulse to pulse will corrupt the return signal and provide an erroneous tracking voltage, and the temporal variations of angle above half, or quarter, of the pulse repetition frequency will be averaged out. The effects of amplitude modulation can be removed if separate antennas and receiving circuits are employed for each angular position and operated in parallel. This arrangement allows the angular

information and tracking signals to be determined on reception of a single pulse and is therefore known as monopulse.

The use of multiple antennas, as in monopulse, provides not only an amplitude reference but also a phase reference. The two receivers in figure 2.4 are offset spatially but have the same angular direction. By measuring the phase difference of the returns from each antenna the angular offset can be determined. If the separation of the antennas, d , is small compared to the target distance the phase difference, $\Delta\phi$, approximates to

$$\Delta\phi = d \frac{2\pi}{\lambda} \sin\theta \quad 2.13$$

where θ is the angular deviation. This again shows an advantage of using a smaller wavelength radiation, to maximise the angular resolution for a given minimum discernible phase shift.

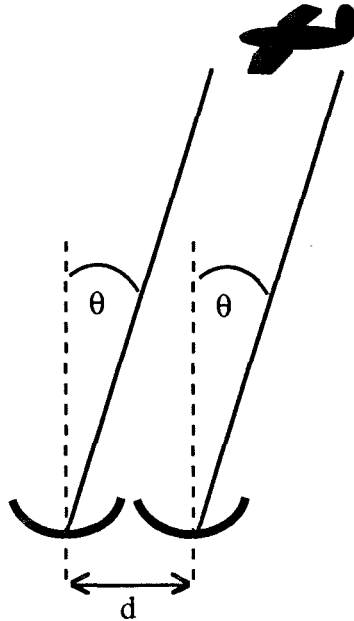


Figure 2.4 Principle of Phase-Comparison Monopulse.

2.1.4 Target Identification.

Reflection from a distant target will produce a distorted return beam. Variations in amplitude and phase across a beam are usually represented by considering higher order modes. As the modes used in free space beams are orthogonal and form a complete set, the return signal, R , can be represented by an infinite series of the form

$$R_x = \sum_{i=0}^{\infty} a_i \cdot E_i \quad 2.14$$

This is analogous to the Fourier components of a periodic waveform and the component amplitudes, a_i , are determined in the same way.

$$a_i = \int_{x=-\infty}^{+\infty} \int_{y=-\infty}^{+\infty} R_x^* \cdot E_i \, dx dy \quad 2.15$$

The representation is complicated by the inclusion of mode sets at different frequencies, and for completion requires the addition of modes for R_y .

A modal analysis of a return signal provides information on the shape and hence the identity of a target. Methods for determining the significant mode contents in a return signal are not as advanced as the signal processing methods used for amplitude and frequency analysis. They are however progressing in an analogous way as is apparent by considering the following examples.

A frequency modulated return can be analyzed using a bank of narrowband filters at the intermediate frequency, the output of which gives a representation of the signal's frequency spectrum. A spatially modulated return incident on a series of spatial filters produces a spatial spectrum in the same way. At optical frequencies, the spatial filters are usually used in transmission, arranged on a wheel and viewed sequentially. At millimetre wave frequencies the filters are more likely to be profiled plates, or kinoforms¹, used in reflection and also viewed sequentially. The frequency modulated signal has the advantage that it can be amplified and buffered so that copies may be sent to each filter in parallel. Recent advances in spatial arrays of amplifying and mixing

¹ S. Jacobsson et al. "Computer Generated Phase Holograms (Kinoforms) for Millimetre and Submillimetre Wavelengths" *Int. J IR & mmW* Vol11 No.11 Nov 1990 p1215.

elements at microwave frequencies suggest that spatial amplification of free space beams at millimetre wave frequencies may soon be possible^{1,2}.

The other main technique used in the frequency domain is that of mixing with a local oscillator to produce an intermediate frequency (IF). Mixing the return with a frequency swept local oscillator also produces an output dependent on the signal's frequency spectrum. This technique again scans the frequency band sequentially and the frequency resolution is determined by the single narrow band IF filter. In principle the use of a scanning IF filter and a fixed frequency local oscillator is equivalent to the swept local oscillator technique described above. In practice it is easier to sweep an oscillator than to scan a filter although linearity of sweep is often a problem. Both techniques have the disadvantage that some phase information is lost in the mixing process.

The swept local oscillator and scanning IF filter techniques have a spatial analogue in the spatial light modulator. The spatial light modulator is used to vary the amplitude and phase distributions in a known and controlled way³. It can be used to generate higher order modes from an incident fundamental mode and in a reciprocal manner convert higher order modes to fundamental modes. Such a device can be used to convert selected higher order modes in a multi-mode return beam into a fundamental mode suitable for detection. By stepping through a number of modes sequentially the modal spectrum is found.

The stepped spatial mode converter acts as a filter at the signal frequency and is analogous to the swept IF filter, whereas conversion to a single mode for detection is analogous to mixing with a local oscillator to produce an IF for detection. The spatial light modulator method is therefore equivalent to a swept filter at the signal frequency, whose output is mixed with a swept local oscillator, locked to the signal filter, to produce a DC level proportional to the spectral power.

The generation of modal spectra provides a further method of identifying targets or of discriminating between targets and surrounding clutter. The aforementioned techniques generate spectra, mode by mode, but can be extended to form pattern recognition aids. The characteristic reflection of a target can be used to form complex multi-mode filters, known as kinoforms, that are analogous to holograms. These can be used to provide a correlation between an unknown return and a list of possible

-
- ¹ L.B. Sjogren et al. "Development of a monolithic 94GHz 360 degree Phase Shifter" 15th Int. Conf. on IR & mmW, Orlando 1990.
 - ² T. Itoh. "Quasi-Optical Power Generation and Measurement Techniques" 16th Int. Conf. on IR & mmW, Lausanne 1991.
 - ³ M.R. Webb. Ph.D Thesis. University of St. Andrews 1992.

targets. Filters incorporating full phase and amplitude information can produce reliable correlations independent of target orientation.

2.2 Selection of Radar Type.

The principle purpose of the project is the development and application of quasi-optical ideas to radar. To save spending considerable effort on re-inventing the wheel, radars which had complex signal processing, transmission and mechanical requirements were avoided, and radars compatible with the qualities of available transmitters were preferred. The transmitter sources envisaged were Gunn effect oscillators. These have powers of a few tens of mW at 94GHz and a few mW at 140GHz. They can be modulated but are not suited to the sort of duty cycles employed by pulse radar. The transmitter is therefore to be CW. The Gunn diodes possess some varactance and the resonant frequency of such a diode in a fixed length cavity can be varied by changing the bias level. Frequency modulation over ~500MHz is possible using this technique, and would provide a timing mechanism for a CW radar. These characteristics of Gunn oscillators have restricted the choice of radar to a frequency modulated CW (FMCW) radar.

The range information is encoded in the return signal frequency, which will be contaminated by Doppler shifts. By suitable choice of modulation waveform (see later) Doppler shifts can be determined and separated from the range frequencies. This makes Doppler measurement a requirement to provide accurate range information, and therefore is easy to incorporate into an FMCW radar.

Significant use is made of polarization in the signal processing and manipulation methods used in quasi-optical systems. The determination of the return signal's polarization state, therefore, is also relatively easy to achieve and can be included in the capabilities of the radar.

The above capabilities are combined to produce a polarization diverse, FMCW Doppler radar.

To be able to identify those tasks that can realized optically, requires a study of the processes required, in an FMCW radar, to extract the information from the return beam.

2.3 Range and Velocity Measurement Techniques in FMCW radar.

Consider frequency modulation of the type shown in figure 2.5a. The frequency of the transmitter varies linearly with time over a range ΔF . As range is directly proportional to elapsed time, the horizontal axis could be labelled R . A signal delayed by a time τ , has a frequency identical to the transmitter τ seconds earlier and hence appears as in figure 2.5b. The difference in frequency of the transmitted and received signals is constant, and proportional to the range, except for a period τ when it 'collapses' through zero and changes sign, figure 2.5c. The difference frequency can be determined by mixing the received signal with a portion of the signal currently being transmitted. The sign of the frequency difference, however, is lost in this process and is shown by the 'beat' frequency of figure 2.5c. The loss of sign is of no consequence if the beat frequency is constant. The inclusion of Doppler shifts in the return produces an asymmetry, figure 2.5d, that can produce range errors if not compensated for. This is discussed in the following section on radial velocity.

The minimum and maximum ranges are determined by the pulse repetition frequency, f_{prf} , and the modulation range ΔF . Consider the diagram in figure 2.5c. By virtue of the fact that the sign information is lost in the mixing process, the time period available for measuring the beat frequency, f_{beat} , is t_{free} where

$$t_{\text{free}} = \frac{1}{2f_{\text{prf}}} - \tau = \frac{1}{2f_{\text{prf}}} - \frac{2R}{c} \quad 2.16$$

The beat frequency at this range is given by

$$f_{\text{beat}} = 2\Delta F f_{\text{prf}} \tau = \frac{4\Delta F f_{\text{prf}} R}{c} \quad 2.17$$

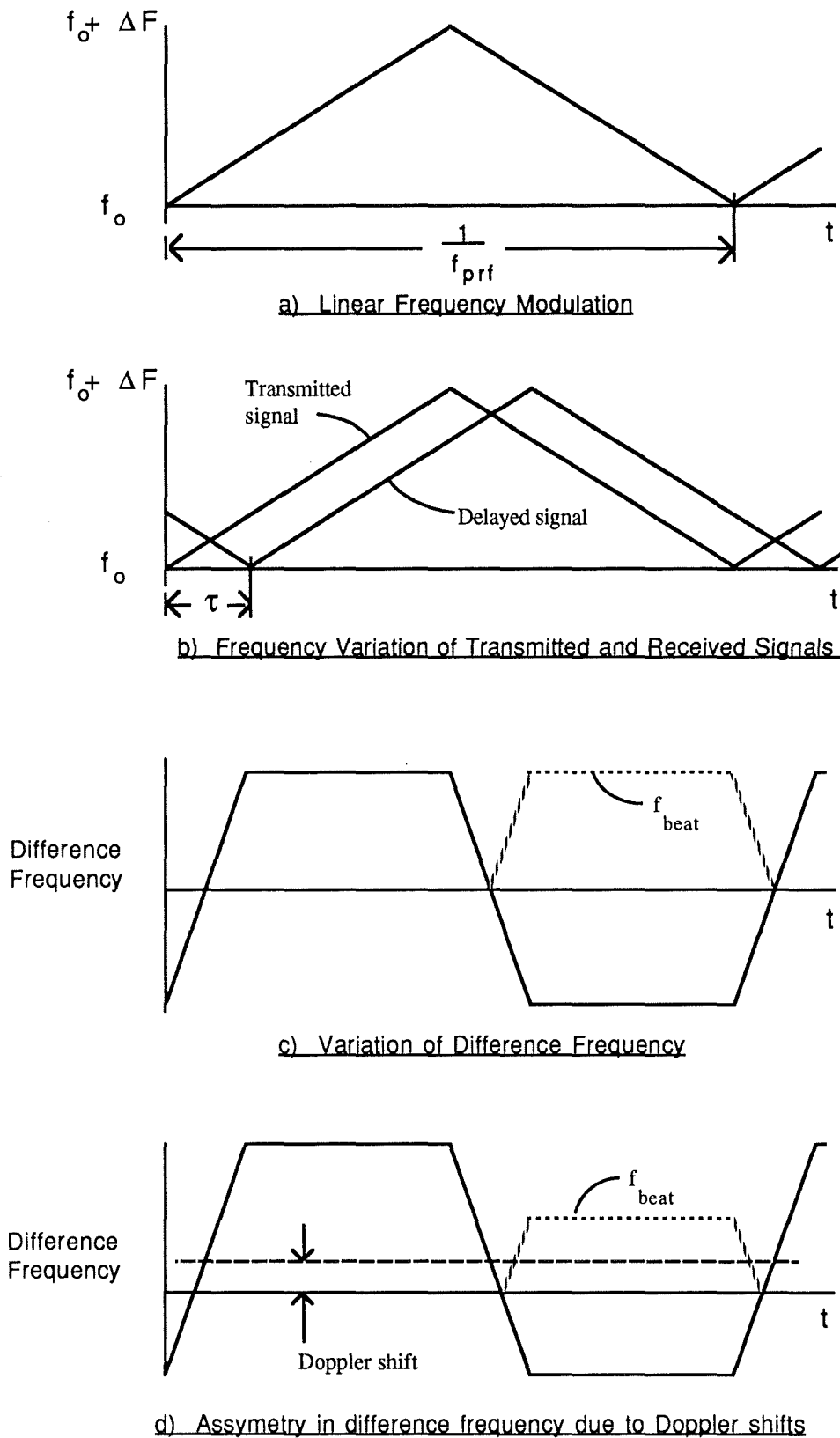


Figure 2.5 Frequency Behaviour in A Linear FM System

The time required to measure this frequency is $T \approx \frac{1}{f_{\text{beat}}}$. In order, therefore, to be able to measure the beat frequency, the time available for measurement must be greater than the required measurement time, hence

$$\frac{1}{2f_{\text{prf}}} - \frac{2R}{c} \geq \frac{c}{4\Delta F f_{\text{prf}} R} \quad 2.18$$

This is shown graphically in figure 2.6.

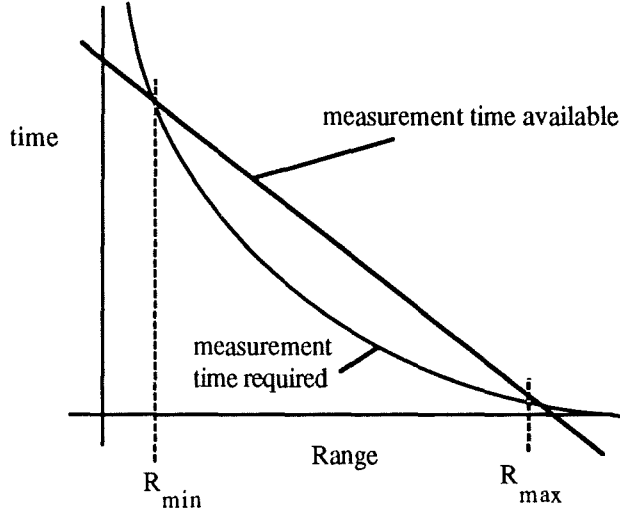


Figure 2.6 Range Restrictions Imposed by Measurement Times

The roots to equation 2.18 give the maximum and minimum ranges for given values of f_{prf} and ΔF . These are evaluated as

$$R_{\text{max}} = \frac{c}{8f_{\text{prf}}} \left\{ 1 + \sqrt{1 - \frac{8f_{\text{prf}}}{\Delta F}} \right\} \approx \frac{c}{2} \left\{ \frac{1}{2f_{\text{prf}}} - \frac{1}{\Delta F} \right\} \quad 2.19$$

$$R_{\text{min}} = \frac{c}{8f_{\text{prf}}} \left\{ 1 - \sqrt{1 - \frac{8f_{\text{prf}}}{\Delta F}} \right\} \approx \frac{c}{2\Delta F} \quad 2.20$$

Where the approximations are for when $f_{\text{prf}} \ll \Delta F$.

A typical Gunn diode may be modulated over a range of 500MHz at a modulation frequency of 5kHz. In this case, and most others, the approximation is valid and the minimum and maximum ranges are 30cm and 15km respectively. To maintain linear modulation the range of frequencies may be reduced to 100MHz at the expense of a larger minimum range, 1.5m, but with an insignificant change in maximum range.

The inclusion of Doppler shifts in the return frequency alters the time required to measure the return frequency but not the time available. Therefore t_{free} is as in equation 2.16 and T becomes

$$T = \frac{c}{\{4\Delta F f_{\text{prf}} R + c f_{\text{Doppler}}\}} \quad 2.21$$

Solving this produces a maximum and minimum range given by

$$R_{\text{max}} \approx \frac{c}{2} \left\{ \frac{1}{2f_{\text{prf}}} - \frac{1}{\Delta F} \right\} + \frac{c f_{\text{Doppler}}}{8\Delta F f_{\text{prf}}} \quad 2.22$$

$$R_{\text{min}} \approx \frac{c}{2\Delta F} - \frac{c f_{\text{Doppler}}}{8\Delta F f_{\text{prf}}} \quad 2.23$$

where f_{Doppler} is the Doppler shift which can be positive or negative. The Doppler shift adds a constant offset to the return frequency. This produces, after mixing, a beat frequency that is different for the up and down ramps of the modulation period as shown in figure 2.5d. To separate the range and Doppler components requires the measurement of the frequency during both the up and down ramps.

To enable the Doppler shifted component to be measured for both ramps and for either sign of shift the range limits must therefore be

$$R_{\text{max}} \approx \frac{c}{2} \left\{ \frac{1}{2f_{\text{prf}}} - \frac{1}{\Delta F} \right\} - \frac{c |f_{\text{Doppler}}|}{8\Delta F f_{\text{prf}}} \quad 2.24$$

$$R_{\text{min}} \approx \frac{c}{2\Delta F} + \frac{c |f_{\text{Doppler}}|}{8\Delta F f_{\text{prf}}} \quad 2.25$$

Having chosen values of ΔF and f_{prf} , the range can be found from the sum of f_{beat} over both up and down ramps, and the velocity found from the difference in f_{beat} in the up and down ramps. Hence

$$\text{Range} = \frac{c(f_{\text{up}} + f_{\text{down}})}{8\Delta F f_{\text{prf}}} \quad 2.26$$

$$\text{Velocity} = \frac{-\lambda(f_{\text{up}} - f_{\text{down}})}{4} \quad 2.27$$

As equation 2.27 shows, it is necessary to know which is the up ramp and which is the down ramp in order to determine the sign of the velocity.

2.3.1 Frequency Measurement Techniques.

To avoid the use of costly IF amplifiers for what is solely for demonstration purposes, operation with IFs of 100MHz and above was ruled out. The mixing process would therefore produce beat frequencies in the range of DC to ~1MHz. Frequencies in this range can be measured by a variety of methods. Frequency counting, period timing (or reciprocal counting) and the use of phase lock loops are described and evaluated here.

2.3.1.1 Frequency Counting.

This method counts the number of zero crossings of the signal in a given time T. The frequency of the signal is given by

$$f = \frac{N}{T} \quad 2.28$$

As N can only be evaluated to the nearest integer, the measured frequency can only assume discrete values spaced at intervals of $\frac{1}{T}$. The error in measuring f is also $\frac{1}{T}$ and this is known as the measurement bandwidth of the input signal. In an FMCW radar T is governed by the modulation frequency, f_{prf} , and the delay time, τ . T is equivalent to t_{free} of equation 2.16. For a modulation frequency of ~500Hz, the error and accuracy for determining f_{beat} are 1kHz. Beat frequencies in the range of 1kHz to 10kHz would be severely limited in accuracy, although the accuracy and error remain constant using this method.

2.3.1.2 Period Timing.

Period timing involves measuring the time between successive zero crossings of the signal frequency. The error in this technique is still determined by the measurement bandwidth, $\frac{1}{T}$, but the average signal frequency can be measured more precisely. The period is measured by counting the number of high frequency clock pulses between successive zero crossings. The frequency is given by

$$f = \frac{1}{P} = \frac{f_{clk}}{N} \quad 2.29$$

For $N \geq 10$ the fractional accuracy in f is $\frac{1}{N}$ and the absolute accuracy is $\frac{f_{clk}}{N^2}$.

For a typical clock frequency of 10MHz, this yields accuracies of 0.1Hz at 1kHz and 100kHz at 1MHz. A pulse repetition frequency of 500Hz yields a measurement bandwidth of 1kHz. At this pulse repetition frequency, period timing gives a more precise frequency than frequency counting for signal frequencies below ~100kHz.

2.3.1.3 Phase lock loops.

A phase lock loop uses a voltage controlled oscillator (VCO) to produce an output at the same frequency as the input signal. The difference in frequency is determined by a phase detector or mixer that produces a control voltage oscillating at the difference frequency. This control voltage is filtered and fed back to the VCO to bring the VCO frequency into lock with the input signal as shown in figure 2.7.

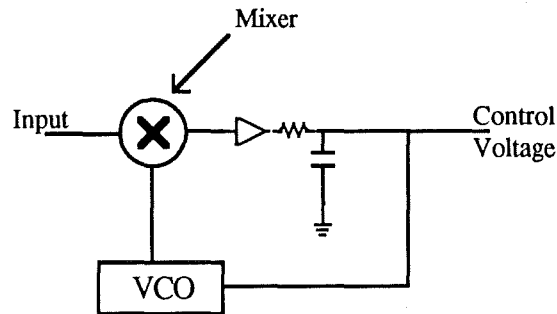


Figure 2.7 Schematic of a Phase Lock Loop

Once the VCO has locked onto the input frequency, the control voltage which is now a DC level is proportional to the VCO and hence the signal frequency. The low-pass filter removes the high frequency components of the control voltage, produced before the loop finds lock, and passes only the underlying DC component to the VCO. This prevents the loop becoming unstable whilst finding the lock position.

Frequency variations in the input signal appear as amplitude variations in the control voltage. Those variations within the pass band of the filter will be tracked by the VCO and the loop then provides FM to AM conversion. Higher frequency components are suppressed by the filter and are not fed back to the VCO.

Once the loop has found lock, the signal frequency is determined by measuring the control voltage. This may contain some modulation, passed by the feedback filter, that is averaged to produce a single voltage, and hence frequency, reading. The measurement bandwidth of the loop is therefore determined by the bandwidth of the low-pass feedback filter. Although the analogue control voltage implies that the frequency can be determined exactly, there are other characteristics of the loop that affect its ability to measure frequency.

To determine the input frequency, the loop first has to lock in. Consider the loop and initial level of control voltage shown in figure 2.8.

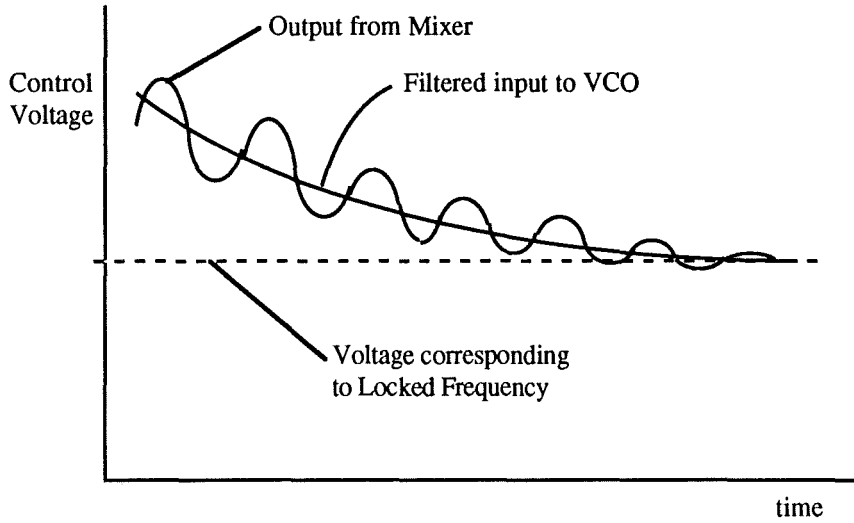


Figure 2.8 Schematic of Control Voltage from Phase Lock Loop.

Initially the input and VCO frequencies are very different, and the mixer output is a high frequency sine wave. Such a sine wave has no DC offset with which to reduce the mean control voltage. When this sine wave is applied to the VCO through the low-pass filter, an asymmetry arises that imposes an overall DC offset on the sine wave. The positive half of the cycle increases the VCO frequency and raises the beat frequency from the mixer, whereas the lower half of the cycle lowers the beat frequency from the mixer. As a result, the time spent in the positive half-cycle is less, being at a higher frequency, than the time spent in the negative half-cycle. The mean level is therefore below the midpoint of the two peaks and constitutes a negative DC offset. This offset is passed by the feedback filter and reduces the VCO frequency until the loop becomes locked.

As a simple example consider a mixer whose output is of constant amplitude and can only assume two states. Such a mixer can be made from an Exclusive-OR gate fed by square waves at the signal and VCO frequencies. The DC offset in this case is proportional to the difference in times spent at each state. The time spent at each state is one half cycle at that frequency, therefore

$$T_1 = \frac{1}{2f_1} \quad 2.30$$

$$T_2 = \frac{1}{2f_2} \quad 2.31$$

and hence the offset voltage is

$$V_{\text{offset}} = k \cdot \frac{\{f_1 - f_2\}}{f_1 f_2} \quad 2.32$$

Assuming the VCO is linear, the difference in frequency between the two states is constant and the offset is then

$$V_{\text{offset}} \propto \frac{1}{f_1 f_2} \quad 2.33$$

At large beat frequencies, when the loop is a long way from lock, the offset voltage is small and increases as the VCO frequency becomes coincident with the signal frequency. This produces a locking 'well' into which the loop can fall. Close to lock the well is steep : small changes in frequency produce large changes in the offset voltage, and lock is achieved quickly. Far from the well the walls are flat and changes in offset voltages are small such that the loop takes a long time to achieve lock, if at all.

The locking bandwidth of a loop is a measure of the width of the well and defines the range of offset frequencies over which lock is achieved in a given time. The slope of the walls is determined by the response of the feedback filter. For a given DC offset the rate of change of the VCO frequency is governed by the charging time of the capacitor through the resistor shown in figure 2.7. A shorter lock-in time is at the expense of a wider measurement bandwidth. In an FMCW radar, lock normally has to be achieved within the duration of the ramp, or more specifically within the time t_{free} of equation 2.16. However, if the beat frequency is reasonably constant, as in figure 2.5c, the Doppler shifts during the two half cycles and the periodic zeroing due to changes in sign of the difference frequency can be considered as frequency modulation on the range 'carrier' frequency. A typical short range radar, of the type envisaged with Gunn diodes as transmitters, will produce Doppler shifts at 94GHz of the order of 10kHz. Delay times corresponding to ranges of a few hundred metres are of the order of $1\mu\text{s}$. The beat frequency will therefore have FM components of a few kHz, due to Doppler shifts, and components at odd multiples of f_{prf} due to the square wave type modulation from the changing sign of the difference frequency. Selective filtering will pass the Doppler shifts to the VCO and reject the zeroing transients. and the loop will therefore track the Doppler shifts and be oblivious to the fact that the difference frequency changes sign.

2.3.2 Summary of Frequency Measurement Requirements.

To measure the range and radial velocity, the beat frequency of the received and transmitted signals needs to be measured during both the up and down ramps of the modulation period. For decoding simplicity, the ramp slopes need to be of equal magnitude and the modulation needs to be linear. The choice of modulation parameters determines the minimum and maximum range and the beat frequencies that these ranges produce. The modulation parameters also affect the precision to which the frequency can be measured and the error in this measurement. Different frequency measurement techniques have different degrees of precision.

The quasi-optical requirements are to guide the received signal to the mixer, and to take a portion of the transmitted signal and guide it to the receiver with the correct polarization.

The decoding requirements are to measure the beat frequency, which is to be in the range 1kHz to 1MHz, during both halves of the modulation cycle and to output the range and velocity components.

2.4 Polarization Measurement Techniques.

The polarization state of the return signal can be determined by measuring the relative amplitude and phase of two orthogonal states as discussed in chapter 1. For practical purposes it is convenient to use linear states. The phase can be measured by mixing the two states which can be done at the signal frequency or at an intermediate frequency. It is not sufficient, however, to obtain only the magnitude of the phase. The sign of the phase is required to distinguish between left and right circular (and elliptical) states but is lost in the mixing process.

Mixing of two signals of the form

$$A = A_0 \cos \{ \omega t \} \quad 2.34$$

and

$$B = B_0 \cos \{ \omega t + \phi \} \quad 2.35$$

produces an output of the form

$$\begin{aligned} M &= A_0^2 \cos^2(\omega t) + B_0^2 \cos^2(\omega t + \phi) + 2A_0B_0 \cos(\omega t) \cos(\omega t + \phi) \\ &= A_0^2 \cos^2(\omega t) + B_0^2 \cos^2(\omega t + \phi) + A_0B_0 \{ \cos(\phi) + \cos(2\omega t + \phi) \} \end{aligned} \quad 2.36$$

The mixer will time average the \cos^2 and $\cos(2\omega t + \phi)$ terms, producing an output of the form

$$M = \frac{1}{2} A_o^2 + \frac{1}{2} B_o^2 + A_o B_o \cos(\phi) \quad 2.37$$

As cosine is an even function, M will be the same whether A lags or leads B . In addition to the loss of sign, mixing the states directly requires knowledge of the amplitudes in order that the cosine term may be separated from equation 2.37.

Mixing each state with a local oscillator at frequency ω_L , produces a pair of beat frequencies of the form

$$M_a = \frac{1}{2} A_o^2 + \frac{1}{2} L_o^2 + A_o L_o \cos \{ [\omega_a - \omega_L]t + \phi_a \} \quad 2.38$$

$$M_b = \frac{1}{2} B_o^2 + \frac{1}{2} L_o^2 + B_o L_o \cos \{ [\omega_b - \omega_L]t + \phi_b \} \quad 2.39$$

The phases ϕ_a and ϕ_b are relative to the local oscillator at $t=0$, but if L_o has the same phase at each mixer the phase difference, $\phi_a - \phi_b$, is equal to the phase difference of the signals A and B . When the two signals A and B are replaced by the polarization states, the phase difference of the mixer outputs is the polarization phase. If the local oscillator is taken from the transmitted signal the mixer outputs will have frequencies containing the range and velocity information, the phase difference will, however, change sign with the up and down ramps. A constant polarization phase will appear as a lagging phase in one half of the modulation period and a leading phase in the other.

The a.c. amplitudes of the two mixer outputs, equations 2.38, 2.39, are proportional to the field strengths of the two polarization states. These can be measured by rectification and smoothing or peak detection. Viewing the two outputs in XY mode on an oscilloscope shows the polarization ellipse of the input beam, with the phasor rotating at the beat frequency rather than the signal frequency.

2.4.1 Summary of Polarization Measurement Requirements.

To measure the amplitude and phase of the polarization states, each state of the return needs to be measured using the same local oscillator. This local oscillator can be the same as that used for measuring range and radial velocity.

The quasi-optical requirements are to guide each polarization state to a separate mixer, and to guide portions of the transmitted signal to each mixer with the same phase.

The decoding requirements are to measure the relative amplitude and phase of the AC coupled components of the two mixer outputs.

Before combining the range radial velocity and polarization requirements it is worthwhile considering a further mode of operation.

2.5 Operation without FM.

It may be useful to measure Doppler and polarization information when there is no FM. The difficulty in this case is finding the sign of the Doppler shift and of the polarization phase. By mixing the transmitted and received signals, the beat frequency can be found as in equation 2.38. The difficulty now is that the beat frequency is a Doppler shift of unknown sign, and that a constant polarization phase can appear as a lag or a lead depending of the sign of the Doppler velocity. A solution is to mix a second reference signal, that is in phase quadrature with the local oscillator, with both of the polarization states of the return. Writing the polarization states as E_x and E_y , and the in phase and in quadrature local oscillators as I and Q, the four mixer outputs can, after AC coupling, be written as

$$M_1 = E_x I \cos(\pm\omega_d t + \alpha) \quad 2.40a$$

$$M_2 = E_x Q \cos\left(\pm\omega_d t + \alpha + \frac{\pi}{2}\right) \quad 2.40b$$

$$M_3 = E_y I \cos\{\pm\omega_d t + \alpha + \phi\} \quad 2.40c$$

$$M_4 = E_y Q \cos\left(\pm\omega_d t + \alpha + \phi + \frac{\pi}{2}\right) \quad 2.40d$$

Where ω_d is the beat frequency, ϕ is the polarization phase and α is the unknown phase difference of the signal and local oscillator at $t=0$.

If ω_d is positive, the outputs of the I and Q channels for E_x will have a phase difference of $\frac{\pi}{2}$, whereas if ω_d is negative, the phase difference will be $-\frac{\pi}{2}$. The sign of the Doppler shift can therefore be found from whether M_1 lags or leads M_2 . The other polarization state, E_y , can be used equally well should E_x be zero.

The phase difference between M_1 and M_3 , or M_2 and M_4 , gives the correct magnitude of the polarization phase, ϕ . If ω_d is positive the sign of the phase will be correct too, whereas if ω_d is negative this phase will have the wrong sign. As the sign of ω_d will have already been determined, the correct polarization phase is easily realized.

For the situation where $\omega_d = 0$, the mixer outputs need to be DC coupled. By assuming equal local oscillator powers in the I and Q states, that are much larger than the return power, the outputs of the form of equation 2.37, approximate to

$$M_i = \frac{1}{2} L^2 + E.L \cos(\phi_{\text{unknown}}). \quad 2.41$$

The constant terms can be determined by varying the local oscillator phase through 2π , and measuring the median mixer level, or by blocking the signal path and measuring the mixer level.

2.5.1 Summary of Measurement Requirements without FM.

To enable operation as a Doppler radar or solely as a polarization analyzer, requires mixing each polarization state with two local oscillators in phase quadrature. The local oscillator is taken from the transmitted signal if Doppler information is required.

The quasi-optical requirements are to guide each polarization state to a pair of mixers, and to generate in phase and in quadrature portions of the transmitted signal. The I and Q local oscillators are then required to be guided to the correct mixer with the appropriate phase.

The decoding requirements are to measure the beat frequency, if it exists, and to measure the relative phases of the four mixer outputs. The amplitude, phase and frequency information from the four mixers is then processed to yield the Doppler velocity and polarization state.

2.6 Combined Quasi-Optical Requirements.

The ability to be used as a Doppler radar requires the use of extra mixers and a second local oscillator. This facility will degrade the performance of a full FMCW radar if it is a permanent fixture because half of the return power is lost in the other two mixers. Re-arranging the circuit layout enables these extra mixers to form two balanced pairs, hence improving the performance. This is discussed in more detail in the next section.

The full quasi-optical requirements are :-

- To launch a beam at a distant target and to couple the reflected signal into the receiver circuit.
- To resolve the return signal into orthogonal polarization states.
- To guide portions of the return signal and the local oscillators to the appropriate mixers with the appropriate phases and amplitudes.
- To take a portion of the transmitted signal to satisfy local oscillator requirements.

The full decoding requirements are :-

- To amplify each mixer output and couple it to the remaining decoding sections in the appropriate way.
- To measure the amplitude, frequency and phase information from the two or four mixers.
- To determine the frequency and phase information over both halves of the modulation cycle.
- To generate and control a modulation signal for the transmitter.
- To retrieve and process the above information and display in a readable form.

Additional requirements include duplexing the transmitter and receiver for antenna sharing, which can be done optically, and linearizing the FM, which can be achieved using a combination of optical and electronic techniques.

2.7 Quasi-Optical Design of the Receiver.

In the millimetre wave region, the losses in transmission and reflection, and cross polarization in wire grid polarizers are very small and are ignored in the following discussions.

A vertical polarizer (vertical wires) splits the return into orthogonal linear states. For an FM radar each of these states is mixed with a single local oscillator. This can be injected at the same polarizer that splits the return, as shown in figure 2.9.

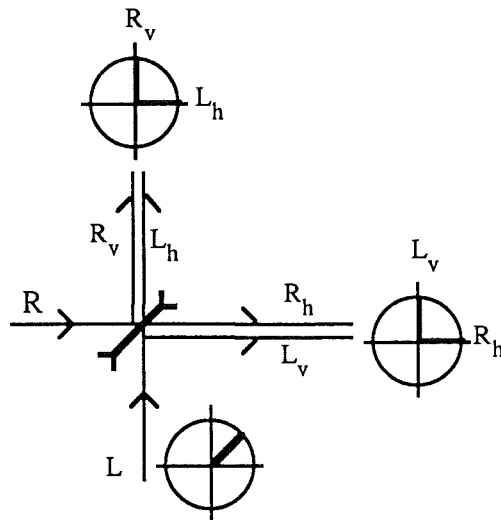


Figure 2.9 Combining Received Signal and Local Oscillator

Each of the two beams leaving the polarizer has the local oscillator in one polarization state and the return signal in the other. If either beam is analyzed by a 45° polarizer (wires at 45° to vertical), the resulting pair of beams each contains portions of the signal and local oscillators in the same polarization.

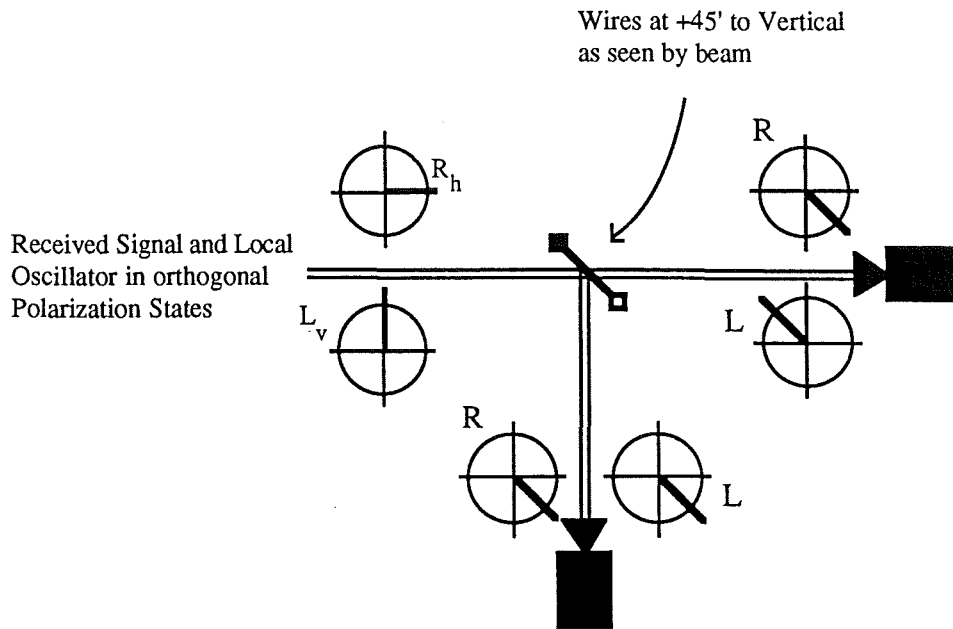


Figure 2.10 Phase Relation of Received Signal and Local Oscillator in a Balanced Mixer.

The phase difference between the signal and local oscillator is different in one beam by 180° with respect to the other as shown by the polarization symbols in figure 2.10. As the return signal and local oscillator are likely to have different frequencies, it is incorrect to say that they are out of phase by 180° . What is true, however, is that outputs of the detectors that mix these beams are in antiphase. Taking the difference of the mixer outputs removes the $\frac{1}{2}L^2$ terms from equation 2.38, and leaves the beat frequency term. Any spurious amplitude modulation of the local oscillator causes variations in $\frac{1}{2}L^2$, and these components may mask the smaller beat frequency components. The effect of local oscillator AM is greatly reduced, though not completely removed, using this method which is known as balanced mixing.

For Doppler radar, with no FM, the requirement is to mix each polarization component with in-phase and in-quadrature local oscillators. It is therefore necessary to split each polarization state into two beams. The local oscillator can be injected in a similar way as before, however the in-phase local oscillator must combine with one beam and the in-quadrature local oscillator with the other.

The beam carrying the local oscillators has the in-phase and in-quadrature components in orthogonal polarization states, where they remain separate. This is shown in figure 2.11. The resultant beam is circularly polarized, though this is of no consequence as the two components are merely sharing the same beam.

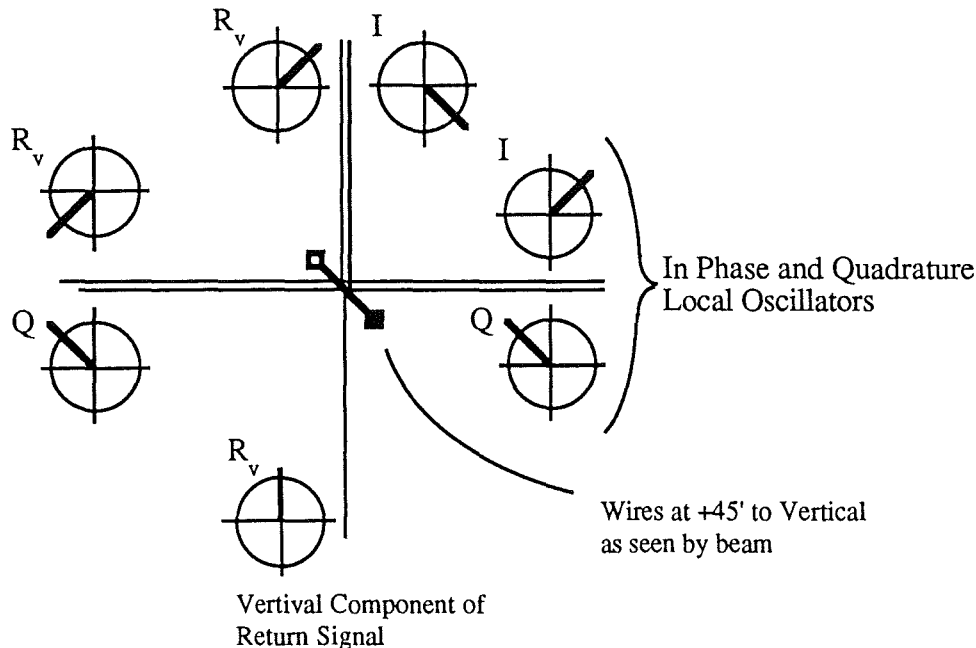


Figure 2.11 Diplexing of Return Signal with In phase and in Quadrature
Local Oscillators

The four output beams : each of the polarization states with each local oscillator, can be analyzed with a polarizer and a balanced pair of mixers, or with a polarizer and a single mixer. In the latter case the polarizer is required because mixers are usually sensitive to one polarization state only. This means that half of the power at each port is thrown away.

The two components of the local oscillator can be taken from a single source by splitting it into two, delaying one part by 90° and recombining. Although this operation is most often carried out by a Martin-Puplett interferometer, it is not possible to split the resulting beam into two identical states using a single polarizer. A circuit for generating two in phase and two quadrature local oscillators is shown in figure 2.12 incorporated into the full receiver circuit. The circuit symbols, as explained in the key, are those of Lesurf¹. The circuit shown in figure 2.12 is the full receiver circuit for which the quasi-optical components were designed and built. This particular optical design also incorporated flexibility for operation at 94GHz or 140GHz. Design decisions taken later in the project meant that a layout for an FMCW radar, that does not require a

¹ J.C.G. Lesurf, "Millimetre wave optics, devices and systems", Adam Hilger/IOPP 1990.

quadrature local oscillator, was actually implemented. This circuit, although simpler, yields more information on the target.

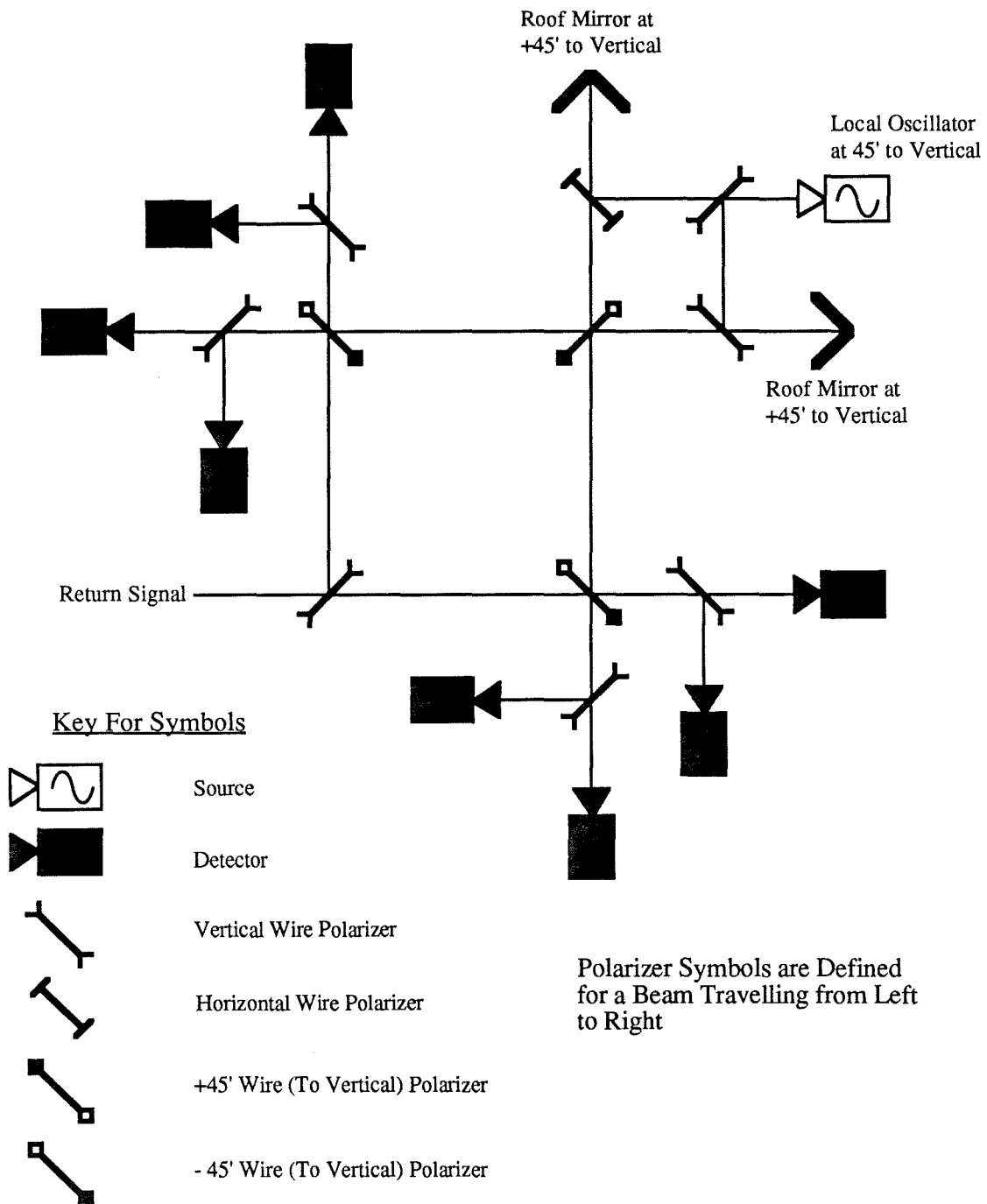


Figure 2.12 Full Receiver Circuit Showing In phase and Quadrature Local Oscillator Circuit

Gaussian Beam Theory and Quasi-Optical Component Design.

3 Abstract

This chapter discusses aspects of Gaussian Beam Theory that are required to design the basic optical components. Coupling, truncation and frequency response are covered and applied to the design of half-cubes, polarizers and lenses. The thermal limits of polarizers and lenses are modelled numerically. A treatment of the effect of alignment tolerances on system performance is also presented.

3.1 Beam Waveguides

The primary aim of quasi-optical hardware is to ensure that sufficient power is transmitted through the system to be detected. Having achieved this the next objective is to reduce the level of 'interference' imposed by the system on the signal.

The use of a sequence of focussing elements, known as a beam waveguide, suits these purposes well. Consecutive focussing elements within the beam waveguide are separated by the sum of their focal lengths. A beam launched by the first element is therefore periodically refocussed and leaves the final element relatively undistorted and with a known beam profile. The losses suffered in the beam waveguide are due to absorption in lens material (or Ohmic losses in mirrors), reflection at a lens and poor coupling to the natural mode of the guide. Large beam sizes and focussing elements will render truncation losses negligible. Truncation is discussed in more detail later.

The following sections discuss coupling, truncation and frequency response as applied to a beam waveguide. They provide the basis on which many of the quasi-optical components were designed. They are then used to gauge the ability of real systems to represent ideal systems.

3.1.1 Coupling of Gaussian Beams.

The efficiency of the beam waveguide is affected by how well the input beam is coupled into the natural mode of the waveguide. Each lens, for example, will only launch the correct beam if it receives the correct beam. The coupling efficiency is a measure of how well the actual beam and the ideal beam match. It is a correlation of the two field patterns taken over a transverse plane and is given by

$$C = \frac{\int_{-\infty}^{\infty} \int_{-\infty}^{\infty} \Phi[x,y] \Psi^*[x,y] \cdot dy \, dx}{\sqrt{\int_{-\infty}^{\infty} \int_{-\infty}^{\infty} |\Phi|^2 \cdot dy \, dx \int_{-\infty}^{\infty} \int_{-\infty}^{\infty} |\Psi|^2 \cdot dy \, dx}} \quad 3.1$$

Φ and Ψ are field patterns of the form given in equation 1.1, and the denominator is for normalization. The power coupling is therefore given by

$$\eta = C \cdot C^* \quad 3.2$$

Beam mismatch is caused either by producing the right beam but in the wrong place, or by producing the wrong beam. A misplaced beam can be described in terms of longitudinal and transverse offsets and by an offset angle.

3.1.1.1 Longitudinal Offsets

Consider initially two fundamental mode beams with a longitudinal offset as shown in figure 3.1.

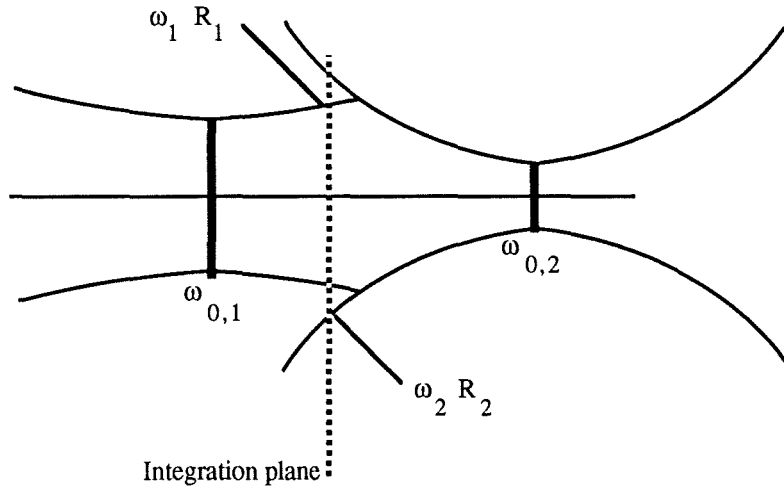


Figure 3.1 Longitudinal Offsets of Two Dissimilar Beams

The transverse field components of two beams are given by

$$\phi(x,y) = \sqrt{\frac{2}{\pi \omega_{\phi}^2}} \exp\left\{\frac{-x^2 - jx^2k}{\omega_{\phi}^2 2R_{\phi}}\right\} \exp\left\{\frac{-y^2 - jy^2k}{\omega_{\phi}^2 2R_{\phi}}\right\} \quad 3.3$$

$$\psi(x,y) = \sqrt{\frac{2}{\pi \omega_{\psi}^2}} \exp\left\{\frac{-x^2 - jx^2k}{\omega_{\psi}^2 2R_{\psi}}\right\} \exp\left\{\frac{-y^2 - jy^2k}{\omega_{\psi}^2 2R_{\psi}}\right\} \quad 3.4$$

The values of ω and R used in equations 3.3 and 3.4 are those taken at the plane of integration. Physically the coupling must be independent of the integration plane which is chosen to simplify the calculations. Kogelnik¹ has solved these integrals to produce

$$\eta = \frac{4}{\left[\frac{\omega_\phi}{\omega_\psi} + \frac{\omega_\psi}{\omega_\phi} \right]^2 + \left\{ \frac{\omega_\psi \omega_\phi k}{2} \right\}^2 \left\{ \frac{1}{R_\phi} - \frac{1}{R_\psi} \right\}^2} \quad 3.5$$

As equation 3.5 shows, the coupling is only unity if $\omega_\phi = \omega_\psi$ and $R_\phi = R_\psi$. This is the case of identical beams. By choosing the integration plane to be at the beam waist plane for one of the beams, equation 3.5 can be simplified. Writing $\omega_\phi = \omega_{o\phi}$ and $R_\phi = \infty$ and substituting expressions for ω_ψ and R_ψ as given by equations 1.2 and 1.3, the coupling can be written in terms of the separation of the waists, z_o , as

$$\eta = \frac{4}{\left[\frac{\omega_{o\phi}}{\omega_{o\psi}} + \frac{\omega_{o\psi}}{\omega_{o\phi}} \right]^2 + \left\{ \frac{2z_o}{k\omega_{o\psi}\omega_{o\phi}} \right\}^2} \quad 3.6$$

3.1.1.2 Lateral Offsets and Tilted Beams.

The reflection of beams from mirrors and polarizers that are not correctly aligned produces laterally offset and tilted beams. Lateral offsets in a beam can be represented by an offset term x_o in equation 3.3. This gives

$$\phi(x,y) = \phi_o \exp \left\{ \frac{-(x-x_o)^2}{\omega_\phi^2} - \frac{jx^2k}{2R_\phi} \right\} \exp \left\{ \frac{-y^2}{\omega_\phi^2} - \frac{jy^2k}{2R_\phi} \right\} \quad 3.7$$

A few steps of algebra are required to arrive at the coupling efficiency which is given by

$$\eta = \kappa \exp \left\{ -\frac{x_o^2 \kappa}{2} \left[\frac{1}{\omega_\phi^2} + \frac{1}{\omega_\psi^2} + \frac{k^2}{4} \left(\frac{\omega_\phi^2}{R_\phi^2} + \frac{\omega_\psi^2}{R_\psi^2} \right) \right] \right\} \quad 3.8$$

where κ is the coupling efficiency with no offset, given in equation 3.6. This result is also produced by Kogelnik, although he expands the exponential term and appears to lose a factor of κ^2 .

1 H. Kogelnik "Coupling and Conversion Coefficients for Optical modes" Symposium on Quasi-Optics, Polytechnic Institute of Brooklyn June 1964

Tilted beams add two further complications to the problem of coupling. The first is that a large tilt angle makes the algebra incredibly complex as small angle approximations are not valid. The second point is how to decide whether or not two tilted beams are transversely offset as well. This second point is illustrated in figure 3.2, in which the tilt angle is exaggerated for clarity.

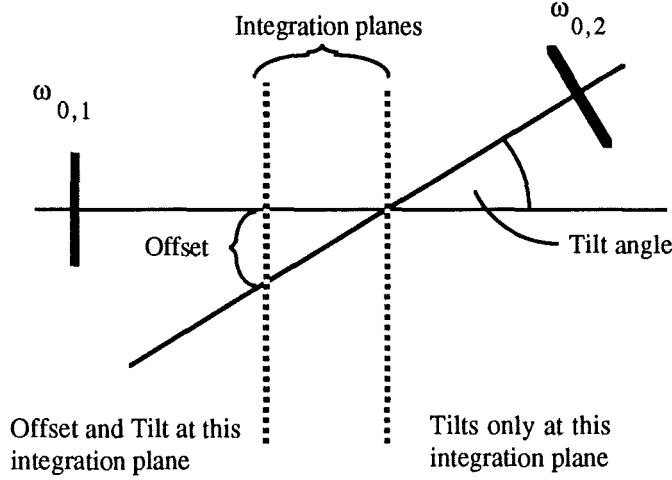


Figure 3.2 The combination of offsets and tilts produced
by choice of integration plane

Choosing the integration plane to be at the point where the axes cross, as Kogelnik does, removes any implicit offsets from the calculation. This seems to imply that the coupling efficiency depends on the choice of integration plane. This cannot be the case, as the coupling must be independent of how the beams are represented and this is shown to be true in the next section.

In Kogelnik's example, the tilting offset is portrayed as an extra phase term such that

$$\phi = \phi_0 \exp \left\{ -(x^2 + y^2) \left[\frac{1}{\omega_\phi^2} - \frac{jk}{2R_\phi} \right] \right\} \exp(-jk\theta x) \quad 3.9$$

This term represents the extra phase length involved in reaching a tilted integration plane. It implicitly assumes that the tilt axis is in the integration plane and that $\sin\theta = \tan\theta = \theta$. The coupling efficiency due to tilted beams is therefore given, after a few more steps of algebra, by

$$\eta = \kappa \exp \left\{ \frac{-\kappa k^2 \theta^2 (\omega_\phi^2 + \omega_\psi^2)}{8} \right\} \quad 3.10$$

where θ is the tilt angle in radians.

3.1.1.3 General Case of Misaligned Beams.

The situation for tilted beams and a general integration plane is represented by figure 3.3. A pair of axes that are skew can also be treated. The shortest distance between two skew lines is always along a line that is perpendicular to both. With a suitable choice of axes (the y axis should lie along the common normal), skew beams can be represented by an offset in the y direction, and a tilt and offset in the x-z plane. The effect of any offset along the y axis is described by an extra factor of the form of equation 3.8.

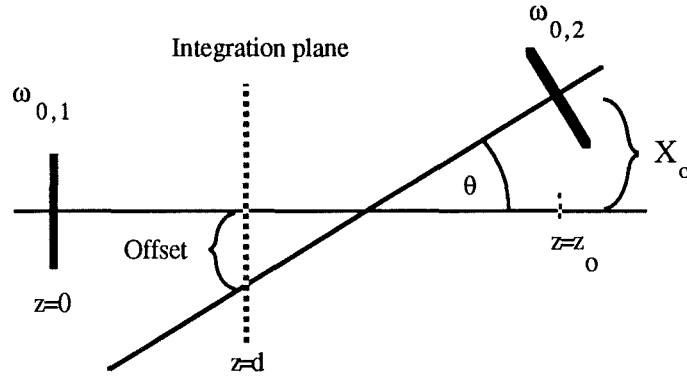


Figure 3.3 A General Representation of Offset and Tilted Beams.

At the integration plane the 'rogue' beam is both offset and tilted with respect to the axis of the other beam and is represented by

$$\psi = \psi_0 \exp \left\{ -y^2 \mathbf{z}_\psi^* \right\} \exp \left\{ -(x-x_0)^2 \mathbf{z}_\psi^* \right\} \exp \left\{ -jk\theta(x-x_0) \right\} \quad 3.11$$

where

$$\mathbf{z}_\psi^* = \frac{1}{\omega_\psi^2} + \frac{jk}{2R_\psi} \quad \text{and} \quad x_0 = X_0 + \theta(d-z_0) \quad 3.12$$

Solving the coupling integrals requires substantial algebraic juggling which is shown in appendix 1. The final coupling efficiency is given by

$$\eta = \kappa \exp \left\{ \frac{-\kappa k^2 \theta^2 (\omega_\phi^2 + \omega_\psi^2)}{8} \right\} \exp \left\{ \frac{k^2 \theta x_0 \kappa}{4} \left(\frac{\omega_\phi^2}{R_\phi} + \frac{\omega_\psi^2}{R_\psi} \right) \right\} \\ \exp \left\{ \frac{-x_0^2 \kappa}{2} \left[\frac{1}{\omega_\phi^2} + \frac{1}{\omega_\psi^2} + \frac{k^2}{4} \left(\frac{\omega_\phi^2}{R_\phi^2} + \frac{\omega_\psi^2}{R_\psi^2} \right) \right] \right\} \quad 3.13$$

Harvey¹ tackles the issue of offset and tilted beams from a separate viewpoint. His co-ordinate system is chosen to give equal angular and linear offsets to each beam. Reassuringly he also obtains the expression given in equation 3.13.

It is now necessary to substitute expressions for ω , R and x_0 to obtain an expression independent of z . This process is also lengthy and is hence also given in appendix 1. The result is

$$\eta = \kappa \exp \left\{ \frac{-\kappa}{2} \left[\frac{X_0^2}{\omega_{o\psi}^2} + \frac{(X_0 - \theta z_0)^2}{\omega_{o\phi}^2} + \frac{\theta^2 k^2}{4} (\omega_{o\phi}^2 + \omega_{o\psi}^2) \right] \right\} \quad 3.14$$

This rather neat result gives the coupling of two beams in terms of the beam waists and their relative positions. In the form above the 'rogue' beam is offset by distances z_0 and X_0 along the z and x axes, and the z axes are skewed by θ radians. As figure 3.3 shows, the lengths X_0 and $(X_0 - \theta z_0)$ are the offsets of each beam waist with respect to the other beam's propagation axis. This demonstrates the symmetry of equation 3.14 and enables the coupling to be expressed in terms of these offsets if they are more convenient to determine.

3.1.2 Beam Truncation.

The coupling integrals required in the previous section are all taken over an infinite plane. Clearly it is not possible to have beams of infinite extent and so some truncation is inevitable. The degree of truncation that is acceptable is determined by how well the truncated beam represents the ideal beam. Consider the truncated beam in figure 3.4. The E field at the aperture has a Gaussian beam profile over the aperture but is zero elsewhere. This aperture distribution can be represented by a set of Gaussian modes propagating away from the aperture. There are an infinite number of mode sets that can be used equally well to describe the aperture field. Each mode set is characterized by its beam waist parameter ω_0 . For many systems the mode set chosen is that which has maximum power in the fundamental mode. This is the criterion chosen by Wylde², from whom the following analysis is taken. The aperture field is represented by

$$\begin{aligned} E_{ap} &= \phi(r, \omega_{oi}) & r &\leq r_{aperture} \\ &= 0 & r &> r_{aperture} \end{aligned} \quad 3.15$$

where $\phi(r, \omega_{oi})$ has the form of equation 3.3.

¹ A.R. Harvey PhD Thesis, University of St. Andrews 1990.

² R.J. Wylde "Millimetre-wave Gaussian beam-mode optics and corrugated feed horns"
Proc. IEE, Vol 131, Pt H No. 4 Aug. 1984 p258

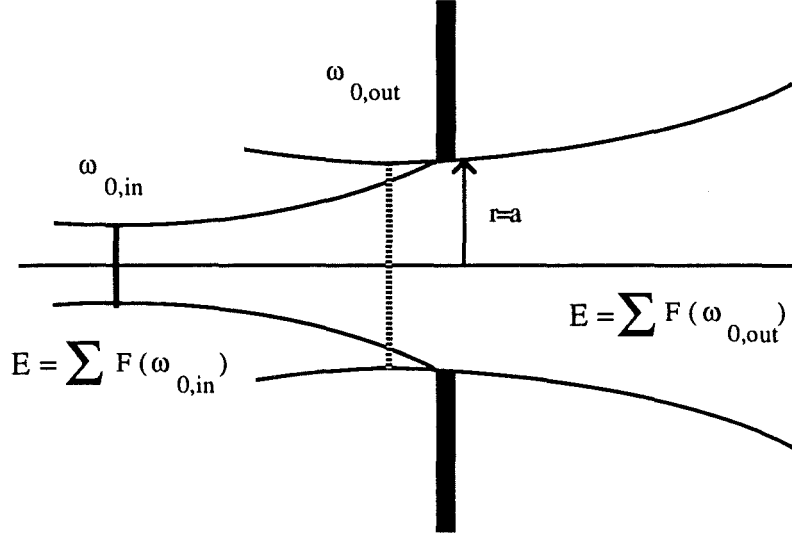


Figure 3.4 The change in output beam parameters due to aperture truncation

The output is represented by a set of Gaussian modes with a unique beam waist parameter ω_{out} such that

$$E_{out} = \sum_{i=0}^{\infty} a_i G_i(\omega_{out}) \quad 3.16$$

The choice of ω_{out} is determined by maximum fundamental mode content. Hence a_0 is maximized with respect to ω_{out} , where a_0 is given by

$$a_0 = \int_{Aperture} E_{ap} G_0^*(\omega_{out}) dA \quad 3.17$$

This process has been carried out by Wylde for different sizes of aperture. He shows that for an input beam with a beam size ω_i at the aperture plane, truncation is negligible for an aperture radius $\geq \frac{3}{2} \omega_i$. For $r_{ap} > \frac{3}{2} \omega_i$, the output beam has the same optimum beam waist size as the input beam, and contains over 98% of the input power in the fundamental mode. This result has been used to define the truncation criterion for the work described in this thesis. The minimum aperture radius, r_{min} , and the maximum beam size, ω_{max} , are therefore related by

$$r_{min} = \frac{3}{2} \omega_{max} \quad 3.18$$

3.1.3 System Bandwidth and Frequency Response.

Real quasi optical systems will need to operate over a range of frequencies. Waveguide systems are usually limited in bandwidth to an octave by the need to suppress higher order modes. Quasi optical systems don't suffer this limitation and hence have wider bandwidths. The impedance bridge of Harvey¹, for example, has a bandwidth of 80GHz to 500GHz - the upper limit being imposed by the use of wire grid polarizers. The continuous operating bandwidth, however, is limited by the waveguide mounted components such as detectors and oscillators.

In a radar the required operating bandwidth is determined by the radar type. An FMCW radar, as described here, may only be swept over $\pm 0.5\text{GHz}$. Pulsed radar and spread spectrum techniques will require an increase in this bandwidth and mode-locked pulse generation² may require a bandwidth of $\sim \pm 10\text{GHz}$. Dual frequency radars put the greatest strain on the continuous system bandwidth.

Changes in frequency affect the performance of a quasi optical system in several ways.

- Increases in wavelength increase beam sizes, which can lead to greater truncation loss. Generally, however, the aperture size is chosen to be greater than the minimum limit for the longest wavelength and truncation is seldom a problem.
- Detector diodes are often mounted in resonant cavities to match their impedances to that of the waveguide. Operation away from the resonant frequency will cause an impedance mismatch and hence a reduction in sensitivity.
- Lenses used in non-confocal arrangements produce beam sizes and waist positions that are wavelength dependent. Confocal arrangements of lenses place restrictions on lens' positions and focal lengths. These restrictions are often unacceptable. In addition, the increase in the number of lenses produces a greater loss and increases the likelihood of generating standing waves. Whilst the loss may be determined and tolerated, the effect of VSWR is difficult to determine and strongly frequency dependent.

Single elements in a system can have their frequency dependence measured to determine the overall response of circuits. It is important during the design of a system to distinguish between the maximum optical system bandwidth and the continuous operating bandwidth. This will avoid placing unnecessary bandwidth requirements on some components - especially those that are waveguide mounted. In the impedance

¹ A.R. Harvey PhD Thesis. University of St. Andrews 1990.

² G.M. Smith Private Communication.

bridge, for example, it is unlikely that measurements will be made at 80GHz and 500GHz simultaneously and hence a small operating bandwidth is acceptable.

3.2 Design of Optical Hardware.

The implementation of the radar is to be achieved using a half-cube system. This technique is used to a great extent at St. Andrews and elsewhere. It provides the maximum flexibility with a minimal number of building blocks. As it turned out, this flexibility proved invaluable!

3.2.1 Half-Cube and Polarizer Design.

The half-cube dimensions were determined by the required size of aperture and a preference towards miniaturization. For the circuit shown in figure 2.12, the longest distance travelled by a beam is 8 cubes. This is the beam from the local oscillator to the detectors. The other beams travel a distance of 4 cubes from antenna to detector. A system capable of supporting a single throw of 8 cubes would be excessively large. The maximum throw of the system was therefore defined to be 4 cubes which requires the use of a thin lens for the longer beams. Substituting the truncation criterion of equation 3.18 into equation 1.10 yields the aperture diameter D as

$$4D = \frac{\pi}{\lambda} \left[\frac{D}{3} \right]^2 \quad 3.19$$

At 94GHz this sets D to 36.5mm, but it does not allow for material to support the lenses and polarizer frames. Initially the polarizer frames were to be copies of Harvey's¹ : rigid frames to define the plane of the wires, located in a recess of the half-cube. This proved too great a restriction on the block design as the polarizers were all frame and not much aperture. The eventual design of half-cube, shown in figure 3.5, uses a raised lip on the diagonal face to define the plane of the wires and a pair of dowel holes to align the angle of the wires. This design allows the polarizer frames to be much thinner and less of a restriction to the aperture. The polarizer frames shown in figure 3.6 use the same pair of dowels to align the frame to the block and to the winding plate. This simplifies much of the construction of the polarizer frames and of the half-cubes. The profiling of the diagonal face of the half-cube can be done to more relaxed tolerances, except for the positioning of the dowel holes, and the polarizer frame becomes less of a precision part. The dimensions of the polarizer determine the relative sizes of the aperture and the cube length. The final sizes were reached by trial and

¹ A.R. Harvey PhD Thesis. University of St. Andrews 1990.

error, and then rounded to a convenient number. A cube length of 70mm and an aperture diameter of 54mm defines the maximum separation of lenses as

$$Z_{\text{sep}} = 319\text{mm} \quad = 4.55 \text{ cubes} \quad @ 94\text{GHz} \quad 3.20$$

$$Z_{\text{sep}} = 475\text{mm} \quad = 6.79 \text{ cubes} \quad @ 140\text{GHz} \quad 3.21$$

Figure 3.5 Half-Cube DRG, ML009

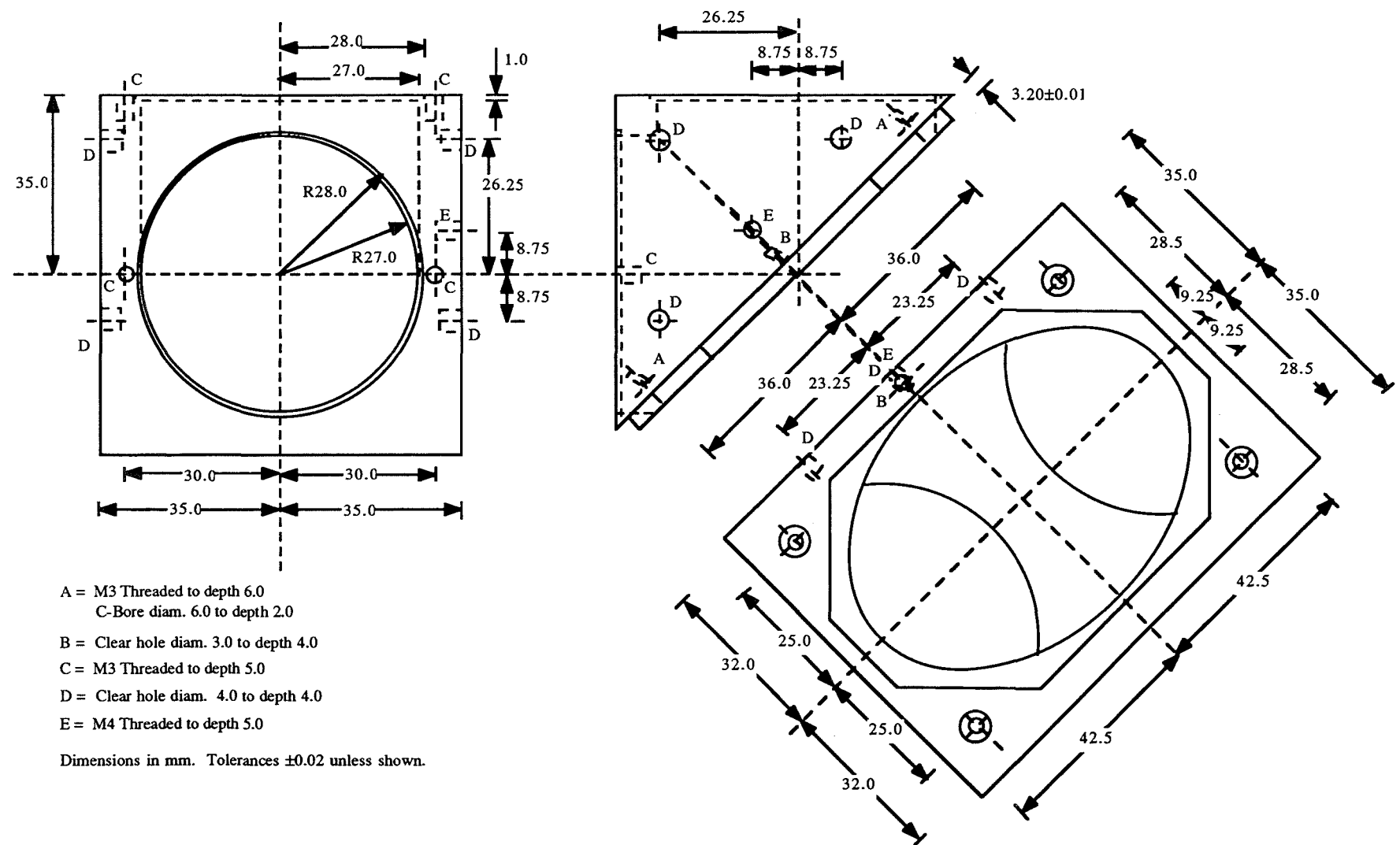
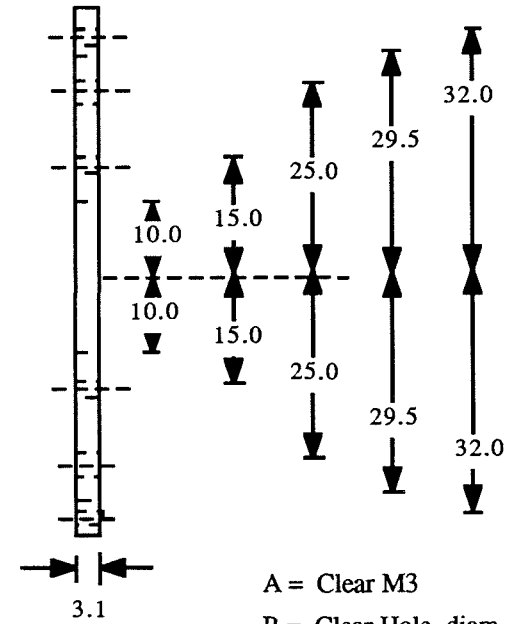
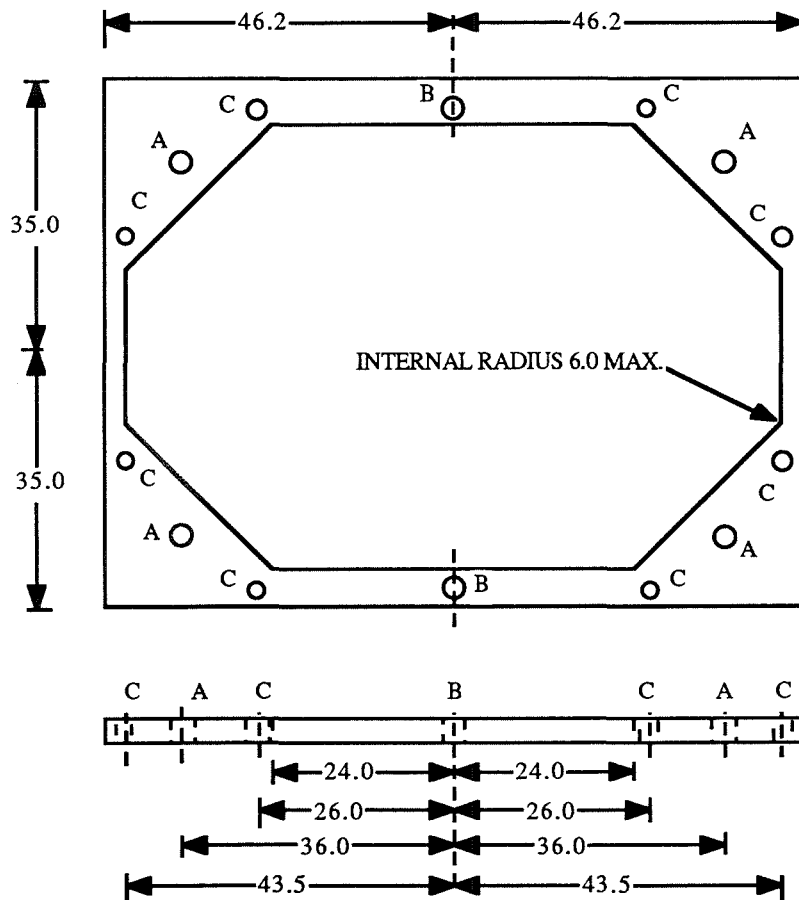


Figure 3.6 Polarizer DRG ML010



A = Clear M3
B = Clear Hole diam. 3.0
C = M2.5 See following note.

Dimensions in mm Tolerances ± 0.02

Note on hole C

Two plates to be made for each polarizer, and bolted together via hole C.

First plate has hole C THREADED M2.5

Second plate has hole C CLEAR M2.5 and CSK.

3.2.2 Lenses.

The design of lenses uses an iterative technique¹ to produce planar convex lenses. This produces a lens profile that equalizes the phase lengths, from input waist to output waist, of all optical paths through the lens. The iteration process has been implemented in Lightspeed PascalTM running on an AppleMacTM². Two modified versions, Beam Lens and Horn Lens listed in appendix 2, use the same core iterating routine but vary different parameters at each iteration.

The iteration routine calculates a specific lens profile, based on the original input and output beams, and then modifies the input and/or the output beam to coincide at the newly formed lens surface. The fixed and variable parameters for these two programs and the original, 'GB Lens', are shown in the following table.

Program Name	Fixed Parameters	Variable Parameters
Beam Lens	$z_{out}, \omega_{o,out}, z_{in}$	$\omega_{o,in}$
Horn Lens	$z_{out}, \omega_{out}, \omega_{o,in}$	z_{in}
GB Lens	$\omega_{o,in}, \omega_{o,out}$	z_{in}, z_{out}

Figure 3.7 Summary of Parameters for Lens Design Programs.

The program 'Horn Lens' designs lenses for coupling quasi-parallel beams to and from a feed horn. The program 'Beam Lens' designs lenses for coupling pairs of quasi-parallel beams. This latter program is used to produce thin lenses.

3.2.3 Thermal Considerations.

In most quasi optical instrumentation the signal power is unlikely to reach a level where significant destructive heating occurs. In radar this is more likely to become a problem. The main areas where heating is a concern are at the transmitter and in any antenna diplexer. The weak optical elements are identified as the lenses and the polarizers. It is assumed that antennae capable of handling high powers already exist, for a given application, in the form of the waveguide analogue. The following sections describe mathematical modelling of thermal effects in lenses and polarizers. The power levels quoted in the following sections are for the specific sizes of lens and polarizer in this radar. The process can be extended to cover any given dimension of lens or polarizer.

¹ A.R. Harvey PhD Thesis. University of St. Andrews 1990.

² G.M. Smith Private Communication.

3.2.3.1 Polarizers - First Model.

The main failure mechanism is melting of the wires through absorption of incident power. The worst case for this is during reflection from vertical wires as these wires are shortest and hence of lowest thermal mass. The power incident on the central wire, which is most likely to fail, is given by

$$P_{\text{inc}} = P_0 \int_{-\frac{1}{2}\text{pitch}}^{+\frac{1}{2}\text{pitch}} \exp\left[-\frac{2x^2}{\omega^2}\right] dx \int_{-\infty}^{+\infty} \exp\left[-\frac{2y^2}{\omega^2}\right] dy \quad 3.22$$

The integral with respect to x can be considered to be constant over the pitch of the wires if $\omega \gg \text{pitch}$. The polarizers constructed have a wire pitch of $50\mu\text{m}$ for use with beam sizes of several millimetres and so this assumption is valid. The **total** beam power is found by integrating equation 3.22 for $x=-\infty$ to $x=+\infty$, with the help of a standard integral¹, and is given by

$$P_{\text{beam}} = P_0 \frac{\pi\omega^2}{2} \quad 3.23$$

and so the fraction of power incident on the central wire is given by

$$\eta = \frac{P_{\text{inc}}}{P_{\text{beam}}} = \frac{\text{pitch}}{\omega} \sqrt{\frac{2}{\pi}} \quad 3.24$$

The power density distribution along the wire will have a Gaussian shape. The normalized power density distribution is hence given by

$$P_{\text{density}} = \frac{1}{\omega} \sqrt{\frac{2}{\pi}} \exp\left\{-\frac{2x^2}{\omega^2}\right\} \quad 3.25$$

The amount of power, δP , incident on a small section of wire, δx , can now be written as

$$\delta P(x) = \delta x \cdot P_{\text{density}} = \frac{\delta x}{\omega} \sqrt{\frac{2}{\pi}} \exp\left\{-\frac{2x^2}{\omega^2}\right\} \quad 3.26$$

Combining equations 3.24 and 3.26 enables the power incident on a small section of wire to be written in terms of the total beam power. By introducing an absorption fraction, α , the input power of a small section of wire becomes

¹ M.R. Spiegel "Mathematical Handbook of Formulas and Tables" McGraw-Hill.

$$\delta P(x) = P_{\text{beam}} \cdot \frac{2\alpha \delta x \text{ pitch}}{\pi \omega^2} \exp\left\{\frac{-2x^2}{\omega^2}\right\} \quad 3.27$$

The value of α is given by the reflectivity of a metal to incident radiation of frequency f . Assuming all that is not reflected is absorbed, α is given by¹

$$\alpha = 4 \sqrt{\frac{\epsilon_0 \pi f}{\sigma}} = 4 \sqrt{\epsilon_0 \pi \rho f} \quad 3.28$$

The resistivity, ρ , is a function of temperature. The resistivity of tungsten can be written as a function of T obtained from a quadratic fit to recorded data² such that

$$\rho = 1.88 \times 10^{-6} T^2 + 2.60 \times 10^{-2} T - 2.82 \quad 3.29$$

where T is in $^{\circ}\text{K}$ and ρ is in $\mu\Omega\cdot\text{cm}$.

Equations 3.27 and 3.28 account for the power input to a section of wire. The main thermal loss mechanisms are conduction, convection and radiation. These are all dependent on the wire temperature and are given by

$$\left[\frac{dQ}{dt}\right]_{\text{radiate}} = \epsilon \sigma A_{\text{surf}} \{T^4 - T_{\text{ambient}}^4\} \quad 3.30$$

$$\left[\frac{dQ}{dt}\right]_{\text{conduct}} = -\lambda A_{\text{section}} \frac{dT}{dx} \quad 3.31$$

$$\left[\frac{dQ}{dt}\right]_{\text{convect}} = h A_{\text{surf}} (T - T_{\text{ambient}}) \quad 3.32$$

where λ is the thermal conductivity [$\text{Wm}^{-2}\text{K}^{-1}$], σ is the Stefan-Boltzmann constant and h is a shape-dependent convection constant. The parameter h is that of a vertical cylinder and is given by³

$$h = 4.186 \sqrt[4]{\frac{(T - T_{\text{ambient}})}{\text{diameter}}} [\text{Wm}^{-2}\text{K}^{-1}] \quad 3.33$$

The emissivity, ϵ , is also a function of temperature. For tungsten this function is

$$\epsilon = -8.31 \times 10^{-12} T^3 + 2.58 \times 10^{-8} T^2 + 1.14 \times 10^{-4} T - 1.09 \times 10^{-2} \quad 3.34$$

where T is in $^{\circ}\text{K}$.

¹ H.J. Pain "The Physics of Vibrations and Waves" 3rd ed. John Wiley & Sons. p211

² Handbook of Chemistry and Physics, 57th ed. CRC

³ Sears, Zemansky and Young University Physics 6th ed. Addison Wesley. p320

small time interval δt . During a period δt , the total heat flow into a section of wire is given by

$$\Delta Q(x) = \delta t \left\{ \delta P(x) - \left[\frac{dQ}{dt} \right]_{\text{radiate}} - \left[\frac{dQ}{dt} \right]_{\text{convect}} - \left[\frac{dQ}{dt} \right]_{\text{conduct}} \right\} \quad 3.35$$

and the temperature therefore becomes

$$T_{t=i}(x) = T_{t=i-1}(x) + \frac{\Delta Q(x)}{C_{\text{spec}} m(x)} \quad 3.36$$

For a wire, $m(x)$ is a constant but will be a varying function of x for a lens. The heating profile of the wire is calculated for each interval δt , as shown in the flow diagram of figure 3.8. It should be noted that it is necessary to calculate the full heat flow profile before updating the temperature profile. This is required because the conductive heat losses are a function of the temperature of the surrounding wire sections. Updating the temperature as the program progresses along the wire causes the conductive losses to be determined over different time intervals. This can lead to non-conservation of energy.

The program was implemented in Lightspeed Pascal™ on an AppleMac™ and the listing is given in appendix 3. The first generation of the model had no temperature dependent absorption and omitted the emissivity. The results of this model show maximum power to be of the order of a few MW. The results for $P_{\text{beam}} = 4\text{MW}$ are typical of those at high powers and have the following interesting properties.

- The temperature increases rapidly with time, figure 3.9, due to the low thermal mass of the wire.
- The heat losses, figure 3.10, are dominated by the T^4 term in the radiative loss.

At lower powers, for example 10kW, the temperature, figure 3.12, tends to a lower plateau. The heat losses, figure 3.13, show an interesting maximum which is an artefact of the modelling process. The temperature recorded is the central temperature of the wire as this was identified as the critical position. The heat loss recorded, however, is the total heat loss from the whole wire. At lower input powers it takes longer to reach a maximum temperature. This extra time is sufficient to allow significant conduction along the wire which flattens the temperature profile, figure 3.14. This reduces the average temperature of the central sections which produces a sharp drop in the total heat loss since the dominant radiative term is strongly temperature dependent. This observation is supported by the narrower width of the temperature profile for 10kW, figure 3.14, than for 4MW, figure 3.11.

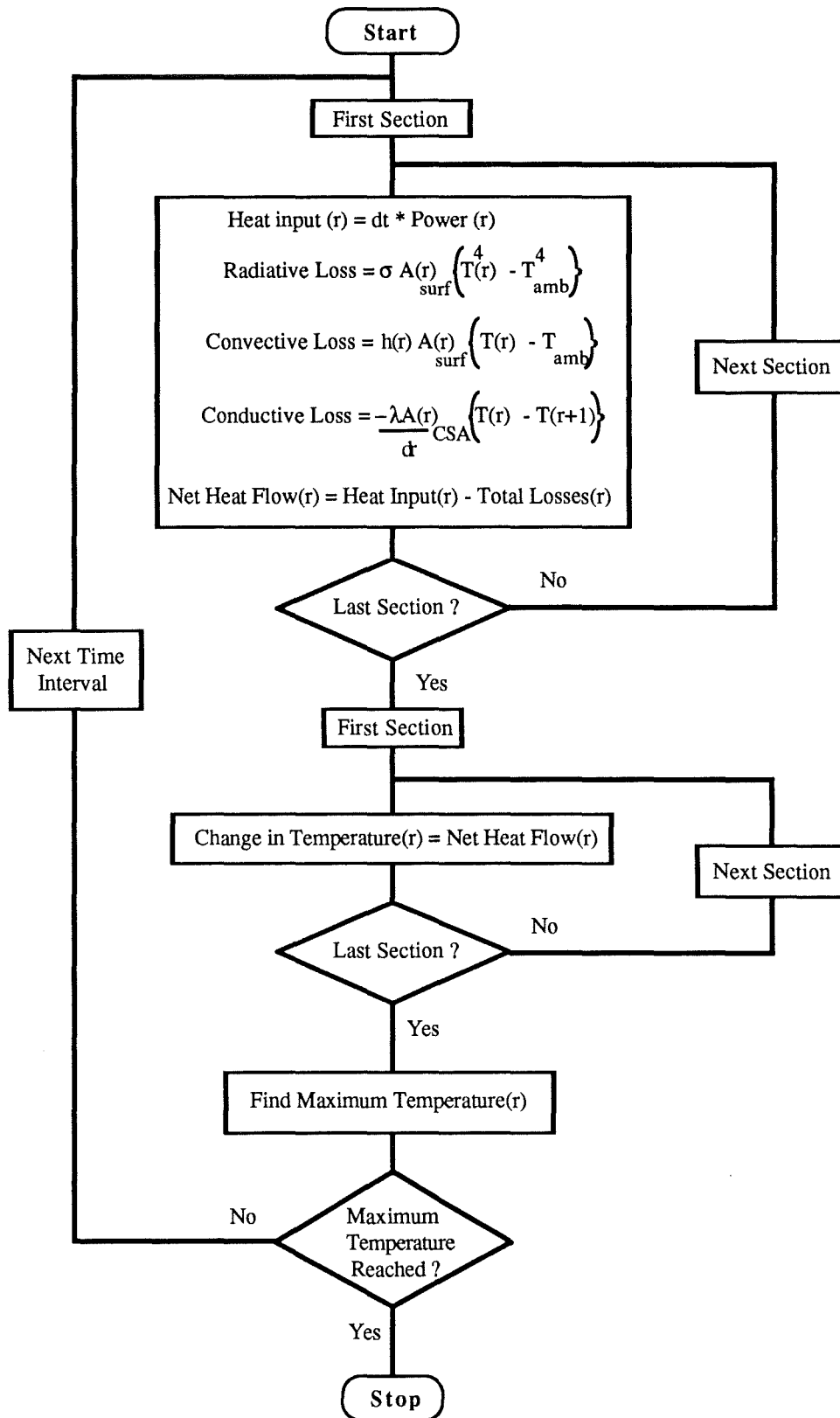


Figure 3.8 Flow Diagram of Wire Heating Routine.

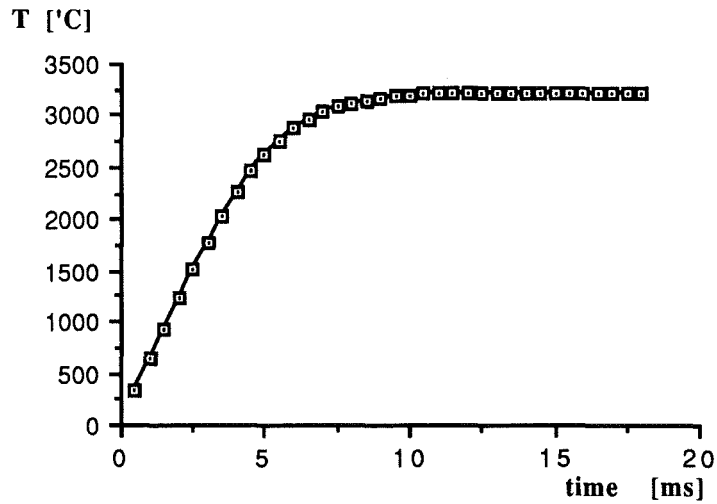


Figure 3.9 Rate of heating of Central Wire. P=4MW

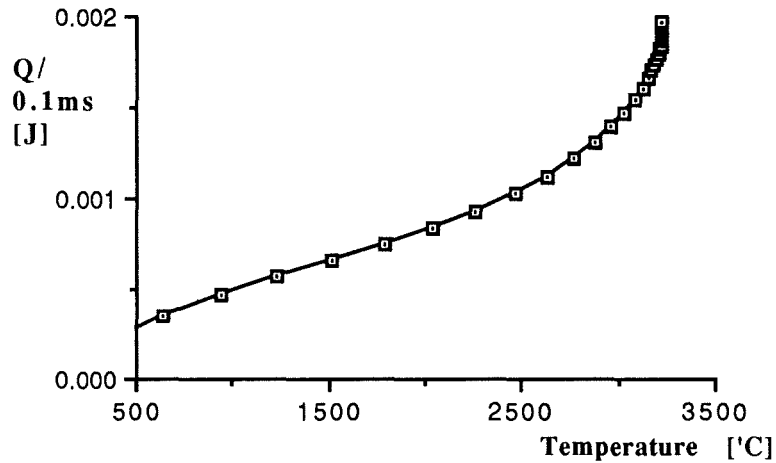


Figure 3.10 Variation of Heat Loss from Central Wire with Temperature. P=4MW

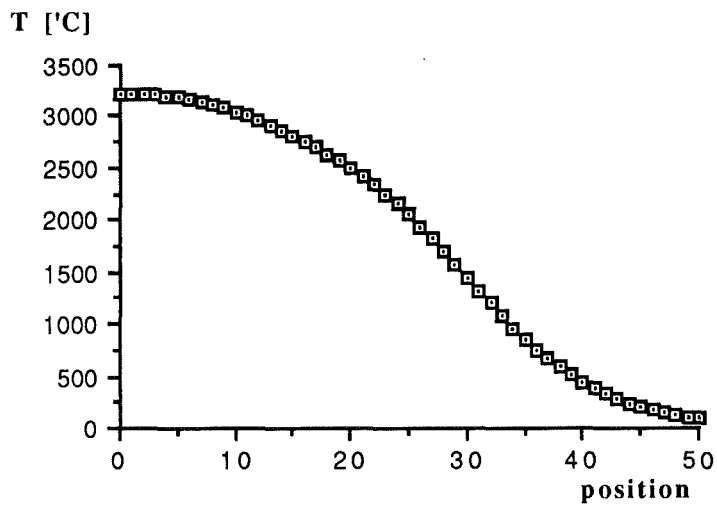


Figure 3.11 Temperature Profile. P=4MW

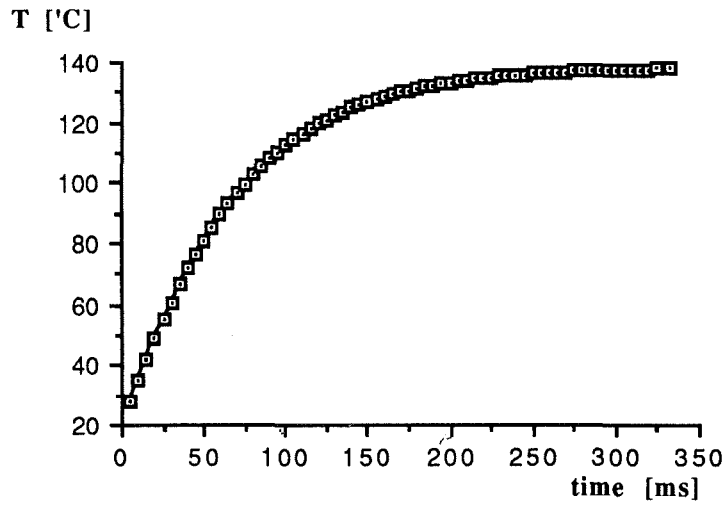


Figure 3.12 Rate of heating of Central Wire. P=10kW

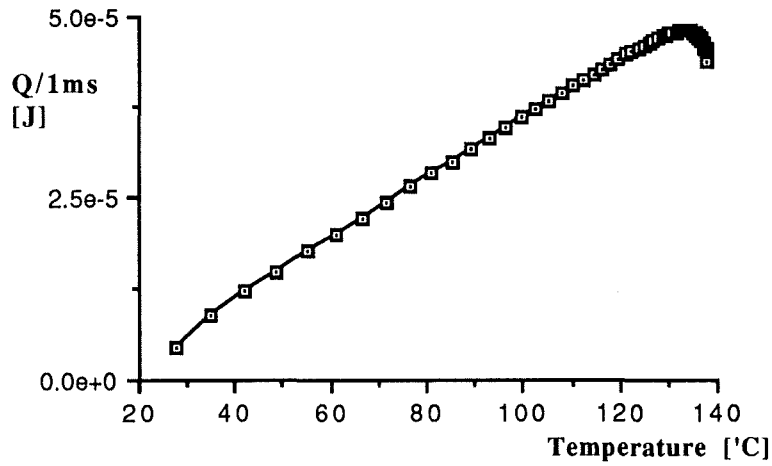


Figure 3.13 Variation of Heat Loss from Central Wire with Temperature. P=10kW

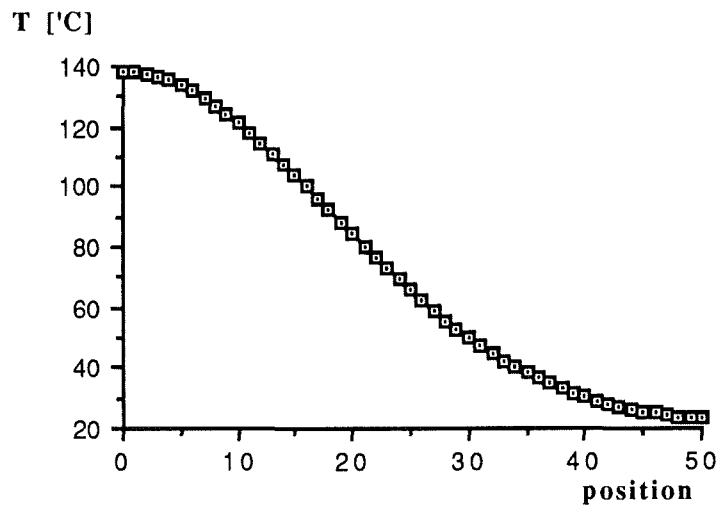


Figure 3.14 Temperature Profile. P=10kW

When used with high powers the program produces sensible looking results : the temperature stabilizes in a well defined time and the temperature profile has a sensible shape. The time intervals are too short to allow a significant amount of heat to reach the block. The problem of how to treat the wire-block interface is therefore of little concern.

3.2.3.2 Polarizers - Second Model.

A second model that included the temperature variations in ρ and ϵ was also implemented in Lightspeed Pascal™. The reduced radiative losses cause a reduction in the maximum input power. The maximum power is now ~200kW as shown in figure 3.15. The variation of maximum temperature with input power is shown in figure 3.16. The criterion for stopping the program is when the change in temperature in successive intervals is less than 0.01°K. The time taken to reach the maximum temperature is also shown. A further modification to the wire heating program, namely the wire-block interaction, was made. The details of this modification are described by equations 3.41 and 3.42 from the next section on lens heating. The changes in performance of the wire heating program were below the 0.01% level and were therefore neglected.

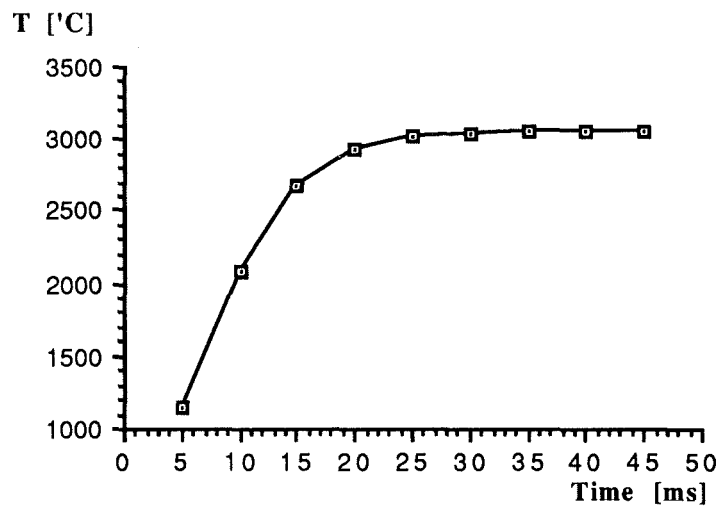


Figure 3.15 Rate of heating of Central Wire. P=200kW

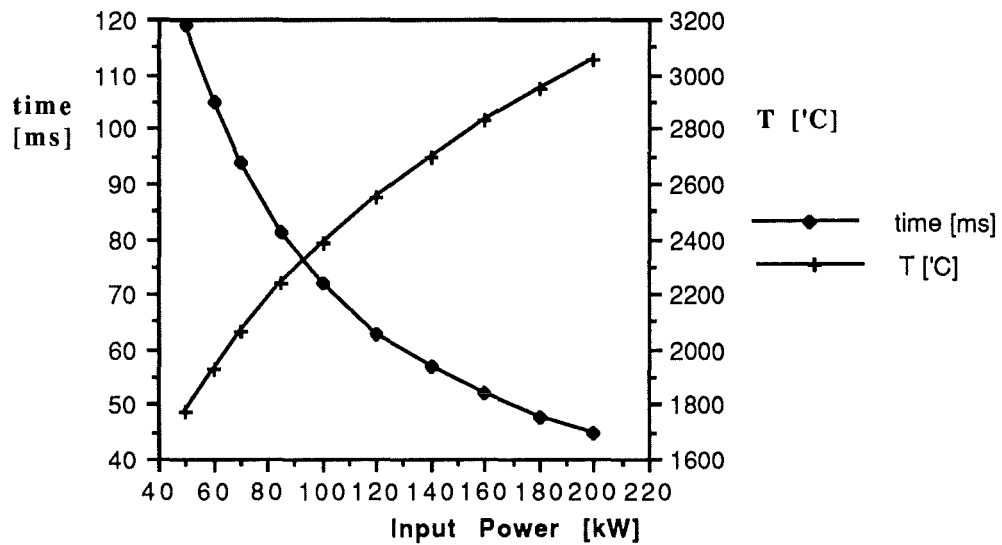


Figure 3.16 Summary of Wire Heating Data

3.2.3.3 Lenses - First Model.

The formulation of incident power for a lens is similar to the wire model. Here it is convenient to use a cylindrical co-ordinate system. The lens is sectioned by dividing the whole lens into concentric rings of equal radial thickness, δr . The normalized power density of a Gaussian beam is given by

$$P = \frac{2}{\pi\omega^2} \exp\left\{\frac{-2r^2}{\omega^2}\right\} \quad 3.37$$

The fraction of power incident on an annular element of thickness δr and radius r is therefore

$$\eta(r) = 4 \frac{r\delta r}{\omega^2} \exp\left\{\frac{-2r^2}{\omega^2}\right\} \quad 3.38$$

The absorption of a lens is due to bulk absorption in the lens material. Typical lenses made in high density polyethylene (HDPE) have losses given by

$$\alpha(r) = 1 - 10^{\left(\frac{g(r)\chi}{10}\right)} \quad 3.39$$

where $g(r)$ is the lens thickness and χ is the loss [dB.m⁻²] at a frequency f [GHz] and is given by¹

$$\chi = -4.16 \times 10^{-2} f \quad 3.40$$

The power absorbed by a particular element is therefore given by

$$\delta P(r) = P_{\text{beam}} \frac{4a(r)r\delta r}{\omega^2} \exp\left\{\frac{-2r^2}{\omega^2}\right\} \quad 3.41$$

The loss mechanisms are essentially the same as for a wire and are given by equations 3.30 to 3.32. The added complication is that the surface and cross sectional areas are functions of r . It should be noted that in formulating the model in terms of discrete elements, the surface and cross sectional areas are not identical to those with infinitesimally small elements.

The lens heating model was implemented in Lightspeed Pascal™. The critical temperature for the lens is lower than its melting point and is taken as ~100°C. The reason for the lower temperature is that the material, HDPE, becomes pliable at this temperature and is not likely to hold its shape². The lower temperatures reached in

¹ J.C.G. Lesurf "Millimetre wave optics, devices and systems", Adam Hilger/IOPP 1990.

² Technical Services Department, Polypenco Limited. Unit E13A, Anniesland Ind. Est., Glasgow G13 1EU.

lenses means that radiative losses are small. The dominant terms are therefore convection and conduction through the lens. The lens-block interaction is therefore more important.

The results of this model show that the maximum power to be less than 1kW, although the heating curves, figures 3.17 and 3.18, do not reach a defined plateau as they do in the wire program. Initially this was thought to be a failing in the iterative approach. It is now thought to be due to poor modelling of the lens-block interaction. Failings in the initial model came to light when low powers and large time intervals were used. The lens profiles usually produced are smoothly varying and 'Gaussian-like'. At low beam powers and large time intervals an oscillation builds up from the edge of the lens and ripples towards the centre. This is due to a large flow of heat into the block which reduces the temperature of the edge section. In the next time interval, the losses from this section are small but a large amount of heat flows in from the adjacent section and from the block. This produces a large rise in temperature for the edge section, and a drop in temperature for the adjacent section. This enables the process to repeat and the temperature wave ripples toward the centre. A typical 'snapshot' of the temperature profile during an oscillation is shown in figure 3.19.

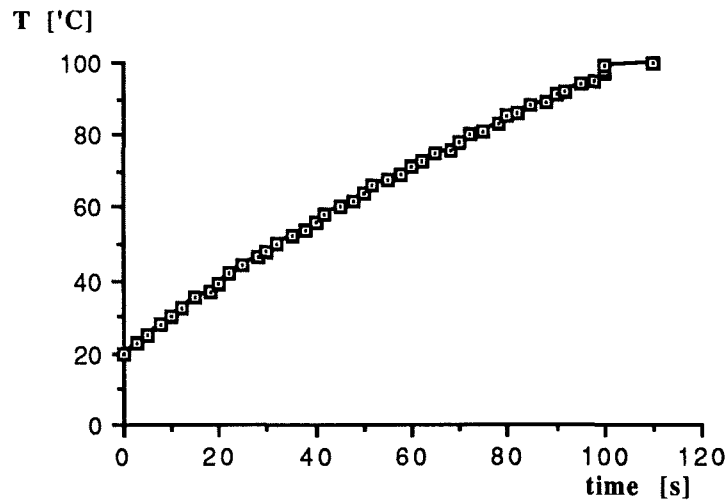


Figure 3.17 Rate of Heating of Lens. $P=750\text{W}$

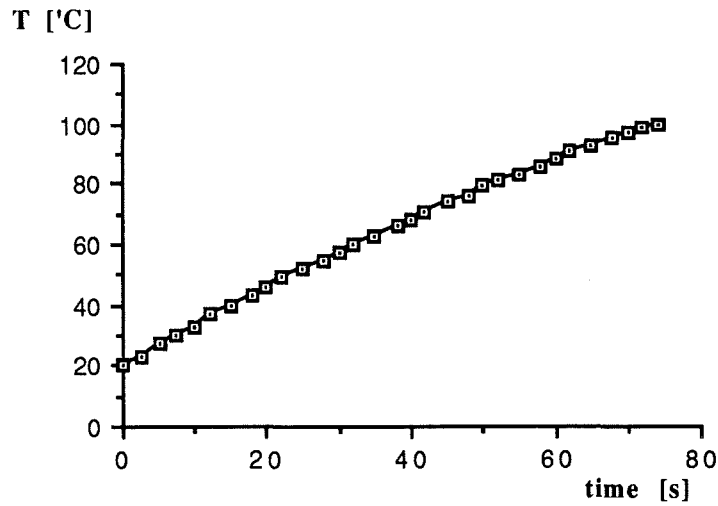


Figure 3.18 Rate of Heating of Lens. $P=1\text{kW}$

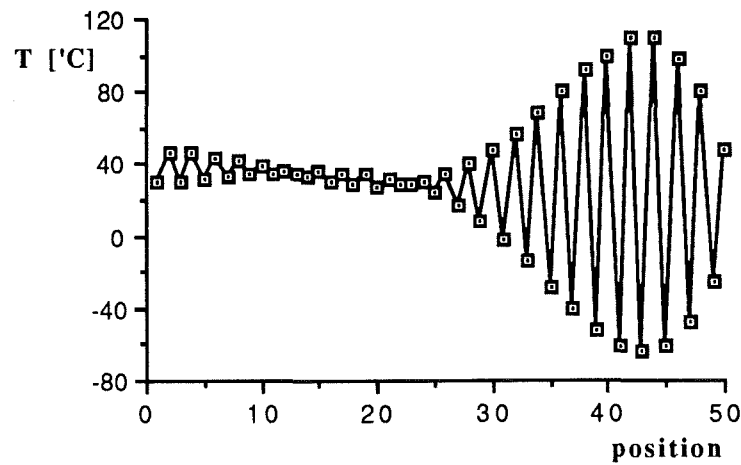


Figure 3.19 Snapshot of Temperature Profile
During Oscillation

It is obvious that the oscillations cannot be real as the flow of heat is a first order problem. There is no means for storing kinetic heat energy, as the inductor does for electrical kinetic energy, and all heat flow is resistive and lossy. The lens and/or wire could be represented electrically by an equivalent circuit such as figure 3.20. The resistances represent the reciprocal of thermal conductivity and the capacitances represent thermal mass, mC_{spec} .

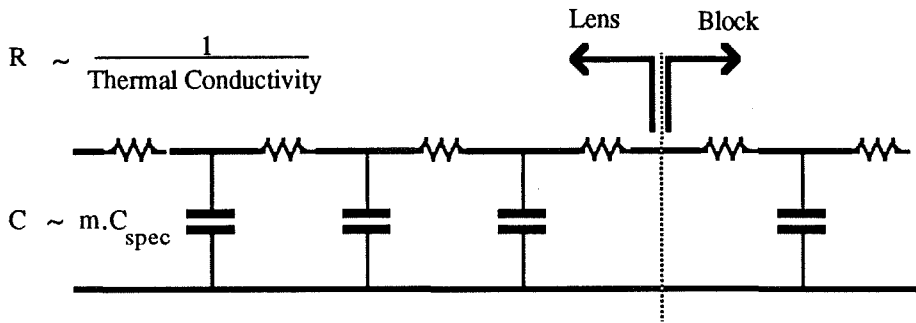


Figure 3.20 An Electrical Representation of Thermal Heat Flow in a Lens

3.2.3.4 Lenses - Second Model.

At the lens-block interface the 'resistance' of the lens dominates the 'resistance' of the block, and so the block receives an amount of energy given by

$$\Delta Q = -\delta t \lambda_{\text{lens}} A_{\text{section}} \frac{(T_{\text{lens}} - T_{\text{block}})}{\delta r} \quad 3.42$$

The temperature T , of the first section of the block increases gradually over the interval, δt , so that

$$T_{t=i} = T_{t=i-1} + (T_{\text{lens}} - T_{t=i-1}) \cdot \left[1 - \exp\left\{\frac{-\delta t}{\tau}\right\} \right] \quad 3.43$$

and then cools through the baseplate such that

$$T_{t=i} \Rightarrow T_{\text{ambient}} + (T_{t=i} - T_{\text{ambient}}) \exp\left\{\frac{-\delta t}{\tau}\right\} \quad 3.44$$

This is not an equality but represents the change in $T_{t=i}$ over the interval δt and is akin to a line of program. The value of τ was determined experimentally by heating a block to $\sim 100^\circ\text{C}$ and measuring its temperature as it cools through the baseplate. The accuracy of the experiment was limited by the inability to keep a constant thermal contact between the block and the baseplate. The value of τ obtained was $100\text{s} \pm 10\text{s}$.

This model was also implemented in BASIC running on an Acorn Archimedes™. This computer was chosen as it was faster than the AppleMac™, and produced profiles whilst running. This enabled the rippling effect of the previous

model to be observed. The omission of ϵ from the radiative loss term had a negligible effect as the temperatures are much lower than those of the wire. The maximum power is $\sim 500\text{W}$ although much depends on the length of heating time. The variation of heating time with power is shown in figure 3.21. From a comparison of these results and those for wire heating it is obvious that the lenses are the weak link. The use of focussing mirrors would be preferable as these would be able to handle more power as well as being easier to cool actively.

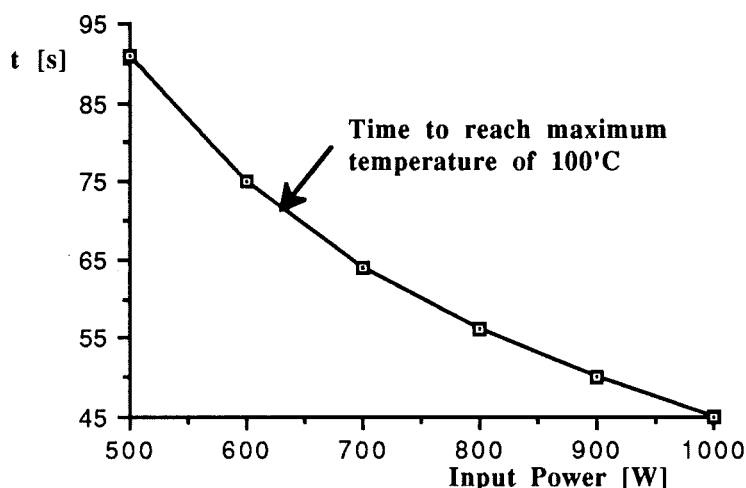


Figure 3.21 Summary of Lens Heating Data

3.3 Oscillator and Detector Block Design.

The source and detector diodes for this project are mounted in tunable co-axial cavities. These cavities are coupled to the output waveguide by a resonant or transforming cap and post arrangement. The design and analysis of these oscillator and detector blocks has received substantial attention from Smith¹. The actual blocks used in this system have minor mechanical differences to those of Smith but are electrically identical. I am indebted to Graham Smith for his guidance in setting up the oscillator and detector blocks. It is through his efforts that these blocks are now standard laboratory equipment and thought of as 'black boxes that require little investigation.' The performance of the oscillators and detectors is presented in chapter 5.

¹ G.M. Smith PhD. Thesis, University of St. Andrews 1990

3.4 A Treatment of Alignment Tolerances.

The half-cube system commonly used in St. Andrews relies on dowelled half-cubes and a grid of holes for the alignment of elements. This type of breadboard provides good alignment accuracy whilst maintaining flexibility in system design. The accuracy to which reflecting elements can be aligned will determine the position of the reflected beam. The uncertainty in the positions and orientations of successive elements may produce an output beam that is misaligned to the ideal beam. The resulting coupling losses can be determined by the following analysis of positional tolerances and the use of the coupling efficiency given in equation 3.14.

Consider initially the positioning of a mirror or reflecting polarizer. The orientation of the reflecting plane is determined by the positions of the three dowels as shown in figure 3.22. Each of these dowels are positioned on the baseplate within a tolerance of $20\mu\text{m}$ along each axis. Each point, therefore, has an uncertainty in its position along each axis which are written as $\sigma(p_x)$ and $\sigma(p_y)$. For the sake of simplicity, the standard deviations, $\sigma(p_x)$ and $\sigma(p_y)$, are both taken as the machining tolerance, denoted $\sigma(p)$ and set to $20\mu\text{m}$.

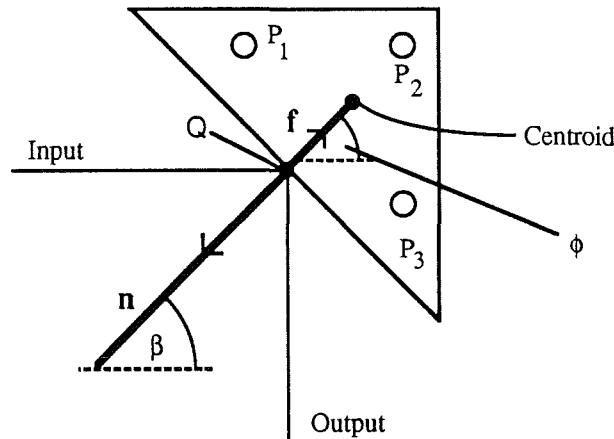


Figure 3.22 The Centroid of the Location Dowels and
its Relation to the Reflecting surface

The overall position of the half-cube is defined by the centroid of these points which has a position vector

$$C = \frac{\mathbf{p}_1 + \mathbf{p}_2 + \mathbf{p}_3}{3} \quad 3.45$$

where \mathbf{p}_i are the position vectors of the three dowels. The error in C is therefore given by $\sigma(C_x)$ and $\sigma(C_y)$ where

$$\sigma^2(C_x) = \frac{1}{3^2} \{ \sigma_1^2(p_x) + \sigma_2^2(p_x) + \sigma_3^2(p_x) \} = \frac{\sigma^2(p)}{3} \quad 3.46$$

$$\sigma^2(C_y) = \frac{1}{3^2} \{ \sigma_1^2(p_y) + \sigma_2^2(p_y) + \sigma_3^2(p_y) \} = \frac{\sigma^2(p)}{3} \quad 3.47$$

The block can also rotate about the centroid, producing an angular error, $\sigma(\theta)$. The angular error is determined by the positional error of each point with respect to the centroid which is given by

$$\delta p_i = |\mathbf{r}_i| \delta \theta \quad 3.48$$

where

$$\mathbf{r}_i = \mathbf{p}_i - \mathbf{C} \quad 3.49$$

The average angular displacement can be written in terms of the average positional error and the average distance, $|\overline{\mathbf{r}_i}|$, such that

$$\delta \theta = \frac{\delta p_1 + \delta p_2 + \delta p_3}{\frac{1}{3} \{ |\mathbf{r}_1| + |\mathbf{r}_2| + |\mathbf{r}_3| \}} \quad 3.50$$

and hence

$$\sigma^2(\theta) = \frac{3\sigma^2(p)}{|\overline{\mathbf{r}_i}|^2} \quad 3.51$$

The point Q in figure 3.22 is the intersection of the reflecting plane and the axis of the input beam. The position of Q and the orientation of the normal \mathbf{n} define the axis of the output beam. An error in the position Q and/or the normal \mathbf{n} will therefore produce an error in the output beam. The point Q is a fixed distance from the centroid and its position is given by

$$\mathbf{Q} = \mathbf{C} - \mathbf{f} = \begin{pmatrix} C_x - f \cos \phi \\ C_y - f \sin \phi \end{pmatrix} \quad 3.52$$

The error in the position of Q is determined by both the translational and rotational errors in C. The angular error in ϕ is also $\sigma(\theta)$ as given by equation 3.51. This enables the positional error in Q to be written as

$$\sigma^2(Q_x) = \sigma^2(C) + f^2 \sin^2 \phi \sigma^2(\theta) \quad 3.53$$

$$\sigma^2(Q_y) = \sigma^2(C) + f^2 \cos^2 \phi \sigma^2(\theta) \quad 3.54$$

where $\sigma^2(C_x) = \sigma^2(C_y) = \sigma^2(C)$ as given by equations 3.46 and 3.47.

For a plane mirror, positional errors parallel to the plane do not affect the position of the output beam, providing the mirror is large enough to avoid truncation. The positional errors along the normal can be found by resolving the positional errors in \mathbf{Q} along \mathbf{n} . The value of this resolved error, $\sigma(s)$, must be independent of \mathbf{Q} since \mathbf{Q} is defined relative to an arbitrary origin. By writing

$$\mathbf{Q} = \mathbf{Q}_0 + \mathbf{E} \quad 3.55$$

where \mathbf{Q}_0 is the mean of \mathbf{Q} , the errors are all contained within \mathbf{E} . The mean value of \mathbf{E} , and hence of its components, is therefore zero. Resolving \mathbf{E} along the normal, \mathbf{n} , produces the parameter s such that

$$s = \mathbf{E} \cdot \mathbf{n} = E_x \cos\beta + E_y \sin\beta \quad 3.56$$

and

$$\sigma^2(s) = \sigma^2(E_x \cos\beta) + \sigma^2(E_y \sin\beta) \quad 3.57$$

The terms on the right of equation 3.57 can each be expanded using the identity¹

$$\frac{\sigma^2(E_x \cos\beta)}{\overline{E_x^2} \cos^2\beta} = \frac{\sigma^2(E_x)}{\overline{E_x^2}} + \frac{\sigma^2(\cos\beta)}{\cos^2\beta} \quad 3.58$$

By invoking the identity $\overline{E_x} = \overline{E_y} = 0$, and knowing that $\sigma^2(E_x) = \sigma^2(Q_x)$, $\sigma^2(E_y) = \sigma^2(Q_y)$ and $\sigma^2(\beta) = \sigma^2(\theta)$, the error in s becomes

$$\sigma^2(s) = \sigma^2(C) + \frac{f^2}{2} \left(1 - \cos(2\phi) \cos(2\beta) \right) \sigma^2(\theta) \quad 3.59$$

This result, and that of equation 3.51, are general results that can be applied to other elements such as translation stages and lenses. Keeping with the example of the mirror, they can now be used to find the errors in the translational position of the output beam axis. The beam errors are in terms of offsets parallel and perpendicular to the axis, δz and δx , and the angular offset $\delta\psi$.

¹ N.C. Barford. 'Experimental Measurements : Precision, Error and Truth', Addison Wesley 1967. p33.

Consider the situation of figure 3.23, which is used to determine the effect of angular errors.

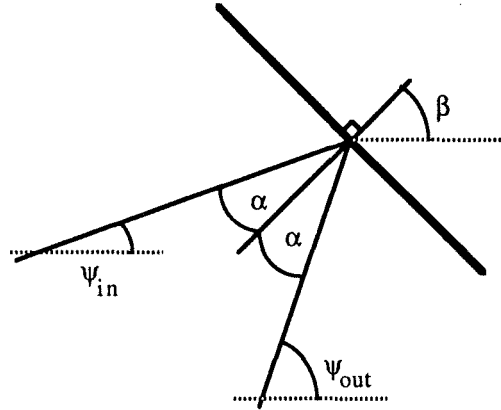


Figure 3.23 Reflection of a Beam by an Angled Surface

The angle of the output axis, ψ_{out} , is given by

$$\psi_{out} = 2\beta - \psi_{in} \quad 3.60$$

The rotational error in β is $\sigma(\theta)$ and this enables the angular error in ϕ_{out} to be written as

$$\sigma^2(\psi_{out}) = \sigma^2(\psi_{in}) + 4\sigma^2(\theta) \quad 3.61$$

The effect of translational misalignment is shown in figure 3.24. The mirror is displaced along the normal by a distance s .

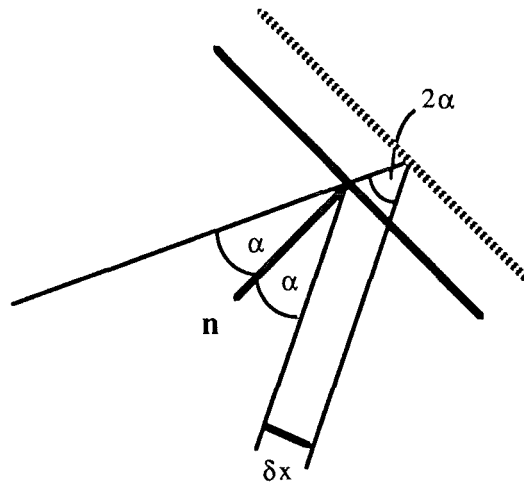


Figure 3.24 Reflection of a Beam by an Angled Surface

The extra path length involved produces an offset along the z axis given by

$$\delta z = \frac{s}{\cos\alpha} (1 + \cos 2\alpha) = 2s \cos\alpha \quad 3.62$$

and an offset along the x axis given by

$$\delta x = \frac{s}{\cos\alpha} \sin 2\alpha = 2s \sin\alpha \quad 3.63$$

As $s = \mathbf{E} \cdot \mathbf{n}$, the error in s is given by equation 3.59 and the mean of s is zero. The alignment errors of the output beam, in the x and z directions, can therefore be found in terms of the errors in the input beam and the error in s . Hence

$$\sigma^2(z_{\text{out}}) = \sigma^2(z_{\text{in}}) + \sigma^2(2s \cos \alpha) \quad 3.64$$

$$\sigma^2(x_{\text{out}}) = \sigma^2(x_{\text{in}}) + \sigma^2(2s \sin \alpha) \quad 3.65$$

Using the identity of equation 3.58, these can be written as

$$\sigma^2(z_{\text{out}}) = \sigma^2(z_{\text{in}}) + 4\cos^2\alpha \sigma^2(s) \quad 3.66$$

$$\sigma^2(x_{\text{out}}) = \sigma^2(x_{\text{in}}) + 4\sin^2\alpha \sigma^2(s) \quad 3.67$$

The results given in equations 3.61, 3.66 and 3.67 enable the alignment errors of a reflected beam to be written in terms of the the initial beam alignment errors and the positional accuracy of the reflecting element. A similar approach can be used to assess the alignment errors produced by other components.

Oscillator and detector blocks are mounted on translation stages that are located on the base plate by two dowels. A similar argument to that above can be used to determine the positional accuracy of the feedhorn and the effective beam waist. In this particular case, the location dowels are a long way from the end of the feedhorn. This gives a large value for f , in equation 3.59, producing a large lateral movement of the feedhorn for a small angular misalignment of the translation stage.

Propagation along a path of length Z_d does not in itself produce additional misalignment errors. It does, however, cause the representation of this misalignment to change. This is described by the following equations.

$$\sigma^2(z_{\text{out}}) = \sigma^2(z_{\text{in}}) \quad 3.68$$

$$\sigma^2(\psi_{\text{out}}) = \sigma^2(\psi_{\text{in}}) \quad 3.69$$

$$\sigma^2(x_{\text{out}}) = \sigma^2(x_{\text{in}}) + Z_d^2 \sigma^2(\psi_{\text{in}}) \quad 3.70$$

A misaligned lens also produces coupling errors. A full treatment would need to involve modal analysis and Gaussian optics. This is not attempted here. An estimate of alignment errors in lenses can, however, be obtained by assuming all lenses to be thin

lenses. This assumption is not valid for many quasi optical lenses, but is a reasonable starting point.

For a thin lens, the focal length is related to the radii of curvature of the input and output beams by

$$\frac{1}{f_l} = \frac{1}{R_{in}} - \frac{1}{R_{out}} \quad 3.71$$

The sign convention is that R is positive for a diverging beam and negative for a converging beam. Assuming that the lens is used to refocus a diverging beam, as in a beam waveguide, and that $R \approx z$, z_{out} can be written as

$$z_{out} = \frac{z_{in} f_l}{(z_{in} - f_l)} \quad 3.72$$

Longitudinal misalignment of the lens will result in an error in z_{in} . This will produce a corresponding error in z_{out} , which can be written as

$$\sigma^2(z_{out}) = \left(\frac{\bar{z}_{out}}{\bar{z}_{in}} \right)^2 \left[1 + \left(\frac{\bar{z}_{out}}{f_l} \right)^2 \right] \sigma^2(z_{in}) \quad 3.73$$

The error in z_{in} will arise from misalignments in both the input beam and the lens. Adding this to equation 3.73 produces

$$\sigma^2(z_{out}) = \left(\frac{\bar{z}_{out}}{\bar{z}_{in}} \right)^2 \left[1 + \left(\frac{\bar{z}_{out}}{f_l} \right)^2 \right] (\sigma^2(z_{in}) + \sigma^2(z_{lens})) \quad 3.74$$

For a lens mounted on a half-cube, the misalignment $\sigma^2(z_{in})$ is equal to $\sigma^2(C)$. A small angular rotation of the input beam about the centre of curvature will not alter the phase front curvature at the lens as this is spherical in the paraxial limit. If the angular offset is small there will be no significant excitation of higher order modes. The output beam will still be a fundamental, but also rotated by a small amount. The input and output beam axes must still intersect at the plane of the lens and so their beam tilt angles are related by

$$\Psi_{out} = \left(\frac{\bar{z}_{in}}{\bar{z}_{out}} \right) \Psi_{in} \quad 3.75$$

A small offset along the x axis will produce an equal and opposite offset in the output beam. Although this means $\sigma^2(x_{out}) = \sigma^2(x_{in})$ this offset will modify the angular error such that

$$\psi_{\text{out}} = \left(\frac{z_{\text{in}} \psi_{\text{in}} + \delta x_{\text{in}}}{\bar{z}_{\text{out}}} \right) \quad 3.76$$

The error in ψ_{out} can now be written in terms of the angular misalignments of the lens and beam. Hence

$$\sigma^2(\psi_{\text{out}}) = \frac{2 \bar{z}_{\text{in}}^2 [\sigma^2(\psi_{\text{in}}) + \sigma^2(\psi_{\text{lens}})] + \sigma^2(x_{\text{in}}) + \sigma^2(x_{\text{lens}})}{\bar{z}_{\text{out}}^2} \quad 3.77$$

Equations 3.74 and 3.77 enable the linear and angular misalignments of a beam leaving a lens to be written in terms of the input beam misalignment and the lens misalignment.

The effect of misalignment of an element on the output beam has been described for the above specific cases. The same arguments can be used to generate data for other elements in a quasi optical system. The representation of this data can be conveniently expressed in matrix form, for example

$$\mathbf{M} \cdot \epsilon_{\text{in}} = \mathbf{M} \cdot \begin{pmatrix} \sigma^2(x_{\text{in}}) \\ \sigma^2(z_{\text{in}}) \\ \sigma^2(\psi_{\text{in}}) \\ 1 \end{pmatrix} = \begin{pmatrix} \sigma^2(x_{\text{out}}) \\ \sigma^2(z_{\text{out}}) \\ \sigma^2(\psi_{\text{out}}) \\ 1 \end{pmatrix} = \epsilon_{\text{out}} \quad 3.78$$

The fourth element in the error vector allows for the independent addition of alignment errors. Defining the matrices for interaction, by the processes described above, enables coupling boundaries to be determined for a given system. Matrices for elements used for this system are given in appendix 4. This approach to the determination of coupling boundaries is obviously specific to a given circuit and a given layout on the baseplate. An example of this analysis would have little meaning unless it was for a genuine circuit. The analysis for the final circuit layout is therefore presented later.

Analysis of Quasi-Optical Circuits.

4 Abstract

The analysis of quasi-optical circuits using the polarization state is described. This technique is incorporated into a computer design tool and used to analyze the receiver and circulator circuits of the radar. Several other circuits are presented and analyzed, though not included in the radar.

4.1 Representation of Polarized Radiation.

The polarization state of a Gaussian beam can be represented in a number of ways. These include Stokes Parameters and Jones Vectors¹. The Stokes formulation is a four parameter vector and is applicable to partially polarized light as well as polarized light. It is formed, however, in terms of irradiances or powers and as such is not applicable to the combination of coherent sources. Jones vectors are a direct, two component representation of the transverse electric vector of a polarized source. As such it is applicable to the combination of coherent sources, but not to partially polarized light. The manipulation of the polarization state, by an optical element, can be described in each case by an appropriate matrix. For the Stokes and Jones vectors these matrices are known as Mueller and Jones matrices respectively. The radiation in most quasi-optic applications is polarized by virtue of the waveguide mounted sources, and so the Jones vector approach is more useful.

Polarizers in the millimetre wave region can be made to perform very efficiently. Wire grid polarizers have less than -30dB cross polar leakage at ~100GHz and are regarded as ideal for most applications. This performance, and the ability to design systems with very low loss using Gaussian beam techniques, enables many circuits to be described and analyzed solely in terms of the polarization state.

4.1.1 Circuit Symbols and Matrices.

The use of a polarization approach to the design and analysis of quasi-optical circuits is very powerful. Many quasi-optical circuits, including all of those presented in this thesis, are derived by considering the polarization content first. Implementation of these circuits is largely straight forward especially if the half-cube system is used. A Jones matrix can be produced for reflection from, and transmission through, each

¹ E. Hecht and A. Zajac "Optics" Addison-Wesely 2nd Ed. 1977 p266.

optical element in a system. For many elements the matrices are simple. Some elements, notably angled polarizers and ferrites, have non-reciprocal transmission matrices : they are dependent on the direction of propagation. The general case for reflection and transmission at a wire grid is given by

$$A_R(\theta) = \begin{pmatrix} -\cos^2\theta & -\cos\theta\sin\theta \\ \cos\theta\sin\theta & \sin^2\theta \end{pmatrix} \quad 4.1$$

$$A_T(\theta) = \begin{pmatrix} \sin^2\theta & -\cos\theta\sin\theta \\ -\cos\theta\sin\theta & \cos^2\theta \end{pmatrix} \quad 4.2$$

where θ is the angle of wires to the vertical and the components of the incident and resultant E-vectors are resolved as

$$E = \begin{pmatrix} E_{\text{vertical}} \\ E_{\text{horizontal}} \end{pmatrix} \quad 4.3$$

The angle convention is that θ is positive for clockwise rotation when viewed in the direction of propagation.

Lesurf¹ has proposed a set of polarization circuit symbols that is used here. The notation for the required Jones matrices is also that of Lesurf and is summarized in the following table. The angles are all measured with respect to the vertical when viewed along the propagation axis. For the symbols shown, the beam is assumed to be moving from left to right.

¹ J.C.G. Lesurf. "Millimetre Wave Optics, devices and Systems" Adam Hilger/IOPP 1990.

Element	Symbol	Transmission	Reflection
Polarizer with wires at +45'.		P_T	P_R
Polarizer with wires at -45'.		N_T	N_R
Polarizer with wires vertical.		V_T	V_R
Polarizer with wires horizontal.		H_T	H_R
Polarizer with wires at variable angle.		A_T	A_R
Roof Mirror.		-	$R(\theta)$
Plane Mirror.		-	M
Absorbing Load.		-	-
Non-polarizing beam splitter.		S_T	S_R
General Source.		-	-
Coherent Source.		-	-
Detector or Mixer.		-	-
Beam Path of Length d.		$[d]$	-

Figure 4.1 Summary of Polarization Matrices and symbols.

The alternative symbols shown above have evolved from those of Lesurf and are used interchangeably. In addition to the above symbols, the following is proposed for a matched free-space Faraday rotator.

Element	Symbol	Transmission	Reflection
Ferrite - Positive Rotation		F_P	-
Ferrite - Negative Rotation		F_N	-

Figure 4.2 Proposed Polarization Matrices and Symbols for Faraday Rotator.

The above representation uses ideal elements. It would be easy to modify the values of the matrix elements to represent real elements if this were required and

justified. This would require, in the majority of cases, adding cross polarization terms to the matrices, and allowing for loss and VSWR. Some additional matrices would be required to fully represent some elements, for example reflection matrices for ferrites, absorbing loads, sources and detectors.

The analysis of a circuit, in terms of the polarization state, can now be reduced to the application of the above matrices, in the appropriate order, to the Jones vector of the input field. For many circuits the manipulation of the polarization vector can be tracked visually through a system from element to element, and the matrix approach is not required. Circuits involving interferometry nearly always require a matrix approach, as the phase relationship of two signals with the same polarization state is important. The matrix approach can be long-winded, especially in the early stages of designing a large circuit. A small change in the circuit will require recalculation of all of the matrices. As matrix multiplication by hand is laborious, a method of automation was produced.

4.2 QOCAD - A Design Tool.

The version of BASIC implemented on the Archimedes™ has a very powerful array handling ability. Matrix and vector multiplication can be achieved by applying simple operators to array variables. High order matrices and vectors can be handled although only 2x2 and 2x1 arrays are required here. The process of multiplying the matrices can be reduced to the selection of the appropriate element from a menu, and inputting the incident polarization vector. It was decided that a visual indication of the elements being combined would benefit the design process and facilitate the correction of mistakes. A program was therefore written that enabled a quasi-optical circuit to be designed on the screen using circuit symbols placed on a grid similar to a baseplate. The polarization properties of the circuit can then be determined for a number of routes through the elements and a particular input vector. Modifications to the circuit can be easily made and the same routes re-evaluated, and/or new routes drawn. The program is called QOCAD and a full listing is contained in appendix 5.

A circuit is designed by positioning the mouse on a grid position and pressing a function key for the required element. The "shift" and "control" keys expand the 12 function keys to cover 36 elements. The 36 elements consist of the first five polarizers in figure 4.1 and a non polarizing beam splitter each in two orientations. The remaining elements are composed of four orientations each of plane mirror, roof mirror, source, detector, absorbing load and Faraday rotator. The orientations refer to the alignment of the element with the beam axis, and not the polarization vector. Some elements require

additional data to define their matrices. Sources have the output polarization vector defined. Roof mirrors and variable angle polarizers have the angle of the roof line and the wire, respectively, defined relative to the vertical. These special characteristics are stored and referenced to the appropriate grid position so that the information is always available.

Routes are drawn using the mouse and the mouse buttons. The number of the currently selected route, 1 to 20, is shown on the screen in red if active and in green if not being used. The colour of the route lines also changes when a route is selected. A route is started by clicking with the left button on the start point. Subsequent steps are drawn by further clicking of the left button on the appropriated grid position. When a route is evaluated, each element along the route is checked to ensure it is correctly aligned and being used properly. This catches errors such as reflecting a beam off a polarizer and sending it the wrong way, and attempting to transmit a beam through a mirror. The route is also checked to ensure it starts on a source and ends at a detector.

The matrix for each element along the route is copied from a look-up table and used to produce the overall matrix for the route. The input polarization vector is then used to produce the resultant polarization vector. The multiplication process involves multiplying the unit matrix by the matrix for the first element to produce a resultant "working" matrix. The working matrix is then multiplied by the next matrix along the route and set equal to the result. This is required as the Archimedes™ only allows matrices to be multiplied in pairs. Should the working matrix become a null matrix at any point along the route, the evaluation process is halted and the offending element identified. The processes for drawing routes and placing elements are entirely separate from the route evaluation process. This enables an offending element to be corrected simply by replacing it with another. It is not necessary to re-draw any routes that passed through the element, and subsequent evaluation of any route will take the new element into consideration. Each evaluated route is displayed in the form of a graphic representation of the polarization vector and the power contained in that state. An example is shown in figure 4.3. The two routes are displayed together as they start on the same source and end on the same detector. There will therefore be interferometric effects to consider. The lengths of each route are also shown. The asterisk indicates that the path, having involved a roof mirror, is not an integer number of grid units (half-cubes) in length. As most roof mirrors are movable the path length is likely to be variable.

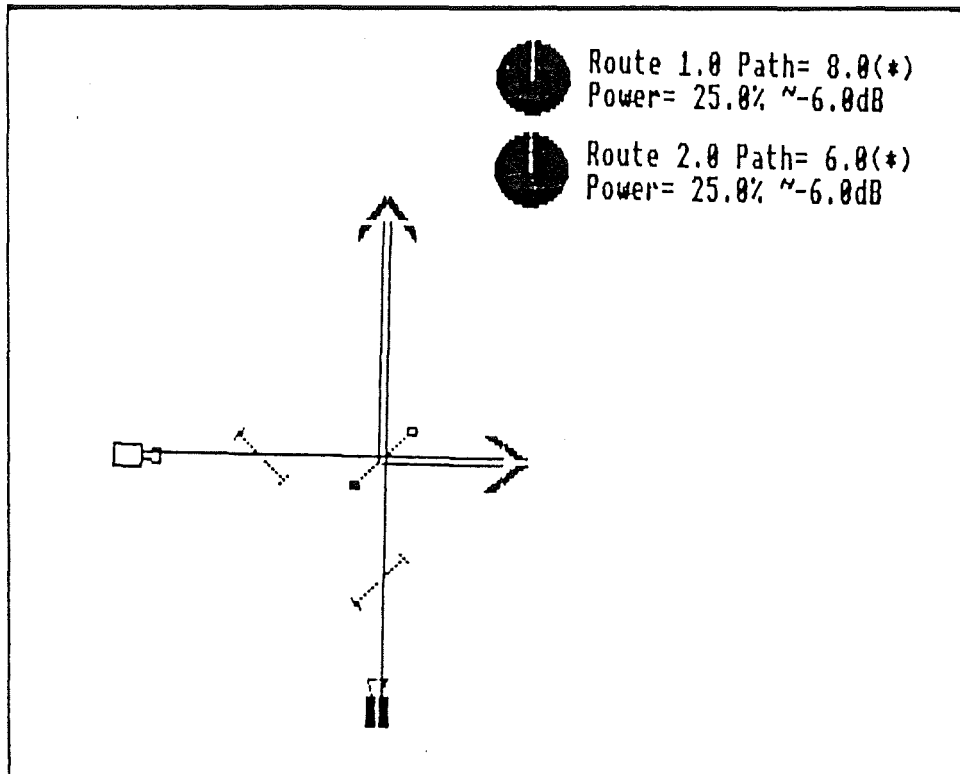


Figure 4.3 The Output of QOCAD for a Martin-Puplett Interferometer.

In its current form, QOCAD is a fast and flexible design aid for quasi-optical circuits. Its main use is for quickly evaluating new circuits to allow modifications to be made. In this sense it is used like a note book during the initial design stage. The structure of the program, however, will allow for many improvements to be quickly added. Such improvements include the incorporation of alignment matrices, as described in chapter 3. Once the initial layout is finalized, the positions and focal lengths of focussing elements can be determined. The knowledge of beam waist sizes and positions can be used in conjunction with the alignment matrices to assess the coupling efficiency.

One technique employed in the practical implementation of this radar is the use of extra layers in a circuit. Whilst propagation along a third axis is complicated to incorporate, the use of parallel layers, linked at strategic points, could readily be added to QOCAD.

4.2.1 Receiver and Circulator Circuits.

Various receiver circuits have been analyzed using QOCAD. The component layout was changed around in order to optimize the space available on the baseplate. The final layout of the receiver is shown in figure 4.4.

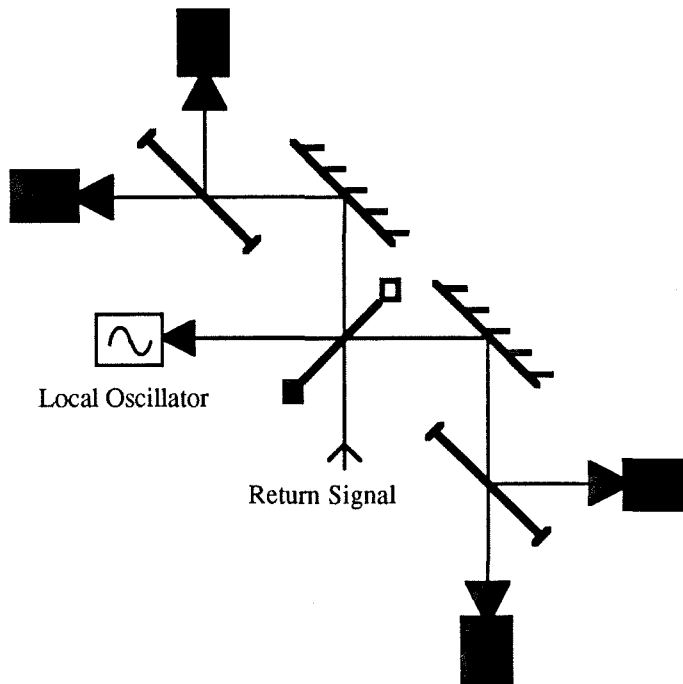


Figure 4.4 Final Layout of Receiver Circuit.

The local oscillator is tapped from the master oscillator using the circuit of figure 4.5.

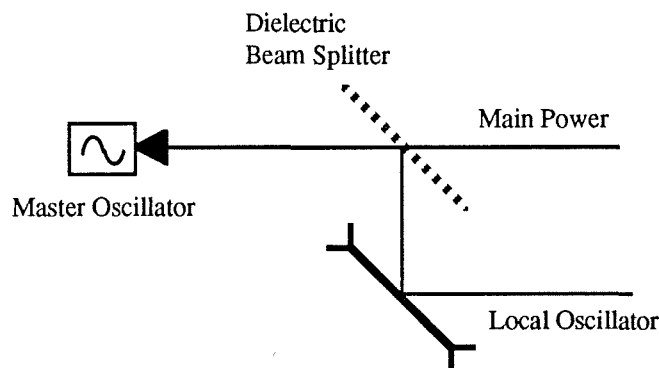


Figure 4.5 Local Oscillator Tapping Circuit.

A non-polarizing beam splitter is used to split the power in the ratio of 10:1. This was preferred to a variable angle polarizer as it was easier to fabricate and the polarization state was maintained. The use of a rotatable roof mirror behind a fixed angle polarizer was rejected due to lack of space. The use of rotating roof mirrors and polarizers varies the amount of local oscillator power by directing some power to a load.

The non-polarizing splitter enables power not required for the local oscillator to be directed at the target.

In conventional waveguide based radar, the transmitter and receiver are able to share an antenna by using a circulator. The optical circulator described by Webb¹, is a single polarization device. A circulator capable of handling both polarizations is required if the full capabilities of the radar are to be used. Figures 4.6 and 4.7 show two circuits that act as full polarization circulators.

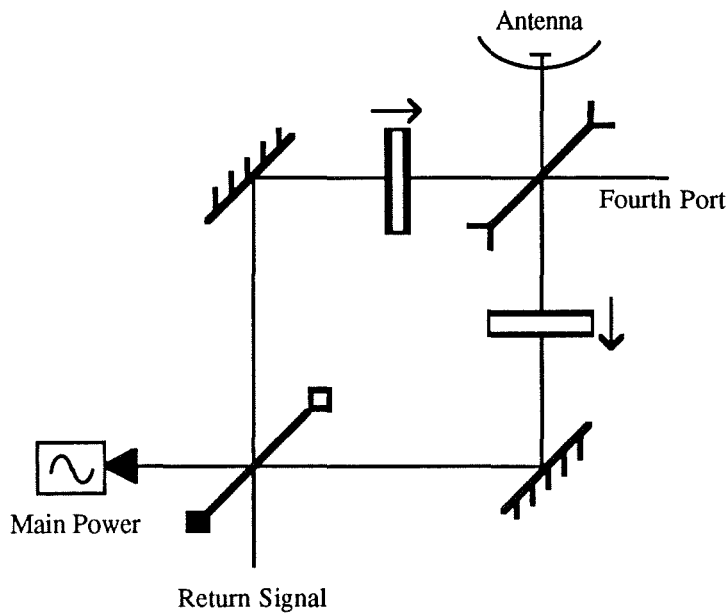


Figure 4.6 Two Ferrite Dual Polarization Circulator.

Figure 4.6 is essentially two single polarization circulators : one for each polarization state. The use of the two plane mirrors enables the two circulators to share the same input and output polarizers. Special note should be made of the orientation of the two ferrite rotators.

¹ M.R. Webb. PhD. Thesis, University of St. Andrews 1992.

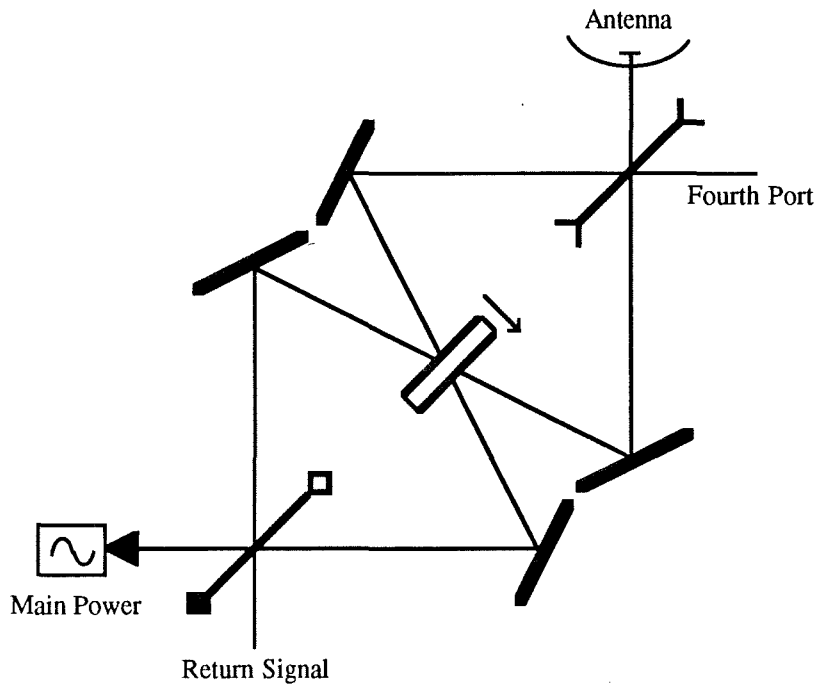


Figure 4.7 Single Ferrite Dual Polarization Circulator.

Figure 4.7 show a full polarization circulator containing only one ferrite rotator. The advantage of this circuit is that both states of the input beam use the same piece of ferrite. This reduces the effects of mismatch between separate rotators. The disadvantages include increased complexity, longer path lengths, beam distortion and poor cross-polar isolation. The increased complexity and longer path lengths are apparent from the diagram. Longer paths may require additional focussing and this will increase insertion loss and VSWR. The distortion is caused by off-normal propagation through the ferrite. The distortion of the beam will upset the coupling of the circuit and may lead to increased loss. An increase in coupling has been observed, by varying the angle of the ferrite¹. This may have been caused by a poor optical set-up in the first place. The effect of off-normal propagation through the ferrite can be measured and allowed for. The off-normal incident angle will, however, cause reflections from the front surface of the ferrite to corrupt a beam transmitted from the other side. As shown in figure 4.7, any reflection from the ferrite surface will appear at the same output port, but in the cross polar component. The ferrite could be tilted to throw such a reflection out of the plane of the circuit. This would, however, present different incident angles to beams from different ports.

The orientation of the plane mirrors appear to have the ideal orientation for low distortion off-axis focussing mirrors. In order to reduce the effects of distortion,

¹ G.M. Smith. Private Communications.

produced by off-axis reflection, focussing mirrors are usually used in complimentary pairs¹. The theory behind this is that an off-axis mirror sets up higher order modes in the reflected beam. In a time reversed situation, these higher order modes would produce a clean Gaussian beam when incident on the same mirror. The phase of a higher order mode changes sign as it passes through the beam waist. The field pattern on the other side of the waist is therefore a mirror image of the field pattern set up by focussing mirror. It follows therefore that a second mirror placed in the appropriate place will convert the higher order modes back into a simple Gaussian.

The higher order modes can be grouped into two categories : those that distort the amplitude of the reflected beam and those that produce power in the orthogonal polarization state. Placing a ferrite rotator between two mirrors will not alter the amplitude distortion provided the incidence angle is normal. For the circuit shown in figure 4.7 this is not the case and the ferrite will alter the mode content. It may be possible to measure the distortion and design the focussing mirrors accordingly though this remains to be seen. A more serious problem is the effect of the ferrite on the cross polarization modes. The action of the ferrite is to rotate the incident polarization state. This will produce a different amount of power in the cross polar modes than would have been the case with no ferrite. Rotating the mirror to counter this problem would increase the problem for beams propagating in the other direction through the ferrite.

For these reasons the circuit of figure 4.7 was rejected and the circulator of figure 4.6 was preferred. To save space, the circulator circuit was placed on a separate layer above the receiver circuit. The ports of the circulator were arranged so that the transmitter port lay above the local oscillator port of the receiver. The local oscillator tap, shown in figure 4.5, is used to take power from the master oscillator and "bounce" it down to the receiver layer. The receiver port of the circulator lies above the input port of the receiver, and the return signal is bounced down to the receiver layer using a pair of mirrors. The physical layout of the receiver layer and of the assembled radar is shown in figure 4.8. The fourth port of the circulator is not used in this application. It could be used by a solid state source to injection lock a higher powered source on the transmitter port.

¹ J.A. Murphy. "Distortion of a Simple Gaussian Beam on Reflection from Off-Axis Ellipsoidal Mirrors" *Int. J. IR & mmW*. Vol 8, No.9 1987. p1165.

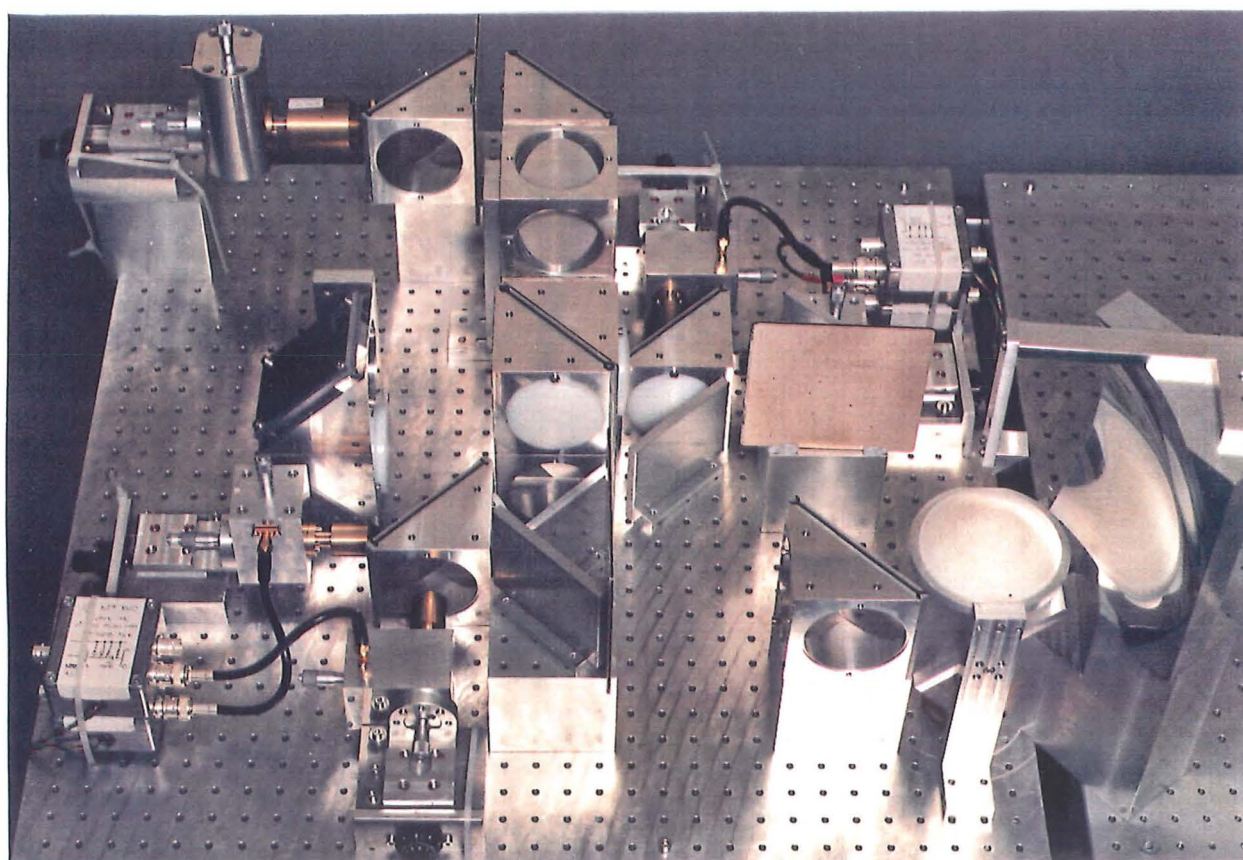
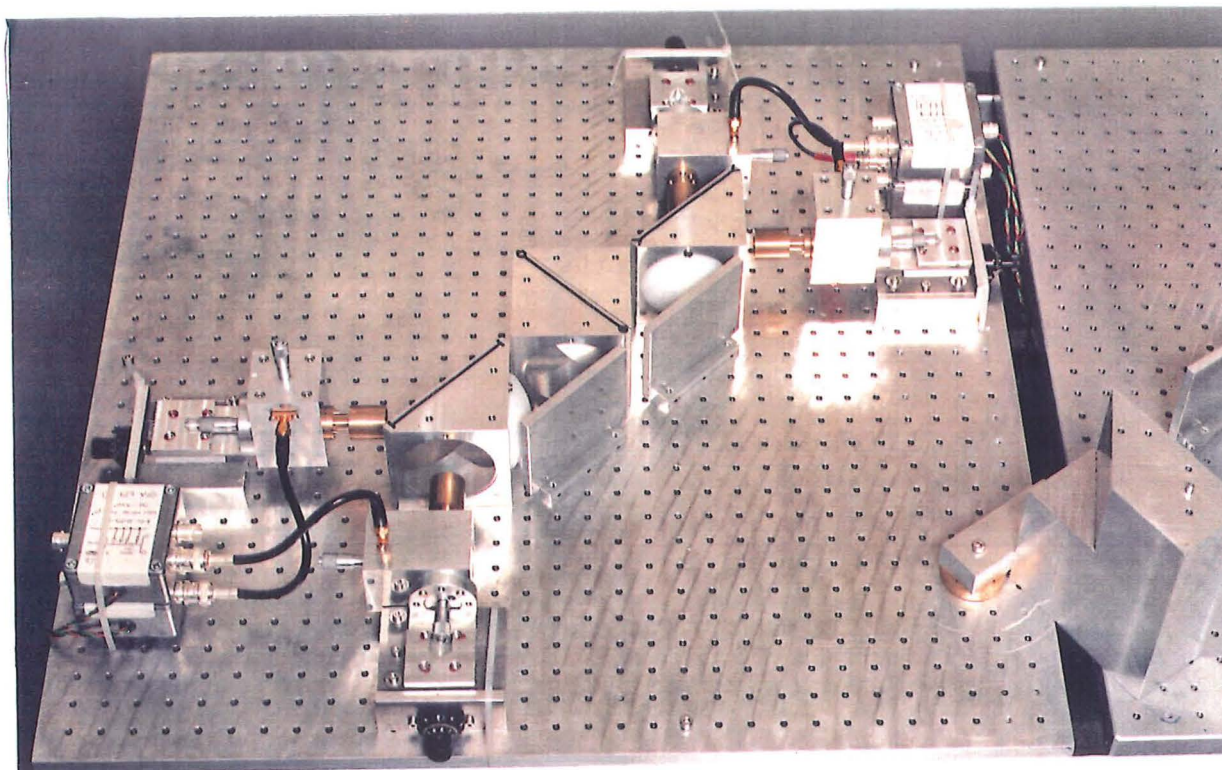


Figure 4.8 Photographs of Receiver Layer (top) and Complete System (bottom).

4.3 Quasi-Optical Circuit Ideas.

The following sections cover circuits that have been designed and evaluated using QOCAD. Some of the practical problems likely to be encountered when implementing these circuits are discussed.

4.3.1 Multi-Modal Signal Processing.

In general a fundamental Gaussian beam, reflected from a complex target will contain a number of higher order modes. The modal content of a beam is a concise and powerful method of representing the phase and amplitude variations across a beam. A portion of such a return beam, coupled into a receiver, will also have spatial amplitude and phase variations. The modal content of the beam reflected from the target will not be the same as that of the beam coupled into the receiver. The modal contents of both beams, however, will be indicative of the type of reflecting surface. The reflection from a particular target may therefore produce a characteristic modal content or signature. Modal analysis can be carried out in a similar way to Fourier analysis, as the higher order spatial modes are orthogonal and form a complete set. The amount of a particular mode is given by the correlation between the unknown field and the field for that mode for example

$$a_i = \int_{\text{beam}} \Psi_i \mathbf{E} \, dS \quad 4.4$$

where \mathbf{E} is the unknown field and Ψ is the field for the i^{th} mode.

Development of the millimetre wave spatial light modulator¹ may lead to mode selective filters. This would convert a particular higher order mode into a fundamental Gaussian mode. The use of a corrugated feed horn as a "fundamental mode passing" filter would enable the amount of power contained in the particular mode to be determined. An active spatial light modulator could scan through a number of higher order modes to determine the mode content of the beam. The circuit of figure 4.9, however, processes the modes in parallel producing a real-time modal content. The return power is split into a number of identical beams by the variable angled polarizers. The angles of the wires are chosen to produce equal powers in each detector arm. Non-polarizing beam splitters could also be used, and the power splitting need not be uniform as long as it was known. The spatial light modulator in each arm is adjusted to convert one particular higher mode to a fundamental. The power in the resulting

¹ M.R. Webb. PhD. Thesis, University of St. Andrews 1992.

fundamental mode, as measured by the detector, defines the amount of that mode present in the return.

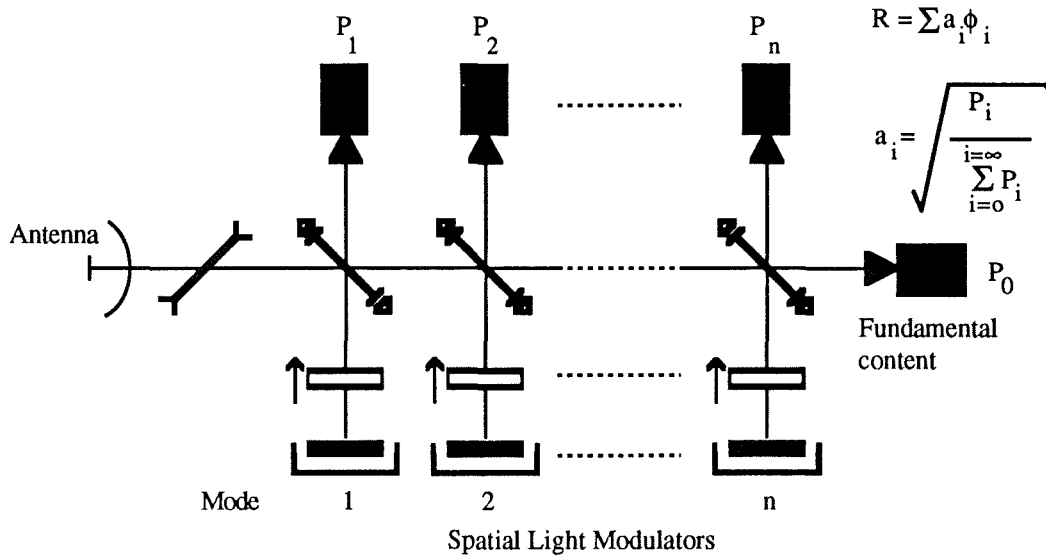


Figure 4.9 Parallel Processing of Spatial Mode Content.

The practical problems likely to be encountered in the implementation of this circuit include the production of clean spatial mode converters, and the efficiency of the corrugated horn in rejecting higher order modes. Although not explicitly shown in figure 4.9, a local oscillator is likely to be used with each detector. These would all be derived from a common source.

4.3.2 Passive Ranging.

Radiation from a distant source, whether real or reflected from a target, appears to emanate from a point. The distance to such a source can be determined by measuring the radius of curvature of the beam's phase front. This technique provides a method of measuring range without illuminating the target. Consider the situation of figure 4.10.

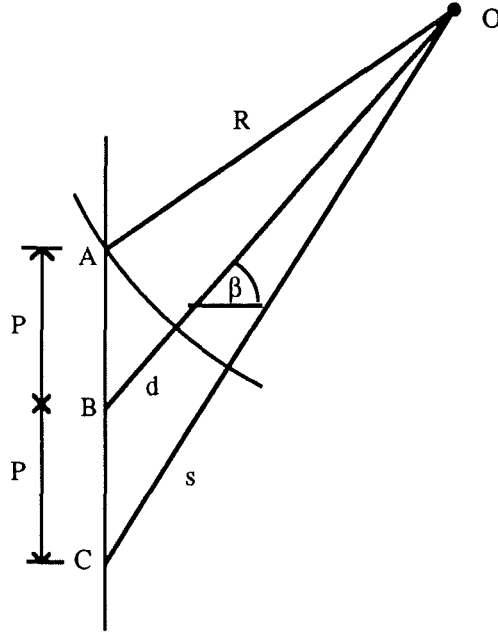


Figure 4.10 Radius of Curvature Measurement.

The phase difference, ϕ_d , between the signals received at A and B is proportional to the path difference d , such that

$$d = \frac{\lambda \phi_d}{2\pi} \pm n\lambda \quad 4.5$$

For a range, R , much larger than the separation, p , the angle of the target to the normal is given by

$$\beta = \arcsin\left(\frac{d}{p}\right) \quad 4.6$$

This assumes that the phase fronts are planar. It will be shown that this assumption is valid for the determination of the angle even when the phase front curvature is taken into consideration.

For a true plane wave, the phase difference, ϕ_s , between the signals received at A and C would be twice ϕ_d . A non-planar phase front will produce a phase difference at C that differs from the expected $2\phi_d$. Detecting and measuring this phase difference will enable the radius of curvature and hence the range to be measured. In figure 4.10,

applying the cosine rule to the triangles $\angle ABO$ and $\angle BCO$ yields the following equations

$$R^2 = (R+d)^2 + p^2 - 2p(R+d)\cos(90-\beta) \quad 4.7$$

$$(R+s)^2 = (R+d)^2 + p^2 - 2p(R+d)\cos(90+\beta) \quad 4.8$$

Applying the identities

$$\cos(90-\beta) \equiv \sin(\beta) \quad 4.8$$

$$\cos(90+\beta) \equiv -\sin(\beta) \quad 4.9$$

and solving the simplified simultaneous equations yields the range as

$$R = \frac{(p^2 + d^2 - s^2)}{(s - 2d)} \approx \frac{p^2}{s - 2d} \quad 4.10$$

and the angle as

$$\sin\beta = \frac{(s^2 + 2Rs)}{4p(R+d)} \approx \frac{2Rs}{4pR} \approx \frac{s}{2p} \approx \frac{d}{p} \quad 4.11$$

The approximations that $R \gg s$, $R \gg d$ and $s \approx 2d$ are valid if $s \approx \lambda$ and R is a few tens of metres. Slightly different expressions are produced if the phases at A and C are measured with respect to B. In this case the range and angle are given by

$$R = \frac{(2p^2 - a^2 - c^2)}{2(a+c)} \approx \frac{p^2}{a+c} \quad 4.12$$

$$\sin\beta = \frac{(c^2 - a^2 + 2R(c - a))}{4pR} \approx \frac{(c - a)}{2p} \quad 4.13$$

where a and c are the phase lengths measured at A and C respectively.

The question of range ambiguity now arises, due to the unknown number of wavelengths that is lost from the measured phase lengths given by equation 4.5. For a wavelength $\sim 3\text{mm}$ and a separation of antennas $\sim 1\text{m}$, the phase measured equals the actual phase provided $R > 330\text{m}$, and the target is along the boresight. This minimum unambiguous range can be reduced by increasing the path length from the central detector. This essentially places the three antennas on a curved phase front and removes some of the offsets from equation 4.5. Increasing the antenna separation will also reduce the minimum range.

For a target that lies off the boresight, the power detected at each antenna will be unequal and this can be used, together with a knowledge of the antenna patterns, to determine the off-boresight angle, β . For a distant target and a small value of β , the

power variation may be small. In this situation the phase difference between A and C may be used.

The maximum range will be determined by one of two factors. The first factor is the smallest phase difference that can be detected between the detectors at A and C. A phase difference smaller than this minimum will not register, and the phase fronts will appear to be planar. The second factor is the ability to determine the boresight angle from the power difference between the detectors at A and C. A large range will produce a small variation in the powers for a given angular change. The smallest angular change that will produce a detectable power variation must be less than the maximum off-boresight angle $\beta \approx \frac{\lambda}{2p}$.

For an example of this, consider antennas with a gain of 35dB, and a minimum detectable power variation of 1%. The worst case will be when the antennas are both approximately on boresight : the angular variation for a 1% power change is largest. A power change of ~1% occurs when the off-boresight angle is γ , given by

$$P(\gamma+\beta) - P(\gamma-\beta) = 0.01 \times P(\gamma) \quad 4.14$$

where, for a Gaussian beam of gain G

$$P(\gamma) = P_0 \exp\left(\frac{-G\gamma^2}{3}\right) \quad 4.15$$

Solving equation 4.14 for a gain of 35dB and $\beta \approx \frac{\lambda}{2p}$, gives

$$\gamma = 1.6 \text{ mrad} \approx 0.1' \quad 4.16$$

from which the maximum range is

$$R_{\max} \approx \frac{p}{\gamma} \approx 600\text{m} \quad 4.17$$

The maximum range could be increased by increasing the antenna gains, increasing the antenna separations or by changing the beam profile. A beam profile that is not flat across the boresight angle, would produce greater power variations for a given angular offset. Such a beam could be produced by pointing the outer antennas in different directions (toeing out) and effectively re-defining the boresight angle, or by using higher order modes. The use of higher order modes to shape such a beam is, however, a whole new ball game.

The circuit shown in figure 4.11 combines the beams at A, B and C. The outputs of the balanced pairs of detectors can be used to produce the phase differences between each pair of antennas and the power received at each antenna. The effective position of the central antenna can be changed by varying the path length using the delay line shown.

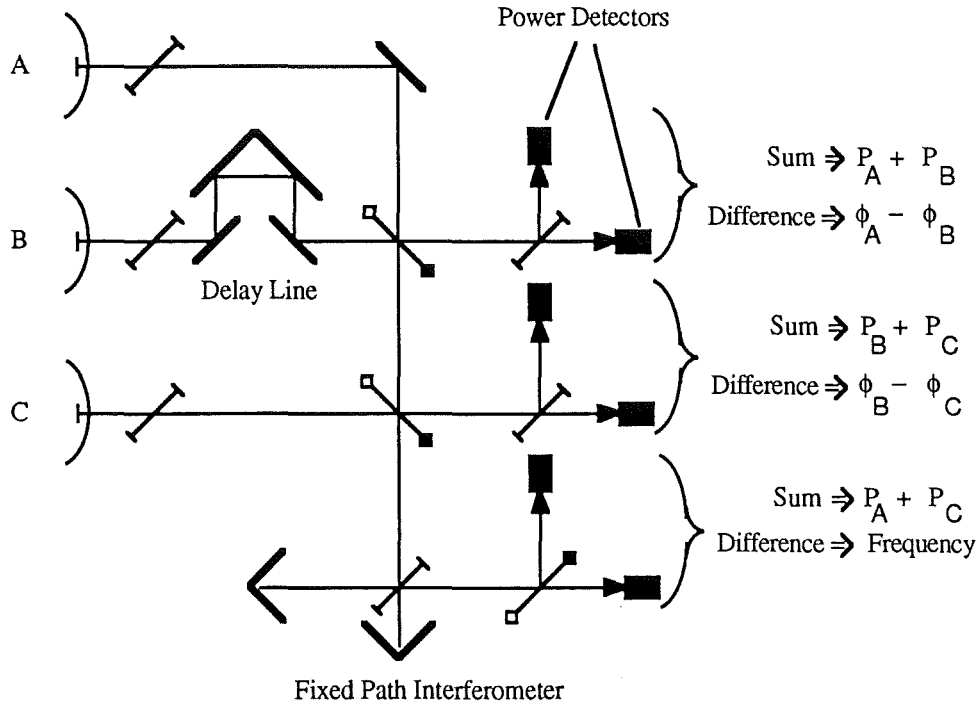


Figure 4.11 Measurement of Phase Front Curvature.

The wavelength of the returning radiation needs to be determined so that the path differences can be determined from the phase differences. This can be achieved by using a frequency counter, the use of scanning interferometry or by fixed path difference interferometry. The last method uses an interferometer with a fixed path difference and a pair of power detectors on the output ports. The power measured in each detector will depend on the phase of the signals in the two paths. The phase difference of the two paths depends on the frequency and hence the frequency can be found by measuring the powers from the two detectors. The signals from ports A and C are used in this way to determine the frequency. The power and the phase difference measured by these detectors will include the effect of the path difference. The path difference will be known, however, and its effect can be removed from the final calculation.

Signal Processing Electronics.

5 Abstract.

This chapter covers the theory, design and construction of the electronic parts of the system. The description starts with the detector diodes and covers first stage amplification, frequency and phase measurement and computer interfacing. The section on the system oscillator covers frequency modulation requirements and oscillator tuning. Methods of linearization are also discussed. The final section covers causes of noise within the system. Receiver noise and oscillator phase noise are discussed and their effect on performance evaluated.

5.1 Receiver Circuitry.

5.1.1 Bias Supply.

The first element in the electronic section of the radar receiver is the mixer diode. The mixer diodes¹ are mounted in detector blocks which are very similar to the oscillator blocks described briefly in chapter 3. The diodes are biased into the operating region, of their IV curves, by the bias circuit shown in figure 5.1. A battery supply is used to maintain low noise levels.

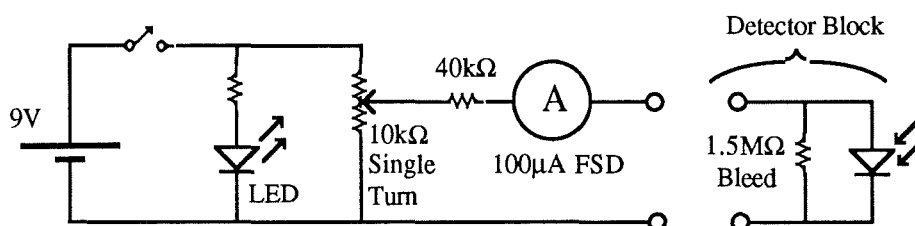


Figure 5.1 Detector Diode Bias Supply.

The meter has a series resistance of $\sim 1.8\text{k}\Omega$, and reads full scale when passing a current of $100\mu\text{A}$. An op-amp was used to buffer an additional meter so that a true output voltage reading could be obtained. The inclusion of an op-amp though, produces a possible hazard. When the supply to an op-amp is turned on or off, the output often leaps to either rail. This can produce voltage spikes at the output that would damage the diode.

¹ Part Number SDO12-014-01 Farran Technology, Ballincollig, Cork, Ireland.

When illuminated with RF power, the IV curve of the diode shifts. The bias point moves along the load line of the diode and bias circuit to the new IV curve. The detection of RF power is achieved by measuring the change in this bias point. A constant current bias produces a varying voltage across the diode, whereas a constant voltage supply produces a varying current through the diode. The power produced by the diode can therefore appear as voltage gain, current gain or both - depending on the nature of the bias circuit. The ammeter has a series resistance of $1.8\text{k}\Omega$ which dominates the output impedance. A further $40\text{k}\Omega$ of series resistance was added to increase the output impedance still further. The high output impedance of the bias circuit means the supply acts like a constant current supply.

5.1.2 First Stage Amplification.

In reality we have to consider noise and signal to noise ratios rather than signal levels. The noise generated in the first stage amplifier can be referred to the input and represented by an ideal amplifier and a noise source. The amount of this noise is described by a power level. More often than not the power level is represented in terms of r.m.s. noise voltages and r.m.s. noise currents produced at the amplifiers input impedance. The amount of input noise produced by an amplifier is a combination of thermal or Johnson noise produced by the source resistance and the effect of current, or shot noise through the source resistance. Shot noise, produced by the quantized nature of carriers, will produce large output voltage noise for a high source impedance. Murphy's law states that the ideal source impedances for power gain and for low noise performance are not one and the same. The application will often determine which is the defining criterion. As an example of this consider the NE5539. This bipolar IC forms the basis of a very wideband amplifier with good voltage noise performance of $4\text{nV}/\sqrt{\text{Hz}}$. Stable operation requires source and load impedances of the order of 100Ω and it is designed for use in 50Ω and 75Ω systems. This would appear to be very suitable as the first stage amplifier for the mixer diodes. The total noise voltage, however, varies over the range of source impedances that the diode presents during normal use, due to the large current noise. In a noise critical system such as the FM noise system of Smith¹ this was unacceptable. A FET input amplifier was preferred because, although the higher input impedance reduced the power gain, the noise performance was constant for a wide range of source impedances.

The same type of FET input amplifier is currently in use as the first stage amplifier for the radar. There appears to be no problem with insufficient signal to noise ratio and so these amplifiers were retained. The first stage amplifiers, or pre-amps, are

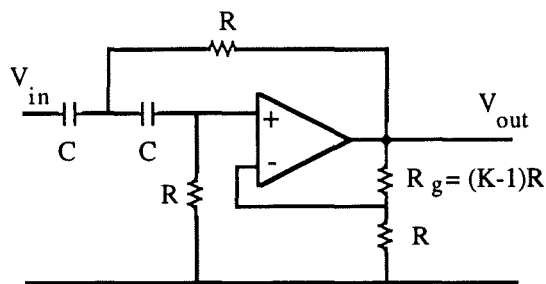
¹ G.M. Smith PhD Thesis, University of St. Andrews 1990.

AC coupled to remove the DC bias signal. The high pass roll-off is at 160Hz. Four amplifiers have been constructed with a nominal voltage gain of 50 and a bandwidth of 160Hz to several MHz. Purely by chance they form two matched pairs. One pair have a gain of 53 and input voltage noise of $16\text{nV}/\sqrt{\text{Hz}}$ The other pair have a gain of 54 and input voltage noise of $16\text{nV}/\sqrt{\text{Hz}}$.

5.1.3 Further Amplification and Signal Isolation.

The signal produced by these amplifiers is sufficient for short range targets : those in the lab.! Further amplification is required to detect more distant targets. The noise performance of these additional amplifiers is less critical than the first stage amplifiers. Further filtering is introduced at this stage to reduce the interference from unwanted signals and from noise. Two types of filter were employed : a wideband, fixed frequency band pass filter and a narrow band tunable band pass filter.

The fixed bandwidth filter consists of a 6-pole Butterworth high pass filter and a 2-pole Butterworth low pass filter. The designed cut-off frequencies are 4.8kHz and 2MHz respectively. The purpose of this filter is to remove signals at the ramp or modulation frequency. These signals are due to power fluctuations of the local oscillator during the modulation cycle. The use of a balanced pair of mixers would normally remove most of this AM noise, but this was not possible due to a mixer failure. Removing the AM noise of the local oscillator whilst retaining a wide passband allows the return signals to be viewed on a spectrum analyzer. The filter consists of three 2-pole sections. The circuit diagram for one section is shown in figure 5.2, along with a table of parameters for all sections. The high pass filter response is shown in figure 5.3.



Stage	K	R _g
1	1.068	680Ω
2	1.586	5.86kΩ
3	2.485	14.85kΩ

$$R = 10.0k\Omega \quad C = 3.3nF$$

Figure 5.2 6-Pole Butterworth Filter Design Showing Circuit for each Stage and Stage Dependent Resistor Values.

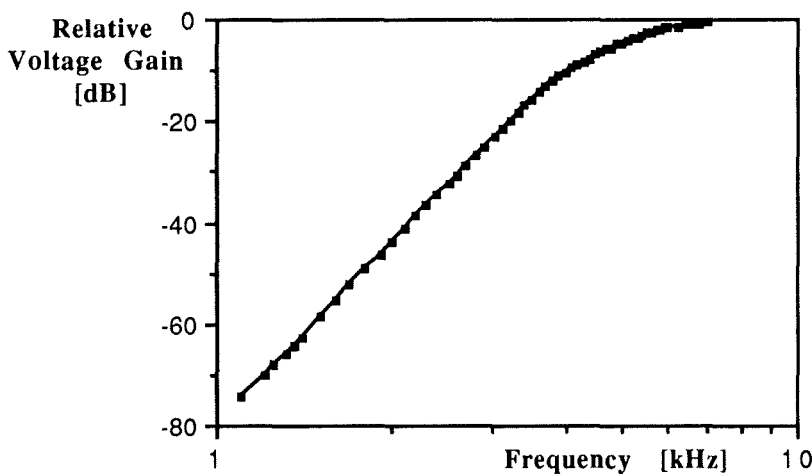


Figure 5.3 Frequency Response of 6-Pole High Pass Filter

The tunable filter consists of a switched capacitor filter based on the LMF100 universal filter IC from National Semiconductor. The second order bandpass filter has a fixed Q of 20, and unity gain at the centre frequency. The centre frequency is defined by the external clock frequency as

$$f_{\text{centre}} = \frac{\sqrt{2}}{50} f_{\text{clk}} \approx \frac{f_{\text{clk}}}{35} \quad 5.1$$

The outputs of the switched capacitor filter are passed through a low pass filter, cut-off at 48kHz, to prevent leakage of the clock. The inputs are filtered to prevent signals near the clock frequency from appearing in the pass band as aliases. These filters, and a maximum clock frequency of 2MHz limits the centre frequency to the range

$$5\text{kHz} < f_{\text{centre}} < 56\text{kHz} \quad 5.2$$

The purpose of this filter is to isolate the return from a single target, and to pass any Doppler components that may be present. The fixed Q of 10 gives a bandwidth of 500Hz at 5kHz and 5.6kHz at 56kHz. This filter allows the radar to be used with the single frequency measurement electronics that are described next.

5.2 Measurement of Return Signal.

The measurement of the two signals' frequency, amplitude and phase is averaged over a number of cycles of the return signal. The number of cycles is variable between 1 and 15, and is defined within the software as N. The number, N, is increased to maximize the accuracy of the measurement up to a limit imposed by the duration of the modulation ramp. As the return signal frequency 'collapses' through zero at the end of each ramp, the use of many RMS measurement ICs is ruled out. The analogue amplitude measurement circuit is physically separate from the digital phase and frequency circuits and so the two circuits shall be described separately.

5.2.1 Frequency and Phase Measurement.

For signal frequencies <100kHz period timing is more accurate than period counting as described in section 2.3.1.2. Although conceptually more elegant, frequency lock loops would face difficulties in this application with locking bandwidths and lock times. The range of return frequencies are comparable to the modulation frequency. At short ranges especially, there would be insufficient time for the loop to achieve lock before the signal was removed. Period timing is implemented by counting pulses of a 10MHz clock. This enables measurement of frequencies down to 153Hz with a 16-bit counter. Two counting channels are used and are designated Master and Slave. The signals from the mixers are amplified further, such that they start to clip, and then 'squared-up' to produce pulse trains. These are routed to the Master and Slave channels by some switching logic. The switching logic ensures that if only one signal is present it is always routed to the Master channel. Counting on both channels is started simultaneously by a positive edge on the Master channel. Counting on the Master channel is stopped by another positive edge on the Master channel and provides the period measurement. Counting on the Slave channel is stopped by a positive edge on the Slave channel. This count measures the time delay between the two channels and hence, with the period, provides the phase difference. The counters are not cleared until the end of the Nth cycle. This produces a cumulative count and hence an average value of the period and time delay. At the end of the Nth period, the valid counts are clocked into output registers. The counters can then be cleared and the logic that measures N is reset. This process takes 5 clock cycles and so for continuous operation, with a 10MHz

clock, the maximum frequency that can be measured is 2MHz. Some of the control lines, from the logic that measures N , are used to control the amplitude measurement circuit. A schematic of the counter circuit is shown in figure 5.4, and a full circuit diagram is given in figure 5.5. Initially there were three Slave channels to enable two further phase measurements to be made. These signals came from the extra ports used in the Doppler radar of figure 2.12. This system was more complex both optically and electronically and provided less information. This was the main reason for choosing the FM version of the radar.

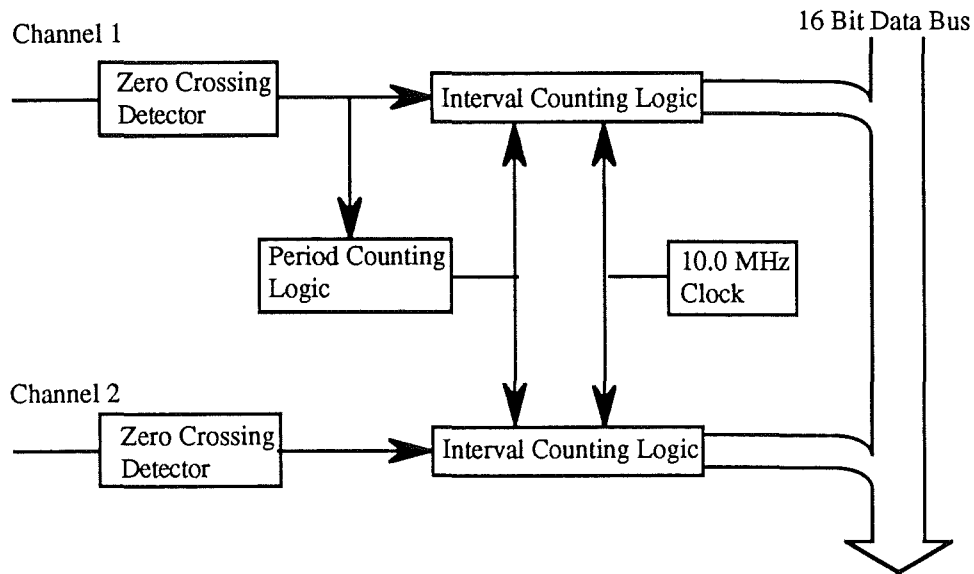


Figure 5.4 Schematic of Counter Circuit.

The two 16-bit output registers from the Master and Slave channels are multiplexed onto an 8-bit data bus and accessed via some interfacing logic described later.

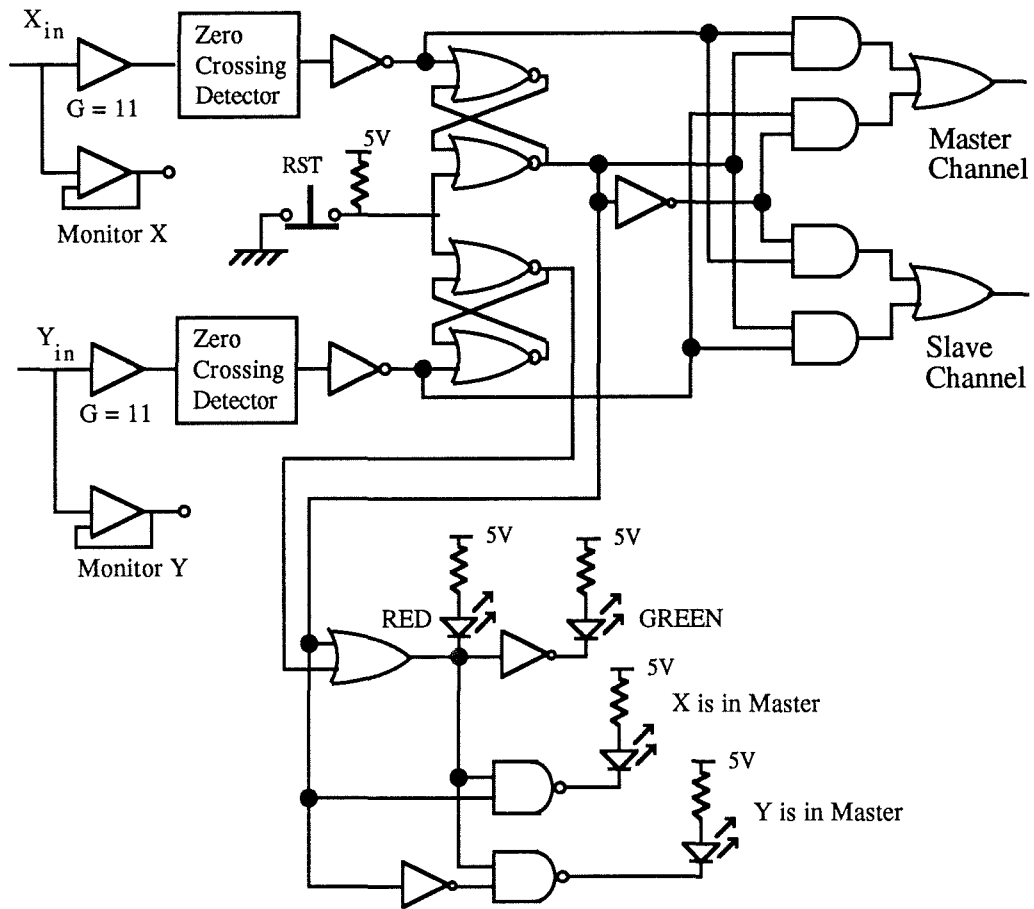


Figure 5.5a Input Buffer and Switching Logic for Counter Board.

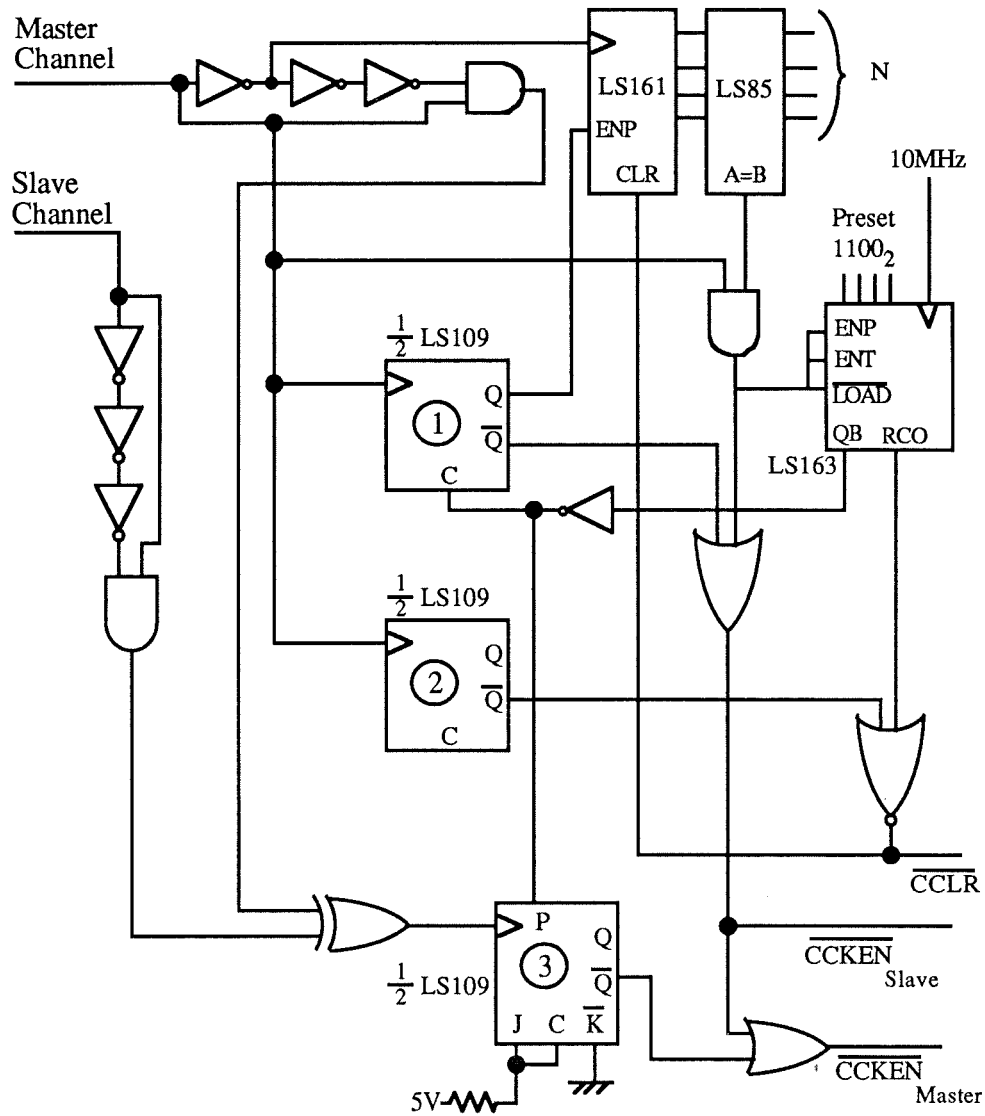


Figure 5.5b Frequency and Phase Measurement Circuits for Counter Board.

5.2.2 Amplitude Measurement.

The amplitudes of the two return signals are measured separately by a pair of identical circuits. Each circuit contains a precision rectifier, an integrator and an ADC. The amplitude comparison is performed in software.

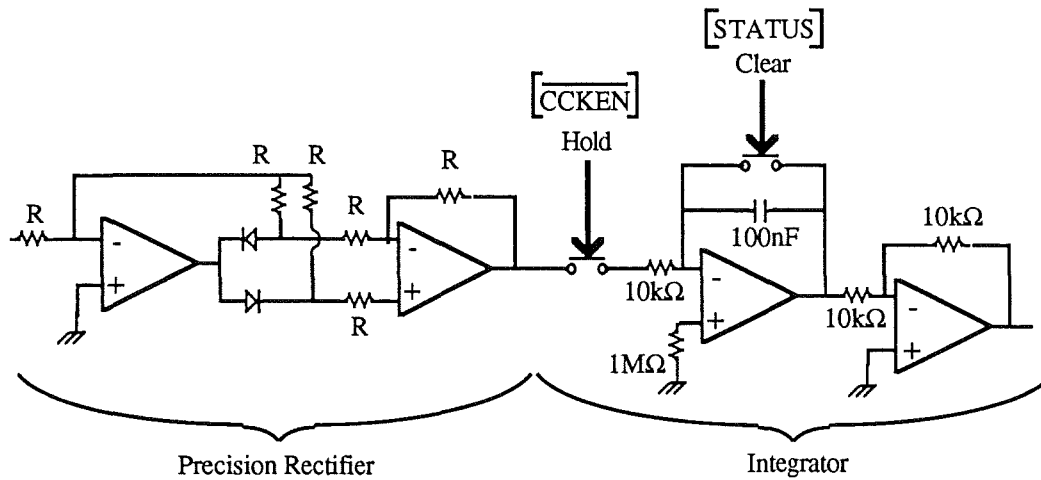


Figure 5.6 Precision Rectifier and Integrator Circuits.

A precision rectifier is used to remove the diode-drop offset voltage present in conventional rectifiers. For small signals this offset can produce significant errors in the ratio of the two amplitudes. The precision rectifier takes advantage of the feedback current of an inverting op-amp. The rectifier, shown in figure 5.6, consists of two amplifiers. The first contains two feedback arms. The diodes in the feedback arms ensure that one arm provides the feedback current for positive inputs and the other provides the current for negative inputs. As it is the feedback *current* that determines the gain, in an inverting configuration, the voltage across the feedback resistor is a half-wave rectified version of the input signal. The diode-drop has been accommodated by the output sitting ~half a Volt above or below the resistor voltage. The second amplifier takes the difference of the half-wave signals to produce a full-wave rectified output. The first amplifier is required to switch its output by two diode-drops in a very short time as the input crosses zero. A high slew rate op-amp is therefore required to reduce distortion especially at high frequencies.

The integration circuit, shown in figure 5.6, uses an op-amp in a conventional integrator configuration, and two analogue switches. The switches are controlled by control lines originating on the counter circuit. The series switch provides a HOLD function, controlled by the clock enable of the Master counter ($\overline{\text{CCKEN}}$), and is for isolating the integrator from the input signal. The switch across the capacitor provides a CLEAR function and is closed at the end of a conversion on the ADC. The HOLD switch is closed to allow integration for the same period that the frequency is measured.

At the end of this period all counters are disabled and the HOLD switch is opened. Conversion is started on the next positive edge of the ADC clock. The STATUS pin on the ADC is pulsed low when the conversion is complete, and this is used to close the CLEAR switch and reset the integrator. The STATUS pin on the ADC does not stay low long enough to allow the capacitor to fully discharge through the switch's ON resistance of 25Ω . The STATUS pin is therefore used to trigger a monostable that provides a suitable $10\mu\text{s}$ pulse.

The ADCs have a conversion time of $5\mu\text{s}$. This allows measurements to be taken at 200kHz or 200 times during the 1ms ramp time. As only one conversion per ramp is required this conversion time is more than adequate. Multiple conversions could be used to provide both an average amplitude and an idea of the temporal variation during the ramp. The temporal variation is not considered important in this application and so an average amplitude was obtained by integrating over several cycles. The ADCs each provide an 8-bit data word that is multiplexed onto the same data bus as the counters.

5.2.3 Interfacing to the Archimedes.

There are six data words to be read during each ramp for a full data set : two 16bit counter words [high byte,low byte] and two 8-bit ADC words. Four bits of data need to be sent to determine N. These two tasks are performed by a separate interfacing circuit. This circuit is to be controlled and accessed by an Archimedes using an external VIA[Versatile Interface Adaptor] card¹. The VIA card simplifies much of the address decoding and data formatting for the Archimedes. The VIA provides two 8-line input/output ports named Port A and Port B. Port B is to become the data bus and Port A the address bus. Only the top 3 bit of Port A are required to address the six registers containing data and the one register containing N. The 8-bit data bus is connected to Port B. A set of four latches is also connected to the data bus, and these are used to store N. A schematic of the interfacing circuit is shown in figure 5.7.

¹ The DACS system. A.R. Harvey. PhD Thesis, University of St. Andrews 1990.

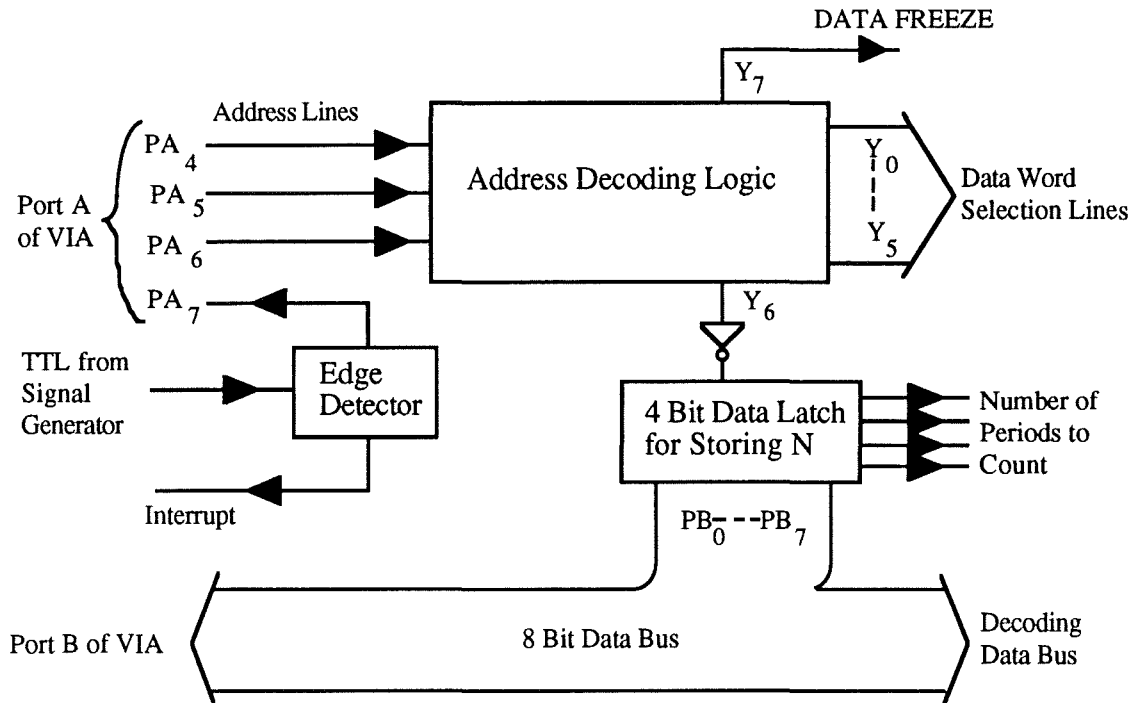


Figure 5.7 Schematic of Interfacing Board

Decoding of the three address lines, PA₄ to PA₆, is achieved using a 3-to-8 line decoder [LS138]. Six of the outputs are connected to the output enables of the six output registers to allow their contents to be placed on the data bus. One output is used to latch data into the data latches that contain N. The remaining output is used to enable all data taking processes. When this output is not selected the data in the counters is frozen and no more conversions are allowed to start. Using the last output in this way ensures that data is frozen in all registers during a read operation.

The top pin of Port A, PA₇, is configured as an input, and connected to the TTL output of a signal generator. The triangular wave output of the signal generator provides the FM ramp for the main oscillator, and the TTL output can therefore be used to define whether the frequency is ramping up or down.

A period of dead time is required at the start of each ramp to allow for data to settle. Physically this is the time required for a transmitted signal to reach the target and return to the receiver. For most targets at ranges of ~100m, a few μ s delay is sufficient. Initially this dead time was timed in hardware and the control line used to disable the counters etc. This produced some spurious results due to the data reading process. When the ADC data is read the STATUS line is reset to a high state. This asynchronous resetting of the STATUS caused spurious clearing of the integrators and the counters. The delay is now implemented in software as part of the data reading

routine. The start of each ramp signals an interrupt in the computer. The data from the previous ramp is read in, which causes new data to be inhibited. On completion of the read process the counters are enabled to allow the registers to be updated. This reading process provides the delay at the start of each ramp.

5.3 System Master Oscillator.

The master oscillator for the radar consists of a Gunn Effect diode mounted in a resonant cavity. The details of this mounting cavity are covered briefly in chapter 3. Three oscillators were investigated as possible master oscillators : two at 140GHz and one at 94GHz. A lack of power at 140GHz, in addition to a lack of measurement equipment, prevented much investigation at this frequency. Effort was therefore concentrated at 94GHz.

5.3.1 Frequency and Power Characteristics.

The variations of frequency and output power, as a function of bias voltage, are dependent on the way in which the oscillator has been set up. Setting up an oscillator involves selecting the required waveguide and co-axial cavity sizes to suit the required frequency range, mounting the chosen diode and optimizing the matching structure. The construction of the block is by no means trivial, but standard sizes have evolved for common applications. Optimizing the matching structure means adjusting the dimensions of the co-axial centre conductor (*the post*) and a radial transmission line (*the cap*) to match the low diode impedance to the higher waveguide impedance at the second harmonic frequency. This is a frustrating task and at the best of times mind-numbingly boring, as each diode is different. The design and analysis of this matching structure has been carried out by Smith¹, based on the work of Carlstrom². I am indebted to Graham Smith for taking much of the blackness out of this art.

¹ G.M. Smith PhD Thesis, University of St. Andrews 1990.

² J.E. Carlstrom et al. "A continuously Tunable 65-115GHz Gunn Oscillator" IEEE Trans. MTT Vol MTT-33 No.7 July 1985 p610.

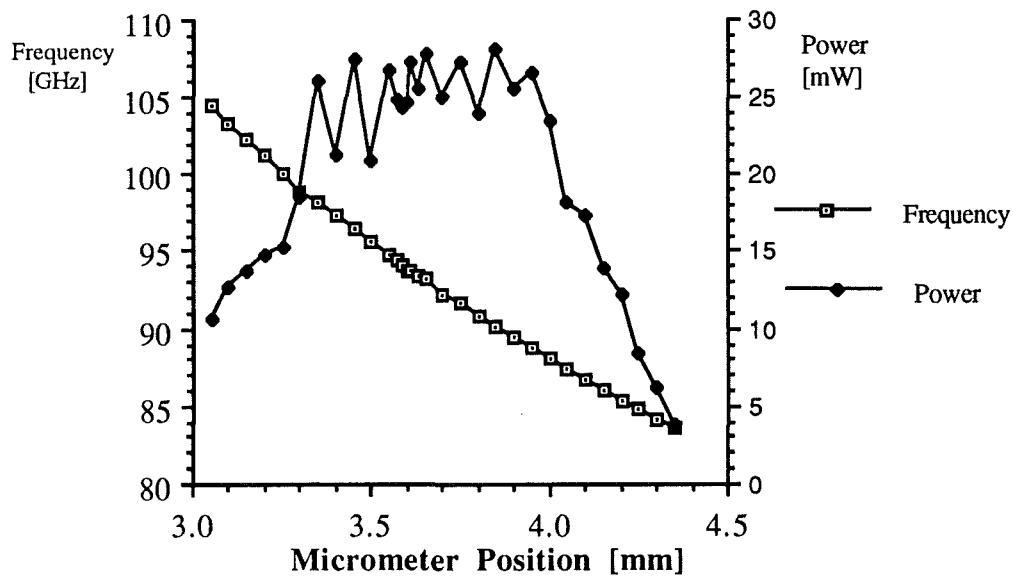


Figure 5.8 Tuning Curve for 94GHz Master Oscillator

Figure 5.8 shows the variation of output power and frequency with the position of the tuning micrometer for the 94GHz Master oscillator. The tuning range of ~20GHz is typical for central frequencies around 90GHz to 100GHz. The peak in power and smooth frequency tuning are also typical for a well set up oscillator. The variations in power around the central maximum are most likely due to standing waves in the measurement set up.

The measurement procedure consists of maximizing the power for a given micrometer setting, by varying the bias voltage and the backshort position. The frequency and the maximum power are then recorded. The bias voltage was limited, for diode preservation, to 10.08V. At this voltage an over voltage protection diode in the oscillator power supply begins to draw significant current. The output power is often still increasing with increasing bias voltage when this self imposed bias limit is reached.

Figure 5.9 shows similar curves for two 140GHz oscillators. The power readings obtained in figure 5.9, were obtained, for block 1.

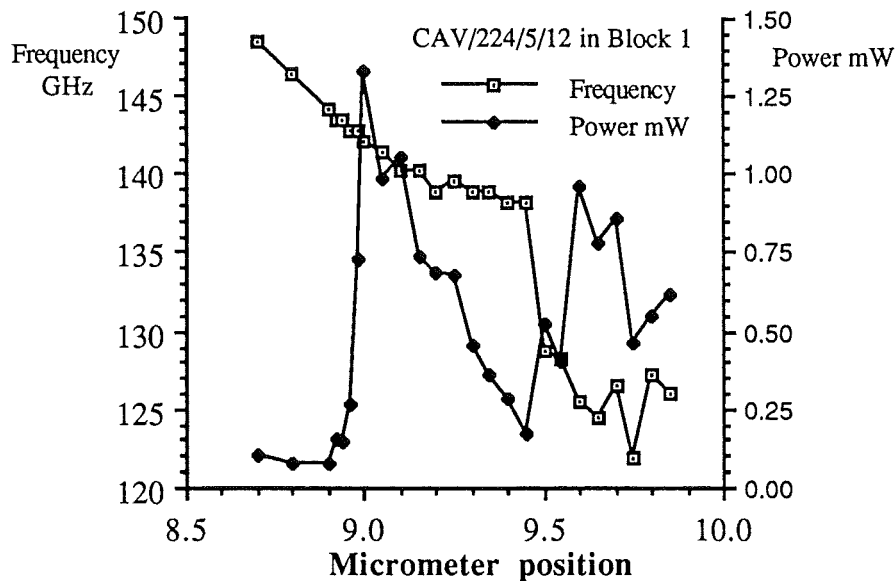


Figure 5.9 Tuning Curve of 140GHz Master Oscillator

The variations of frequency and output power as a function of bias voltage, are shown in figure 5.10 for three micrometer positions of the 94GHz oscillator. In each case the bias and backshort are adjusted to give maximum output power as before. The frequency and output power are then recorded as a function of bias voltage only. Figure 5.10b shows a tuning curve well suited to linear frequency modulation. Modulation of the bias between 9.2V and 9.8V produces ~240MHz of linear frequency variation and very little power variation. The curves are taken in static conditions which, as mentioned above, may differ from the dynamic curve when modulating at ~1kHz.

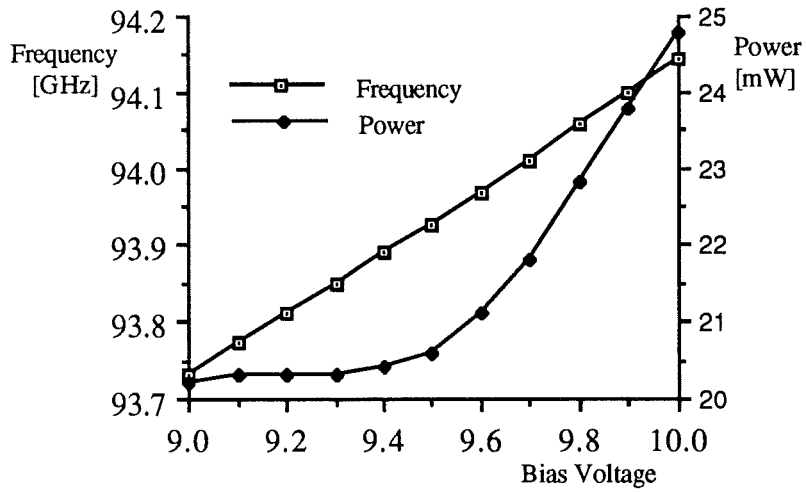


Figure 5.10a Bias tuning of 94GHz Master Oscillator
Choke=3.585mm Backshort=2.82

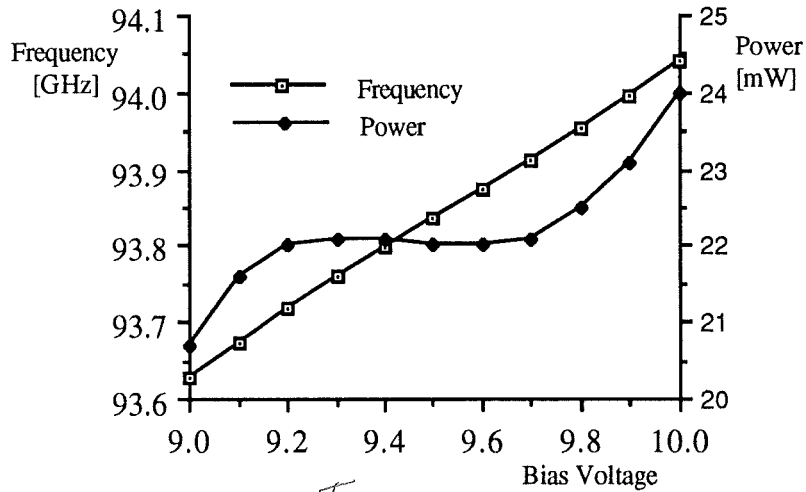


Figure 5.10b Bias tuning of 94GHz Master Oscillator
Choke=3.59mm Backshort=2.87

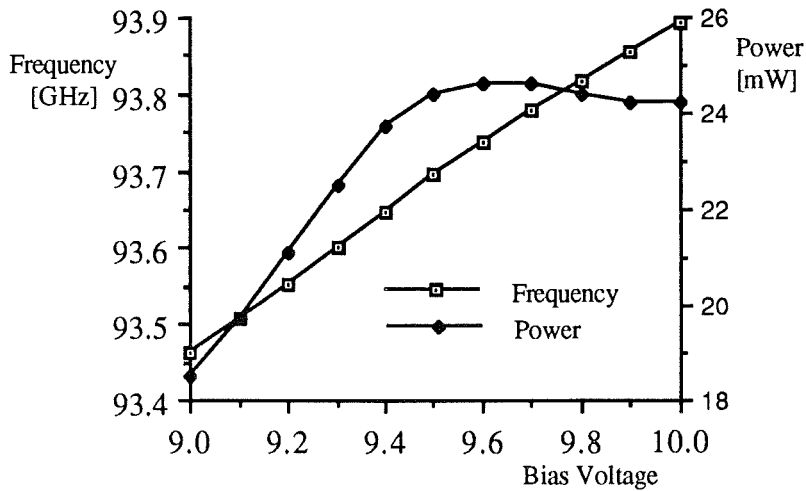


Figure 5.10c Bias Tuning of 94GHz Master Oscillator
Choke=3.6mm Backshort=2.79

5.3.2 Frequency Modulation.

For a given range, the beat frequency is a measure of the average slope of the frequency modulation curve. Provided that the temporal variations of the modulation curve occur over periods much longer than the delay time, this slope approximates the differential of the modulation curve.

$$f_{\text{beat}} = F(t) - F(t - \tau) \approx \tau \frac{dF(t)}{dt} \quad 5.3$$

If $F(t)$ is linear then $\frac{dF}{dt}$ is a constant and needs only to be evaluated once. For any other function, $\frac{dF}{dt}$ is also a function of time and needs to be determined for each frequency measurement to allow τ to be determined. It is not always possible to determine $\frac{dF}{dt}$ accurately due to heating effects in Gunn diodes. The measured bias tuning curve is obtained under static conditions : ample time is available before each measurement is taken to allow thermal equilibrium to be reached in the diode. In normal use the bias variations may occur over shorter times, preventing thermal equilibrium from being reached. In this dynamic situation the frequency and power output of a diode, at a given voltage, may differ from the static situation.

Using $\frac{dF(t)}{dt}$, and the time during the ramp that the measurement is taken, t , the time delay can be evaluated as

$$\tau = \frac{f_{\text{beat}}(t)}{\left[\frac{dF(t)}{dt} \right]} \quad 5.4$$

If f_{beat} is measured as a function of time during the ramp, it is possible to deduce the shape of $\frac{dF}{dt}$ by making sufficient independent measurements. To reduce the amount of computation, and to reduce the burden on the decoding electronics, the use of linear modulation is preferred. The use of a small modulation range, $\sim 100\text{MHz}$, produces a linear modulation curve when measured statically. It is assumed that the dynamic tuning curve is not significantly different for this small range of modulation.

Modulation of the bias supplied to the diode produces frequency modulation by virtue of the diode's inherent varactance. Modulating this way also produces power variations which are generally to be avoided. The power variations produce AM fluctuations in the local oscillator which can cause spurious frequency components to appear in the IF. As mentioned above, filtering has been employed to reduce this effect.

Methods for the linearization of frequency modulation waveforms have been the subject of previous work at St. Andrews¹ and is currently receiving further attention². The method centres around varying the shape of the modulation waveform to produce a linear frequency sweep. This is a non-active form of sweep linearization. Active methods of sweep linearization require the modulated frequency to be monitored. Deviations from linear behaviour can then be used to change the bias voltage accordingly. The voltage-frequency tuning characteristic allows the Gunn oscillator to be used as the Voltage Controlled Oscillator (VCO) in a lock loop. The beat frequency obtained from a fixed reference target should be constant for a linear ramp. The variation of the actual beat frequency from the expected frequency can be used to pull the oscillator into lock.

One method of producing a control voltage from the frequency difference is to phase detect using the actual frequency and a reference source at the required frequency. A drawback with this method is that only a few cycles of the intermediate frequency (IF) may occur during the ramp time. This makes it difficult for the loop to achieve lock within the duration of the ramp and still allow time for measurement of the unknown return signal. The use of a higher IF eases this problem, but complicates the positioning of the reference target which is now further away and more likely to interfere with real targets.

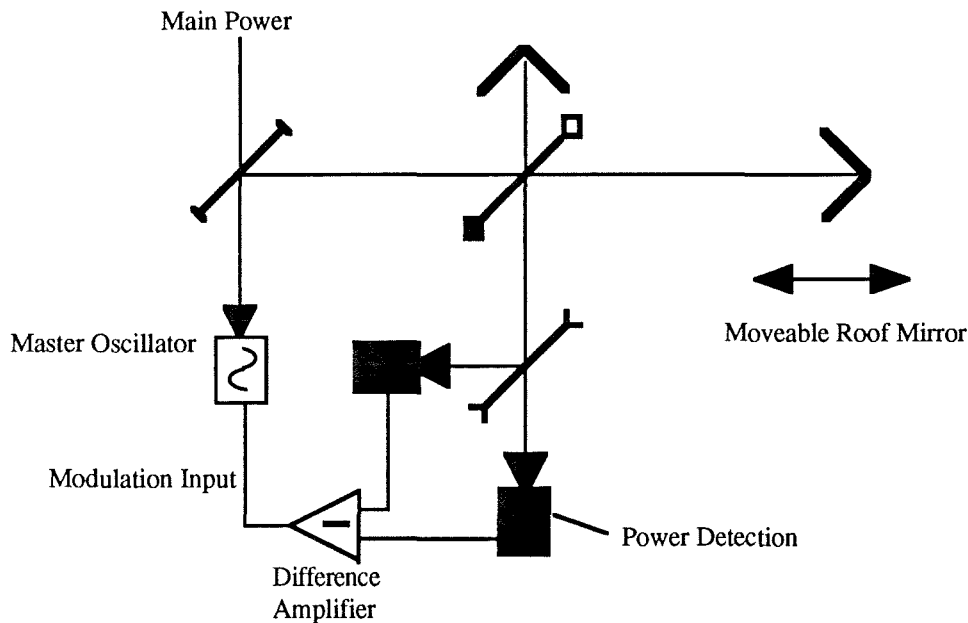


Figure 5.11 An Optical FM Linearization Method

¹ A.R. Harvey Private Communication.

² D.A. Robertson Private Communication.

The quasi-optical circuit of figure 5.11 provides a means for sweep linearization at the signal frequency. The long arm of the interferometer provides the reference target and the short arm provides the local oscillator. The path difference is arranged to be an integer number of wavelengths at the start frequency of the ramp. The two detectors therefore see equal power and the output of the difference amplifier is zero. Offsetting one mirror produces an imbalance of power at the detectors since the polarization state at the vertical wire polarizer has changed. This imbalance produces a non-zero voltage at the output of the difference amplifier which changes the output frequency of the oscillator. When the oscillator frequency is such that the new path difference is an integer number of the new wavelength, the power balance is restored and the oscillator is locked to the new frequency. Strictly speaking the control voltage would return to zero if the path difference was exactly an integer number of new wavelengths. The frequency actually stabilizes at a value where there is sufficient imbalance to produce the necessary control voltage. For a control loop with a very large gain : large voltage swings for a small power imbalance, the frequency reached by the oscillator will be very close to the ideal frequency, and the oscillator will track the mirror position. Linearly sweeping the position of the mirror produces linear wavelength modulation which is a very good approximation to linear frequency modulation for small frequency deviations at ~100GHz. Frequency sweeps with a linearity of better than 1% over a range of 1GHz can be achieved using this method.

Modulation of the source with a 1kHz triangular wave is well within the capabilities of the oscillator power supply. Modulation frequencies up to 20MHz are possible with suitable power supplies¹. The maximum and minimum ranges for a modulation frequency of 1kHz and a modulation range of 240MHz are given by equations 2.19 and 2.20 respectively as

$$R_{\max} = 75\text{km} \quad 5.5$$

$$R_{\min} = 62.5\text{cm} \quad 5.6$$

The range is related to the beat frequency, using equation 2.17, by

$$\text{Range}[\text{m}] = 0.313 \times f_{\text{beat}}[\text{kHz}] \quad 5.7$$

Having a maximum beat frequency of ~1MHz, imposed by analogue gain and bandwidth requirements, prevents detection of targets beyond ~313m. By reducing the modulation range to 150MHz, and modulating with a 500Hz triangular wave (1ms ramp time) the minimum range is only increased to 1m, and the range is then given by

$$\text{Range}[\text{m}] \approx f_{\text{beat}}[\text{kHz}] \quad 5.8$$

¹ D.A. Robertson Private Communication.

5.4 Detection of Signals in Noise and Clutter.

There are two main mechanisms by which a return signal may be rendered undetectable. The first is the degradation of signal to noise ratio by a combination of path loss and receiver noise. The second is the masking of an otherwise detectable signal by spurious reflections from clutter. In the IF these two mechanisms manifest themselves in much the same way : the signal power is not detectable above the background power. Consider initially the first mechanism.

5.4.1 Receiver Noise Performance.

The path losses to and from a target are not generally known or adjustable. The ability of a receiver to detect a small signal is therefore determined by the receiver's noise performance. As with an amplifier, the amount of noise produced by a receiver is measured at the output as a power level over a given bandwidth. The actual meaning of the output and the frequency band needs to be defined, but the principle is much the same. The difficulty with a receiver is knowing how to refer the noise power back to the input. The receiver analogue of voltage or current gain is conversion gain. This is the efficiency at which the incident RF power is converted to IF power. For a mixer diode alone, this gain is always a loss. Various pre-amps, however, are often included in the definition of the receiver. The overall conversion gain is then greater than unity. Once referred to the input, the noise power is expressed as a power source for use with an ideal receiver. The most common method of representing a source of noise power is a black body radiator at a given temperature. The amount of noise power produced by a black body is well known to be

$$P = 2kTB \quad 5.9$$

where k is Boltzmann's Constant, B is the frequency bandwidth and T is the absolute temperature. Many mixers and detectors are only sensitive to one polarization state, as they are often waveguide mounted. Half of the power given in equation 5.9 appears in each polarization state.

The bandwidth of the receiver is usually set by the IF amplifiers, and needs to be known when the output noise power is first measured. The noise produced within the receiver can therefore be represented solely by a noise temperature.

An ideal receiver, consisting of a mixer, IF amplifiers and a bandpass filter, converts RF power to IF power which appears at the output as an r.m.s. voltage. For an external black body source at temperature T_s , this voltage is given by

$$V = kT_s BGA \quad 5.10$$

where G is the conversion gain [Volts per Watt] and A is the amplifier voltage gain.

The noise produced in a real receiver can be added as an extra thermal source at temperature T_N . The output of the receiver is now

$$V = k(T_s + T_N)BGA \quad 5.11$$

There are two unknowns in equation 5.11 : T_N and G . It is assumed that the gain, A , of the IF amplifiers can readily be measured as can the temperature of the external source T_s . Measuring V for two external thermal sources T_{s1} and T_{s2} , produces a pair of simultaneous equations from which T_N and G are determined as

$$T_N = \frac{(V_2 T_{s1} - V_1 T_{s2})}{(V_1 - V_2)} \quad 5.12$$

$$G = \frac{(V_1 - V_2)}{kBA(T_{s1} - T_{s2})} \quad 5.13$$

When the receiver is used with a local oscillator, as is most often the case, some other concepts have to be introduced. Firstly, the local oscillator produces amplification of the unknown signal thus changing the effective conversion gain. Secondly, the local oscillator produces its own noise which appears in the IF. Thirdly, the concept of sidebands needs to be introduced. Mixing with a local oscillator causes the frequency bands either side of the local oscillator to overlap when they appear in the IF. Care must be taken, when referring noise back to the input, in defining where in the frequency band to put the noise source. This becomes apparent in the next section.

The output noise voltage can be measured, using a local oscillator, for two known thermal sources. The two noise voltages can then be substituted into equations 5.12 and 5.13 to give a noise temperature and a conversion gain as before. The power from the known sources is contained in both sidebands of the local oscillator and so it is sensible to distribute the noise source in the same way. The noise temperature T_N , given by equation 5.12, is therefore known as the Double Side Band (DSB) receiver noise temperature.

When the signals of interest all appear in one sideband of the local oscillator, the other sideband is filtered out. The use of a Single Side Band (SSB) filter in this way, removes unwanted signals and unwanted noise from the other sideband. Placing a SSB filter at the input of a receiver does not alter the amount of noise produced by the

receiver. It is often convenient, however, to refer the receiver noise to the front of the SSB filter so that it can be added to the unknown signal easily. A SSB filter has a gain of $\frac{1}{2}$ as far as the noise source is concerned. When the receiver noise is referred to the input of a SSB filter, the figure quoted is $2T_N$, and is known as the SSB receiver noise temperature.

The DSB noise temperature is quoted most as it is a smaller number and makes the performance look better! Another figure, often quoted by diode manufacturers, is the mixer noise temperature. This is a smaller number still, as it represents only the noise generated by the diode. The effects of any necessary pre-amps have been removed from this figure, and need to be replaced to produce the noise performance of a real system. The mixer noise temperature is a convenient method for comparing one diode against another as it is independent of the amplifier performance. It is important, when quoting noise temperatures, to compare like with like, especially regarding SSB and DSB noise temperatures. SSB and DSB noise temperatures are merely different ways of representing the same amount of noise.

In the above treatment, the local oscillator has been assumed to be ideal. In general this is not the case, as the local oscillator will produce some AM noise. This noise will add to the receiver noise and hence increase the measured output noise. This can be treated in two ways. Firstly the receiver noise can be measured with and without a local oscillator. The contribution from the local oscillator can then be deduced. Secondly, the receiver noise temperature can be measured with the local oscillator and quoted as an equivalent or effective noise temperature under conditions of normal use. The latter method gives the more useful figure, but is dependent on the local oscillator. The former method is an attempt to separate receiver and local oscillator contributions, but ignores the amplifying effect of the local oscillator. You pay your money and take your choice.

The set up for measuring the noise temperature is shown in figure 5.12. The sensitivities of the two mixers are adjusted to minimize the effect of local oscillator power variations. The local oscillator is modulated to produce some sideband power which appears as power in the IF. The mixers are adjusted to null the output of the differential amplifier. This gives maximum rejection of local oscillator AM noise. The noise voltage at the amplifier output is converted to a DC level by the rectifying circuit. This does not produce a true r.m.s. reading but is proportional to the true r.m.s. Integration of the half-wave rectified signal produces an output that is smaller than the true r.m.s. by a factor of $\frac{\sqrt{2}}{\pi}$ or roughly $\frac{1}{2}$. The integration time of the RC network is several seconds. It is not necessary to know the gains of the amplifiers and the rectifier circuit in order to evaluate T_N . These gains would need to be measured to determine G .

The output of the integrator was sampled continuously by an ADC linked to an Acorn Archimedes™. Using a program called ADCread¹ the voltage can be measured a number of times and some statistics generated. The computer takes 600 measurements of the voltage. Each measurement is itself the mean of 100 samples, although no statistical data is available on the spread of these 100 samples. The 600 measurements are used to produce a mean and standard deviation, from which the standard error is calculated. A set of 600 measurements was made several times, usually 10, for both the hot and the cold loads. These were combined to produce a single output voltage for each load.

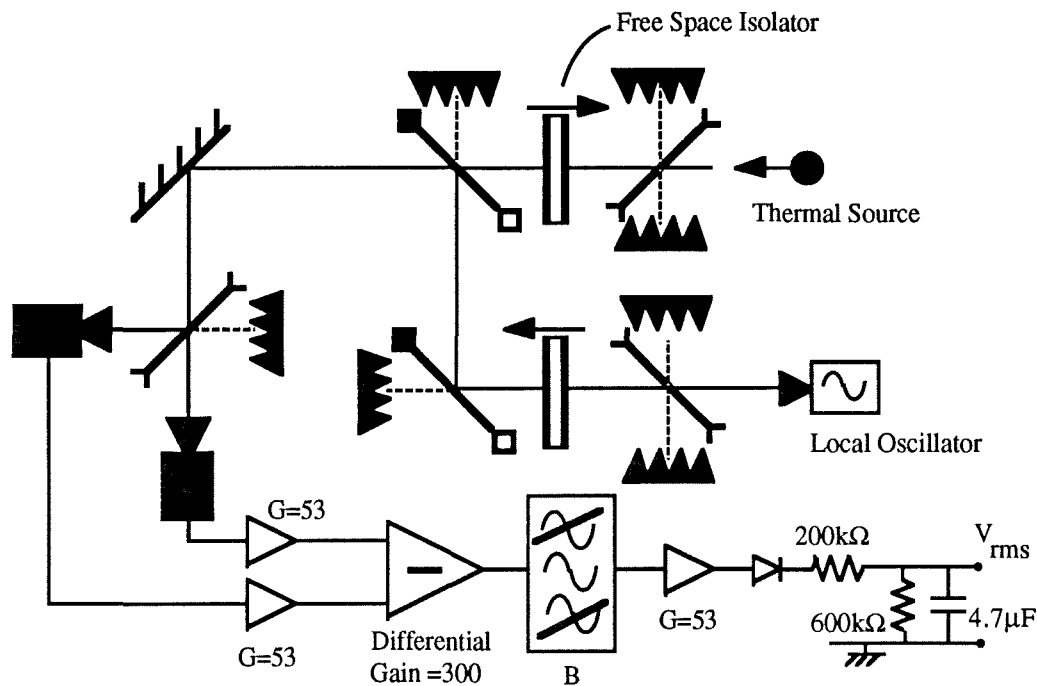


Figure 5.12 Receiver Noise Temperature Measurement Set-Up

The two known thermal sources are both made of an absorbing material, Eccosorb™. One is left at room temperature (290K) and the other is cooled to 77K using liquid Nitrogen. The cold load was left in a polystyrene bucket containing the liquid Nitrogen, and viewed through the bucket wall. The attenuation due to the bucket is negligible.

¹ A.R. Harvey PhD Thesis, University of St. Andrews. 1990.

Several attempts were made to determine the noise temperature in this way and are summarized in the following table.

Expt. No.	$V_{\text{hot}}(\text{arbs})$	$V_{\text{cold}}(\text{arbs})$	$T_N \text{ 'K}$
1	2540 ± 5.3	2530 ± 6.1	45900
2	2490 ± 16.7	2478 ± 5.4	33400
3	3500 ± 34.5	3490 ± 9.1	47200
4	3482 ± 10.0	3470 ± 6.0	70400

Figure 5.13 Summary of Noise Temperature Measurement Attempts

The accuracy stated in the above table reflects the stability of the voltages being measured. The calculated errors in T_N are larger than 100%, This shows that the errors in V are too large and that V is not stable enough to determine T_N in this way. Several experiments produced a value for V_{cold} that was greater than V_{hot} which is confirmation that all is not well. The reason for stating the above inconclusive results is to demonstrate the inability to determine the noise temperature by the conventional experimental route. This is a clear sign that the actual noise temperature is far greater than originally expected.

There are several possible reasons for the uncertainty in these results:

- 1 T_N is actually much larger than $\sim 100,000\text{K}$ and changes of $\sim 200\text{K}$ on top of this are not detectable.
- 2 The VSWR of the detector+horn is large such that little local oscillator and signal power enters the mixer. This would reduce conversion gains and thereby increase the effective noise temperature.
- 3 Reflections from the detectors are again reflected by the thermal source and pump the local oscillator. This would cause variations in the conversion gain that were dependent of the position of the source and that varied between the hot and cold loads.

The effects of 1,2 and 3 are inter-related. Isolation was introduced between the thermal source and the rest of the measurement system. Experiment 1 is with no isolation and experiments 2,3 and 4 are without. It can be seen that this had little, if any, effect.

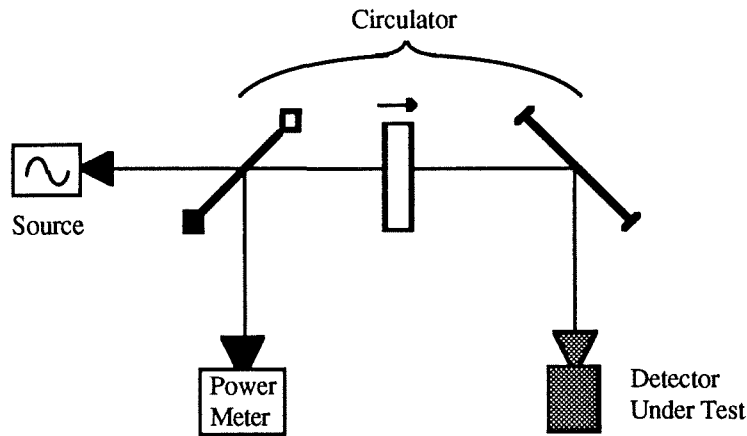


Figure 5.14 Optical Circuit for Measurement of VSWR

The VSWR of the detector was measured using the circuit shown in figure 5.14. The power reflected from the detector was compared with the power reflected by a mirror and an absorbing load. This enables the incident power to be determined and the system losses removed. The same experiment was carried out with the horn on its own. The power reflected when the wave guide was terminated with a short and a matched load was also measured. This enables the horn loss to be determined. The power reflected from the mirror varied with the mirror position. Several peaks and troughs were observed as the position was continuously varied. These are due to interference between the power reflected from the mirror and the power reflected within the system. The underlying trend shows a maximum in the reflected power as the mirror position coincides with the beam waist.

The horn and detector together had a VSWR of 1.74. The horn by itself had a VSWR of 1.46 and ohmic losses of 35.7% of incident power. The combination of reflection and ohmic losses gives the power transmission as 60.8% or -2.16dB.

It is not possible to easily combine the two VSWR values to obtain a VSWR of the detector. The phase of the reflections would need to be known as it is possible that reflections from the horn and from the detector cancel to some extent thereby increasing the power coupling.

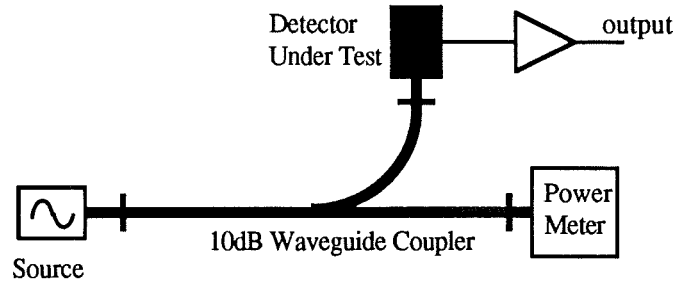


Figure 5.15 A Method of Measuring Noise Temperature.

An alternative method was used for measuring the noise temperature. The experimental set up is shown in figure 5.15. The local oscillator power falling on the detector is monitored by the power meter. When the local oscillator power is varied, the sideband power appears in the IF. When the degree of modulation is known, the measured IF power can be used to determine the conversion gain. Modulation with a sine wave is ideal as the side band content is well known. The variation of output power with modulation was not linear, however, and so a square wave modulation was used. This essentially steps the local oscillator power between two known power levels. The difference in these power levels was measured as 0.08mW or -10.97dBm. The power in the IF side band was measured using a spectrum analyzer to be +6.3dBm in the 10kHz side band and -3.4dBm in the 30kHz side band. There were several other side bands present due to the square wave modulation and also to frequency modulation. These were all observed to be more than 15dB below the first side band and were therefore ignored. The total IF power was therefore taken as 6.7dBm or 4.7mW. By removing the power gain of the amplifier, =34.5dB, the conversion gain is given by

$$G = \frac{P_{out}}{P_{in}} = 6.7\text{dBm} - 34.5\text{dB} - -10.97\text{dBm} = -16.83\text{dB} \quad 5.14$$

At 400kHz the system output noise is -102dBm/Hz. This is referred to the input using the amplifier and conversion gains, and is written as

$$P_{noise} = -102\text{dBm/Hz} - 34.5\text{dB} + 16.83\text{dB} = -119.67\text{dBm/Hz} \quad 5.15$$

This noise can be represented by a mythical thermal source at the mixer input. As the power spectrum extends either side of the local oscillator, the mixed down contribution will be the sum of the two sidebands. T_N is therefore given by

$$T_N = \frac{P_{noise}}{2k} = 39 \times 10^6 \text{ K} \quad 5.16$$

and is known as the Double Side Band (DSB) receiver noise temperature.

This value is larger than expected : typical noise temperatures are $\sim 10,000\text{K}$. The conversion gain of -16.83dB is typical and the amplifier performance is reasonable though not excellent. The voltage noise of the amplifier, referred to the input, is $16\text{nV}/\sqrt{\text{Hz}}$. This is for a source impedance of 0Ω to $2.7\text{k}\Omega$. The source impedance of the diode is likely to be \sim few hundred Ω and so the amplifier noise will be similar to $16\text{nV}/\sqrt{\text{Hz}}$. This implies that the amplifier contributes about a quarter (0.23) of the noise power that is measured at its output. The remaining output power is amplified mixer noise. This gives the mixer a noise temperature of $1.3 \times 10^6\text{K}$. This is the temperature of a mythical thermal source at the *output* of an ideal mixer, and hence is not side band dependent.

5.4.2 Phase Noise and Clutter Rejection.

Frequency modulation provides a means for measuring range in a CW radar. The range resolution is therefore related to the frequency resolution in the IF. For the radar described here, the duration of the modulating ramp is $\sim 1\text{ms}$ which means that at best the beat frequency is only stable for this time. Larger ranges reduce the available measurement time, see figure 2.6, and hence increase the measurement bandwidth. If the IF detection system were to consist of a filter bank, the width, and hence spacing, of each filter would be $\sim 1\text{kHz}$. Narrower filters would it seems increase the resolution but this is wrong for two related reasons. Firstly, the beat frequency at the IF filter has a modulation envelope imposed by the 1ms ramp time. This increases the spectral width of even the purest sinusoid to $\sim 1\text{kHz}$. Such a beat frequency would excite several IF filters. Secondly, the spectral width of each filter is inversely related to its response time. A 1Hz filter, for example, takes about a second to respond to a signal applied to its input. The beat frequency will have changed significantly during this time, or even vanished. The same arguments can be applied to the IF detection method described above. In order for the counting circuit to operate well, the beat signal is filtered by a tunable bandpass filter. The width of this filter defines the measurement bandwidth. for this radar, a switched capacitor filter is used as a tunable bandpass filter with a Q of 20. The fixed Q means that the measurement bandwidth depends on the beat frequency.

The range resolution is determined, from the above arguments, by the ability to measure and resolve beat frequencies from adjacent targets. This ability is determined by the width of the measurement bandwidth and the frequency stability of the beat frequency. The frequency stability is itself determined by the phase or frequency noise of the transmitter and on the linearity of the sweep.

The question of resolution can be posed in terms of detection of a small target in the vicinity of many other targets of a similar range. This is the problem of detection of targets in clutter. Consider the situation shown in figure 5.16.

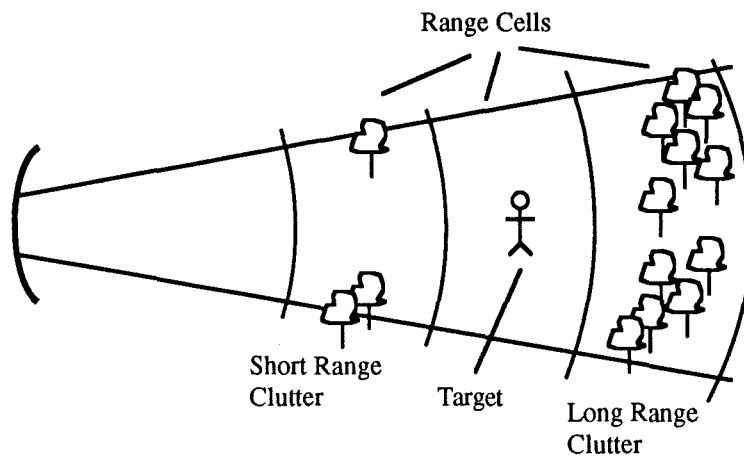


Figure 5.16 The Detection of Targets in Clutter.

The size of the range cell is determined by the width of the measurement bandwidth. The clutter appears in the range cells either side of the target cell and would ordinarily be rejected by the IF filter. Variations in the beat frequency of the clutter, may cause some power to appear in a side band that lies at the target frequency. Large clutter returns may mask the return from the target. How severe a problem this is depends on the frequency stability of the transmitter and the local oscillator. In this case the local oscillator is derived from the transmitter and will have the same frequency stability. This stability is described by the oscillator's phase noise side bands.

The phase noise of the 94GHz Master oscillator is shown in figure 5.17 and was measured using the FM noise measurement system of Smith¹.

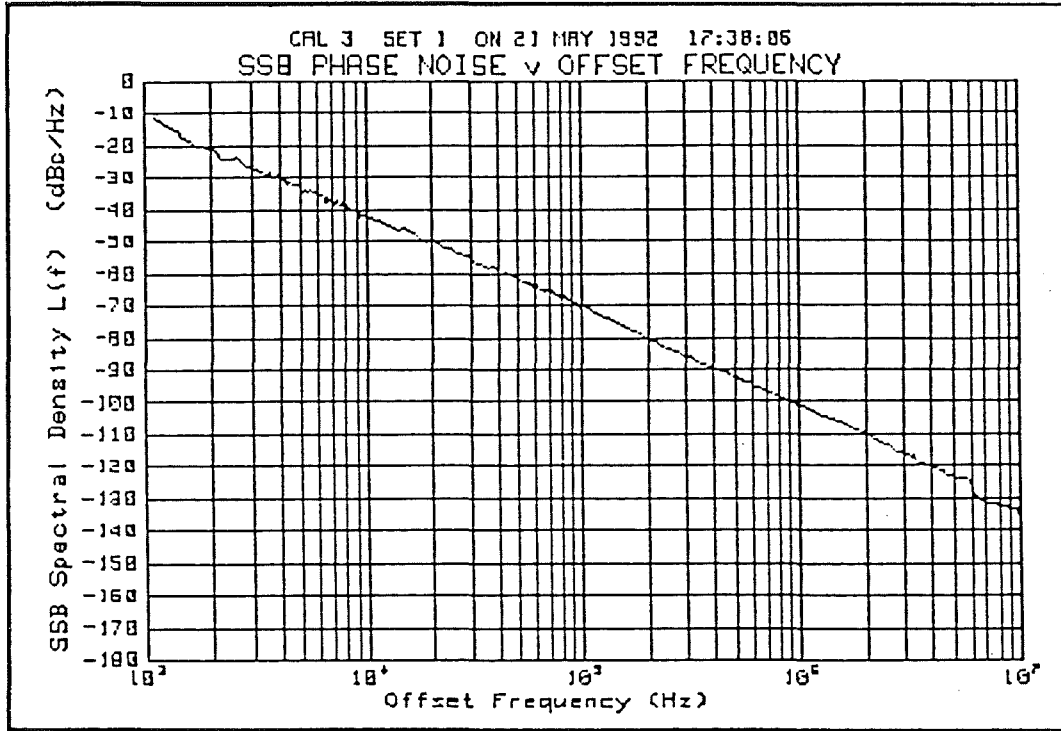


Figure 5.17 SSB Phase Noise Density Against Offset Frequency.

In order for the target to be visible, the signal power must be greater than the combined noise and clutter power. For a ratio $S[\text{dB}]$, of signal to combined noise and clutter, and a clutter power χdB above the signal power then

$$S = P_{\text{sig}} - \{ P_{\text{sig}} + \chi + L(f_0) + 10\log(\text{BW}) \} \quad 5.17$$

where BW is the measurement bandwidth and $L(f_0)$ is the SSB phase noise power density at an offset frequency f_0 in dBc/Hz. A correction factor needs to be applied to $L(f_0)$ to determine the IF power density when the local oscillator and the signal are derived from the same source. If the time delay between the two signals is zero then the frequency variations of the two sources are identical. The difference frequency would then be stable. When a delay is introduced, the side bands of the two sources are phase shifted with respect to each other and no longer cancel in the IF. The amount of phase shift depends on the offset frequency of the side band being considered, and the time delay. The worst case occurs when the side bands add in the IF and increase the side band noise. This produces a doubling of the field amplitude and an increase in noise power of 6dB. When talking in terms of side bands it is important to note the following points. With AM or FM modulation the phase difference of the side bands at a given

¹ G.M. Smith PhD Thesis, University of St. Andrews 1990.

offset frequency is often mentioned : the side bands are in phase for AM and in anti-phase for FM. This is not correct as the side bands are at different frequencies and hence have a constantly changing phase difference. What can be correctly stated is that the *sum* of the two side bands is in phase with the carrier for AM, and in quadrature with the carrier for FM. The effect of a time delay, τ , on the phase modulation index, θ , is described by

$$\theta'(\tau) = 2\theta(\tau=0) \sin\left(\frac{2\pi f_o \tau}{2}\right) \quad 5.18$$

where f_o is the offset frequency of the sideband being considered. The range for this radar is given by

$$R[\text{metres}] = f_{\text{beat}} [\text{kHz}] \quad 5.19$$

At a given beat frequency, f_b , the measurement bandwidth, BW, is defined by the filter Q (=20) as

$$BW = \frac{f_b}{Q} \quad 5.20$$

Since the clutter is in the adjacent range cell, the offset frequency is also $\frac{f_b}{Q}$. This enables equation 5.18 to be written as

$$\theta' = 2\theta \sin\left\{\frac{\pi \cdot R \times 10^3 \cdot R \cdot 6.7 \times 10^{-9}}{Q}\right\} = 2\theta \sin\left\{\frac{6.7 \times 10^{-6} \pi R^2}{20}\right\} \quad 5.21$$

By fitting a curve to figure 5.17, an approximate expression for the phase noise as a function of frequency can be obtained. For f_o in Hz this is given by

$$L(f_o) \approx 78.1 - 30\log(f_o) \text{ dB} \quad 5.22$$

Using equation 5.22 it is possible to obtain a general expression for the SNR in the presence of clutter for *this particular radar* provided the following assumptions are made

- 1 The clutter appears in the range cell adjacent to the target cell.
- 2 The approximation $2\sin(\pi f_o \tau) \approx 2\pi f_o \tau$ is valid.
- 3 The range in metres = the beat frequency in kHz.

The first assumption states that the IF bandwidth and the offset frequency are equal.

The other two allow equation 5.21 to be written as

$$\left(\frac{\theta'}{\theta}\right)_{\text{dB}} = 20\log\left(\frac{\theta'}{\theta}\right) = -147.6 + 20\log(R) + 20\log(f_o) \quad 5.23$$

The noise power is found by integrating the adjusted phase noise density over the interval $\frac{1}{2}f_0$ to $\frac{3}{2}f_0$. The adjusted phase noise density is found by combining equations 5.22 and 5.23. The integrated noise power is then

$$\int_{\frac{1}{2}f_0}^{\frac{3}{2}f_0} L(f_0) = \{-69.1 + 20\log(R)\} \text{ dB} \quad 5.24$$

and the signal to noise ratio is

$$S[\text{dB}] = -\chi + 69.1 - 20\log(R) \quad 5.25$$

This is valid as long as the approximation $2\sin(\pi f_0 \tau) \approx 2\pi f_0 \tau$ holds. This condition can be written as

$$R \cdot \delta R \lesssim 9500 \text{ m}^2 \quad 5.26$$

It is interesting to note that the SNR does not depend upon the size of the range cell although obviously the resolution will. Some typical values of R and δR for this radar are 100m and 1m respectively. These satisfy equation 5.26 and give an SNR of 20dB for clutter power 9.1dB above the target power.

If the clutter is situated more than one range cell from the target the SNR is given by

$$S[\text{dB}] = -\chi + 69.1 + Y(n) - 20\log(R) \quad 5.27$$

where $Y(n)$ is an additional factor when the clutter is situated n range cells from the target cell. Figure 5.18 shows a plot of $Y(n)$ against n .

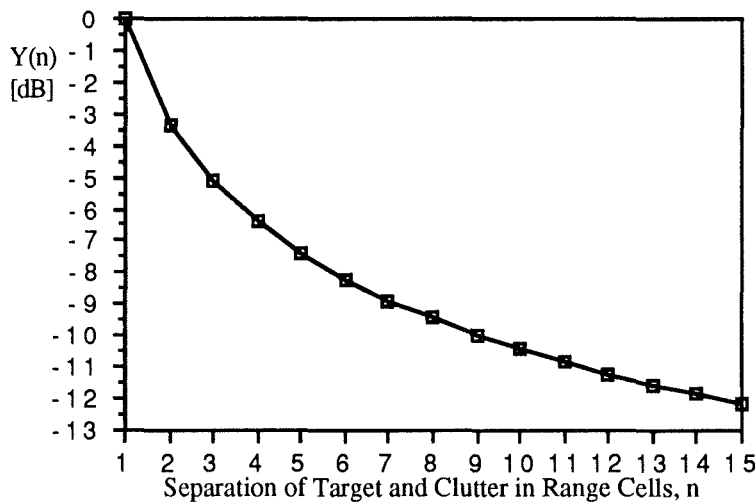


Figure 5.18 Additional Attenuation of Clutter Noise due to Target-Range Separation.

Feedhorn Design and Evaluation.

6 Abstract.

The design of a Potter horn with a variable phase length is described and the evaluation of the antenna pattern presented. The design and evaluation of a single-mode conical feedhorn is also presented. Some limitations of the present pattern measurement system are discussed. An alternative feedhorn measurement technique is proposed and discussed.

6.1 Dual Mode Feedhorns.

Feedhorns are required to launch a free space Gaussian beam from a waveguide source, and to couple Gaussian beams into waveguide detectors. The most common feedhorn, for this frequency range, is the corrugated feedhorn. This is chosen mainly for two reasons. Firstly is the efficiency : nearly 98% of the power can be coupled into the fundamental mode¹, and with good symmetry. Secondly, the bandwidth is typically 10% to 20% making them particularly useful for broadband instrumentation.

6.1.1 Corrugated Feedhorns.

The corrugated horn produces a higher order mode to reduce the sidelobe level in the E plane and to equalize the E plane and H plane beam widths. The higher order cylindrical mode, $TM_{1,1}$, is generated from the incident $TE_{1,1}$ mode by the first corrugations in the cylindrical wave guide. Some of the power is converted to $TM_{1,1}$ and the rest remains as $TE_{1,1}$. These two modes have different phase velocities, and would ordinarily have the wrong phase difference at the aperture if allowed to propagate along a smooth horn. The remaining corrugations in the guide provide a reactive surface that presents different boundary conditions to each mode. Careful design of the depth and width of the corrugations, produces a surface that enables the $TE_{1,1}$ and the $TM_{1,1}$ modes to propagate at the same phase velocity. As the two modes are produced together and propagate together they are often called a hybrid mode and named $HE_{1,1}$.

The production of corrugated horns in the millimetre wave region involves electroforming copper onto an aluminium mandrill. The outer profile of the horn, including any reference faces, is machined and the aluminium is etched out. Finally

¹ R.J. Wyld. "Millimetre-wave Gaussian Beam-Mode Optics and Corrugated Feedhorns" Proc. IEE Vol 131. Pt H. No.4 Aug 1984.

flanges are added and the completed horn is gold flashed. These processes make a quality feedhorn difficult to make, if attempted in the lab., and expensive to buy.

6.1.2 Potter Horns.

An alternative feedhorn was designed that could be produced more easily in-house. This feedhorn is a derivative of the dual mode feedhorn produced by Potter¹. The Potter horn, as it has become known, also uses the higher order $TM_{1,1}$ mode and actually pre-dates the corrugated horn.

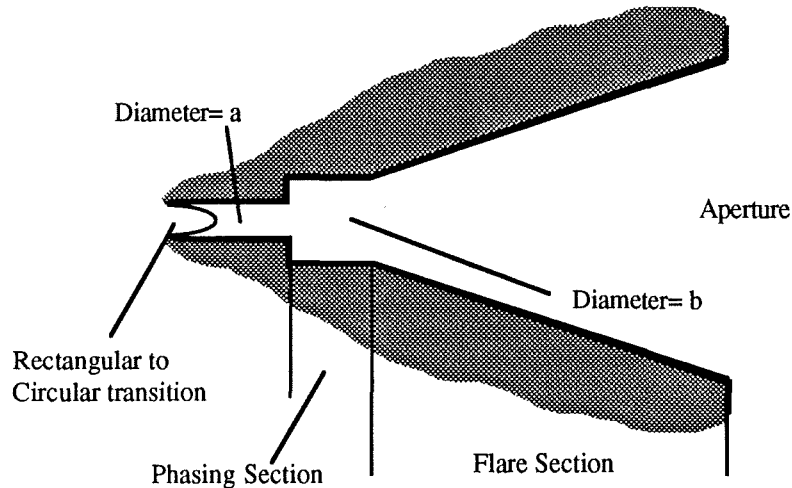


Figure 6.1 Section of Potter Horn.

The Potter horn, shown in figure 6.1, produces the higher order $TM_{1,1}$ mode by an abrupt change in the radius of the cylindrical guide. The dimensions of the larger guide are chosen to cut-off all but the $TE_{1,1}$ and $TM_{1,1}$ modes. The relative amount of the $TM_{1,1}$ mode that is produced depends on the size of the step. The two modes propagate away from the step along the phasing section before reaching the flare section and the aperture. The lengths of the phasing and flare sections are chosen such that the two modes have the appropriate phase at the aperture despite their different phase velocities. The horn described by Potter operates at 9.6GHz, and many of his dimensions are determined empirically. The main drawback with this type of horn is the narrow band of operation defined by the lengths of the phasing and flare sections. Operation away from the design frequency alters the phase velocities of the two modes. They are now no longer in phase at the aperture and the benefits of using the higher mode are lost. The lengths of the phasing and flare sections are chosen such that the two modes have the appropriate phase at the aperture despite their different phase velocities.

¹ P.D. Potter. "A New Horn Antenna with Suppressed Sidelobes and Equal Beamwidths"
Microwave Journal Vol. VI, June 1963.

6.1.3 A Tunable Potter Horn.

A Potter horn with a tunable phasing section was designed and evaluated. The variable length of the phasing section will allow the narrow operating band to be tuned over a wide range of frequencies. The mechanical design of the horn is shown in figure 6.2. The initial design, shown in figure 6.2a, did not provide adequate support for the flare section and the range of tuning was limited. The second design was more mechanically stable and allowed a larger tuning range. This range allowed the differential phase length to be tuned through a whole cycle ensuring that equal phase paths can be achieved.

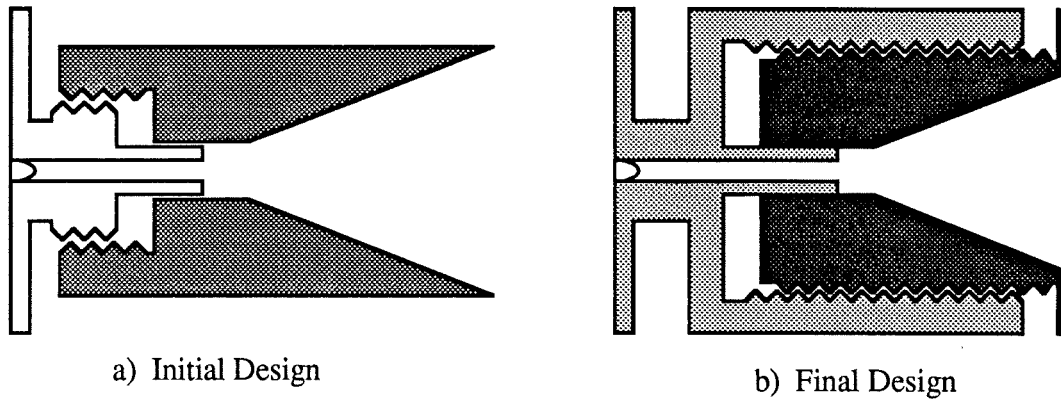


Figure 6.2 Mechanical Construction of Tunable of Potter Horn.

The first stage of the design is to determine the radii of the two guides, a and b . The relative radii of the two guides are chosen to satisfy the following criteria.

- The smaller guide must be cut-off to all modes except $TE_{1,1}$.
- The larger guide must propagate the $TE_{1,1}$ and $TM_{1,1}$ modes, but cut-off any other higher order modes.
- The step size, $t = \frac{a}{b}$, must be chosen to produce the required power ratio of $TE_{1,1}$ and $TM_{1,1}$ in the larger guide. This is required for cancellation of sidelobes and equalization of beam widths.
- The phase velocities of the $TE_{1,1}$ and $TM_{1,1}$ modes in the larger guide should be significantly different to allow the phase difference to be removed in a short length of guide.
- The phasing section should be short enough to reduce loss, but long enough to allow transient modes to die away before the flare section. Transient modes are set up at the step but do not propagate as they are beyond cut-off.

The transverse field at the plane of the step can be represented in terms of the cylindrical waveguide modes in the smaller and larger guides. The full analysis of what happens at the step would need to include all of the modes, transient and propagating, in both guides propagating in both directions. This requires the solution of an infinite

number of simultaneous equations. Some limits have to be imposed in order to make the problem solvable. Cole et al¹, use an iterative matrix approach to solve this problem and their results show good agreement with experiment. Some assumptions can be made to reduce the number of equations to a practical level.

The field in the smaller guide can be represented by a single TE_{1,1} mode propagating towards the step. This has been shown to be a reasonable assumption, in both theory and practice², when the larger guide is well above cut-off for the TM_{1,1} mode. The propagating modes in the larger guide can be limited to TE_{1,1}, TM_{0,1}, TE_{2,1}, TE_{0,1} and TM_{1,1} by restricting the radius, b. The unwanted modes, TM_{0,1}, TE_{2,1} and TE_{0,1} are not excited due to the symmetry of the radius step. These restrictions essentially reduce the field in the larger guide to the sum of TE_{1,1} and TM_{1,1} modes. The step will also set up a number of transient modes. Although they do not propagate, they do, in part, determine the amplitudes and phases of the propagating modes.

The transverse field at the step can therefore be represented approximately by

$$\begin{aligned} E_{ap} &= TE_{1,1} \left[\frac{r}{a} \right] & r \leq a \\ &= 0 & r > a \end{aligned} \quad 6.1$$

This aperture field can also be written in terms of the two propagating modes in the larger guide.

$$E_{ap} = p TE_{1,1} \left[\frac{r}{b} \right] + q TM_{1,1} \left[\frac{r}{b} \right] \quad 6.2$$

The transverse electric fields for TE and TM modes are given in a number of papers and books. The following are taken from Ludwig³ and given by

$$\begin{aligned} E_{TE_{m,n}}(\rho, \phi) &= \frac{m}{\rho} J_m(\epsilon'_{m,n} \rho) \sin(m\phi) \mathbf{r} \\ &\quad + \epsilon'_{m,n} J'_m(\epsilon'_{m,n} \rho) \cos(m\phi) \phi \end{aligned} \quad 6.3$$

$$\begin{aligned} E_{TM_{m,n}}(\rho, \phi) &= \epsilon_{m,n} J'_m(\epsilon_{m,n} \rho) \sin(m\phi) \mathbf{r} \\ &\quad + \frac{m}{\rho} J_m(\epsilon_{m,n} \rho) \cos(m\phi) \phi \end{aligned} \quad 6.4$$

-
- 1 W.J. Cole et al. "Iterative Solution of Waveguide Discontinuity Problems" Bell Syst. Tech. Jour. Vol 46 1967.
 - 2 W.J. English. "The Circular Waveguide Step-Discontinuity Mode Transducer" IEEE Trans. MTT Vol. MTT-21. 1973
 - 3 A.C. Ludwig. "Radiation Pattern Synthesis for Circular Aperture Horn Antennas" IEEE Trans. AP Vol. AP-14 July 1966.

where $\rho = \frac{r}{r_o}$ with r_o = radius of guide

$J_m(x)$ = Bessel function of first kind, order m .

$\epsilon_{m,n}$ = n^{th} root of $J_m(x)$

$\epsilon'_{m,n}$ = n^{th} root of $\frac{d}{dx} J_m(x)$

The values of p and q can be found from a Fourier type expansion since the modes are orthogonal and form a complete set. Hence

$$p = \frac{1}{p_o} \int_{\phi=0}^{\phi=2\pi} \int_{r=0}^{r=a} E_{ap} \cdot E_{TE_{1,1}} \left(\frac{r}{b}, \phi \right) r \cdot dr \cdot d\phi \quad 6.5$$

$$q = \frac{1}{q_o} \int_{\phi=0}^{\phi=2\pi} \int_{r=0}^{r=a} E_{ap} \cdot E_{TM_{1,1}} \left(\frac{r}{b}, \phi \right) r \cdot dr \cdot d\phi \quad 6.6$$

The mode functions of equations 6.3 and 6.4 need to be normalized. This is normally achieved for free space modes by setting

$$\int_s |E|^2 dS = 1 \quad 6.7$$

This is equivalent to setting the power in each mode to $\frac{1}{Z_o}$, where z_o is the characteristic impedance. In free space the characteristic impedance is the same for all modes, this is not the case for waveguide modes. In order that p and q be representative of the powers in each mode, the different characteristic impedances must be considered when normalizing. For $TE_{1,1}$ and $TM_{1,1}$ modes the normalization factors are p_o and q_o respectively where

$$p_o = \frac{\int_{\phi} \int_r \left| E_{TE_{1,1}} \left(\frac{r}{r_o}, \phi \right) \right|^2 r \cdot dr \cdot d\phi}{Z_{TE_{1,1}}(r_o, \lambda)} \quad 6.8$$

$$q_o = \frac{\int_{\phi} \int_r \left| E_{TM_{1,1}} \left(\frac{r}{r_o}, \phi \right) \right|^2 r \cdot dr \cdot d\phi}{Z_{TM_{1,1}}(r_o, \lambda)} \quad 6.9$$

The integrals in equations 6.8 and 6.9 can be solved using recurrence formulae for Bessel functions and the standard integral¹

$$\int_{\rho=0}^{\rho=1} \{J_n(\epsilon'\rho)\}^2 \rho \cdot d\rho = \frac{1}{2} \left[\{J'_n(\epsilon')\}^2 + \left(1 - \frac{n^2}{\epsilon'^2}\right) \{J_n(\epsilon')\}^2 \right] \quad 6.10$$

The characteristic impedance is given in many texts, for example Collin², so that the coefficients p and q can be written as

$$p_o = \left[\frac{Z_o}{1.27 r_o^2 \sqrt{1 - \frac{\lambda^2}{11.64 r_o^2}}} \right]^{\frac{1}{2}} \quad 6.11$$

$$q_o = \left[\frac{Z_o \sqrt{1 - \frac{\lambda^2}{2.69 r_o^2}}}{3.73 r_o^2} \right]^{\frac{1}{2}} \quad 6.12$$

The integrals in equations 6.5 and 6.6 are solved to give

$$p = \frac{\pi a^2 \epsilon'}{2 p_o (t^2 - 1)} \left\{ J_o(\epsilon't) J'_o(\epsilon') - t J_o(\epsilon') J'_o(\epsilon't) \right. \\ \left. + J_2(\epsilon't) J'_2(\epsilon') - t J_2(\epsilon') J'_2(\epsilon't) \right\} \quad 6.13$$

$$q = \frac{\pi a^2 \epsilon' \epsilon}{2 q_o (\epsilon^2 t^2 - \epsilon'^2)} \left\{ \epsilon' J_o(\epsilon t) J'_o(\epsilon') - \epsilon t J_o(\epsilon') J'_o(\epsilon t) \right. \\ \left. - \epsilon' J_2(\epsilon t) J'_2(\epsilon') + \epsilon t J_2(\epsilon') J'_2(\epsilon t) \right\} \quad 6.14$$

where $t = \frac{a}{b}$

$\epsilon = 1^{\text{st}} \text{ root of } J_1(x) = 3.8317$

$\alpha. = 1^{\text{st}} \text{ root of } J'_1(x) = 1.8412$

$J'_1(x) = \frac{d}{dx} J_m(x)$

The values of p and q have been evaluated, for a range of values of b, for two separate cases. The first is for 94GHz, where a=1.5mm, $\lambda=3.19\text{mm}$. The second is for

¹ M.R. Spiegel "Mathematical Handbook of Formulas and Tables" McGraw-Hill 1990.

² R.E. Collin "Foundations for Microwave Engineering" McGraw-Hill.

140GHz where $a=1\text{mm}$, $\lambda=2.14\text{mm}$. The value of $\frac{q}{p}$ as a function of b is shown in figures 6.3 and 6.4.

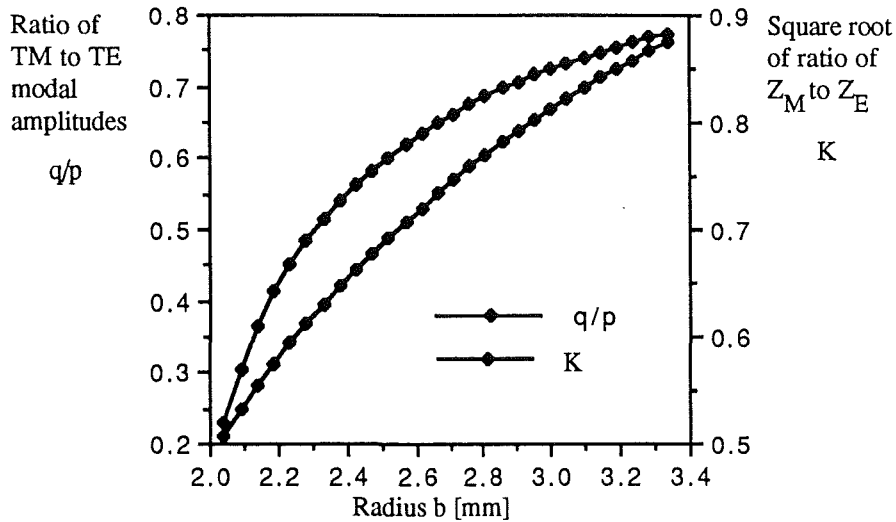


Figure 6.3 Relative Mode Content $a=1.5\text{mm}$ $f=94\text{GHz}$.

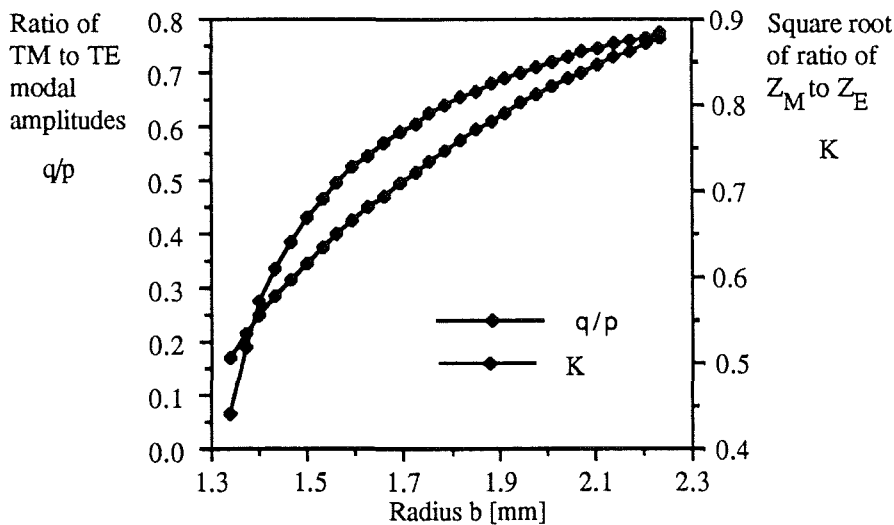


Figure 6.4 Relative Mode Content $a=1\text{mm}$ $f=140\text{GHz}$.

Potter examined the individual field patterns produced by $TE_{1,1}$ and $TM_{1,1}$ modes radiating from an open guide. He uses these patterns to determine the required mode content for a given far field beam pattern. The relative amounts of the two modes is described by a factor α . Although Potter states that α is a measure of the relative power, his use of α suggests it is the ratio of the fields. Different values for α are required for different applications. Equal beam widths or minimum sidelobes require different values of α . To produce a beam with equal widths in the E plane and the H plane a value of $\alpha=0.653$ is required.

The relation of Potter's α to $\frac{q}{p}$, as given in figures 6.3 and 6.4, is determined by the characteristic impedances of the two modes and is given by

$$\alpha = \frac{q}{p} \sqrt{\frac{Z_{TM_{1,1}}}{Z_{TE_{1,1}}}} = K \frac{q}{p} \quad 6.15$$

Two tunable Potter horns were made, one for operation at 94GHz the other for 140GHz. An incorrect value of b was chosen using $\frac{q}{p} = 0.653$ rather than $\alpha = 0.653$. This is equivalent to choosing $\alpha = 0.553$, which is still a useful value : the sidelobe level is lowest although the beam widths are not equal. The evaluation of the 94GHz source is discussed in the following section. There was insufficient power at 140GHz to allow the second horn to be evaluated as the signal to noise ratio was too low to obtain repeatable results.

The studies of Agarwal and Nagelberg¹ show that the amplitude ratio of the two modes is approximately constant over a wide range of frequencies, well above the cut-off frequency of the $TM_{1,1}$ mode. The launch phase of the two modes is, however, strongly frequency dependent. Agarwal and Nagelberg reduce the frequency dependence by loading the step with a ring of dielectric. The details of how this works are not described, but are attributed to the effect of the dielectric on the initial launch phase, and the relative phase velocities in the material itself. The use of a variable phasing length should enable the frequency dependent launch phase to be tuned out.

6.1.4 Antenna Measurements.

The antenna pattern of the horn was measured using a detector, mounted on an arm, that pivots about the phase centre. The source was modulated and a lock-in amplifier used to recover the signal and reduce the background noise. The angular position was measured using a single turn potentiometer mounted to the arm spindle and the whole movement process was motorized. A logarithmic amplifier was used to increase the dynamic range of the power measurement and the voltages corresponding to the angular position and the power were read by an ADC on the ArchimedesTM. A program was written that calibrated the set-up, read in the data and displayed it on the screen. The recorded traces can then be normalized and the beam widths found. The program is called Gausspat, and is listed in appendix 6.

¹ K.K. Agarwal & E.R. Nagelberg. "Phase Characteristics of a Circularly Symmetric Dual-Mode Transducer" IEEE Trans. MTT vol MTT-18 Jan 1970.

To obtain a good beam pattern, the pivot of the arm needs to be at the phase centre of the horn. This allows the resulting pattern to be easily expanded in terms of Gaussian modes. For a corrugated horn the position of the apparent beam waist lies behind the aperture plane by a distance, t . Wyld¹ has shown how t varies with the dimensions of the horn and with the wavelength. The Potter horn also radiates the $TE_{1,1}$ and $TM_{1,1}$ modes that constitute the $HE_{1,1}$ mode of the corrugated horn. It is reasonable, therefore, to apply the same analysis to get a measure of the apparent waist position of the Potter horn.

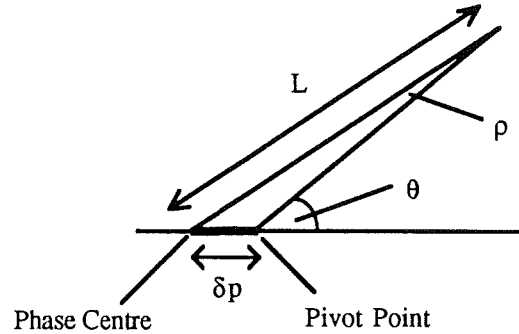


Figure 6.5 Misalignment of the Pivot Point.

The accuracy in positioning the pivot point is not critical. As shown in figure 6.5, the error, ρ , in the beam angle, θ , is larger for larger values of θ . As $L \approx 0.5\text{m}$ and $\theta \approx 15^\circ$ the angular error, ρ , is given by

$$L \cdot \sin \rho = \delta p \cdot \sin \theta \quad 6.16$$

where δp is the error in the position of the pivot point. An offset of $\delta p = 1\text{mm}$ produces an angular error, $\rho = 0.03^\circ$, in the measured beamwidth of $\sim 15^\circ$. The corresponding errors in the calculated beam waist size and waist position are 0.01mm and 0.1mm respectively.

There was a problem with standing waves when the source was pointing at the detector. There is sufficient power reflected from the detector to pull the source and produce power variations. The on axis power was found to vary periodically with the separation of the source and detector. The separation of consecutive peaks was found to be 1.6mm . This corresponds to a round trip path length of λ at 94GHz . As no waveguide isolator was available for the waveguide size of the horn, the pumping of the source could not be avoided. In practice the horn position, on axis, was varied to mid

¹ R.J. Wyld. "Millimetre-wave Gaussian Beam-Mode Optics and Corrugated Feedhorns" Proc. IEE Vol 131. Pt H. No.4 Aug 1984.

way between a trough and a peak. It was hoped that the reflected power would then be in quadrature with the main power and not alter the signal power. This was often difficult to achieve and the beam patterns show peaks and dips around the axis as a result.

The beam patterns are normalized by setting the peak power to 0dB. The beam width, at $\frac{1}{e}$ peak power, is then calculated by fitting a quadratic to the curve of $\ln(P)$ vs angle. As the peak power depends on the separation of the horns, it is sometimes difficult to define the beam width with any confidence. Free space isolation of the source was attempted. The physical size of the ferrite and the difficulty of supporting them without distorting the beam, prevented this being a viable option.

Figure 6.6 shows the H plane pattern of the 94GHz Potter horn. The side lobes are ~27dB below the main lobe and this agrees well with theory. The beam pattern in this plane is not affected by the presence of the $TM_{1,1}$ mode. The E plane pattern is therefore adjusted to achieve the same shape. The E plane pattern at 94GHz is shown in figure 6.7. The main lobe is heavily distorted, due to standing waves, making it difficult to determine the beam width. The main lobe, however, looks to be about the right size and shape. The side lobes are at least 22dB below the main lobe and this is evidence of a higher mode. The first side lobe for $TE_{1,1}$ alone is, in theory, 17.7dB below the main lobe.

Figures 6.8 and 6.9 show two extreme effects of tuning the phase of the $TM_{1,1}$ mode. Figure 6.8 shows broadening of the mainlobe below the -10dB level. This is caused by the $TM_{1,1}$ mode adding to the side lobes of the $TM_{1,1}$ mode. Figure 6.9 shows the extreme reduction in the level of one side lobe and slight narrowing of the main lobe. The actual power level in this side lobe was difficult to measure. The use of a logarithmic amplifier improved the dynamic range to 10 decades in theory. In practice, noise at the input to the logarithmic amplifier reduces the usable range to about 5 decades. The noise on low level signals causes the net input of the logarithmic amplifier to go below zero. The response of the logarithmic amplifier to a negative input is for the output to move towards the negative rail. The gains on the lock-in amplifier were increased to their maximum levels with the detector positioned on this side lobe. There was still no detectable signal.

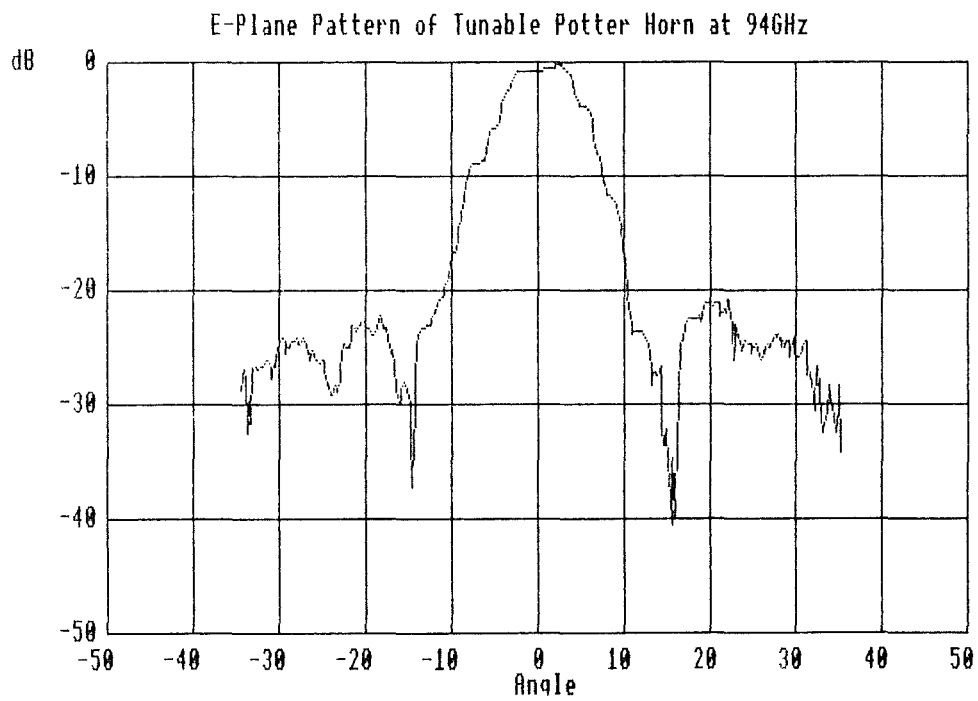
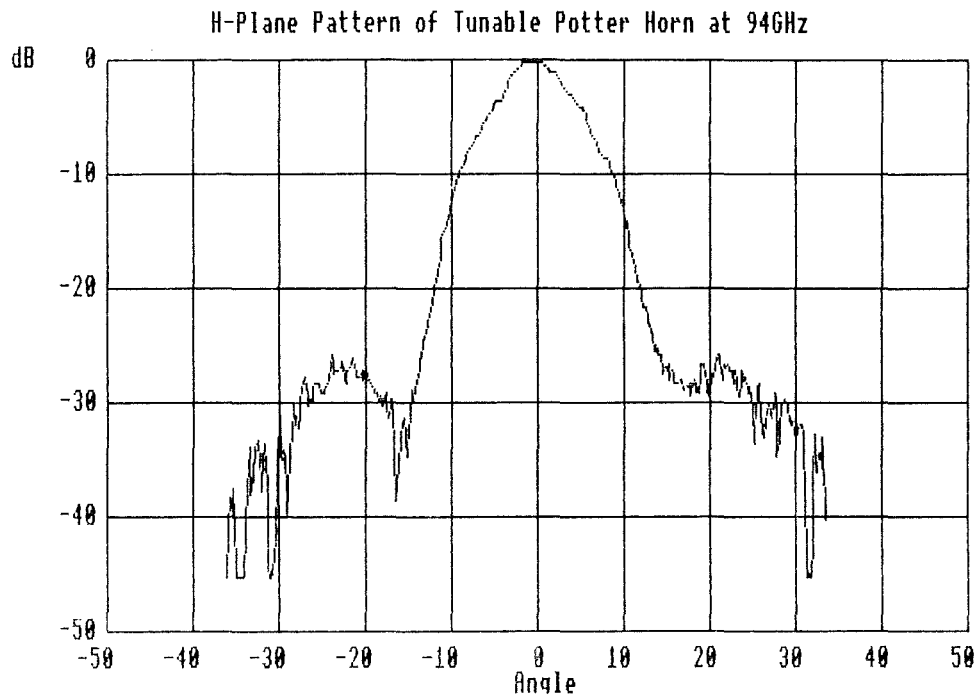


Figure 6.6 (Top) H Plane Antenna Pattern. Figure 6.7 E Plane Antenna Pattern.

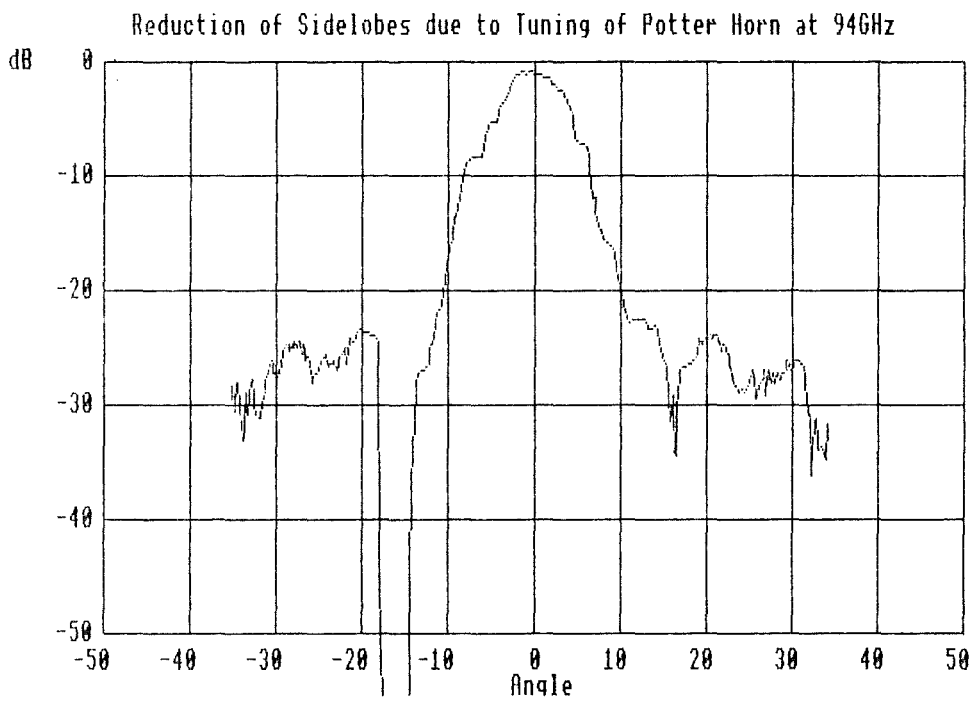
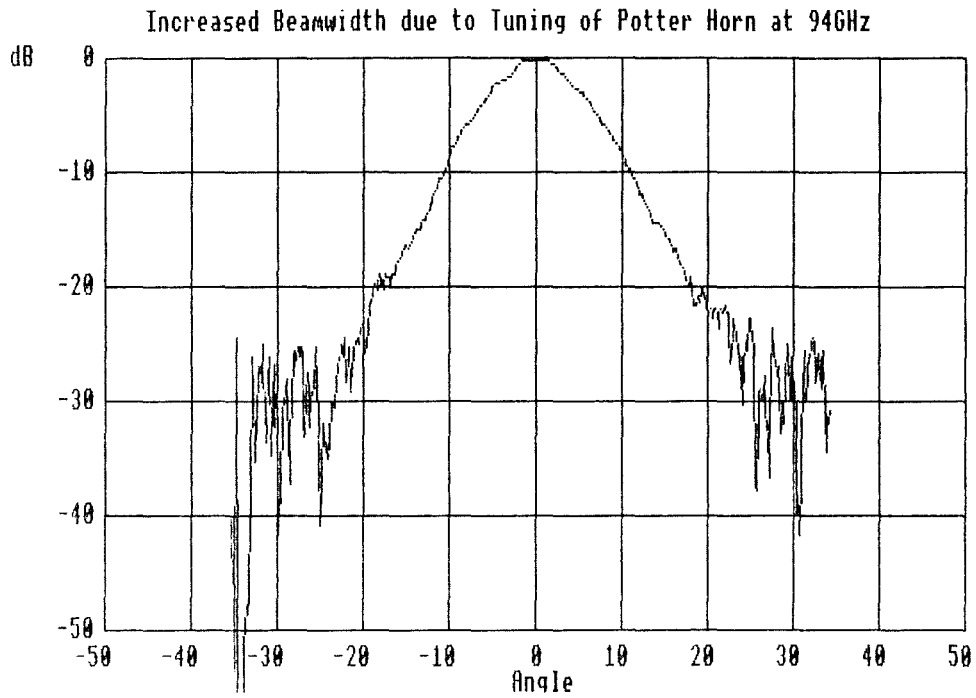


Figure 6.8 (Top) An Increase in the E plane Beam Width Produced by Changing the Phase of the $TM_{1,1}$ Mode.

Figure 6.9 (Bottom) A Reduction in the Side Lobe Level Produced by Changing the Phase of the $TM_{1,1}$ Mode.

6.2 Single-Mode Conical Feed Horns.

To allow the detectors to operate at 94GHz and 140GHz they were built in WG28¹. The feedhorns for these detectors need to be equally wide band and this rules out multi-mode horns such as corrugated and Potter horns.

Four single-mode conical feed horns were designed and built for this frequency range. The E field for the cylindrical TE_{1,1} mode dies away gradually in the H plane, at the walls of the waveguide, but ends abruptly in the E plane. The non zero fields at the waveguide wall set up large side lobes in the E plane antenna pattern. It is accepted that the performance of these horns will not be comparable to a dedicated corrugated feed horn, but will be able to couple at least some power into the detectors at 94GHz and 140GHz.

The horns were designed using the data produced by King². He produced graphs of absolute gain as functions of the horn shape and horn dimensions. These graphs show that there is an optimum aperture diameter, d , for a given length of flare section, L . King recommends that the optimum diameter should not be exceeded as this causes severe distortion of the main lobe. The flare angle was determined by the shape of a special tapered cutting tool produced for the manufacture of the Potter horns³. This angle was 12.9'. The dimensions chosen were $L=30\text{mm}$ and $d=13.7\text{mm}$. Figure 6.10 shows how these compare with the optimum dimensions at 94GHz and 140GHz.

λ	L	d	d_{opt}	Gain	H plane FWHM	E plane FWHM
2.14mm	14λ	6.42λ	6.5λ	23dB	10.9'	9.3'
3.19mm	9.4λ	4.3λ	5.5λ	22dB	16.3'	14'

Figure 6.10 Conical Horn Parameters at 94GHz and 140GHz.

Four nominally identical feed horns were made and their antenna patterns were almost identical. An H plane and E plane pattern are shown in figures 6.11 and 6.12 respectively. The H plane pattern shows the expected profile down to ~-20dB. The E plane pattern shows the characteristic side lobes of a single mode conical horn.

-
- 1 WG28 2.032mm by 1.016mm. Cut-off at 74GHz. Normally used from 90GHz to 140GHz.
 - 2 A.P. King. "The Radiation characteristics of Conical Horn Antennas" Proc IRE, vol 38, March 1950.
 - 3 Produced by W. Smith, Department of Physics and Astronomy Mechanical Workshop, University of St. Andrews.

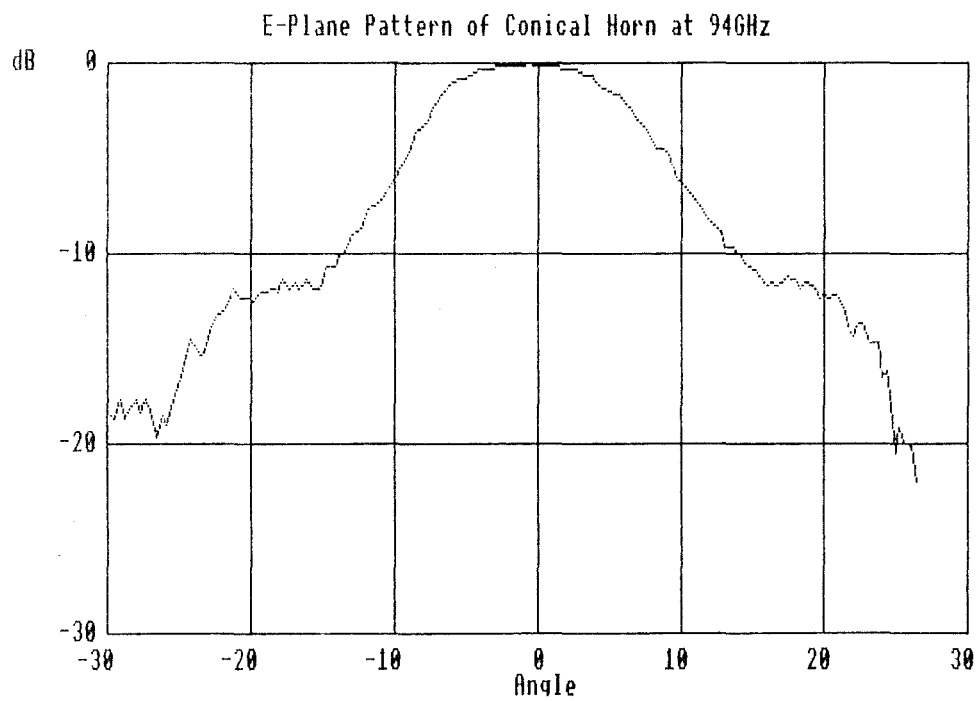
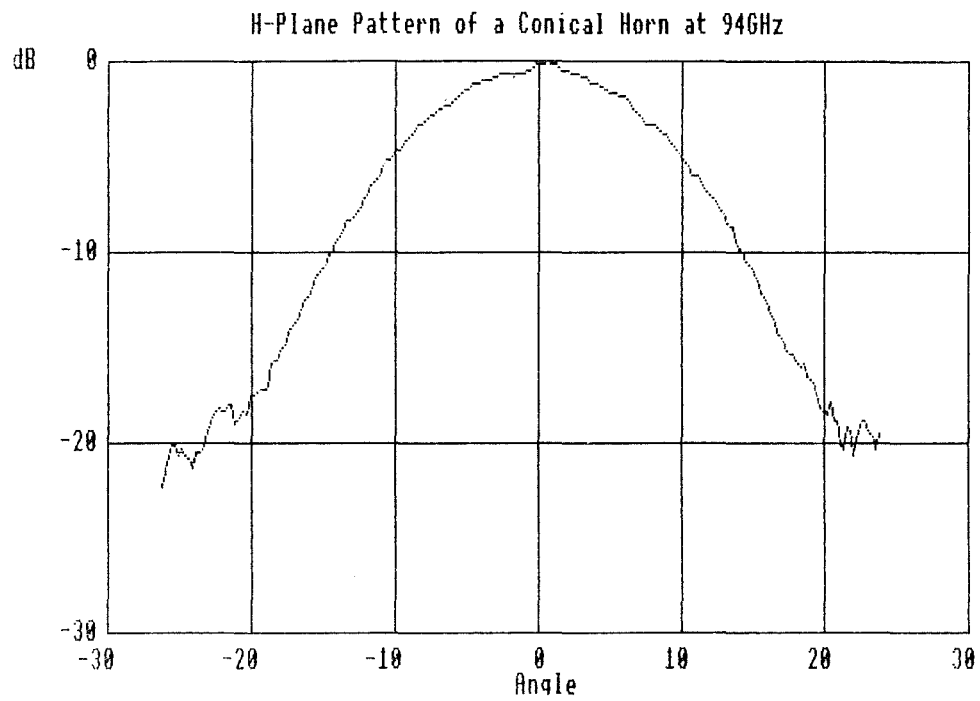


Figure 6.11 (Top) H Plane Antenna Pattern. Figure 6.12 E Plane Antenna Pattern.

6.3 An Alternative Measurement Technique.

A question often posed in antenna measurement set-ups concerns the effect of the receiver horn on the antenna pattern. The ideal receiver horn would have an isotropic radiation pattern such that its sensitivity was independent of angle. A good approximation to an isotropic antenna can be obtained by using an antenna in the far field that always points at the unknown horn. This technique was used in the above pattern measurements.

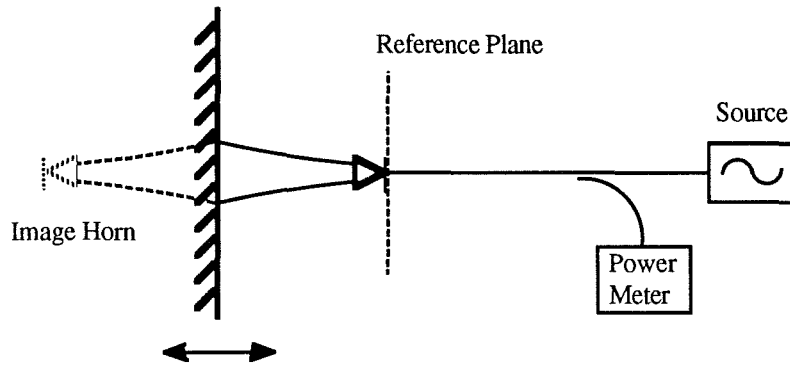


Figure 6.13 Image of Unknown Feedhorn.

The receiver horn can be replaced by an image of the unknown horn by using a mirror as shown in figure 6.13. The problem now is in varying the angle about the phase centre. If the angle of the mirror is varied, and the separation of the mirror and the phase centre is known, the angular antenna pattern may be deduced. A similar method is proposed that enables the unknown quantities of a horn producing a Gaussian beam to be determined.

An image of the unknown horn is created using a mirror. The power coupled back into the horn is a measure of the coupling between the unknown horn and its image. For an axial arrangement the power coupling, as given in equation 3.6, is

$$\eta = \frac{4}{\left(\frac{\omega_{o1}}{\omega_{o2}} + \frac{\omega_{o2}}{\omega_{o1}}\right)^2 + \left(\frac{2Z_o}{k \cdot \omega_{o1} \omega_{o2}}\right)^2} \quad 6.17$$

The beam waists are, by definition, identical and the distance Z_o can be written as

$$Z_o = 2(x+t) \quad 6.18$$

where x is the distance from the aperture plane to the mirror, and t is the distance from the effective beam waist plane to the aperture. The detected power consists of the

transmitted power less the coupling and ohmic losses. The ohmic losses occur for each pass through the horn and so the received power is

$$P_R = \gamma^2 \eta P_T \quad 6.19$$

where γ is the transmitted power as a fraction of the incident power. The received power as a function of x can now be written as

$$\left(\frac{P_T}{P_R} \right) = \frac{1}{\gamma^2 \eta} = \frac{4(x^2 + xt + t^2)}{k^2 \gamma^2 w_0^4} + \frac{1}{\gamma^2} \quad 6.20$$

Writing equation 6.20 as a quadratic in x gives

$$\left(\frac{P_T}{P_R} \right) = x^2 \left\{ \frac{4}{k^2 \gamma^2 w_0^4} \right\} + x \left\{ \frac{4t}{k^2 \gamma^2 w_0^4} \right\} + \left\{ \frac{4t^2}{k^2 \gamma^2 w_0^4} + \frac{1}{\gamma^2} \right\} \quad 6.21$$

Measuring $\left(\frac{P_T}{P_R} \right)$ as a function in x , and fitting a quadratic will produce an equation of the form

$$\left(\frac{P_T}{P_R} \right) = a_2 x^2 + a_1 x + a_0 \quad 6.22$$

from which the unknown quantities are found as

$$t = \frac{a_1}{a_2} \quad 6.23$$

$$\omega_0 = \sqrt[4]{\frac{4}{k^2} \left(\frac{a_0}{a_2} - \left(\frac{a_1}{a_2} \right)^2 \right)} \quad 6.24$$

$$\gamma = \sqrt{\frac{a_2}{a_0 a_2 - a_1^2}} \quad 6.25$$

The circuit in figure 6.14 can be used to measure the return power as a function of the mirror position. An optical circulator is used to diplex the source and the detector, and the use of a local oscillator enables the phase of the reflection to be determined. The system losses and internal reflections are determined by placing a mirror and an absorbing load at the output plane.

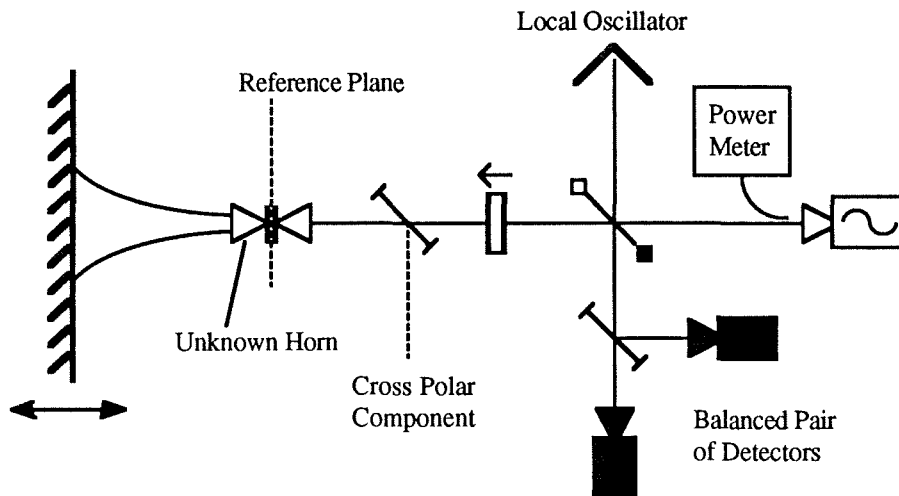


Figure 6.14 Optical Circuit for Characterizing Feedhorns.

Theoretically the quadratic in equation 6.22 can be determined with three power measurements. In practice the effects of VSWR will cause rapid variations in the power about a slowly varying mean level. The mean level can be used to determine the quadratic, whereas the fluctuations will be a measure of the VSWR.

Analysis of System Performance.

7 Abstract.

A description of the antenna is presented. The optical loss of the radar is measured and the comparison with theory is discussed. The range, velocity and polarization measurement ability is demonstrated. The performance of the radar as a whole is described, and suggestions for improvements to several sections are made.

7.1 The Radar Antenna.

The antenna used in this radar consisted of a section of a paraboloidal mirror¹ fed by a small primary mirror. The primary mirror is placed at the focal point of the paraboloid. The angle of the primary mirror is such that it reflects a beam travelling vertically upwards onto the paraboloidal mirror. The mirror is mounted so that it can be rotated about the vertical axis centred on the focal point. The mirror can then be rotated to scan the beam in a plane parallel with the base plate. A lens at the output of the circulator focuses the beam to a waist, $\omega_0 = 3.0\text{mm}$, near the primary mirror. The exact position of this waist is chosen such that the phase centre of the beam, at the mirror, lies at the focus of the paraboloid. The phase fronts of the beam leaving the mirror are theoretically planar. The output beam therefore has a beam waist at the mirror. The size of this waist is calculated as $\omega_0 = 24.7\text{mm}$, giving a gain of 32.3dB.

7.2 Performance Tests.

The assembled radar was subjected to several tests to assess its performance. The results of these tests are discussed in the following sections.

7.2.1 Loss.

The transmission loss, from source to antenna, will depend on several factors. These include ohmic losses in the feedhorns, optical coupling losses, absorption in the lenses and ferrites and reflection losses.

¹ P.D.E. Components. PO Box 814. DELL D.O. Edinburgh. EH14 4AX.

7.2.1.1 Insertion Loss.

The power produced by the source was measured with a waveguide power meter to be 21.9mW. The power radiated by the horn can be measured by a free-space power meter¹. The radiated power is partially absorbed by a resistive membrane. The resultant heat causes an increase in pressure within a pressure cell, of which the membrane forms one wall. The change in pressure is detected by a microphone near the pressure cell. The unknown r.f. power is compared to the known ohmic heating produced by an applied low frequency signal. The membrane is best used at the Brewster angle to minimize the reflected power, and maximize the power absorbed in the film. When measuring the output power from the Potter horn it was not possible to operate at the Brewster angle. The physical size of the horn and the need for a mechanical chopper prevented the power meter from being placed close to the horn. To avoid truncation the power meter was used normal to the beam axis and the effects of reflection taken into consideration. A similar measurement was made with the power meter in the position of the primary focus mirror. In this position the mirror could be used at the Brewster angle. The power at the antenna was measured as 4.28mW. This was repeated several times and the result was consistent to within 0.02mW. The power at the output of the Potter horn could not be consistently measured. The readings ranged from 11.88mW to 13.10 mW. The output power was reduced by de-tuning the back short of the oscillator and the power measured again. The power at the antenna was measured as 2.85mW and again was consistent to within 0.02mW. The power at the Potter horn, however, was still 11.9mW! This discrepancy is thought to be due to the reflected power from the power meter pumping the oscillator. It was not possible, however, to isolate the oscillator, optically or in waveguide, to demonstrate this. The ohmic losses of the Potter horn can only be estimated as between -2.2dB and -2.6dB. The total optical loss can also only be estimated as between -4.4dB and -6.2dB. The total r.f. insertion loss can be determined as -7.1dB.

¹ Thomas Keating Ltd. Station Mills, Billingshurst, West Sussex. RH14 9SH.

7.2.1.2 Coupling Losses.

The layout of the elements for the full receiver circuit was subjected to an alignment analysis as described in chapter 3. The alignment matrices, shown in appendix 4, were completed for each appropriate lens and path length. Three paths through the system were analyzed :

- A Oscillator to antenna, via the full polarization circulator circuit.
- B Antenna to detector, via the full polarization circulator and receiver circuits.
- C Oscillator to detector, via the local oscillator tap and receiver circuits.

The resulting alignment tolerances, $\sigma(x)$, $\sigma(z)$, and $\sigma(\theta)$, were used to produce the power coupling efficiency, η , as per equation 3.14. The results are summarized in figure 7.1.

	With Lenses			Without Lenses		
	A	B	C	A	B	C
$\sigma(x)$	4.32mm	6.88mm	3.16mm	1.32mm	1.72mm	1.04mm
$\sigma(z)$	0.056mm	0.17mm	0.08mm	0.069mm	0.089mm	0.079mm
$\sigma(\theta)$	0.051rad	0.077rad	0.036rad	6.8×10^{-3} rad	9.1×10^{-3} rad	7.6×10^{-3} rad
$\eta \%$	12.3%	7.5%	57.9%	82.4%	85.5%	94.4%
η dB	-9.1	-11.2	-2.37	-0.84	-0.68	-0.25

Figure 7.1 Summary of Results from Alignment Error Analysis.

The alignment errors are based on worst case positional accuracy and hence the coupling efficiency should be regarded as a minimum expected level. Even so the calculated efficiencies are disappointingly small for the two long paths A and B. The effects of the lenses were removed, as these are based on large assumptions, and the coupling efficiencies calculated again. These efficiencies show that the effects of the lenses dominate, although no conclusions can be drawn directly from the numeric values. A new analysis of the effect of a misaligned lens, based on Gaussian beam analysis, would seem to be much needed.

7.2.1.3 Absorption in Lenses and Ferrites.

The lens material, High Density Poly-Ethylene (HDPE), absorbs and reflects some of the power incident on it. The lens surface is blazed to produce a quarter wave matching layer to reduce reflections. The absorption of HDPE at 94GHz¹ is 0.04dB/cm. For a typical lens of thickness 12mm, the loss per lens is 0.05dB.

The ferrite material has a high refractive index and requires the addition of quarter wave matching layers. Typical values of VSWR and insertion loss are 1.3 and -0.49dB respectively². The total expected insertion loss from the source to the antenna is then given by

$$L = (-0.1\text{dB})_{\text{lens}} + (-0.98\text{dB})_{\text{ferrite}} + (-0.1\text{dB})_{\text{antenna lens}} + (-0.46\text{dB})_{\text{LO tap}} = -1.69\text{dB} \quad 7.1$$

The coupling between two corrugated horns using a pair of lenses ought to be ~90%. This takes the lens losses and the efficiency of the feedhorn into account. In practice a coupling of 70% is regarded as good and 60% as typical³. The reason for this discrepancy is not fully understood. Possible reasons include amplitude distortion of the beam by the lens, and reflection at the surfaces. Whatever the cause of this extra 1.2dB to 1.8dB, it is reasonable to assume it is present in the coupling for this radar. The theoretical coupling loss is then given by

$$-2.89\text{dB} \geq L_{\text{Theory}} \geq -3.49\text{dB} \quad 7.2$$

This value takes horn losses, coupling losses, absorption losses and reflection into account. The difference between this and the measured -7.1dB may be due to the ohmic losses in the Potter horn or the poor coupling due to element misalignment. Until an improved representation of lens misalignment is produced, the latter factor remains unknown.

¹ J.C.G. Lesurf. "Millimetre-wave Optics, Devices and Systems" Adam Hilger/IOPP.

² M.R. Webb. "A MM-Wave Four-Port Quasi-Optical Circulator" Int. Jour. IR & MMW Vol 12 No.1

³ G.M. Smith. Private Communication.

7.2.2 Range Measurement.

The range of the frequency modulation and the ramp frequency were set at 150MHz and 500Hz respectively. At these settings the beat frequency should be 1kHz per 1m range. The actual range of a corner cube target was measured, referenced to the front edge of the base plate, and the resulting beat frequency measured. The results of this experiment are shown in figure 7.2.

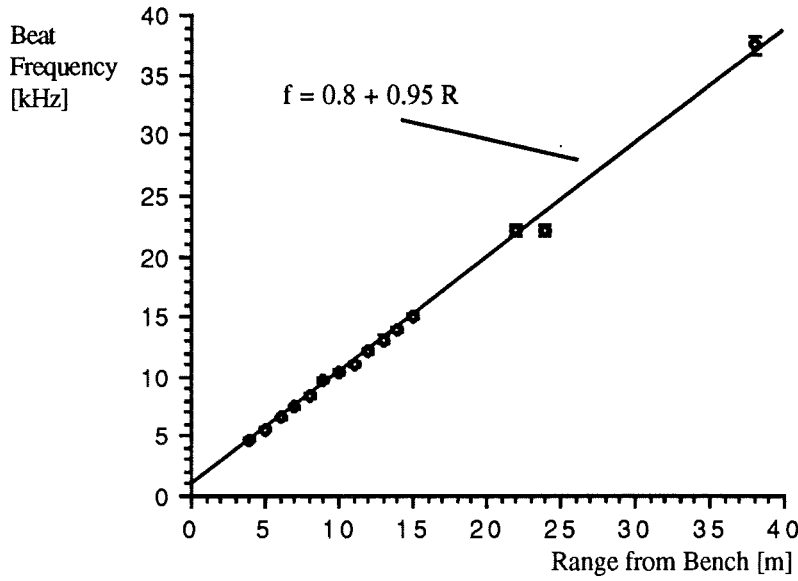


Figure 7.2 Calibration of Range Measurement.

The fitted curve gives the beat frequency as a function of range as

$$f_{\text{beat}}[\text{kHz}] = 0.95.R[\text{m}] + 0.8 \quad 7.3$$

The range of an unknown target can then be deduced from the beat frequency by

$$R[\text{m}] = 1.05f_{\text{beat}}[\text{kHz}] - 0.84 \quad 7.4$$

The error in the gradient is 6%, and this is a measure of the linearity of the FM sweep and of the accuracy in positioning the bandpass filter.

The above experiment was performed in a corridor, hence the maximum range of 38m. The waveguiding effect of the corridor is not likely to effect the frequency of the target return. It may however effect the strength of the return. The measurement of the radar's maximum range was therefore undertaken outdoors.

The maximum clock frequency for the switched capacitor bandpass filter was determined by the signal generator as 2.03MHz. This limited the centre frequency of the bandpass filter to 57kHz. To enable measurements to be made to larger distances the modulation frequency was decreased. A modulation frequency of 200Hz was used,

which increases the ramp time to 2.5ms. The beat frequency for a given range is now smaller by a factor of 2.5.

The return signal at a beat frequency of 57kHz was visible with an estimated signal to noise ratio of 3dB. The range, calculated from equation 7.4, is 148.9m. This was again limited by the clock frequency of the filter. The ramp frequency was not reduced again as the range of the target could not be increased any further. The theoretical performance of the radar can be determined from the following analysis of the reflection of a corner cube.

The power coupled into the receiver, after reflection from an infinite plane mirror, can be expressed as the power coupled between the receiver and an image of the transmitter as shown in figure 7.3

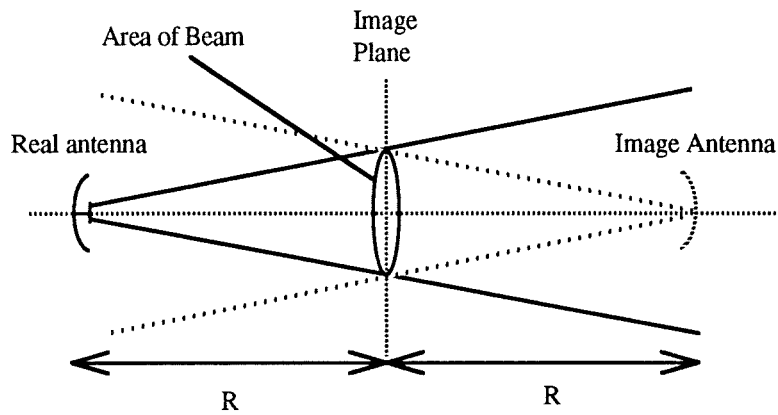


Figure 7.3 Image of Antenna in an Infinite Mirror

The transmitted power density, for an antenna of gain G is

$$P_{\text{density}} = \frac{P_T G}{4\pi r^2} \quad 7.5$$

The power collected by an identical receiving antenna, at a distance $2R$, is determined by its effective area A_{eff} , such that

$$P_R = \frac{P_T G}{4\pi(2R)^2} \cdot A_{\text{eff}} \quad 7.6$$

The effective area of the receiving antenna is given in terms of the gain and the wavelength as

$$A_{\text{eff}} = \frac{\lambda^2 G}{4\pi} \quad 7.7$$

The received power can now be written as

$$P_R = \frac{P_T G^2 \lambda^2}{(4\pi)^2 (2R)^2} \quad 7.8$$

The beam area at a range R, is given by the beam width θ as

$$A_{\text{beam}} = (R\theta)^2 = \frac{4R^2}{G} \quad 7.9$$

where θ is the full width at half maximum.

A corner cube reflector essentially reflects all of the power incident on it, back towards the source. The use of such a reflector with an area less than A_{beam} is equivalent to placing an aperture at the image plane. The power received by the detector is now given by

$$P_R = \frac{P_T G^2 \lambda^2}{(4\pi)^2 (2R)^2} \cdot \frac{A_{\text{aperture}}}{A_{\text{beam}}} = \frac{P_T G^3 \lambda^2}{(4\pi)^2 (2R)^4} \cdot A_{\text{aperture}} \quad 7.10$$

Equation 7.10 is evaluated using $G=32.3\text{dB}$, $R=148.9$, $P_T=4.28\text{mW}$ and $A_{\text{aperture}}=0.02\text{m}^2$, to give

$$P_R = 3.45\text{pW} = -84.6\text{dBm} \quad 7.11$$

The minimum detectable signal, in the absence of any significant clutter, is determined by the AM noise of the local oscillator and the thermal noise produced by the receiver. The combination of these noise sources was measured in chapter 5. The system noise, referred to the input is $\sim -120\text{dBm/Hz}$. At $R=148.9\text{m}$ the measured beat frequency was 57kHz . The Q of the bandpass filter was 14.1 and not the designed value of 10 due to a wiring error. The IF bandwidth at this frequency is therefore 4kHz and the noise power contained in it is

$$P_N = -120\text{dBm/Hz} + 10\log(4 \times 10^3) = -84\text{dBm} \quad 7.12$$

The estimated signal power from the corner cube, and the noise power are comparable. The observed signal power was $\sim 3\text{dB}$ above the noise power. This discrepancy can be attributed to errors in determining the measured range and the reflectivity of the corner cube.

7.2.3 Polarization.

The transmitter was configured to send a linearly polarized beam at 45° to the vertical. The return signal is split into orthogonal linear states that are equivalent to the horizontal and vertical states when referred back through the circulator to the antenna. The power in each state was observed to vary as a roof mirror, used as a target, was rotated about the beam axis. Equal powers were observed when the roof line was horizontal, vertical or at $\pm 45^\circ$. The power appeared all at one detector when the roof line was rotated to $\pm 22.5^\circ$. The phase of the return signals would have enabled the full polarization state to be determined. It was not possible, unfortunately, for the decoding electronics to be used for the measurements taken "in the field", for two reasons.

Firstly, the computer and DACS¹ crate could not easily be transported from location to location. Secondly, the existence of multiple return signals confused the detection electronics, which essentially expect a single signal frequency.

The measurement of Doppler shifts was not possible for the same reasons. Doppler shifts were observed, however, as the target was moved radially and, at shorter ranges, as people moved through the range cell.

7.3 Conclusions.

An FMCW-Doppler radar, with a facility for polarization analysis has been designed, constructed and tested. The ability of the radar to measure the range, velocity and polarization state has been demonstrated at 94GHz, and the range-finding calibrated. The actual performance, in terms of the system loss and sensitivity, is not as high as expected. This is due partly to the use of experimental feedhorns, which do not perform as well as commercially available horns. The other main reason for the lower performance is that flexibility for operation at 94GHz and 140GHz was designed into the radar from an early stage. The lack of available power at 140GHz prevented this flexibility from being demonstrated. The actual insertion loss of -7.1dB is still comparable to existing radars implemented in waveguide. Holm² has demonstrated a pulse radar operating at 70GHz with an r.f. insertion loss of 6dB. McGee and Loomis³ report separate pulse radar tracking at 94GHz and 140GHz with losses of -3.5dB and -6.5dB respectively. Lynn⁴ cites a representative 94GHz radar with a two-way system loss of -11dB.

The radar described here can be made to operate over a very wide bandwidth. The oscillator itself can be tuned over 20GHz and the detectors tuned to follow. The optical circuit can be used up to ~500GHz, at which point the polarizing properties of the wire grids begins to deteriorate, by changing 8 lenses and using suitable sources and detectors. The present detectors are capable of operating to 140GHz, and have been observed to detect at this frequency. The use of a dedicated corrugate horn is recommended.

¹ A.R. Harvey. PhD Thesis, University of St. Andrews. 1990.

² W.A. Holm et al. "Combined Electro-Optical Millimetre Wave Radar Sensor System" DARPA-Tri Service Millimetre Waves Conf. 1977.

³ R.A. McGee & J.M. Loomis "Radar tracking of an M-48 Tank at 94GHz and 140GHz" 6th DARPA-Tri Service Millimetre Waves Conf. 1977.

⁴ V.L. Lynn. "HOWLS Radar Development" AGARD-AVP/GCP Joint Symp. Florence 1976.

7.4 Further Work.

The radar described here is an experimental set-up. The performance could be improved by changing the design and construction of some of the components. With available time and money, the following improvements would be made.

7.4.1 Detectors.

The noise temperature of the detectors is several orders of magnitude higher than expected or desired. This may be due to a diode with a poor r.f. performance, which would necessitate a new diode. The detector blocks, initially designed to cover 94GHz to 140GHz continually, would operate better if designed for a narrower frequency band. At 94GHz this would consist of changing to a larger waveguide size, and replacing the existing coaxial post with a post and cap.

7.4.2 Feedhorns.

The feedhorns for the detector are best replaced with dedicated corrugated horns. The E plane antenna pattern of the conical horns does not match with the free space Gaussian mode. This produces large VSWR and poor power coupling. The master oscillator would also benefit from the use of a corrugated feed horn.

Appendix 1

Mathematical Derivation of a General Coupling Integral

This appendix contains the algebra required to produce the coupling efficiency for a general case of offset and tilted beams shown in figure A1.1.

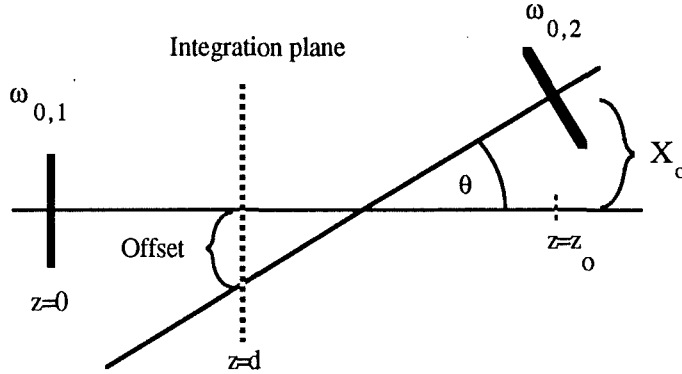


Figure A1.1 A General Representation of Offset and Tilted Beams.

The two beams are represented by equations 3.3 and 3.11 and are

$$\phi = \phi_0 \exp(-x^2 z_1) \exp(-y^2 z_1) \quad \text{A1.1}$$

$$\psi = \psi_0 \exp(-y^2 z_2^*) \exp(-(x-x_0)^2 z_2^*) \exp(-jF(\theta)) \quad \text{A1.2}$$

where

$$z_1 = \frac{1}{\omega_\phi^2} + j \frac{k}{2R_\phi} \quad \text{A1.3}$$

$$z_2^* = \frac{1}{\omega_\psi^2} + j \frac{k}{2R_\psi} \quad \text{A1.4}$$

$$x_0 = X_0 - (z_0 - d)\theta \quad \text{A1.5}$$

$$F(\theta) = (x - x_0)k\theta = \theta^2 k(z_0 - d) + \theta k(x - X_0) \quad \text{A1.6}$$

Equation 2 can be expanded to give

$$\begin{aligned} \psi = \psi_0 \exp(-y^2 z_2^*) \exp \left\{ -x^2 z_2^* x \left(2x_0 z_2^* - jk\theta \right) \right. \\ \left. + x_0^2 z_2^* - j \left(\theta^2 k(z_0 - d) - \theta k X_0 \right) \right\} \end{aligned} \quad A1.7$$

It is convenient to express some terms using x_0 and some terms using the expansion of equation 5.

The second exponential term contains a quadratic in x . The constant term in this quadratic can be written as

$$x_0^2 z_2^* - j \left(\theta^2 k(z_0 - d) - \theta k X_0 \right) = a + jb \quad A1.8$$

where

$$a = \frac{-x_0^2}{\omega_\psi^2} \quad A1.9$$

$$b = \frac{x_0^2 k}{2R_\psi} - \theta^2 k(z_0 - d) + \theta k X_0 \quad A1.10$$

The coupling integral is now evaluated using the standard integral¹

$$\int_{-\infty}^{+\infty} \exp \left\{ -(at^2 + bt + c) \right\} dt = \sqrt{\frac{\pi}{a}} \exp \left\{ \frac{b^2 - 4ac}{4a} \right\} \quad A1.11$$

as

$$\begin{aligned} \int_{-\infty}^{+\infty} \int_{-\infty}^{+\infty} \phi \psi^* dx dy = I = \phi_0 \psi_0 \exp(a - jb) \int_{-\infty}^{+\infty} \exp \left\{ -y^2(z_1 + z_2) \right\} dy \\ \cdot \int_{-\infty}^{+\infty} \exp \left\{ -x^2(z_1 + z_2) + x(2x_0 z_2 + jk\theta) \right\} dx \end{aligned} \quad A1.12$$

and so

$$I = \phi_0 \psi_0 \exp(a - jb) \frac{\pi}{(z_1 + z_2)} \exp A \exp \{ jB \} \quad A1.13$$

¹ M.R. Spiegel "Mathematical Handbook of Formulas and Tables" McGraw-Hill.

where

$$A = \Re \left\{ \frac{(2x_0 z_2 + jk\theta^2)^2}{4(z_1 + z_2)} \right\} = \Re \{ Q \} \quad A1.14$$

$$B = \Im \left\{ \frac{(2x_0 z_2 + jk\theta^2)^2}{4(z_1 + z_2)} \right\} = \Im \{ Q \} \quad A1.15$$

The power coupling is given by

$$\eta = \mathbf{I} \cdot \mathbf{I}^* \quad A1.16$$

and so

$$\eta = \frac{\phi_0^2 \psi_0^2 \pi^2}{(z_1 + z_2)(z_1 + z_2)^*} \exp\{2a\} \exp\{2A\} \quad A1.17$$

Introducing κ as

$$\kappa = \frac{4}{\omega_\psi^2 \omega_\phi^2 |z_1 + z_2|^2} \quad A1.18$$

allows η to be written as

$$\eta = \frac{\omega_\psi^2 \omega_\phi^2 \kappa \psi_0^2 \phi_0^2 \pi^2}{4} \exp\{2(a+A)\} \quad A1.19$$

The exponential in equation A1.19 can be expanded using equations A1.9 and A1.14 to give

$$2(a+A) = \frac{2E}{|z_1 + z_2|^2} \quad A1.20$$

$$E = \frac{-x_0^2}{\omega_\psi^2} \left\{ |z_1|^2 + |z_2|^2 + 2\Re(z_2 z_1^*) \right\} + \Re(x_0^2 z_2 z_1^*) + \frac{x_0^2 |z_2|^2}{\omega_\psi^2}$$

$$-\left(\frac{k\theta}{2}\right)^2 \left(\frac{1}{\omega_\psi^2} + \frac{1}{\omega_\phi^2} \right) - k\theta x_0 \Im(z_1^* z_2) \quad A1.21$$

$$\begin{aligned}
 &= \frac{-x_o^2}{\omega_\psi^2} \left\{ |z_1|^2 + 2\Re(z_2 z_1^*) \right\} + x_o^2 \Re(z_2(z_1^* z_2)) - \left(\frac{k\theta}{2}\right)^2 \left(\frac{1}{\omega_\psi^2} + \frac{1}{\omega_\phi^2}\right) \\
 &\quad - \frac{j\theta^2 x_o}{2} \left(\frac{1}{R_\phi \omega_\psi^2} + \frac{1}{R_\psi \omega_\phi^2}\right)
 \end{aligned} \tag{A1.22}$$

Using the expressions for z_1 and z_2 in equations A1.3 and A1.4, it follows that

$$\Re(z_2 z_1^*) = \frac{1}{\omega_\psi^2 \omega_\phi^2} - \frac{k^2}{4R_\phi R_\psi} \tag{A1.23}$$

$$\Im(z_2 z_1^*) = -\frac{k}{2} \left(\frac{1}{R_\phi \omega_\psi^2} + \frac{1}{R_\psi \omega_\phi^2}\right) \tag{A1.24}$$

This allows E to be written as

$$\begin{aligned}
 E &= \frac{-x_o^2}{\omega_\psi^2 \omega_\phi^2} \left\{ \frac{1}{\omega_\psi^2} + \frac{1}{\omega_\phi^2} + \frac{k^2}{4} \left(\frac{\omega_\psi^2}{R_\psi^2} + \frac{\omega_\phi^2}{R_\phi^2}\right) \right\} + \left(\frac{k\theta}{2}\right)^2 \left(\frac{1}{\omega_\psi^2} + \frac{1}{\omega_\phi^2}\right) \\
 &\quad + \frac{k^2 \theta x_o}{2} \left(\frac{1}{R_\phi \omega_\psi^2} + \frac{1}{R_\psi \omega_\phi^2}\right)
 \end{aligned} \tag{A1.25}$$

The constants ϕ_o and ψ_o are to normalize the beam powers and can be determined using the standard integral of equation A1.11 to be

$$\phi_o^2 = \frac{2}{\pi \omega_\phi^2} \tag{A1.26}$$

$$\psi_o^2 = \frac{2}{\pi \omega_\psi^2} \tag{A1.27}$$

These expressions are then substituted into equation A1.19, and combined with equations A1.20 and A1.25 to give

$$\begin{aligned}
 \eta &= \kappa \exp\left\{ \frac{-\kappa k^2 \theta^2 (\omega_\phi^2 + \omega_\psi^2)}{8} \right\} \exp\left\{ \frac{k^2 \theta x_o \kappa}{4} \left(\frac{\omega_\phi^2}{R_\phi} + \frac{\omega_\psi^2}{R_\psi}\right) \right\} \\
 &\quad \exp\left\{ \frac{-x_o^2 \kappa}{2} \left[\frac{1}{\omega_\phi^2} + \frac{1}{\omega_\psi^2} + \frac{k^2}{4} \left(\frac{\omega_\phi^2}{R_\phi^2} + \frac{\omega_\psi^2}{R_\psi^2}\right) \right] \right\}
 \end{aligned} \tag{A1.28}$$

which appears in chapter 3 as equation 3.13.

The explicit appearance of the position of the integration plane, d , has dropped out from the coupling efficiency, but it is still implicit in the expressions for ω , R and x_0 . The implicit dependance on d will now be removed.

The variables ω and R can be written as

$$\omega^2 = \omega_0^2(1 + \alpha) \quad A1.29$$

$$R = \frac{z}{\alpha}(1 + \alpha) \quad A1.30$$

$$\alpha = \frac{4z^2}{k^2\omega_0^4} \quad A1.31$$

Dividing A1.29 by A1.30 therefore produces

$$\frac{\omega^2}{R} = \frac{4z}{k^2\omega_0^2} \quad A1.32$$

Representing the terms inside the exponential of equation A1.28 by M , and substituting equations A1.29 to A1.32 produces

$$\begin{aligned} \frac{-2M}{\kappa} = x_0^2 & \left\{ \frac{k^2\omega_{0\phi}^2}{4zR_\phi} + \frac{k^2\omega_{0\psi}^2}{4(z-z_0)R_\psi} + \frac{z}{R_\phi\omega_{0\phi}^2} + \frac{(z-z_0)}{R_\psi\omega_{0\psi}^2} \right\} \\ & + \theta^2 \left\{ \frac{zR_\phi}{\omega_{0\phi}^2} + \frac{(z-z_0)R_\psi}{\omega_{0\psi}^2} \right\} - 2\theta x_0 \left(\frac{z}{\omega_{0\phi}^2} + \frac{(z-z_0)}{\omega_{0\psi}^2} \right) \end{aligned} \quad A1.33$$

Equation A1.30 can be used to show that

$$\frac{k^2\omega_0^2}{4Rz} = \frac{1}{\omega_0^2} - \frac{z}{R\omega_0^2} \quad A1.34$$

and hence

$$\begin{aligned} \frac{-2M}{\kappa} = x_0^2 & \left(\frac{1}{\omega_{0\phi}^2} + \frac{1}{\omega_{0\psi}^2} \right) + \theta^2 \left(\frac{zR_\phi}{\omega_{0\phi}^2} + \frac{(z-z_0)R_\psi}{\omega_{0\psi}^2} \right) \\ & - 2\theta x_0 \left(\frac{z}{\omega_{0\phi}^2} + \frac{(z-z_0)}{\omega_{0\psi}^2} \right) \end{aligned} \quad A1.35$$

Equation A1.30 can also be used to show that

$$\frac{zR}{\omega_o^2} = \frac{z^2}{\omega_o^2} + \frac{k^2\omega_o^2}{4} \quad A1.36$$

which is substituted into equation A1.35 to give

$$\begin{aligned} \frac{-2M}{\kappa} = & x_o^2 \left(\frac{1}{\omega_{o\phi}^2} + \frac{1}{\omega_{o\psi}^2} \right) + \theta^2 \left(\frac{z^2}{\omega_{o\phi}^2} + \frac{(z-z_o)^2}{\omega_{o\psi}^2} \right) \\ & + \frac{\theta^2 k^2}{4} (\omega_{o\phi}^2 + \omega_{o\psi}^2) - 2\theta x_o \left(\frac{z}{\omega_{o\phi}^2} + \frac{(z-z_o)}{\omega_{o\psi}^2} \right) \end{aligned} \quad A1.37$$

The expression for x_o , in equation A1.5, can now be substituted into equation A1.37 to give

$$\begin{aligned} \frac{-2M}{\kappa} = & \left(\frac{1}{\omega_{o\phi}^2} + \frac{1}{\omega_{o\psi}^2} \right) \left\{ X_o^2 + \theta^2 (z-z_o)^2 + 2\theta X_o (z-z_o) \right\} \\ & + \theta^2 \left(\frac{z^2}{\omega_{o\phi}^2} + \frac{(z-z_o)^2}{\omega_{o\psi}^2} \right) + \frac{\theta^2 k^2}{4} (\omega_{o\phi}^2 + \omega_{o\psi}^2) \\ & - 2\theta X_o \left(\frac{z}{\omega_{o\phi}^2} + \frac{(z-z_o)}{\omega_{o\psi}^2} \right) - 2\theta^2 (z-z_o) \left(\frac{z}{\omega_{o\phi}^2} + \frac{(z-z_o)}{\omega_{o\psi}^2} \right) \end{aligned} \quad A1.38$$

The terms in equation A1.38 cancel at an alarming rate to give

$$\frac{-2M}{\kappa} = \frac{\theta^2 k^2}{4} (\omega_{o\phi}^2 + \omega_{o\psi}^2) + X_o^2 \left(\frac{1}{\omega_{o\phi}^2} + \frac{1}{\omega_{o\psi}^2} \right) + \frac{\theta z_o (\theta z_o - 2X_o)}{\omega_{o\phi}^2} \quad A1.39$$

Equation A1.39 can be simplified further and inserted into equation A1.28 to give the coupling efficiency as

$$\eta = \kappa \exp \left\{ \frac{-\kappa}{2} \left[\frac{X_o^2}{\omega_{o\psi}^2} + \frac{(X_o - \theta z_o)^2}{\omega_{o\phi}^2} + \frac{\theta^2 k^2}{4} (\omega_{o\phi}^2 + \omega_{o\psi}^2) \right] \right\} \quad A1.40$$

This appears in chapter 3 as equation 3.14.

Appendix 2

Horn Lens Design.

```

PROGRAM lens_design_for_horns (input, output);
  CONST
    n_lens = 1.5250; {HDPE}
    no_of_points = 100;
    z_spacing = 0.1;
  TYPE
    parameter = ARRAY[0..no_of_points] OF real;
    radial_parameter = ARRAY[0..150] OF real;
  VAR
    f : text;
    prompt, defstring, filename : STRING;
    answer : char;
    i, radial_no_of_points : integer;
    calc_wmaxlens, correction, A, B, C, D, TangRin, TangRout, PlanarRin,
    PlanarRout : real;
    Tang_focal_length, Planar_focal_length, focal_length, oldzl_lens, zl_lens :
    real;
    Real_zrin, zrin, zrou, zin, Real_zin, zout, Rin, Rout, maxthrow : real;
    lens_thickness, blazing_depth, lambda, w0in, w0out, wmaxatlens,
    zout_to_planar, freq : real;
    lens_size, radial_spacing, zoutmax, w0outmax : real;
    r, zl : parameter;
    rad_r, rad_zl : radial_parameter;
    window : rect;
    reply : boolean;
  FUNCTION zr_fn (n, lambda, w0 : real) : real;
  BEGIN
    zr_fn := pi * w0 * w0 * n / lambda;
  END;

  FUNCTION z_fn (wmaxlens, w0, zr : real) : real;
  BEGIN
    z_fn := zr * sqrt(sqrt(wmaxlens / w0) - 1);
  END;

  FUNCTION w0_parallel_fn (w, z, wl : real) : real;
  BEGIN
    w0_parallel_fn := sqrt(w * w / 2 + sqrt((w * w * w * w / 4) - sqrt(wl * z /
    pi)));
  END;

  FUNCTION w0_focus_fn (w, z, wl : real) : real;
  BEGIN
    w0_focus_fn := sqrt(w * w / 2 - sqrt((w * w * w * w / 4) - sqrt(wl * z / pi)));
  END;

  FUNCTION w_fn (w0, z, zr : real) : real;
  BEGIN
    w_fn := w0 * sqrt(1 + sqrt(z / zr));
  END;

```

```

FUNCTION Rz_fn (z, zr : real) : real;
BEGIN
    IF z = 0 THEN
        Rz_fn := 1E20
    ELSE
        Rz_fn := z * (1 + sqr(zr / z));
    END;

FUNCTION zl_at_wmaxlens (wmaxlens : real; r, zl : parameter) : real;
    VAR
        i : integer;
    BEGIN
        FOR i := 1 TO no_of_points DO
            BEGIN
                IF (wmaxlens <= r[i]) AND (wmaxlens > r[i - 1]) THEN
                    zl_at_wmaxlens := zl[i - 1] + (zl[i] - zl[i - 1]) * (wmaxlens - r[i - 1]) /
(r[i] - r[i - 1]);
                    IF r[no_of_points] < wmaxlens THEN
                        writeln('ERROR - INSUFFICIENT POINTS');
                    END;
                END;
            END;

PROCEDURE sort_radially (r_points, z_points : integer; r_pitch : real);
    VAR
        i, j : integer;
    BEGIN
        rad_r[0] := 0;
        rad_zl[0] := 0;
        FOR j := 1 TO r_points DO
            FOR i := 1 TO z_points DO
                BEGIN
                    rad_r[j] := j * r_pitch;
                    IF (rad_r[j] <= r[i]) AND (rad_r[j] > r[i - 1]) THEN
                        rad_zl[j] := zl[i - 1] + (zl[i] - zl[i - 1]) * (rad_r[j] - r[i -
1]) / (r[i] - r[i - 1]);
                        IF r[no_of_points] < rad_r[j] THEN
                            writeln('ERROR - INSUFFICIENT POINTS');
                        END;
                    END;
                END;
            END;

BEGIN
    setrect(window, 0, 20, 512, 342);
    settextrct(window);
    showtext;
    writeln;
    writeln(' GAUSSIAN BEAM LENS DESIGN PROGRAM');
    writeln;
    writeln(' This program designs lenses to couple beams from a horn to a given
output beam. The input waist is');
    writeln('fixed and the horn position is determined by the program. ');
    writeln;
    writeln(' To design a lens for coupling an input beam of unknown waist but fixed
position, use the program BEAM LENS DESIGN');
    writeln;
    writeln('Dimensions in mm');
    write('Frequency [GHz] = ');
    readln(freq);
    lambda := 299.79 / freq;

```

```

writeln('Wavelength = ', lambda : 6 : 3);
write('Diameter of aperture = ');
readln(lens_size);
write('lens_thickness = ');
readln(lens_thickness);
write('Maximum field beamsize at aperture = ');
readln(wmaxatlens);
blazing_depth := lambda / (4 * sqrt(n_lens));
writeln('Blazing depth = ', blazing_depth : 6 : 3);
writeln('Radial pitch ought to be less than ', blazing_depth : 6 : 3);
write('Radial pitch = ');
readln(radial_spacing);
radial_no_of_points := 1 + round(lens_size / (2 * radial_spacing));
writeln('Radial no of points = ', radial_no_of_points);
write('w0in = ');
readln(w0in);
writeln;
zoutmax := zr_fn(0.5, lambda, wmaxatlens);
w0outmax := wmaxatlens / sqrt(2.0);
writeln('For a maximum throw, zout to planar = ', zoutmax : 6 : 3);
writeln('and the beamwaist, w0 out = ', w0outmax : 6 : 3);

REPEAT
{choose output beamwaist position relative to the planar surface - working from the}
{maximum beamsize at the planar surface}
    write('Focussed or Parallel waist at output, or Maximum throw? [F/P/M] ');
    readln(answer);
    reply := true;
    CASE answer OF
        'F', 'f' :
            BEGIN
                write('zout_to_planar = ');
                readln(zout_to_planar);
                w0out := w0_focus_fn(wmaxatlens, zout_to_planar,
lambda);
                writeln('w0 out = ', w0out : 6 : 3);
            END;
        'P', 'p' :
            BEGIN
                write('zout_to_planar = ');
                readln(zout_to_planar);
                w0out := w0_parallel_fn(wmaxatlens, zout_to_planar,
lambda);
                writeln('w0 out = ', w0out : 6 : 3);
            END;
        'M', 'm' :
            BEGIN
                zout_to_planar := zoutmax;
                w0out := w0outmax;
                writeln('zout to planar = ', zoutmax : 6 : 3);
                writeln('w0 out = ', w0outmax : 6 : 3);
            END;
        OTHERWISE
            reply := false
    END;
UNTIL reply;
{calculate the Rayleigh lengths}
zrin := zr_fn(n_lens, lambda, w0in);

```

```
zrout := zr_fn(1, lambda, w0out);
{first value for zin calculated from beamsize on planar surface}
zin := z_fn(wmaxatlens, w0in, zrin);
{zout is fixed as that measured from the planar surface but z=0 is at the tangential
surface}
zout := zout_to_planar - lens_thickness;
writeln;
writeln;
writeln('PRINCIPLE PARAMETERS');
writeln('(all dimensions in mm)');
writeln;
writeln('wavelength =', lambda : 10 : 3);
writeln('w0in =', w0in : 10 : 3);
writeln('w0out =', w0out : 10 : 3);
writeln('zout to planar surface =', zout_to_planar : 10 : 3);
writeln('w max =', wmaxatlens : 10 : 3);
writeln('Refractive Index of lens =', n_lens : 10 : 3);
writeln('Lens Thickness =', lens_thickness : 10 : 3);
oldzl_lens := 0;
calc_wmaxlens := wmaxatlens;
writeln;
writeln;
writeln('ITERATIVE CALCULATION');
writeln;
REPEAT
  writeln('new calculated w at lens =', calc_wmaxlens : 10 : 8);
  FOR i := 0 TO no_of_points DO
    BEGIN
      zl[i] := i * Z_spacing;
      A := n_lens / Rz_fn(zin - zl[i], zrin) + 1 / Rz_fn(zout + zl[i],
zrout);
      B := 2 * pi * (n_lens - 1) * zl[i] / lambda;
      C := arctan((zin - zl[i]) / zrin) - arctan(zin / zrin);
      D := arctan((zout + zl[i]) / zrout) - arctan(zout / zrout);
      r[i] := sqrt(lambda * (B + C + D) / (pi * A));
    END;
  {find where the output beamsize hits the new curved surface}
  zl_lens := zl_at_wmaxlens(calc_wmaxlens, r, zl);
  correction := zl_lens - oldzl_lens;
  {this is a measure of the change in the curved surface}
  writeln('correction to ZL(w) =', correction);
  {find the new beamsize at the curved surface due to the output beam}
  calc_wmaxlens := w_fn(w0out, zout_to_planar - lens_thickness + zl_lens,
zrout);
  {move the input beam until its beamsize at the curved surface equals the output
beamsize}
  zin := z_fn(calc_wmaxlens, w0in, zrin);
  oldzl_lens := zl_lens;
  UNTIL abs(correction) < 0.0000001;
  writeln('iteration end');
  writeln;
  writeln;
  writeln(' RADIAL LENS PROFILE (mm)');
  writeln;
  sort_radially(radial_no_of_points, no_of_points, radial_spacing);
  writeln('D' : 10, 'Z' : 8, 'Z-blazing' : 14);
  FOR i := 0 TO radial_no_of_points DO
```

```

        writeln(2 * rad_r[i] : 10 : 1, rad_zl[i] : 10 : 3, rad_zl[i] + blazing_depth : 10 :
3);
    writeln;
    writeln;
    writeln('PARAMETERS AT THIN LENS PLANE (Curved Surface)');
    Real_zin := (zin + (n_lens - 1) * (lens_thickness - zl_lens)) / n_lens;
    Real_zrin := zr_fn(1, lambda, w0in);
    Rin := Rz_fn(Real_zin, Real_zrin);
    Rout := Rz_fn(zout + zl_lens, zROUT);
    focal_length := 1 / (1 / Rin + 1 / Rout);
    writeln('zin to lens =', Real_zin : 10 : 3);
    writeln('w at thin lens plane =', w_fn(w0out, zout_to_planar - lens_thickness +
zl_lens, zROUT) : 10 : 3);
    writeln('imaginary zin =', zin : 10 : 3);
    writeln('zout to lens =', zout_to_planar - lens_thickness + zl_lens : 10 : 3);
    writeln('Rin =', Rin : 10 : 3);
    writeln('Rout =', Rout : 10 : 3);
    writeln('Focal Length =', focal_length : 10 : 3);
    writeln;
    writeln('PARAMETERS AT TANGENTIAL PLANE');
    TangRout := Rz_fn(zout_to_planar - lens_thickness, zROUT);
    TangRin := Rz_fn(Real_zin + zl_lens, Real_zrin);
    Tang_focal_length := 1 / (1 / TangRin + 1 / TangRout);
    writeln('w at lens =', calc_wmaxlens : 10 : 3);
    writeln('zout to lens =', zout_to_planar - lens_thickness : 10 : 3);
    writeln('zin to lens =', Real_zin + zl_lens : 10 : 3);
    writeln('Corrected Real Rin =', TangRin : 10 : 3);
    writeln('Corrected Rout =', TangRout : 10 : 3);
    writeln('Corrected Focal Length =', Tang_focal_length : 10 : 3);
    writeln;
    writeln('PARAMETERS ON PLANAR SURFACE');
    PlanarRout := Rz_fn(zout_to_planar, zROUT);
    PlanarRin := Rz_fn(Real_zin - lens_thickness + zl_lens, Real_zrin);
    Planar_focal_length := 1 / (1 / PlanarRin + 1 / PlanarRout);
    writeln('w at lens =', w_fn(w0in, Real_zin - lens_thickness + zl_lens, Real_zrin)
: 10 : 3);
    writeln('zout to lens =', zout_to_planar : 10 : 3);
    writeln('zin to lens =', Real_zin - lens_thickness + zl_lens : 10 : 3);
    writeln('Rin =', PlanarRin : 10 : 3);
    writeln('Rout =', PlanarRout : 10 : 3);
    writeln('Corrected Focal Length =', Planar_focal_length : 10 : 3);
    writeln;
    write('OUTPUT TO FILE? (Y/N): ');
    readln(answer);
    IF (answer = 'Y') OR (answer = 'y') THEN
        BEGIN
            prompt := 'INPUT FILENAME';
            defstring := 'Horn lens ';
            filename := newfilename(prompt, defstring);
            IF filename <> '' THEN
                BEGIN
                    rewrite(f, filename);
                    writeln(f, 'File =', filename);
                    writeln(f, '    PRINCIPLE PARAMETERS');
                    writeln(f, '    (all dimensions in mm)');
                    writeln(f, 'wavelength =', lambda : 6 : 3);
                    writeln(f, 'w0out =', w0out : 6 : 3);
                    writeln(f, 'Z out to planar =', zout_to_planar : 6 : 3);

```

```

        writeln(f, 'w0in = ', w0in : 6 : 3);
        writeln(f, 'Lens Thickness =', lens_thickness : 6 : 3);
        writeln(f);
        writeln(f, '    PARAMETERS AT THIN LENS PLANE
(Curved Surface)');
        writeln(f, 'zin to lens =', Real_zin : 10 : 3);
        writeln(f, 'w at thin lens plane =', w_fn(w0out,
zout_to_planar - lens_thickness + zl_lens, zroun) : 10 : 3);
        writeln(f, 'imaginary zin =', zin : 10 : 3);
        writeln(f, 'zout to lens =', zout_to_planar - lens_thickness +
zl_lens : 10 : 3);
        writeln(f, 'Rin =', Rin : 10 : 3);
        writeln(f, 'Rout =', Rout : 10 : 3);
        writeln(f, 'Focal Length =', focal_length : 10 : 3);
        writeln(f);
        writeln(f, '    PARAMETERS AT TANGENTIAL PLANE');
        writeln(f, 'w at lens =', calc_wmaxlens : 10 : 3);
        writeln(f, 'zout to lens =', zout_to_planar - lens_thickness :
10 : 3);
        writeln(f, 'zin to lens =', Real_zin + zl_lens : 10 : 3);
        writeln(f, 'Corrected Real Rin =', TangRin : 10 : 3);
        writeln(f, 'Corrected Rout =', TangRout : 10 : 3);
        writeln(f, 'Corrected Focal Length =', Tang_focal_length :
10 : 3);
        writeln(f);
        writeln(f, '    PARAMETERS ON PLANAR SURFACE');
        writeln(f, 'w at lens =', w_fn(w0in, Real_zin -
lens_thickness + zl_lens, Real_zrin) : 10 : 3);
        writeln(f, 'zout to lens =', zout_to_planar : 10 : 3);
        writeln(f, 'zin to lens =', Real_zin - lens_thickness + zl_lens
: 10 : 3);
        writeln(f, 'Rin =', PlanarRin : 10 : 3);
        writeln(f, 'Rout =', PlanarRout : 10 : 3);
        writeln(f, 'Corrected Focal Length =', Planar_focal_length :
10 : 3);
        writeln(f);
        writeln(f, 'File =', filename);
        writeln(f, 'Lens thickness without blazing =', lens_thickness
: 6 : 3);
        writeln(f, '    RADIAL LENS PROFILE (mm) Blazing
Depth =', blazing_depth : 6 : 3);
        writeln(f);
        writeln(f, '    D          Z absolute          Z relative');
        writeln(f);
        writeln(f, 2 * rad_r[0] : 6 : 1, CHR(9), rad_zl[0] : 6 : 3);
        FOR i := 1 TO radial_no_of_points DO
            BEGIN
                writeln(f, 2 * rad_r[i] : 6 : 1, CHR(9), rad_zl[i] : 6
: 3, CHR(9), rad_zl[i] - rad_zl[i - 1] : 6 : 3);
            END;
        close(f);
    END;
    writeln;
    writeln('FINISHED');
END;
END.
```

Beam Lens Design.

PROGRAM lens_design_for_horns (input, output);

CONST

n_lens = 1.5250; {HDPE}
no_of_points = 160;
z_spacing = 0.1;

TYPE

parameter = ARRAY[0..no_of_points] OF real;
radial_parameter = ARRAY[0..150] OF real;

VAR

f : text;
prompt, defstring, filename : STRING;
answer : char;
i, radial_no_of_points : integer;
calc_wmaxlens, correction, A, B, C, D, TangRin, TangRout, PlanarRin,
PlanarRout : real;
Tang_focal_length, Planar_focal_length, focal_length, oldzl_lens, zl_lens :
real;
Real_zrin, zrin, zrout, zin, z_lens, Real_zin, zout, Rin, Rout, maxthrow :
real;
lens_thickness, blazing_depth, lambda, w0in, w0out, wmaxatlens,
zout_to_planar, freq : real;
zin_to_planar, lens_size, radial_spacing, zoutmax, w0outmax : real;
r, zl : parameter;
rad_r, rad_zl : radial_parameter;
window : rect;
reply, focus_input : boolean;

FUNCTION zr_fn (n, lambda, w0 : real) : real;

BEGIN

zr_fn := pi * w0 * w0 * n / lambda;

END;

FUNCTION z_fn (wmaxlens, w0, zr : real) : real;

BEGIN

z_fn := zr * sqrt(sqr(wmaxlens / w0) - 1);

END;

FUNCTION w0_parallel_fn (w, z, wl : real) : real;

BEGIN

w0_parallel_fn := sqrt(w * w / 2 + sqrt((w * w * w * w / 4) - sqr(wl * z /
pi)));

END;

FUNCTION w0_focus_fn (w, z, wl : real) : real;

BEGIN

w0_focus_fn := sqrt(w * w / 2 - sqrt((w * w * w * w / 4) - sqr(wl * z / pi)));

END;

FUNCTION w_fn (w0, z, zr : real) : real;


```

BEGIN
    w_fn := w0 * sqrt(1 + sqr(z / zr));
END;

FUNCTION Rz_fn (z, zr : real) : real;
BEGIN
    IF z = 0 THEN
        Rz_fn := 1E20
    ELSE
        Rz_fn := z * (1 + sqr(zr / z));
    END;
END;

FUNCTION zl_at_wmaxlens (wmaxlens : real;
                        r, zl : parameter) : real;
    VAR
        i : integer;
    BEGIN
        FOR i := 1 TO no_of_points DO
            BEGIN
                IF (wmaxlens <= r[i]) AND (wmaxlens > r[i - 1]) THEN
                    zl_at_wmaxlens := zl[i - 1] + (zl[i] - zl[i - 1]) * (wmaxlens -
r[i - 1]) / (r[i] - r[i - 1]));
                    IF r[no_of_points] < wmaxlens THEN
                        writeln('ERROR - INSUFFICIENT POINTS');
                    END;
                END;
            END;
        END;

    PROCEDURE sort_radially (r_points, z_points : integer;
                            r_pitch : real);
        VAR
            i, j : integer;
        BEGIN
            rad_r[0] := 0;
            rad_zl[0] := 0;
            FOR j := 1 TO r_points DO
                FOR i := 1 TO z_points DO
                    BEGIN
                        rad_r[j] := j * r_pitch;
                        IF (rad_r[j] <= r[i]) AND (rad_r[j] > r[i - 1]) THEN
                            rad_zl[j] := zl[i - 1] + (zl[i] - zl[i - 1]) * (rad_r[j] - r[i -
1]) / (r[i] - r[i - 1]));
                            IF r[no_of_points] < rad_r[j] THEN
                                writeln('ERROR - INSUFFICIENT POINTS');
                            END;
                        END;
                    END;
                END;
            END;

    BEGIN
        setrect(window, 0, 20, 512, 342);
        settextrct(window);
        showtext;
        writeln;
        writeln(' GAUSSIAN BEAM LENS DESIGN PROGRAM');
        writeln;
        writeln('This program designs lenses to couple beams from an input waist of
unknown ');
        writeln('size but fixed position, to a given output beam . The waist size is
determined ');
    
```

```

writeln('by the program .');
writeln;
writeln(' To design a lens for coupling a beam from a horn use the program ');
writeln(' *** HORN LENS DESIGN *** ');
writeln;
writeln('Dimensions in mm');
write('Frequency [GHz] = ');
readln(freq);
lambda := 299.79 / freq;
writeln('Wavelength = ', lambda : 6 : 3);
write('Diameter of aperture = ');
readln(lens_size);
write('lens_thickness = ');
readln(lens_thickness);
write('Maximum field beamsize at aperture = ');
readln(wmaxatlens);
blazing_depth := lambda / (4 * sqrt(n_lens));
writeln('Blazing depth = ', blazing_depth : 6 : 3);
writeln('Radial pitch ought to be less than ', blazing_depth : 6 : 3);
write('Radial pitch = ');
readln(radial_spacing);
radial_no_of_points := 1 + round(lens_size / (2 * radial_spacing));
writeln('Radial no of points = ', radial_no_of_points);
writeln;
zoutmax := zr_fn(0.5, lambda, wmaxatlens);
w0outmax := wmaxatlens / sqrt(2.0);
writeln('For a maximum throw, z to planar = ', zoutmax : 6 : 3);
writeln('and the beamwaist, w0 = ', w0outmax : 6 : 3);
writeln;
writeln('***** Characteristics of INPUT beam *****');
REPEAT
{choose input beamwaist position relative to the planar surface - working from the}
{maximum beamsize at the planar surface}
    write('Focussed or Parallel waist at input, or Maximum throw? [F/P/M] ');
    readln(answer);
    reply := true;
    CASE answer OF
        'F', 'f' :
            BEGIN
                write('zin_to_planar = ');
                readln(zin_to_planar);
                focus_input := true;
            END;
        'P', 'p' :
            BEGIN
                write('zin_to_planar = ');
                readln(zin_to_planar);
                focus_input := false;
            END;
        OTHERWISE
            reply := false
    END;
UNTIL reply;
writeln;
writeln('***** Characteristics of OUTPUT beam *****');
REPEAT
{choose output beamwaist position relative to the planar surface - working from the}
{maximum beamsize at the planar surface}

```

```

write('Focussed or Parallel waist at output, or Maximum throw? [F/P/M] ');
readln(answer);
reply := true;
CASE answer OF
    'F', 'f' :
        BEGIN
            write('zout_to_planar = ');
            readln(zout_to_planar);
            w0out := w0_focus_fn(wmaxatlens, zout_to_planar,
lambda);
            writeln('w0 out = ', w0out : 6 : 3);
        END;
    'P', 'p' :
        BEGIN
            write('zout_to_planar = ');
            readln(zout_to_planar);
            w0out := w0_parallel_fn(wmaxatlens, zout_to_planar,
lambda);
            writeln('w0 out = ', w0out : 6 : 3);
        END;
    'M', 'm' :
        BEGIN
            zout_to_planar := zoutmax;
            w0out := w0outmax;
            writeln('zout to planar = ', zoutmax : 6 : 3);
            writeln('w0 out = ', w0outmax : 6 : 3);
        END;
    OTHERWISE
        reply := false
END;
UNTIL reply;
{ first value for w0in calculated from beamsizes on planar surface and zin }
IF focus_input THEN
    BEGIN
        w0in := w0_focus_fn(wmaxatlens, zin_to_planar, lambda)
    END
ELSE
    BEGIN
        w0in := w0_parallel_fn(wmaxatlens, zin_to_planar, lambda)
    END;
{ calculate the Rayleigh lengths }
zrin := zr_fn(n_lens, lambda, w0in);
zrout := zr_fn(1, lambda, w0out);
{ zout is fixed as that measured from the planar surface }
zout := zout_to_planar;
{ z_lens is the distance from the input waist to the principle plane, but is transformed }
{ into the equivalent length in the dielectric }
z_lens := n_lens * zin_to_planar + lens_thickness;
{ zin is fixed as that measured from the curved surface, but is transformed }
{ into the equivalent length in the dielectric }
zin := z_lens;
writeln;
writeln;
writeln('PRINCIPLE PARAMETERS');
writeln('(all dimensions in mm)');
writeln;
writeln('wavelength =', lambda : 10 : 3);
writeln('zin to planar surface =', zin_to_planar : 10 : 3);

```

```

writeln('w0out = ', w0out : 10 : 3);
writeln('zout to planar surface =', zout_to_planar : 10 : 3);
writeln('w max = ', wmaxatlens : 10 : 3);
writeln('Refractive Index of lens =', n_lens : 10 : 3);
writeln('Lens Thickness =', lens_thickness : 10 : 3);
oldzl_lens := 0;
calc_wmaxlens := wmaxatlens;
writeln;
writeln;
writeln('ITERATIVE CALCULATION');
writeln;
REPEAT
    writeln('w0 in = ', w0in : 6 : 3, ' new calculated w at lens = ',
calc_wmaxlens : 10 : 8);
    FOR i := 0 TO no_of_points DO
        BEGIN
            zl[i] := i * Z_spacing;
            A := n_lens / Rz_fn(zin - zl[i], zrin) + 1 / Rz_fn(zout + zl[i],
zrout);
            B := 2 * pi * (n_lens - 1) * zl[i] / lambda;
            C := arctan((zin - zl[i]) / zrin) - arctan(zin / zrin);
            D := arctan((zout + zl[i]) / zrout) - arctan(zout / zrout);
            r[i] := sqrt(lambda * (B + C + D) / (pi * A));
        END;
    {find where the new curved surface has a radius equal to the old beamsize}
    zl_lens := zl_at_wmaxlens(calc_wmaxlens, r, zl);
    correction := zl_lens - oldzl_lens;
    {this is a measure of the change in the curved surface}
    writeln('correction to ZL(w) = ', correction);
    {find the new beamsize at the curved surface due to the output beam}
    calc_wmaxlens := w_fn(w0out, zout_to_planar - lens_thickness + zl_lens,
zrout);
    {calculate the input beamwaist required to give this beamsize at the lens}
    IF focus_input THEN
        BEGIN
            w0in := w0_focus_fn(calc_wmaxlens, z_lens - zl_lens, lambda /
n_lens)
        END
    ELSE
        BEGIN
            w0in := w0_parallel_fn(calc_wmaxlens, z_lens - zl_lens, lambda /
n_lens)
        END;
    {calculate the new input Rayleigh length}
    zrin := zr_fn(n_lens, lambda, w0in);
    zin := z_lens - zl_lens;
    oldzl_lens := zl_lens;
    UNTIL abs(correction) < 0.0000001;
    writeln('iteration end');
    writeln;
    writeln;
    writeln(' RADIAL LENS PROFILE (mm)');
    writeln;
    sort_radially(radial_no_of_points, no_of_points, radial_spacing);
    writeln('D' : 10, 'Z' : 8, 'Z-blazing' : 14);
    FOR i := 0 TO radial_no_of_points DO
        writeln(2 * rad_r[i] : 10 : 1, rad_zl[i] : 10 : 3, rad_zl[i] + blazing_depth : 10 :
3);

```

```
writeln;
writeln;
writeln('PARAMETERS AT THIN LENS PLANE (Curved Surface)');
Real_zin := (zin + (n_lens - 1) * (lens_thickness - zl_lens)) / n_lens;
Real_zrin := zr_fn(1, lambda, w0in);
Rin := Rz_fn(Real_zin, Real_zrin);
Rout := Rz_fn(zout, zrou);
focal_length := 1 / (1 / Rin + 1 / Rout);
writeln('zin to lens =', Real_zin : 10 : 3);
writeln('w at thin lens plane =', w_fn(w0out, zout_to_planar - lens_thickness +
zl_lens, zrou) : 10 : 3);
writeln('imaginary zin =', zin : 10 : 3);
writeln('zout to lens =', zout_to_planar - lens_thickness + zl_lens : 10 : 3);
writeln('Rin =', Rin : 10 : 3);
writeln('Rout =', Rout : 10 : 3);
writeln('Focal Length =', focal_length : 10 : 3);
writeln;
writeln('PARAMETERS AT TANGENTIAL PLANE');
TangRout := Rz_fn(zout_to_planar - lens_thickness, zrou);
TangRin := Rz_fn(Real_zin + zl_lens, Real_zrin);
Tang_focal_length := 1 / (1 / TangRin + 1 / TangRout);
writeln('w at lens =', calc_wmaxlens : 10 : 3);
writeln('zout to lens =', zout_to_planar - lens_thickness : 10 : 3);
writeln('zin to lens =', Real_zin + zl_lens : 10 : 3);
writeln('Corrected Real Rin =', TangRin : 10 : 3);
writeln('Corrected Rout =', TangRout : 10 : 3);
writeln('Corrected Focal Length =', Tang_focal_length : 10 : 3);
writeln;
writeln('PARAMETERS ON PLANAR SURFACE');
PlanarRout := Rz_fn(zout_to_planar, zrou);
PlanarRin := Rz_fn(Real_zin - lens_thickness + zl_lens, Real_zrin);
Planar_focal_length := 1 / (1 / PlanarRin + 1 / PlanarRout);
writeln('w at lens =', w_fn(w0in, Real_zin - lens_thickness + zl_lens, Real_zrin)
: 10 : 3);
writeln('zout to lens =', zout_to_planar : 10 : 3);
writeln('zin to lens =', Real_zin - lens_thickness + zl_lens : 10 : 3);
writeln('Rin =', PlanarRin : 10 : 3);
writeln('Rout =', PlanarRout : 10 : 3);
writeln('Corrected Focal Length =', Planar_focal_length : 10 : 3);
writeln;
write('OUTPUT TO FILE? (Y/N): ');
readln(answer);
IF (answer = 'Y') OR (answer = 'y') THEN
  BEGIN
    prompt := 'INPUT FILENAME';
    defstring := 'Beam lens ';
    filename := newfilename(prompt, defstring);
    IF filename <> '' THEN
      BEGIN
        rewrite(f, filename);
        writeln(f, 'File =', filename);
        writeln(f, '  PRINCIPLE PARAMETERS');
        writeln(f, '    (all dimensions in mm)');
        writeln(f, 'wavelength =', lambda : 6 : 3);
        writeln(f, 'w0out =', w0out : 6 : 3);
        writeln(f, 'Z out to planar =', zout_to_planar : 6 : 3);
        writeln(f, 'Z in to planar =', zin_to_planar : 6 : 3);
        writeln(f, 'Lens Thickness =', lens_thickness : 6 : 3);
```

```

                                writeln(f);
                                writeln(f, '  PARAMETERS AT THIN LENS PLANE
(Curved Surface)');
                                writeln(f, 'zin to lens =', Real_zin : 10 : 3);
                                writeln(f, 'w at thin lens plane =', w_fn(w0out,
zout_to_planar - lens_thickness + zl_lens, zroun) : 10 : 3);
                                writeln(f, 'imaginary zin =', zin : 10 : 3);
                                writeln(f, 'zout to lens =', zout_to_planar - lens_thickness +
zl_lens : 10 : 3);
                                writeln(f, 'Rin =', Rin : 10 : 3);
                                writeln(f, 'Rout =', Rout : 10 : 3);
                                writeln(f, 'Focal Length =', focal_length : 10 : 3);
                                writeln(f);
                                writeln(f, '  PARAMETERS AT TANGENTIAL PLANE');
                                writeln(f, 'w at lens =', calc_wmaxlens : 10 : 3);
                                writeln(f, 'zout to lens =', zout_to_planar - lens_thickness :
10 : 3);
                                writeln(f, 'zin to lens =', Real_zin + zl_lens : 10 : 3);
                                writeln(f, 'Corrected Real Rin =', TangRin : 10 : 3);
                                writeln(f, 'Corrected Rout =', TangRout : 10 : 3);
                                writeln(f, 'Corrected Focal Length =', Tang_focal_length :
10 : 3);
                                writeln(f);
                                writeln(f, '  PARAMETERS ON PLANAR SURFACE');
                                writeln(f, 'w at lens =', w_fn(w0in, Real_zin -
lens_thickness + zl_lens, Real_zrin) : 10 : 3);
                                writeln(f, 'zout to lens =', zout_to_planar : 10 : 3);
                                writeln(f, 'zin to lens =', Real_zin - lens_thickness + zl_lens
: 10 : 3);
                                writeln(f, 'Rin =', PlanarRin : 10 : 3);
                                writeln(f, 'Rout =', PlanarRout : 10 : 3);
                                writeln(f, 'Corrected Focal Length =', Planar_focal_length :
10 : 3);
                                writeln(f);
                                writeln(f, 'File =', filename);
                                writeln(f, 'Lens thickness without blazing =', lens_thickness
: 6 : 3);
                                writeln(f, '  RADIAL LENS PROFILE (mm) Blazing
Depth =', blazing_depth : 6 : 3);
                                writeln(f);
                                writeln(f, '  D          Z absolute      Z relative');
                                writeln(f);
                                writeln(f, 2 * rad_r[0] : 6 : 1, CHR(9), rad_zl[0] : 6 : 3);
                                FOR i := 1 TO radial_no_of_points DO
                                    BEGIN
                                        writeln(f, 2 * rad_r[i] : 6 : 1, CHR(9), rad_zl[i] : 6
: 3, CHR(9), rad_zl[i] - rad_zl[i - 1] : 6 : 3);
                                    END;
                                close(f);
                                END;
                                writeln;
                                writeln('FINISHED');
                                END;
END.
```

Appendix 3

Wire Heating Program.

```
PROGRAM hot_wire (input, output);
  CONST
    no_of_sections = 50;
    sigma = 5.7E-08;
  TYPE
    profile = ARRAY[0..no_of_sections] OF real;
  VAR
    f : text;
    prompt, defstring, filename : STRING;
    answer : char;
    p_unit : STRING;
    p_factor : real;
    window : rect;
    reply, stop_run : boolean;
  { wire parameters }
    L_wire, diam_wire, mass_wire, therm_cond_wire : real;
    rho_wire, Tmax_wire, Cspec_wire, min_T_step : real;
    T_ambient, T_start, T_block, alpha, delta_Temp, dTemp, w_at_wire,
    A_surface, A_csa : real;
    pitch, dt, dx, h, Tmax_so_far, Old_Tmax, t_average : real;
    Pout_max, Pout_total, P_beam : real;
    P_beam_scaled, P_wire, Q_out_total, Qout_to_block : real;
    P_vs_T : ARRAY[0..201, 0..1] OF real;
    Q_in, Q_out, P_in, T_wire : profile;
    time_response_of_wire : ARRAY[0..201] OF real;
    i, j, k, x, x_hot, time, stop_time, Temperature : integer;

  PROCEDURE units (power : real);
  BEGIN
    IF power < 0 THEN
      BEGIN
        p_unit := ' negative ';
        p_factor := 1;
      END;
    IF power > 0.001 THEN
      BEGIN
        p_unit := ' mW';
        p_factor := 0.001;
      END;
    IF power > 1 THEN
      BEGIN
        p_unit := ' W';
        p_factor := 1;
      END;
    IF power > 1000 THEN
      BEGIN
        p_unit := ' kW';
        p_factor := 1000;
      END;
    END;
```

```

IF power > 1000000 THEN
    BEGIN
        p_unit := ' MW';
        p_factor := 1000000;
    END;
END;

FUNCTION epsilon (t_abs : real) : real;
BEGIN
    epsilon := -1.089E-02 + (1.1339E-04 * t_abs) + (2.5823E-08 * sqr(t_abs)) -
(8.3074E-12 * t_abs * sqr(t_abs));
END;

FUNCTION radiate (i : integer) : real;
VAR
    T, T_local : real;
BEGIN
    T_local := 273 + T_ambient;
    T := T_wire[i] + 273; {absolute temp required}
    radiate := epsilon(T) * sigma * A_surface * (sqr(sqr(T)) -
sqr(sqr(T_local))); {Watts}
END;

FUNCTION conduct (i : integer) : real;
VAR
    Qin, Qout : real;
BEGIN
    {Qout is heat flowing from i to i+1}
    IF i = no_of_sections THEN
        BEGIN
            Qout := -therm_cond_wire * A_csa * (T_block - T_wire[i]) / dx;
            T_block := T_block + (T_wire[i] - T_block) * (1 - exp(-dt /
100)); {heating up}
            T_block := T_ambient + (T_block - T_ambient) * exp(-dt /
100); {cooling down}
            { 100 seconds is an experimentally determined time constant}
            { T_block := exp(-dt / 100) * (T_block + Qout / 0.5)}
            { 0.5 is a value for mC for a small ring of Aluminium}
            {exp() is the cooling during the time interval dt}
            Qout_to_block := Qout;
        END
    ELSE
        BEGIN
            Qout := -therm_cond_wire * A_csa * (T_wire[i + 1] - T_wire[i]) /
dx
        END;
    {Qin is heat flowing from i-1 to i}
    IF i = 0 THEN
        BEGIN
            Qin := 0;
            Qout := 2 * Qout; {heat leaves from both sides}
        END
    ELSE
        BEGIN

```



```

dx;
        Qin := -therm_cond_wire * A_csa * (T_wire[i] - T_wire[i - 1]) /
END;
        END;
        conduct := (Qout - Qin); { Watts}
END;

FUNCTION convect (i : integer) : real;
BEGIN
    h := 4.186 * sqrt(sqrt(abs(T_wire[i] - T_ambient) / diam_wire));
    convect := A_surface * h * (T_wire[i] - T_ambient); { Watts}
END;

FUNCTION absorption (T_abs : real) : real;
VAR
    resistivity : real;
BEGIN
    resistivity := (-2.8151 + 2.5964E-02 * T_abs + 1.8816E-06 * sqrt(T_abs)) *
1E-08;
    absorption := 4 * sqrt(2.7816 * resistivity);
END;

FUNCTION P_density (i : integer;
                    T_rel : real) : real;
VAR
    fraction : real;
BEGIN
    fraction := pitch * 2 / (pi * sqrt(w_at_wire));
    P_density := P_beam * absorption(T_rel + 273) * exp(-2 * sqrt(i * dx /
w_at_wire));
END;

PROCEDURE Input_parameters;
BEGIN
    write('Usual data? [y/n] ');
    readln(answer);
    IF (answer = 'Y') OR (answer = 'y') THEN
        BEGIN
            L_wire := 60E-03;
            diam_wire := 25.0E-06;
            rho_wire := 19300.0;
            therm_cond_wire := 173.0;
            Cspec_wire := 133.0;
            pitch := 50.0E-06;
        END
    ELSE
        BEGIN
            writeln(' Input wire parameters');
            write('Length of wire [mm] = ');
            readln(L_wire);
            L_wire := L_wire / 1000;
            write('Diameter of wire [um] = ');
            readln(diam_wire);
            diam_wire := diam_wire * 1E-06;
            write('Pitch of wires [um] = ');
            readln(pitch);
            pitch := pitch * 1E-06;
        END
    END;
END;

```

```

        write('Density of wire [kg/m3] = ');
        readln(rho_wire);
        write('Thermal conductivity [W/m/K] = ');
        readln(therm_cond_wire);
        write('Specific Heat capacity [J/K/kg] = ');
        readln(Cspec_wire);
    END;
    write('Maximum temperature of wire [deg C] = ');
    readln(Tmax_wire);
    write('Ambient temperature [deg C] = ');
    readln(T_ambient);
    write('Minimum temperature step if T max is not reached [deg C] = ');
    readln(min_T_step);
    writeln;
    write('Beam size at wire [mm] =');
    readln(w_at_wire);
    w_at_wire := w_at_wire / 1000;
END;

```

```

PROCEDURE set_up;
    VAR
        x, t, Temp : integer;

```

```

    BEGIN
    {*****Calculate parameters for each section*****}
        A_csa := pi * sqr(diam_wire) / 4; {m2}
        dx := 0.5 * L_wire / no_of_sections; {m}
        A_surface := pi * diam_wire * dx; {m2}
        mass_wire := rho_wire * A_csa * dx; {kg}

        write('Required power in input beam [W] = ');
        readln(P_beam);
        write('Time interval [msec] = ');
        readln(dt);
        dt := dt / 1000;
        writeln('Setting up data .....');
        writeln;
        T_start := T_ambient;
        T_block := T_ambient;
        alpha := 100000; {found empirically}
        FOR x := 0 TO no_of_sections DO
            BEGIN
                Q_in[x] := 0;
                P_in[x] := dx * P_density(x, T_start);
                T_wire[x] := T_start;
                Q_out[x] := 0;
                FOR t := 0 TO 200 DO
                    BEGIN
                        time_response_of_wire[t] := T_start;
                    END;
                END;
            END;
            Tmax_so_far := T_start;
            Old_Tmax := T_start;
            stop_run := false;
            Temperature := 0;
            dTemp := (Tmax_wire - T_ambient) / 100;

```

```

END;

PROCEDURE output_data;
  VAR
    x, t : integer;
    T_hot : real;

  BEGIN
    writeln('Time taken to reach maximum temperature [sec] =', dt * stop_time :
10 : 6);
    writeln;
    Pout_total := Q_out_total;
    units(Pout_total);
    writeln('Actual maximum rate of heat removal = ', Pout_total / p_factor : 6 :
2, p_unit);
    writeln;
    T_hot := T_ambient;
    FOR x := 0 TO no_of_sections DO
      BEGIN
        IF T_wire[x] >= T_hot THEN
          BEGIN
            T_hot := T_wire[x];
            x_hot := x;
          END;
        END;
      BEGIN
        writeln('Position of hot spot = section ', x_hot : 2);
        writeln('Last temperature step = ', delta_temp : 6 : 3);
        writeln('Maximum temperature reached [deg C] = ', Tmax_so_far : 6 : 2);
        units(P_beam);
        writeln('Power in input beam = ', P_beam / p_factor : 6 : 2, p_unit);
        writeln;
        writeln;
        write('OUTPUT PROFILES TO FILE? (Y/N): ');
        readln(answer);
        IF (answer = 'Y') OR (answer = 'y') THEN
          BEGIN
            prompt := 'INPUT FILENAME';
            defstring := 'Wire profile';
            filename := newfilename(prompt, defstring);
            IF filename <> '' THEN
              BEGIN
                rewrite(f, filename);
                {position  Temp  }
                FOR x := 0 TO no_of_sections DO
                  BEGIN
                    writeln(f, x, CHR(9), T_wire[x] : 14);
                  END;
                writeln(f);
                {temp[0]  Q_out_total}
                FOR t := 0 TO Temperature - 1 DO
                  BEGIN
                    writeln(f, P_vs_T[t, 0] : 14, CHR(9),
P_vs_T[t, 1] : 14);
                  END;
                FOR t := 1 TO stop_time DO
                  BEGIN
                    IF (t MOD 5) = 0 THEN

```

```

                                BEGIN
                                writeln(f, t, CHR(9),
time_response_of_wire[(t DIV 5)] : 14);
                                END;
                                END;
                                writeln(f, stop_time, CHR(9),
time_response_of_wire[1 + (stop_time DIV 5)] : 14);
                                close(f);
                                END;
                                END;
                                END;

{ *****MAIN PROGRAM***** }
BEGIN
    setrect(window, 0, 20, 512, 342);
    settextrct(window);
    showtext;
    writeln;
    writeln('          THERMAL EFFECTS IN A WIRE');
    writeln;
    Input_parameters;
    set_up;
    writeln('Working ...');
    writeln;
    time := 0;
    REPEAT
        write('.');
        time := time + 1;
        IF (time MOD 20) = 0 THEN
            writeln('time =', time : 3, '    T max so far =', Tmax_so_far : 4 : 1, '
Temp step =', delta_temp : 6 : 3);
            Q_out_total := 0;
            FOR x := 0 TO no_of_sections DO
                BEGIN
                    Q_in[x] := dt * P_in[x];
                    Q_out[x] := dt * (radiate(x) + convect(x) + conduct(x));
                    Q_out_total := Q_out_total + radiate(x) + convect(x);
                END;
            { Total heat loss is sum of radiative and convective losses for all sections plus }
            { conductive losses from the end section }
            Q_out_total := (Q_out_total + Qout_to_block) * dt;

            { Update the temperature profile based on the new heat losses }
            Old_Tmax := Tmax_so_far;
            FOR x := 0 TO no_of_sections DO
                BEGIN
                    T_wire[x] := T_wire[x] + (Q_in[x] - Q_out[x]) / (mass_wire *
Cspec_wire);
                    IF T_wire[x] > Tmax_so_far THEN
                        BEGIN
                            Tmax_so_far := T_wire[x];
                            x_hot := x;
                        END;
                    END;
            END;

```

```
{output interim data}
{** record Heat loss as a function of temperature **}
  IF (time MOD 5) = 0 THEN
    BEGIN
      P_vs_T[Temperature, 0] := T_wire[0];
      P_vs_T[Temperature, 1] := Q_out_total;
      Temperature := Temperature + 1;
      IF Temperature >= 200 THEN
        stop_run := true;
      END;
    {** record central temp as a function of time **}
    IF (time MOD 5) = 0 THEN
      BEGIN
        time_response_of_wire[(time DIV 5)] := T_wire[1];
        IF (time DIV 5) > 200 THEN
          stop_run := true;
        END;
      {** Check for ending conditions **}
      delta_Temp := Tmax_so_far - Old_Tmax;
      {ask_to_stop;}
      IF delta_Temp < min_T_step THEN
        stop_run := true;
      IF Tmax_so_far >= Tmax_wire THEN
        stop_run := true;
      UNTIL stop_run;

      writeln;{end the dots}
      time_response_of_wire[(1 + time DIV 5)] := T_wire[1];
      stop_time := time;
      output_data;
      writeln('Finished');
    END.
```

Appendix 4

Matrix Representation of Misalignment Parameters

The use of a matrix to represent the misalignment of a beam is presented in chapter 3, equation 3.78. The elements in the matrix are determined using the processes discussed in chapter 3. It would be tedious, even in an appendix, to lay out these processes for every element and hence they are summarized here. Much use is made of

- The centroid position Equation 3.45.
- Its positional error Equations 3.46 and 3.47.
- Its rotational error Equation 3.51.
- The *active* plane position Equation 3.52.
- Its positional error Equations 3.53 and 3.54.

The active plane is defined as the plane at which the beam transformation effectively takes place : a thin-lens plane, a mirror or polarizer etc.

The general form of the matrix is

$$\begin{array}{c}
 \begin{array}{cccc}
 & x & z & \psi & \text{const} \\
 x & \left(\begin{array}{cccc} 1 & - & - & - \end{array} \right) & \left(\begin{array}{c} \sigma^2(x) \\ \sigma^2(z) \\ \sigma^2(\psi) \\ 1 \end{array} \right)_{\text{in}} & = & \left(\begin{array}{c} \sigma^2(x) \\ \sigma^2(z) \\ \sigma^2(\psi) \\ 1 \end{array} \right)_{\text{out}} \\
 z & & & & \\
 \psi & & & & \\
 \text{const} & \left(\begin{array}{cccc} 0 & 0 & 0 & 1 \end{array} \right) & & &
 \end{array}
 \end{array} \quad \text{A4.1}$$

Note that it is convenient to work in terms of variances (σ^2). The specific matrices are given below and, where appropriate evaluated numerically. The numerical form is for the specific components used within this system and the appropriate parameters are listed.

Reflection at a 45° Mirror or Polarizer.

$$E_R = \begin{pmatrix} 1 & 0 & 0 & 4\sin^2\alpha \cdot \sigma^2(s) \\ 0 & 1 & 0 & 4\cos^2\alpha \cdot \sigma^2(s) \\ 0 & 0 & 1 & 4\sigma^2(\theta) \\ 0 & 0 & 0 & 1 \end{pmatrix} = \begin{pmatrix} 1 & 0 & 0 & 1.24 \times 10^{-3} \text{mm}^2 \\ 0 & 1 & 0 & 1.24 \times 10^{-3} \text{mm}^2 \\ 0 & 0 & 1 & 9.2 \times 10^{-6} \text{rad}^2 \\ 0 & 0 & 0 & 1 \end{pmatrix}$$

where
 $\sigma^2(C) = 1.33 \times 10^{-4} \text{mm}^2$
 $\sigma^2(\theta) = 2.3 \times 10^{-6} \text{rad}^2$
 $f = 20.6 \text{mm}$
 $\alpha = 45^\circ$
 $\phi = 45^\circ$
 $\beta = 45^\circ$
 $\sigma^2(s) = 2.11 \times 10^{-4} \text{mm}^2$

Free Path of Length z_d .

$$E_Z = \begin{pmatrix} 1 & 0 & z_d^2 & 0 \\ 0 & 1 & 0 & 0 \\ 0 & 0 & 1 & 0 \\ 0 & 0 & 0 & 1 \end{pmatrix}$$

where z_d = path length in mm.

Transformation at a Lens of Focal Length F.

$$E_L = \begin{pmatrix} 1 & 0 & 0 & 0 \\ 0 & \left(\frac{z_o}{z_i}\right)^2 \left(1 + \frac{z_o^2}{F^2}\right) & 0 & \left(\frac{z_o}{z_i}\right)^2 \left(1 + \frac{z_o^2}{F^2}\right) \sigma^2(C) \\ \frac{1}{z_o^2} & 0 & \frac{2z_i^2}{z_o^2} & \frac{2z_i^2 \sigma^2(\theta) + \sigma^2(C)}{z_o^2} \\ 0 & 0 & 0 & 1 \end{pmatrix}$$

where
 $\sigma^2(C) = 1.33 \times 10^{-4} \text{mm}^2$
 $\sigma^2(\theta) = 2.3 \times 10^{-6} \text{rad}^2$
 F = Focal Length mm
 z_i = Input Distance
 z_o = Output Distance

Beam Positioning by a Translation Stage.

$$E_T = \begin{pmatrix} 1 & 0 & 0 & \sigma^2(C) + f^2 \sigma^2(\theta) \\ 0 & 1 & 0 & \sigma^2(C) \\ 0 & 0 & 1 & \sigma^2(\theta) \\ 0 & 0 & 0 & 1 \end{pmatrix} = \begin{pmatrix} 1 & 0 & 0 & 4.5 \times 10^{-3} \text{mm}^2 \\ 0 & 1 & 0 & 2.0 \times 10^{-4} \text{mm}^2 \\ 0 & 0 & 1 & 2.1 \times 10^{-6} \text{rad}^2 \\ 0 & 0 & 0 & 1 \end{pmatrix}$$

where
 $\sigma^2(C) = 2.0 \times 10^{-4} \text{mm}^2$
 $\sigma^2(\theta) = 2.1 \times 10^{-6} \text{rad}^2$
 $f \approx 45-50 \text{mm}$
 $\phi = 0^\circ$
 $\beta = 0^\circ$

Appendix 5

QOCAD - A Design Tool.

```

REM *****VERSION 2.01*****
REM **Set up Global variables **
REM *****
ON ERROR PROCerror :END
DIM grid_data%(7,7)
DIM grid_specials(7,7)
DIM route_roof%(20)
DIM element_DRN%(36,1)
DIM grid_DRN%(7,7,1)
DIM routes%(20,50,1)
DIM element_data(36,1,1,1)
DIM results(20,1,1)
DIM output(20,1)
PROCfind_where_is
PROCinitialise
filename$=""
used_sources%=0
route_number%=1
current_path%=0
current_step_number%=0
total_steps%=0
gmx%=0
gmy%=0
PROCdraw_grid
PROCflag
*FX 15,1
REM flush input buffer

REPEAT
  aa% = INKEY(1)

  CASE aa% OF
    WHEN -1 : PROCcheck_mouse
    WHEN ASC("S"),ASC("s") : PROCroute_step(route_number%+1)
    WHEN ASC("E"),ASC("e") : PROCeval_route:PROCshow_route(1)
    WHEN ASC("D"),ASC("d") : PROCinfo
    WHEN ASC("G"),ASC("g") : PROCgo_to_route
    WHEN ASC("I"),ASC("i") : PROCinput_from_disk
    WHEN ASC("O"),ASC("o") : PROCoutput_to_disk
    WHEN ASC("Q"),ASC("q") : PROCexit : END
    WHEN ASC("P"),ASC("p") : OSCLI("Qprint")
    WHEN ASC("T"),ASC("t") : OSCLI("ScreenSave RAM:Thesis")
    WHEN 5 : PROCsum_all_routes : REM ctrl E
    WHEN 19 : PROCroute_step(route_number%-1) : REM ctrl S
    OTHERWISE
      IF aa%>=150 AND aa%<=186 THEN PROCupdate_circuit(aa%)
  ENDCASE
UNTIL FALSE
END

DEF FNgrid(screen_co_ord%)
=INT(0.5 + (screen_co_ord% - 40)/130)

DEF FNscreen(grid_co_ord%)
=40 + (130*grid_co_ord%)

DEF FNdot(a%(),b%())

```



```

LOCAL amod,bmod,c%()
DIM c%(1)
amod = a%(0)*a%(0) + a%(1)*a%(1)
amod=SQR(amod)
bmod = b%(0)*b%(0) + b%(1)*b%(1)
bmod=SQR(bmod)
IF amod=0 OR bmod=0 THEN
    amod=1
    bmod=1
    REM prevent div by zero, but leave c() as 0,0 so result is zero
ELSE
    c%()=a%()*b%()
ENDIF
=(c%(0) + c%(1))/(amod*bmod)

```

```

DEF PROCgo_to_route
LOCAL route%
INPUT TAB(0,26)"Go to route"route%
PRINT TAB(0,26)"      "
PROCroute_step(route%)
ENDPROC

```

```

DEF PROCflag
IF total_steps%=0 THEN
    GCOL 2
ELSE
    GCOL 1 : REM red if route used, green if empty
ENDIF
RECTANGLE FILL 890,1000,100,20
GCOL 7
@%=&202
PRINT TAB(0,0)"ROUTE No."route_number%
@%=&1020101
ENDPROC

```

```

DEF PROCdraw_grid
GCOL 6
FOR I%=40 TO 950 STEP 130
    LINE I%,0,I%,990
    LINE 0,I%,990,I%
NEXT I%
GCOL 7
ENDPROC

```

```

DEF PROCcheck_mouse
LOCAL x%,y%,z%
MOUSE x%,y%,z%
IF y%>990 THEN y%=990
IF x%>990 THEN x%=990
gmx%=FNgrid(x%)
gmy%=FNgrid(y%)
CASE z% OF
    WHEN 4 : PROCstart_stop_line
    WHEN 2 : PROCroute_step(route_number%+1)

```

```

    WHEN 1 : PROCerase_step
ENDCASE
REM prevent bouncing by waiting for release
REPEAT
    MOUSEx%,y%,z%
UNTIL z%=0
ENDPROC

```

```

DEF PROCstart_stop_line
LOCAL x1%,x2%,y1%,y2%
IF total_steps%=0 THEN
REM new route
    current_step_number%=0
    total_steps%=1
    current_path%=0
    routes%(route_number%,0,0)=gmx%
    routes%(route_number%,0,1)=gmy%
ELSE
    x1%=routes%(route_number%,current_step_number%,0)
    y1%=routes%(route_number%,current_step_number%,1)
    IF gmx%=x1% AND gmy%=y1% THEN PROCroute_step(route_number%+1) : ENDPROC
REM if same point clicked then exit
    x2%=gmx%
    y2%=gmy%
    IF x1%<>x2% AND y1%<>y2% THEN ENDPROC:REM diagonal steps not allowed
    total_steps%=total_steps% + 1
    current_step_number%=current_step_number%+1
    current_path%=current_path% + ABS(x2%-x1%) + ABS(y2%-y1%)
    PROC_line(x1%,y1%,x2%,y2%)
    routes%(route_number%,current_step_number%,0)=gmx%
    routes%(route_number%,current_step_number%,1)=gmy%
ENDIF
PROCflag
ENDPROC

```

```

DEF PROC_line(a1%,b1%,a2%,b2%)
LOCAL xoff_set,yoff_set
REM use offset to show direction of line
yoff_set=0
xoff_set=0
IF a1%>a2% THEN yoff_set=-4
IF a2%>a1% THEN yoff_set= 4
IF b1%>b2% THEN xoff_set= 4
IF b2%>b1% THEN xoff_set=-4
a1%=FNscreen(a1%) + xoff_set
a2%=FNscreen(a2%) + xoff_set
b1%=FNscreen(b1%) + yoff_set
b2%=FNscreen(b2%) + yoff_set
LINE a1%,b1%,a2%,b2%
ENDPROC

```

```

DEF PROCroute_step(which_route%)
REM Close down existing route and open next
GCOL 1

```

```

REM erase current route
PROCrefresh_route
GCOL 7
IF current_step_number%=0 THEN total_steps%=0 :REM one point only
routes%(route_number%,50,0)=total_steps% : REM store in last place
routes%(route_number%,50,1)=current_path%
REM got to route number
route_number%=which_route%
IF route_number%>=21 THEN route_number%=1
IF route_number%<=0 THEN route_number%=20
total_steps%=routes%(route_number%,50,0) : REM for new route
current_path%=routes%(route_number%,50,1)
current_step_number%=total_steps% - 1
REM draw route
PROCrefresh_route
PROCflag
ENDPROC

DEF PROCerase_step
LOCAL i%,j%,step_x%,step_y%,element_id%
LOCAL x1%,x2%,y1%,y2%
REM check a step exists
IF current_step_number%<=0 AND total_steps%=0 THEN ENDPROC :REM empty
IF current_step_number%<=0 AND total_steps%=1 THEN
REM one point only - doesn't count as a route
routes%(route_number%,0,0)=0 : REM erase initial point
routes%(route_number%,0,1)=0
total_steps%=0
current_path%=0
ENDPROC
ENDIF
REM draw route in black
GCOL 0
PROCrefresh_route
GCOL 7
REM redraw icons on last step
x1%=routes%(route_number%,current_step_number%-1,0)
y1%=routes%(route_number%,current_step_number%-1,1)
x2%=routes%(route_number%,current_step_number%,0)
y2%=routes%(route_number%,current_step_number%,1)
step_x%=1
step_y%=1
IF x1%>x2% THEN step_x%=-1
IF y1%>y2% THEN step_y%=-1
FOR i%=x1% TO x2% STEP step_x%
FOR j%=y1% TO y2% STEP step_y%
element_id%=grid_data%(i%,j%) : REM find element at that point
PROCplace_element(element_id%,i%,j%) : REM redraw it
NEXT j%
NEXT i%
REM reset steps
current_step_number%= current_step_number% - 1
current_path%=current_path% - (ABS(x2%-x1%) + ABS(y2%-y1%))
total_steps%= total_steps% - 1
IF current_step_number%=0 THEN
total_steps%=0 : REM clears route used flag

```

```

routes%(route_number%,0,0)=0 : REM erase initial point
routes%(route_number%,0,1)=0
current_path%=0
ENDIF
REM redraw new route
PROCrefresh_route
PROCflag
ENDPROC

```

```

DEF PROCrefresh_route
LOCAL i%,x1%,y1%,x2%,y2%
IF total_steps%<=1 AND current_step_number%<=0 THEN ENDPROC
REM one point only in route and next point thought of as at 0,0
FOR i%=1 TO total_steps%-1
x1%=routes%(route_number%,i%-1,0)
y1%=routes%(route_number%,i%-1,1)
x2%=routes%(route_number%,i%,0)
y2%=routes%(route_number%,i%,1)
PROC_line(x1%,y1%,x2%,y2%)
NEXT i%
ENDPROC

```

```

DEF PROCplace_element(element_id%,x%,y%)
x%=FNscreen(x%)-40
y%=FNscreen(y%)-40
VDU 23,27,0,element_id%,0,0,0,0,0,0
PLOT &ED,x%,y%
ENDPROC

```

```

DEF PROCeval_route
LOCAL i%,k%,l%,a%,b%,x1%,y1%,x2%,y2%,x3%,y3%
LOCAL xstep%,ystep%,el_id%,dotprod1,dotprod2,dotprod3,Tx%
LOCAL v_in%(1),v_out%(1),v_DRN%(1),work(),buff()
DIM v_in%(1)
DIM v_out%(1)
DIM v_DRN%(1)
DIM work(1,1)
DIM buff(1,1)
REM prepare to count number of roof mirrors
route_roof%(route_number%)=0
IF total_steps%<=0 THEN ENDPROC : REM nothing to evaluate
REM initialize working matrix
work(0,0)=1
work(0,1)=0
work(1,0)=0
work(1,1)=1
REM select each line of route
FOR i%=0 TO total_steps%-1
a%=routes%(route_number%,i%,0)
b%=routes%(route_number%,i%,1)
IF i%=0 THEN
x1%=a% : REM prevent wrong subscripts
y1%=b%
ELSE
x1%=routes%(route_number%,i%-1,0)

```

```

    y1%=routes%(route_number%,i%-1,1)
ENDIF
IF i%=total_steps%-1 THEN
    x3%=x2%
    y3%=y2% : REM prevent reading array past end of route
ELSE
    x3%=routes%(route_number%,i%+1,0)
    y3%=routes%(route_number%,i%+1,1)
ENDIF
REM if line contains more than one element then check them all
IF a%>x3% THEN xstep%=-1 ELSE xstep%=1
IF b%>y3% THEN ystep%=-1 ELSE ystep%=1
FOR x2%=a% TO x3%-xstep% STEP xstep%
    FOR y2%=b% TO y3%-ystep% STEP ystep%
REM find element at selected point
        el_id%=grid_data%(x2%,y2%)
REM calculate input and output vectors
        v_in%(0)=x2%-x1%
        IF v_in%(0)<>0 THEN v_in%(0)=v_in%(0)/ABS(v_in%(0))
        v_in%(1)=y2%-y1%
        IF v_in%(1)<>0 THEN v_in%(1)=v_in%(1)/ABS(v_in%(1))
        v_out%(0)=x3%-x2%
        IF v_out%(0)<>0 THEN v_out%(0)=v_out%(0)/ABS(v_out%(0))
        v_out%(1)=y3%-y2%
        IF v_out%(1)<>0 THEN v_out%(1)=v_out%(1)/ABS(v_out%(1))
        v_DRN%(0)=grid_DRN%(x2%,y2%,0)
        v_DRN%(1)=grid_DRN%(x2%,y2%,1)
        dotprod1 = FNdot(v_in%(),v_DRN%()) : REM i/p with DRN of element
        dotprod2 = FNdot(v_in%(),v_out%()) : REM of o/p with i/p
        dotprod3 = FNdot(v_DRN%(),v_out%()) : REM o/p with DRN of element
        IF FNdot(v_in%(),v_in%())=0 AND i%<>0 THEN PRINT"***in***"
REM check that v_in exists if not the first step
        IF FNdot(v_out%(),v_out%())=0 AND i%<>total_steps% THEN PRINT"***out***"
REM check that v_out exists if not the last step
        PROCget_matrix : REM pull data into buffer
        PROCorientation : REM check beams are reflected OK, and that nothing
            REM obviously silly is happening eg Tx thru mirror
        work%=buff().work() : REM evaluate step
        PROCnull(work()) : REM if null then stop evaluating
        REM solve the problem when x2,y2 rounds a corner
        x1%=x2%
        y1%=y2%
    NEXT y2%
NEXT x2%
NEXT i%
REM at end of route store final matrix, null stored if null found
FOR k%=0 TO 1
    FOR l%=0 TO 1
        results(route_number%,k%,l%)=work(k%,l%)
    NEXT l%
NEXT k%
ENDPROC

DEFPROCshow_route(r%)
REM save a window, print data, wait for key, replace window
PROCwindow(r%)
GCOL 7

```

```

PROCgraphout(route_number%,r%)
delay%=GET
IF delay%=ASC("P") OR delay%=ASC("p") THEN OSCLI("Qprint")
PROCrestore(r%)
ENDPROC

DEF PROCget_matrix
LOCAL factor
IF dotprod2=1 THEN Tx%=1 ELSE Tx%=0
REM if i/p and o/p beams are parallel then transmitted else reflected
CASE el_id% OF
  WHEN 5,6,7,8 :
    PROCget_buff(el_id%)
    REM if approached from other side swap signs on trailing diagonal
    IF dotprod1 < 0 THEN
      buff(0,1) = -buff(0,1)
      buff(1,0) = -buff(1,0)
    ENDIF

  WHEN 33,34 :
    REM partial reflect or transmit
    PROCget_buff(el_id%)
    IF Tx%=0 THEN
      REM need field reflection NOT power reflection
      factor = grid_specials(x2%,y2%)
      factor = SQR(1 - factor*factor)
    ELSE
      factor = grid_specials(x2%,y2%)
    ENDIF
    buff() = buff() * factor

  WHEN 21,22,23,24 :
    CASE grid_specials(x2%,y2%) OF
      WHEN -45 : PROCget_buff(21)
      WHEN 0 : PROCget_buff(22)
      WHEN 45 : PROCget_buff(23)
      WHEN 90 : PROCget_buff(24)
    OTHERWISE
      buff(0,0) = COS(2*RAD(grid_specials(x2%,y2%)))
      buff(0,1) = -SIN(2*RAD(grid_specials(x2%,y2%)))
      buff(1,0) = SIN(2*RAD(grid_specials(x2%,y2%)))
      buff(1,1) = COS(2*RAD(grid_specials(x2%,y2%)))
    ENDCASE
    route_roof%(route_number%)=route_roof%(route_number%) + 1

  WHEN 29,30,31,32 :
    IF dotprod1 = 1 THEN PROCget_buff(29)
    REM no reflection, but transmission with or against +ve rotation dirn
    IF dotprod1 = -1 THEN PROCget_buff(30)

  WHEN 35,36 :
    angle=grid_specials(x2%,y2%)
    IF Tx%=0 THEN
      buff(0,0) = - COS(RAD(angle))*COS(RAD(angle))
      buff(0,1) = -COS(RAD(angle))*SIN(RAD(angle))
      buff(1,0) = COS(RAD(angle))*SIN(RAD(angle))
      buff(1,1) = SIN(RAD(angle)) * SIN(RAD(angle))
    
```

```

ELSE
  buff(0,0) = SIN(RAD(angle)) * SIN(RAD(angle))
  buff(0,1) = -COS(RAD(angle))*SIN(RAD(angle))
  buff(1,0) = -COS(RAD(angle))*SIN(RAD(angle))
  buff(1,1) = COS(RAD(angle))*COS(RAD(angle))
ENDIF

WHEN 13,14,15,16 :
  IF dotprod1=0 AND dotprod3=1 THEN Tx%=1 ELSE Tx%=0
  PROCget_buff(el_id%)

WHEN 17,18,19,20 :
  IF dotprod1=1 AND dotprod3=0 THEN Tx%=0 ELSE Tx%=1
  PROCget_buff(el_id%)

  OTHERWISE PROCget_buff(el_id%)
  REM rest are 'normal'
ENDCASE

ENDPROC

DEF PROCorientation
LOCAL cond%()
DIM cond%(1)
CASE el_id% OF
  WHEN 1,2,3,4,5,6,7,8,33,34,35,36 :
    REM polarizers of all angles and non-polarizing beam splitters
    IF Tx% = 1 THEN ENDPROC : REM transmit regardless of orientation
    REM check o/p beam for orientation
    IF dotprod1<0 THEN
      cond%()=v_out%()-v_DRN%():cond%()=cond%()-v_in%()
    ELSE
      cond%()=v_in%()-v_DRN%():cond%()=cond%()-v_out%()
    ENDIF
    IF Tx%=0 AND cond%(0)=0 AND cond%(1)=0 THEN ENDPROC

  WHEN 9,10 :
    REM check o/p beam for orientation
    IF dotprod1<0 THEN
      cond%()=v_out%()-v_DRN%():cond%()=cond%()-v_in%()
    ELSE
      cond%()=v_in%()-v_DRN%():cond%()=cond%()-v_out%()
    ENDIF
    IF Tx%=0 AND cond%(0)=0 AND cond%(1)=0 THEN ENDPROC

  WHEN 11,12 :
    REM check o/p beam for orientation
    cond%()=v_in%()+v_out%()
    IF Tx%=0 AND dotprod1=1 AND cond%(0)=0 AND cond%(1)=0 THEN ENDPROC
    IF Tx%=0 AND dotprod1=-1 AND cond%(0)=0 AND cond%(1)=0 THEN ENDPROC

  WHEN 13,14,15,16 :
    REM if a source and start of route its OK
    IF dotprod3=1 AND i%=0 THEN ENDPROC

```

```

WHEN 17,18,19,20,25,26,27,28 :
  REM if a detector or dump and END of route its OK
  IF dotprod1=1 AND i%=total_steps%-1 THEN ENDPROC

WHEN 21,22,23,24 :
  REM if roof mirror, then check it points right way
  cond%()=v_in%() + v_out%()
  IF Tx%=0 AND dotprod1=1 AND cond%(0)=0 AND cond%(1)=0 THEN ENDPROC

WHEN 29,30,31,32 :
  REM check beam direction is perp to face, and that beam is transmitted
  IF dotprod1=1 AND Tx%=1 THEN ENDPROC
  IF dotprod1=-1 AND Tx%=1 THEN ENDPROC

OTHERWISE ENDPROC
  REM component not defined yet, endproc to avoid error

ENDCASE
PRINT TAB(0,26)"Error in"
PRINT TAB(0,27)"orientation"
GCOL 9
RECTANGLE FNscreen(x2%)-40,FNscreen(y2%)-40,80
TIME=0 : REPEAT UNTIL TIME>250
GCOL 0
RECTANGLE FNscreen(x2%)-40,FNscreen(y2%)-40,80
GCOL 7
PROCdraw_grid
PROCrefresh_route
PRINT TAB(0,26)"      "
PRINT TAB(0,27)"      "
ENDPROC

DEF PROCget_buff(number%)
LOCAL k%,l%
FOR k%=0 TO 1
  FOR l%=0 TO 1
    buff(k%,l%)=element_data(number%,Tx%,k%,l%)
  NEXT l%
NEXT k%
ENDPROC

DEF PROCnull(R())
REM *****
REM check for null matrix
REM *****
IF R(0,0)=0 AND R(0,1)=0 AND R(1,0)=0 AND R(1,1)=0 THEN
  GCOL 9
  RECTANGLE FNscreen(x2%)-40,FNscreen(y2%)-40,80
  PRINT TAB(0,26)"Zero Field"
  TIME=0 : REPEAT UNTIL TIME>250
  GCOL 0
  RECTANGLE FNscreen(x2%)-40,FNscreen(y2%)-40,80

```



```

GCOL 7
PRINT TAB(0,26) "
PROCdraw_grid
PROCrefresh_route
x2%=x3% : y2%=y3% : REM ensure control leaves inner loops
i%=total_steps%-1 : REM leave outer loop
ENDIF
ENDPROC

```

```

DEF PROCupdate_circuit(element_id%)
element_id%=element_id% - 150
IF element_id%<0 OR element_id%>36 THEN ENDPROC
PROCcheck_mouse
REM if old element was a source then subtract from count
CASE grid_data%(gmx%,gmy%) OF
WHEN 13,14,15,16 : used_sources%=used_sources%-1
ENDCASE
CASE element_id% OF
WHEN 0 :
REM delete element
grid_specials(gmx%,gmy%)=0 : REM clear special data

WHEN 21,22,23,24 :
PRINT TAB(0,26)"Angle of roof"
VDU 23,1,11
INPUT TAB(0,27)"to Vertical "angle
VDU 23,1,01
REM i/p angle and store at grid position
grid_specials(gmx%,gmy%)=angle
PRINT TAB(0,26) " "
PRINT TAB(0,27) " "

WHEN 33,34 :
PRINT TAB(0,26)"Percentage FIELD"
VDU 23,1,11
INPUT TAB(0,27)"transmission "angle
VDU 23,1,01
REM i/p % Tx and store at grid position
grid_specials(gmx%,gmy%)=angle
PRINT TAB(0,26) " "
PRINT TAB(0,27) " "

WHEN 35,36 :
PRINT TAB(0,26)"Angle of wires"
VDU 23,1,11
INPUT TAB(0,27)"to Vertical "angle
VDU 23,1,01
REM i/p angle and store at grid position
grid_specials(gmx%,gmy%)=angle
PRINT TAB(0,26) " "
PRINT TAB(0,27) " "

WHEN 13,14,15,16 :
PRINT TAB(0,26)"Angle of E-field"
VDU 23,1,11
INPUT TAB(0,27)"to vertical "angle

```

```

VDU 23,1,0I
  grid_specials(gmx%,gmy%)=angle
REM if a source then increment count
  used_sources%=used_sources%+1
  PRINT TAB(0,26)"      "
  PRINT TAB(0,27)"      "

ENDCASE
PROCplace_element(element_id%,gmx%,gmy%)
  grid_data%(gmx%,gmy%) = element_id%
  grid_DRN%(gmx%,gmy%,0) = element_DRN%(element_id%,0)
  grid_DRN%(gmx%,gmy%,1) = element_DRN%(element_id%,1)
PROCrefresh_route
ENDPROC

DEF PROCsum_all_routes
LOCAL a%,b%,i%,j%,pos_count%,no_routes%,R%
LOCAL in(),out(),route_list%(),inter_list%(),working()
DIM route_list%(20)
DIM inter_list%(20,20)
DIM working(1,1)
DIM in(1)
DIM out(1)
REM find selected detector
PROCcheck_mouse
CASE grid_data%(gmx%,gmy%) OF
  WHEN 17,18,19,20 :
    REM for detectors only
    REM evaluate all routes
    FOR a%=1 TO 20
      PROCeval_route
      PROCroute_step(route_number%+1)
    NEXT a%
    REM this ensures all output arrays are filled
    no_routes%=0
    FOR a%=1 TO 20
      IF routes%(a%,50,0)>=2 THEN
REM if route contains at least one line(two points)
        last_x%=routes%(a%,routes%(a%,50,0)-1,0)
        last_y%=routes%(a%,routes%(a%,50,0)-1,1)
REM check if route ends at selected detector
        IF last_x%=gmx% AND last_y%=gmy% THEN
          no_routes%=no_routes%+1
          route_list%(no_routes%)=a%
        ENDIF
      ENDIF
    NEXT a%

REM for each selected route, check first step to see if same source is used
    FOR a%=1 TO no_routes%
      FOR b%=1 TO no_routes%
        IF a%<>b% THEN
          REM only if routes are different
          first_x_a%=routes%(route_list%(a%),0,0)
          first_y_a%=routes%(route_list%(a%),0,1)
          first_x_b%=routes%(route_list%(b%),0,0)
          first_y_b%=routes%(route_list%(b%),0,1)

```

```

IF first_x_a%=first_x_b% AND first_y_a%=first_y_b% THEN
  inter_list%(route_list%(a%),route_list%(b%))=1
  inter_list%(route_list%(a%),0)=1
ENDIF
ENDIF
NEXT b%
NEXT a%

REM combine outputs depending on whether or not interferometry is used
pos_count%=1
PROCwindow(no_routes%)
REM if not interferometry then list power etc
FOR a%=1 TO no_routes%
  IF inter_list%(route_list%(a%),0)=0 THEN
    GCOL 7
    PROCgraphout(route_list%(a%),pos_count%)
    pos_count%=pos_count%+1
  ENDIF
NEXT a%
REM if interferometry then work out all outputs
FOR a%=1 TO 20
  FOR i%=0 TO 1
    FOR j%=0 TO 1
      working(i%,j%) = results(a%,i%,j%)
    NEXT j%
  NEXT i%
  out()=working().in()
  output(a%,0)=out(0)
  output(a%,1)=out(1)
NEXT a%
REM ask for data on cubesize etc and work out final phase, but not now!!!
REM just print separately
FOR a%=1 TO no_routes%
  IF inter_list%(route_list%(a%),0)=1 THEN
    GCOL 2
    RECTANGLE FILL 800,1033-100*pos_count%,479,100
    GCOL 5
    PROCgraphout(route_list%(a%),pos_count%)
    pos_count%=pos_count%+1
  ENDIF
NEXT a%
delay%=GET
IF delay%=ASC("P") OR delay%=ASC("p") THEN OSCLI("Qprint")
IF delay%=ASC("T") OR delay%=ASC("t") THEN OSCLI("Screensave RAM:Thesis")
PROCrestore(no_routes%)

OTHERWISE
  PRINT TAB(0,26)"Move to a "
  PRINT TAB(0,27)"DETECTOR "
  TIME = 0
  REPEAT UNTIL TIME>300
    PRINT TAB(0,26)"      "
    PRINT TAB(0,27)"      "
  ENDCASE
ENDPROC

DEF PROCgraphout(R%,YPOS%)

```

```

LOCAL perc, dB, fract, path_length%, norm, R$, DB$, angle%, out(), mat(), in()
DIM out(1)
DIM in(1)
DIM mat(1,1)
IF YPOS% < 1 OR YPOS% > 10 THEN ENDPROC
REM find the input angle
in(0) = COS(RAD(grid_specials(routes%(R%,0,0), routes%(R%,0,1))))
in(1) = SIN(RAD(grid_specials(routes%(R%,0,0), routes%(R%,0,1))))
IF in(0) = 0 AND in(1) = 0 THEN ENDPROC
FOR i% = 0 TO 1
  FOR j% = 0 TO 1
    mat(i%, j%) = results(R%, i%, j%)
  NEXT j%
NEXT i%
out() = mat().in()
fract = (out(0)*out(0) + out(1)*out(1)) / (in(0)*in(0) + in(1)*in(1))
perc = 0.1 * INT(0.5 + 1000*fract)
IF fract < > 0 THEN
  dB = 0.1 * INT(0.5 + 100*LOG(fract))
  DB$ = " " + STR$(dB) + "dB"
ELSE
  DB$ = ""
ENDIF
path_length% = routes%(R%, 50, 1)
IF R% = route_number% THEN path_length% = current_path%
IF route_root%(R%) >= 1 THEN R$ = "(" ELSE R$ = ""
norm = SQR(out(0)*out(0) + out(1)*out(1))
IF norm = 0 THEN norm = 1
VDU 5
REM print at graphics cursor
YPOS% = 1113 - 100*YPOS%
MOVE 905, YPOS%
PRINT "Route "R%" Path= "path_length%; R$
MOVE 905, YPOS%-36
PRINT "Power= "perc"% "DB$
COLOUR 5, 0, 0, 155
GCOL 5
CIRCLE FILL 845, YPOS%-32, 40
GCOL 14
LINE 845, YPOS%-32, 845+40*out(1)/norm, YPOS%-32+40*out(0)/norm
GCOL 7
VDU 4
VDU 23, 1, 0!
ENDPROC

DEF PROCinfo
LOCAL angle
PROCcheck_mouse
CASE grid_data%(gmx%, gmy%) OF
  WHEN 21, 22, 23, 24, 35, 36 :
    REM if roofmirror, beamsplitter, rot-polarizer then correct angle / % Tx
    angle = grid_specials(gmx%, gmy%)
  WHEN 13, 14, 15, 16, 33, 34 :
    angle = grid_specials(gmx%, gmy%)
    REM source has angle in correct form
    angle = grid_specials(gmx%, gmy%)
OTHERWISE

```

```
ENDPROC
ENDCASE
MOVE FNscreen(gmx%),FNscreen(gmy%)-40
MOVE 100+FNscreen(gmx%),60+FNscreen(gmy%)
*SGET infowindow
GCOL 7
RECTANGLE FILL FNscreen(gmx%),FNscreen(gmy%)-40,100
COLOUR 5,0,0,155
GCOL 5
RECTANGLE FILL 5+FNscreen(gmx%),5+FNscreen(gmy%)-40,95
GCOL 7
VDU 5
MOVE 15+FNscreen(gmx%),50+FNscreen(gmy%)
IF grid_data%(gmx%,gmy%)=33 OR grid_data%(gmx%,gmy%)=34 THEN
  PRINT " % Tx"
ELSE
  PRINT "Angle"
ENDIF
MOVE 25+FNscreen(gmx%),FNscreen(gmy%)
PRINT angle
TIME=0
REPEAT UNTIL TIME>250
VDU 4
*SCHOOSE infowindow
PLOT &ED,FNscreen(gmx%),FNscreen(gmy%)-40
*SDELETE infowindow
ENDCASE
ENDPROC
```

```
DEF PROCwindow(a%)
REM save a% window areas for replacing later
y%=1033-100*a%
MOVE 800,y%
MOVE 1279,1023
*SGET window
GCOL 0
RECTANGLE FILL 800,y%,479,1023-y%
ENDPROC
```

```
DEF PROCrestore(a%)
REM replace the previously saved window
y%=1033-100*a%
*SCHOOSE window
PLOT &ED,800,y%
*SDELETE window
VDU 23,1,0!
ENDPROC
```

```
DEF PROCoutput_to_disk
LOCAL a%,b%,c%,d%,e%,f%,g%,h%,i%,j%,l%,m%
PROCroute_step(route_number%)
MOVE 300,400
MOVE 900,600
*SGET filewindow
```

```

GCOL 4
RECTANGLE FILL 300,400,600,200
GCOL 7
MOVE 350,550
VDU 5
PRINT"Input filename for data or RTN "
MOVE 350,480
oldfile$="<"+filename$+">"
PRINT oldfile$;
GCOL 15
PLOT &00,5,-32
PLOT &01,20,0
PLOT &00,0,32
GCOL 7
INPUT file$
VDU 4
VDU 23,1,0!
IF file$="" THEN
filename$=filename$
ELSE
filename$=file$
ENDIF
A=OPENOUT filename$
REM store elements first
FOR i%=0 TO 7
  a%=grid_data%(i%,0)
  b%=grid_data%(i%,1)
  c%=grid_data%(i%,2)
  d%=grid_data%(i%,3)
  e%=grid_data%(i%,4)
  f%=grid_data%(i%,5)
  g%=grid_data%(i%,6)
  h%=grid_data%(i%,7)
  PRINT# A,a%,b%,c%,d%,e%,f%,g%,h%
NEXT i%
REM store special data
FOR i%=0 TO 7
  a%=grid_specials(i%,0)
  b%=grid_specials(i%,1)
  c%=grid_specials(i%,2)
  d%=grid_specials(i%,3)
  e%=grid_specials(i%,4)
  f%=grid_specials(i%,5)
  g%=grid_specials(i%,6)
  h%=grid_specials(i%,7)
  PRINT# A,a%,b%,c%,d%,e%,f%,g%,h%
NEXT i%
REM store DRN data
FOR i%=0 TO 7
  FOR j%=0 TO 1
    a%=grid_DRN%(i%,0,j%)
    b%=grid_DRN%(i%,1,j%)
    c%=grid_DRN%(i%,2,j%)
    d%=grid_DRN%(i%,3,j%)
    e%=grid_DRN%(i%,4,j%)
    f%=grid_DRN%(i%,5,j%)
    g%=grid_DRN%(i%,6,j%)

```

```

h%=grid_DRN%(i%,7,j%)
PRINT# A,a%,b%,c%,d%,e%,f%,g%,h%
NEXT j%
NEXT i%
REM store route data
FOR i%=0 TO 50
  FOR l%=0 TO 1
    FOR m%=0 TO 10 STEP 10
      a%=routes%(1 + m%,i%,l%)
      b%=routes%(2 + m%,i%,l%)
      c%=routes%(3 + m%,i%,l%)
      d%=routes%(4 + m%,i%,l%)
      e%=routes%(5 + m%,i%,l%)
      f%=routes%(6 + m%,i%,l%)
      g%=routes%(7 + m%,i%,l%)
      h%=routes%(8 + m%,i%,l%)
      j%=routes%(9 + m%,i%,l%)
      k%=routes%(10 + m%,i%,l%)
      PRINT# A,a%,b%,c%,d%,e%,f%,g%,h%,j%,k%
    NEXT m%
  NEXT l%
NEXT i%
PRINT# A,used_sources%
CLOSE# A
*SCHOOSE filewindow
PLOT &ED,300,400
*SDELETE filewindow
ENDPROC

DEF PROCinput_from_disk
LOCAL a%,b%,c%,d%,e%,f%,g%,h%,i%,j%,l%,m%
MOVE 0,0
MOVE 290,1000
*SGET dirwindow
GCOL 0
RECTANGLE FILL 0,0,290,1000
GCOL 4
RECTANGLE 0,0,290,1000
REM set up text window
VDU 28,1,30,16,4
*.<QoCad$Dir>
REM restore text window
VDU 28,62,31,79,0
MOVE 300,400
MOVE 900,600
*SGET filewindow
GCOL 4
RECTANGLE FILL 300,400,600,200
GCOL 7
MOVE 350,550
VDU 5
PRINT"Filename for loading data "
MOVE 350,480
GCOL 15
PLOT &00,5,-32
PLOT &01,20,0
PLOT &00,0,32

```

```

GCOL 7
INPUT ""file$
VDU 4
VDU 23,1,0!
IF file$="" THEN
*SCHOOSE filewindow
PLOT &ED,300,400
*SDELETE filewindow
*SCHOOSE dirwindow
PLOT &ED,0,0
*SDELETE dirwindow
ENDPROC
ELSE
filename$=file$
ENDIF
A=OPENIN (FileSys$+"."+filename$)
REM load elements first
FOR i%=0 TO 7
INPUT# A,a%,b%,c%,d%,e%,f%,g%,h%
grid_data%(i%,0)=a%
grid_data%(i%,1)=b%
grid_data%(i%,2)=c%
grid_data%(i%,3)=d%
grid_data%(i%,4)=e%
grid_data%(i%,5)=f%
grid_data%(i%,6)=g%
grid_data%(i%,7)=h%
NEXT i%
REM load special data
FOR i%=0 TO 7
INPUT# A,a%,b%,c%,d%,e%,f%,g%,h%
grid_specials(i%,0)=a%
grid_specials(i%,1)=b%
grid_specials(i%,2)=c%
grid_specials(i%,3)=d%
grid_specials(i%,4)=e%
grid_specials(i%,5)=f%
grid_specials(i%,6)=g%
grid_specials(i%,7)=h%
NEXT i%
REM load DRN data
FOR i%=0 TO 7
FOR j%=0 TO 1
INPUT# A,a%,b%,c%,d%,e%,f%,g%,h%
grid_DRN%(i%,0,j%)=a%
grid_DRN%(i%,1,j%)=b%
grid_DRN%(i%,2,j%)=c%
grid_DRN%(i%,3,j%)=d%
grid_DRN%(i%,4,j%)=e%
grid_DRN%(i%,5,j%)=f%
grid_DRN%(i%,6,j%)=g%
grid_DRN%(i%,7,j%)=h%
NEXT j%
NEXT i%
REM load route data
FOR i%=0 TO 50
FOR l%=0 TO 1

```



```

FOR m%=0 TO 10 STEP 10
  INPUT# A,a%,b%,c%,d%,e%,f%,g%,h%,j%,k%
  routes%(1+m%,i%,l%)=a%
  routes%(2+m%,i%,l%)=b%
  routes%(3+m%,i%,l%)=c%
  routes%(4+m%,i%,l%)=d%
  routes%(5+m%,i%,l%)=e%
  routes%(6+m%,i%,l%)=f%
  routes%(7+m%,i%,l%)=g%
  routes%(8+m%,i%,l%)=h%
  routes%(9+m%,i%,l%)=j%
  routes%(10+m%,i%,l%)=k%
NEXT m%
NEXT l%
NEXT i%
INPUT# A,a%
used_sources%=a%
CLOSE# A
*SCHOOSE filewindow
PLOT &ED,300,400
*SDELETE filewindow
*SCHOOSE dirwindow
PLOT &ED,0,0
*SDELETE dirwindow
REM redraw elements
FOR i%=0 TO 7
  FOR j%=0 TO 7
    PROCplace_element(grid_data%(i%,j%),i%,j%)
  NEXT j%
NEXT i%
REM redraw all routes
route_number%=1
current_path%=routes%(1,50,1)
total_steps%=routes%(1,50,0)
current_step_number%=total_steps%-1
PROCrefresh_route
FOR i%=1 TO 20
  PROCroute_step(route_number%+1)
NEXT i%

ENDPROC

```

```

DEF PROCinitialise
LOCAL EL%,T%
MODE 12
VDU 28,62,31,79,0
*POINTER
MOUSE RECTANGLE 0,0,989,989
MOUSE ON
@%=&1020101
*FX 221,150
*FX 222,162
*FX 223,174
*FX 224,186
*FX 225,150
*FX 226,162

```

```
*FX 227,174
*FX 228,186
VDU 23,1,0I
```

```
G=OPENIN "<QoCad$Dir>.mainfile.ELEM36C"
FOR EL%=0 TO 36
FOR T%=0 TO 1
INPUT# G,A,B,C,D,E
element_data(EL%,T%,0,0)=A
element_data(EL%,T%,0,1)=B
element_data(EL%,T%,1,0)=C
element_data(EL%,T%,1,1)=D
element_DRN%(EL%,T%) = E
NEXT T%
NEXT EL%
CLOSE# G
*SLOAD <QoCad$Dir>.mainfile.SPR36
ENDPROC
```

```
DEF PROCexit
VDU 26
*FX 221,0
*FX 222,0
*FX 223,0
*FX 224,0
*FX 225,0
*FX 226,0
*FX 227,0
*FX 228,0
MOUSE OFF
@%=2314
CLS
VDU 23,1,1I
ENDPROC
```

```
DEF PROCfind_where_is
DIM SysVarVal% 80, SysVarName% 80
$SysVarVal%="QoCad$Dir"+CHR$(0)
SYS "OS_ReadVarVal",SysVarVal%,SysVarName%,80,0 TO ,,VarEnd%
SysVarName%?VarEnd%=13
FileSys$=$SysVarName%
ENDPROC
```

```
DEF PROCerror
REPORT
PRINT ERL
ENDPROC
```

Appendix 6

Gausspat.

```
REM MPATTERN last modified 23.30 15th Jan 92
OFF
PROCadcread MODE 12 PROCinitialize REPEAT
  PROCmenu
  UNTIL FALSE
END
:
:
DEF PROCinitialize
  total_points% = 4000
  VDU 23,1,0,0,0,0,0,0,0
  Y=OPENIN ":Horn_patts$.g_c_hyst"
  INPUT#Y,g,c,hyst
  CLOSE#Y
  @%=&01000505
  VDU 24, 0;0;1279;820;
  CLS : CLG
  INPUT"Enter path and directory for datafiles";user$
  IF user$="" THEN user$="ML"
  CLS
  user$=user$+"."
  PRINT "Check connections to adc module number ONE :": PRINT
  PRINT "channel for angle voltage    2"
  PRINT "channel for detector voltage  3": PRINT
  PRINT "Modify ?"
  x$=GET$: CLS
  IF (x$="Y") OR (x$="y") THEN PROCset_adc
  dotty=FALSE
  logs=FALSE
  a_delay=FALSE
  the_delay%=150
  no_avs%=10
  this_scan%=0
  old_av%=10
  dirn%=0
  plus%=1
  minus%=-1
  no_decades%=4
  no_tens%=4
  y_factor%=180
  x_factor%=135
  x_scale%=10
  ang_range=45
  angres=0.5
  DIM points(4,1,total_points%)
  DIM scan_ID$(4)
  DIM title$(4)
  DIM scan_width(4)
```

```

title$()="untitled"
scan_ID$()="Empty "
scan_width()=0
PROCbox
REM scan_ID$(3)="Active"
COLOUR 12
VDU 28,2,23,7,17
PRINTTAB(0,this_scan%)scan_ID$(this_scan%)
delay%=0
A%=1
C%=no_avs%
a_channel%=2
s_channel%=3
power_offset=0
angle_offset=0
PROCtrim
old_pwr=FNpower(FNtalk_adc(s_channel%,10))
old_value=FNtalk_adc(a_channel%,10)
old_position=FNangle(old_value)
VDU 28,0,5,79,0
ENDPROC
:
:
DEF PROCzero_offset
LOCAL buff%
VDU 28,0,5,79,0
COLOUR 7
CLS
PRINTTAB(0,0)"You will need to null any offsets in the ADC to give correct angles and pow
PRINTTAB(20,2)"Zero the inputs to the ADC and press SPACEBAR";
REPEAT UNTIL GET=32
power_offset=FNtalk_adc(s_channel%,500)
angle_offset=FNtalk_adc(a_channel%,500)
CLS
ENDPROC
:
:
DEF PROCwindows
VDU 28,0,23,7,15
COLOUR 6
CLS
@%=&01000101
FOR i%=0 TO 4
PRINT TAB(0,2+i%)i%+1;" scan_ID$(i%)
NEXT i%
PRINT TAB(0,0)" Scan"
COLOUR 12
VDU 28,2,23,7,17
PRINTTAB(0,this_scan%)scan_ID$(this_scan%)
VDU 28,0,30,7,25
CLS
COLOUR 2
PRINTTAB(0,0)"Angle"
PRINTTAB(0,3)"Power"
ENDPROC
:
:

```

```

DEF PROCquit
VDU 26
CLS:CLG
QUIT
END
ENDPROC
:
:
DEF PROCscan
VDU 28,0,5,79,0
COLOUR 7
PRINT TAB(0,4)"Scanning";
count%=0 : old_ang = ang_range
title$(this_scan%)="modified"
scan_width(this_scan%)=0
first_value=FNtalk_adc(a_channel%,no_avs%)
first_position=FNangle(first_value)
REPEAT
    second_value=FNtalk_adc(a_channel%,no_avs%)
    second_position=FNangle(second_value)
    change=second_position - first_position
UNTIL (ABS(change)>angres) AND (ABS(second_position)<=(ang_range -0.5))
IF change>0 THEN
    dirn%=plus%
    GCOL 1
    COLOUR 1
ELSE
    dirn%=minus%
    GCOL 3
    COLOUR 3
ENDIF
PRINT TAB(0,4)"Scanning";
old_ang=FNangle(second_value - dirn%*hyst)
SOUND 1,-9,200,5
REPEAT
    IF a_delay THEN
        SOUND 1,-7,190,4
        TIME=0 : REPEAT UNTIL TIME>the_delay%
        SOUND 1,-7,220,1
    ENDIF
    REPEAT
        ang=FNangle(FNtalk_adc(a_channel%,no_avs%) - dirn%*hyst)
        signal=FNpower(FNtalk_adc(s_channel%,no_avs%))
    UNTIL dirn%*(ang - old_ang)>angres
    old_ang=ang
    count% = count%+1
    IF dotted THEN
        POINT FNscreenx(ang),FNscreeny(signal)
    ELSE
        IF count%=1 THEN
            MOVE FNscreenx(ang),FNscreeny(signal)
        ELSE
            DRAW FNscreenx(ang),FNscreeny(signal)
        ENDIF
    ENDIF
    points(this_scan%,0,count%)=ang
    points(this_scan%,1,count%)=signal

```

```

@ %=&01020104
VDU 28,0,24,7,23
CLS
PRINTTAB(0,0)count%;
VDU 28,0,27,7,26
CLS
PRINTTAB(0,0)ang;
VDU 28,0,30,7,29
CLS
PRINTTAB(0,0)-10*signal;
@ %=&01000505
UNTIL ABS(ang)>=ang_range + angles
VDU 28,0,24,7,23
CLS
points(this_scan%,0,0)=count% : REM store no. of data points
points(this_scan%,1,0)=no_avs% : REM store no. of averages
scan_ID$(this_scan%)="Active" : REM scan now in use
SOUND 1,-10,100,7:SOUND 1,0,100,7:SOUND 1,-10,100,7
SOUND 1,0,100,7:SOUND 1,-10,100,7
PROCup_scan
VDU 28,0,5,79,0
ENDPROC
:
:
DEF PROClimits
VDU 28,0,5,79,0
COLOUR 7
CLS
REPEAT
  CLS
  INPUT"Angular resolution [>0.05 deg] ";angles
UNTIL angles>=0.05
REPEAT
  CLS
  INPUT "Enter maximum angular deviation ";ang_range
UNTIL ABS(ang_range)<=85
REPEAT
  INPUT"How many decades of dynamic range "no_decades%
UNTIL (no_decades%<=10) AND (no_decades%>0)
y_factor%=INT(720/no_decades%)
CLS
ang_range = ABS(ang_range)
title$="untitled"
no_tens%=1 + INT(ang_range/10)
x_factor%=INT(540/no_tens%)
CLS
PROCbox
VDU 28,2,23,7,17
COLOUR 12
PRINTTAB(0,this_scan%)scan_ID$(this_scan%)
ENDPROC
:
:
DEF PROCpre_amp
VDU 28,0,5,79,0
COLOUR 7
CLS

```

```

PRINT "Do you want to use the log amplifier? [y/n] "
as$=GET$
IF as$="Y" OR as$="y" THEN
    logs=TRUE
    PRINT "Set up the log amplifier [y/n]"
    a$=GET$
    IF a$="Y" OR a$="y" THEN
        CLS
        PRINT "Maximum input to the log amp = 10Volts"
        INPUT "Output scale factor "log_scale
        INPUT "Input reference voltage "log_ref
    ENDIF
ELSE
    logs=FALSE
ENDIF
CLS
ENDPROC
:
:
DEF PROCcalibrate
VDU 28,0,5,79,0
CLS
COLOUR 7
PRINT "Move the arm to the following calibration positions and press SPACEBAR when"
PRINT "each one is reached"
PRINT "FIRST POSITION = one end marker"
REPEAT UNTIL GET=32
    calpos1=FNtalk_adc(a_channel%,500)
    INPUT "Enter calibration angle or <RTN> for default "calang1
    IF calang1=0 THEN calang1=81.53
    CLS
    PRINT "SECOND POSITION = other end marker"
    REPEAT UNTIL GET=32
        calpos2=FNtalk_adc(a_channel%,500)
        INPUT "Enter calibration angle or <RTN> for default "calang2
        IF calang2=0 THEN calang2=81.53
        CLS
        PRINT "THIRD POSITION = any marked central position. Move directly to it and"
        PRINT "      DO NOT REVERSE DIRECTION OF ARM"
        REPEAT UNTIL GET=32
            calpos3=FNtalk_adc(a_channel%,500)
            CLS
            PRINT "Continue moving in same direction for at least 15 degrees (end moves 6 inches)"
            PRINT "      REVERSE DIRECTION OF ARM and move to "
            PRINT "FOURTH POSITION = same central position as used in position three"
            PRINT "Move directly to it and DO NOT REVERSE DIRECTION OF ARM"
            REPEAT UNTIL GET=32
                calpos4=FNtalk_adc(a_channel%,500)
            IF (calang1=81.53) AND (calang2=81.53) THEN
                IF calpos1>calpos2 THEN
                    calang2=-calang2
                ELSE
                    calang1=-calang1
                ENDIF
            ENDIF
        ENDIF
    offset=ABS(calpos4-calpos3)
    slope=(calang2-calang1)/(calpos2-calpos1)

```

```

IF calpos1<>calpos2 THEN
  IF slope<0 THEN
    g = -ABS(calang2 - calang1)/(ABS(calpos2 - calpos1) - offset)
  ELSE
    g = ABS(calang2 - calang1)/(ABS(calpos2 - calpos1) - offset)
  ENDIF
ELSE
  PRINT "Check connection to POT and/or move the arm!"
ENDIF
IF g<>0 THEN
  IF calpos1>calpos2 THEN
    c = calang1 - g*(calpos1 - offset)
  ELSE
    c = calang2 - g*(calpos2 - offset)
  ENDIF
ENDIF
hyst=offset/2
PROCtrim
Y=OPENOUT ":Horn_patts$.g_c_hyst"
PRINT#Y,g,c,hyst
CLOSE#Y
ENDPROC
:
:
DEF FNangle(x)
=x*g +c
:
:
DEF FNpower(j)
IF logs THEN
  TP=-(1.26*j/(4096*log_scale) + LOG(log_ref/10.5))
REM 10.5V is the maximum output of the lock in amplifier - set this to 0dB
ELSE
  IF j<=0.4096 THEN TP=4.0 ELSE TP=-LOG(j/4096)
ENDIF
=TP
:
:
DEF PROCbox
@%=&01000505
CLG
GCOL 7
MOVE 190,80
DRAW 190,800
DRAW 1270,800
DRAW 1270,80
DRAW 190,80
FOR i%=-no_tens%+1 TO no_tens%-1
MOVE FNscreenx(x_scale%i%),80
DRAW FNscreenx(x_scale%i%),800
NEXT i%
FOR i%=1 TO no_decades%-1
MOVE 190,FNscreeny(i%)
DRAW 1270,FNscreeny(i%)
NEXT i%
VDU 5
FOR i%=-no_tens% TO no_tens%

```



```

MOVE (FNscreenx(x_scale%*i%)-70),60
PRINT x_scale%*i%
NEXT i%
MOVE 700,30 : PRINT"Angle"
FOR i%=0 TO no_decades%
MOVE 98,(FNscreeny(i%)+16)
PRINT -10*i%
NEXT i%
MOVE 70,816 :PRINT"dB"
VDU 4
PROCwindows
ENDPROC
:
:
:
DEF FNscreenx(a)
=INT(730 + x_factor%*a/10)
:
:
:
DEF FNscreeny(a)
=INT(800 - y_factor%*a)
:
:
:
DEF PROCflush
points()=0
scan_ID$()="Empty "
title$()="untitled"
scan_width()=0
this_scan%=0
PROCbox
ENDPROC
:
:
:
DEF PROCgive(a_scan%)
VDU 28,0,5,79,0
COLOUR 7
CLS
PRINTTAB(0,0)"Space on disk = "
*FREE :horn_patts
INPUT TAB(0,4)"filename ";name$ : PRINT TAB(0,4)"
IF name$<>" THEN
INPUT TAB(0,4)"Title ";title$(a_scan%)
CLS : centre%=44 - 0.5*LEN(title$(a_scan%))
PRINT TAB(centre%,5);title$(a_scan%);
name$=user$+name$
X=OPENOUT name$
PRINT#X,points(a_scan%,0,0),points(a_scan%,1,0),x_factor%,x_scale%
PRINT#X,title$(a_scan%)
no_points%=points(a_scan%,0,0)
FOR c1%=1 TO no_points%
PRINT#X,points(a_scan%,0,c1%),points(a_scan%,1,c1%)
NEXT c1%
CLOSE#X
ELSE
PRINTTAB(0,4)"No file saved"
TIME=0
REPEAT UNTIL TIME>200
ENDIF

```

```

ENDPROC
:
:
DEF PROCtake(a_scan%)
VDU 28,0,5,79,0
COLOUR 7
INPUT TAB(0,4)"filename ";name$ : PRINT TAB(0,4)"
name$=user$+name$
X=OPENIN name$
old_av%=no_avs%
INPUT#X,no_points%,no_avs%,x_f%,x_s%
points(a_scan%,0,0)=no_points% : points(a_scan%,1,0)=no_avs%
INPUT#X,title$(a_scan%)
FOR c1%=1 TO no_points%
INPUT#X,points(a_scan%,0,c1%),points(a_scan%,1,c1%)
NEXT c1%
CLOSE#X
scan_width(a_scan%)=0
IF scan_ID$(a_scan%)="Active" THEN
  FOR i%=points(a_scan%,0,0)+1 TO total_points%
    points(a_scan%,0,i%)=0
    points(a_scan%,1,i%)=0
  NEXT i%
ELSE
  scan_ID$(a_scan%)="Active"
ENDIF
GCOL 7
PROCmemory(a_scan%)
VDU 28,2,23,7,17
COLOUR 12
PRINTTAB(0,this_scan%)scan_ID$(this_scan%)
ENDPROC
:
:
DEF PROCprint_graph
VDU 28,0,5,79,0
CLS
centre%=44 - 0.5*LEN(title$(this_scan%))
PRINT TAB(32,0)TIMES
IF scan_width(this_scan%)<>0 THEN PRINT TAB(40,4)scan_width(this_scan%)
PRINT TAB(centre%,5);title$(this_scan%);
VDU 28,0,30,7,25
CLS
VDU 26
OSCLI("Qprint")
PROCwindows
VDU 28,2,23,7,17
COLOUR 12
PRINTTAB(0,this_scan%)scan_ID$(this_scan%)
ENDPROC
:
:
DEF PROCmenu
VDU 28,0,5,79,0
COLOUR 2
CLS
PRINT TAB(9,0)"(C)alibrate  (L)imits  (P)re-amp  (Z)ero  (S)can"

```

```

PRINT TAB(9,2)"(A)verages  (W)ipe  (D)ata menu  (Q)uit  (X)amine"
IF a_delay THEN
  COLOUR 10
ELSE
  COLOUR 0
ENDIF
PRINTTAB(0,0)"DELAY";
COLOUR 2
@%=&01000505
VDU 5
GCOL 3
MOVE 0,700 : PRINT"Averages"
GCOL 0
MOVE 0,650 : PRINTold_av%
GCOL 3
MOVE 0,650 : PRINTno_avs%
VDU 4
COLOUR 7
centre%=44 - 0.5*LEN(title$(this_scan%))
IF scan_width(this_scan%)<>0 THEN
  PRINT TAB(30,4)"Half width at 1/e = "scan_width(this_scan%)/2;
ELSE
  PRINT TAB(30,4)"          ";
ENDIF
PRINT TAB(centre%,5);title$(this_scan%);
*FX 21,0
exit=FALSE
REPEAT
  PROCdirect_and_trim
  ans$=INKEY$(40)
  CASE ans$ OF
    WHEN "C" , "c" : exit=TRUE : PROCcalibrate
    WHEN "L" , "l" : exit=TRUE : PROClimits
    WHEN "A" , "a" : exit=TRUE : PROCaverage
    WHEN "S" , "s" : exit=TRUE : PROCscan
    WHEN "W" , "w" : exit=TRUE : PROCflush
    WHEN "Q" , "q" : exit=TRUE : PROCquit
    WHEN "D" , "d" : exit=TRUE : PROCdata_menu
    WHEN "Z" , "z" : exit=TRUE : PROCzero_offset
    WHEN "P" , "p" : exit=TRUE : PROCpre_amp
    WHEN "X" , "x" : exit=TRUE : PROCexamine
    WHEN "!" : exit=TRUE : PROCmake_delay : REM secret option
    WHEN "U" : exit=TRUE : PROCup_scan : REM secret option
  OTHERWISE
    PROCdirect_and_trim
  ENDCASE
UNTIL exit
ENDPROC
:
:
DEF PROCdata_menu
REPEAT
  VDU 28,0,5,79,0
  VDU 4
  CLS
  COLOUR 6
  PRINT TAB(0,0) "(V)iew scans  (R)efresh  (I)nput  (O)utput  (D)ots  (F)ile path"

```

```

PRINT TAB(0,2) "(N)ormalize (W)idth (P)rint (M)ain menu (L)ines (X)amine"
centre%=44 - 0.5*LEN(title$(this_scan%))
IF scan_width(this_scan%)<>0 THEN
  PRINT TAB(30,4)"Half width at 1/e = "scan_width(this_scan%)/2;
ELSE
  PRINT TAB(30,4)"          ";
ENDIF
PRINT TAB(centre%,5);title$(this_scan%);
*FX 21,0
exit=FALSE
leave=FALSE
REPEAT
  PROCdirect_and_trim
  ans$=INKEY$(30)
  COLOUR 7
  CASE ans$ OF
    WHEN "V" , "v" :leave=TRUE : PROCview_scans
    WHEN "R" , "r" :leave=TRUE : PROCbox
    WHEN "I" , "i" :leave=TRUE : PROCtake(this_scan%)
    WHEN "O" , "o" :leave=TRUE : PROCgive(this_scan%)
    WHEN "N" , "n" :leave=TRUE : PROCnormalize
    WHEN "W" , "w" :leave=TRUE : PROCscan_width(this_scan%)
    WHEN "P" , "p" :leave=TRUE : PROCprint_graph
    WHEN "X" , "x" :leave=TRUE : PROCexamine
    WHEN "F" , "f" :leave=TRUE : PROCdirectory
    WHEN "M","m","q","Q" : exit=TRUE : leave=TRUE
    WHEN "D" , "d" :leave=TRUE : dotty=TRUE
    WHEN "L" , "l" :leave=TRUE : dotty=FALSE
    WHEN "U"      :leave=TRUE : PROCup_scan : REM secret option
  OTHERWISE
    PROCdirect_and_trim
  ENDCASE
UNTIL leave
UNTIL exit
ENDPROC
:
:
DEF PROCdirectory
VDU 28,0,5,79,0
CLS
PRINTTAB(0,0)"Current path and directory = "user$
INPUTTAB(0,2)"Enter path and directory for data files ";new_user$
IF new_user$<>"" THEN user$=new_user$
ENDPROC
:
:
DEF PROCdirect_and_trim
new_pwr=FNpower(FNtalk_adc(s_channel%,no_avs%))
second_value=FNtalk_adc(a_channel%,no_avs%)
second_position=FNangle(second_value)
change=second_position - old_position
IF (ABS(change)>angres) OR (ABS(new_pwr-old_pwr)>0.001) THEN
  IF change>angres THEN
    dirn%=plus%
  ENDIF
  IF change<-angres THEN
    dirn%=minus%

```

```

ENDIF
PROCtrim
old_pwr=new_pwr
old_value=second_value
old_position=second_position
ENDIF
ENDPROC
:
:
DEF PROCmake_delay
SOUND 1,-9,58,7
a_delay=NOT(a_delay)
ENDPROC
:
:
DEF PROCview_scans
previous%=this_scan%+1
REPEAT
VDU 28,0,5,79,0
COLOUR 7
inner_loop%=FALSE
outer_loop%=FALSE
REPEAT
CLS
PRINTTAB(0,0)"Enter scan 1 to 5 to view scans, <SPACE>=SELECT ";
CASE GETS OF
WHEN "1" : inner_loop%=TRUE : scan_wanted%=1
WHEN "2" : inner_loop%=TRUE : scan_wanted%=2
WHEN "3" : inner_loop%=TRUE : scan_wanted%=3
WHEN "4" : inner_loop%=TRUE : scan_wanted%=4
WHEN "5" : inner_loop%=TRUE : scan_wanted%=5
WHEN " " : inner_loop%=TRUE : outer_loop%=TRUE
OTHERWISE
inner_loop%=FALSE
ENDCASE
UNTIL inner_loop%
IF NOT outer_loop% THEN
GCOL 7
COLOUR 6
PROCselect_scan(previous%-1)
GCOL 15
COLOUR 12
PROCselect_scan(scan_wanted%-1)
previous%=scan_wanted%
ENDIF
UNTIL outer_loop%
this_scan%=previous%-1
GCOL 7
COLOUR 12
PROCselect_scan(this_scan%)
ENDPROC
:
:
DEFPROCselect_scan(a_scan%)
VDU 28,2,23,7,17
IF scan_IDS(a_scan%)="Active" THEN PROCmemory(a_scan%)
PRINTTAB(0,a_scan%)scan_IDS(a_scan%)

```

```

ENDPROC
:
:
DEF PROCmemory(a_scan%)
no_points%=points(a_scan%,0,0)
IF dotty THEN
FOR t%=1 TO no_points%
POINT FNscreenx(points(a_scan%,0,t%)),FNscreeny(points(a_scan%,1,t%))
NEXT t%
ELSE
IF no_points%>=2 THEN
MOVE FNscreenx(points(a_scan%,0,1)),FNscreeny(points(a_scan%,1,1))
FOR t%=2 TO no_points%
DRAW FNscreenx(points(a_scan%,0,t%)),FNscreeny(points(a_scan%,1,t%))
NEXT t%
ENDIF
ENDIF
ENDPROC
:
:
DEF PROCexamine
COLOUR 15
VDU 28,0,24,7,23
CLS
PRINTTAB(0,0)"Examine";
COLOUR 7
*POINTER
MOUSE ON
@%=&01020104
REPEAT
MOUSE x,y,z
VDU 28,0,27,7,26
CLS
PRINTTAB(0,0)FNscreen_angle(x);
VDU 28,0,30,7,29
CLS
PRINTTAB(0,0)-10*FNscreen_power(y);
UNTIL z<>0
MOUSE OFF
VDU 28,0,24,7,23
CLS
@%=&01000505
ENDPROC
:
:
DEF FNscreen_angle(a)
=10*(a - 730)/x_factor%
:
:
DEF FNscreen_power(a)
=(800 - a)/y_factor%
:
:
DEF PROCtrim
IF dirn%=plus% THEN
COLOUR 1
ELSE

```

```

    COLOUR 3
ENDIF
@%=&01020104
VDU 28,0,27,7,26
CLS
PRINTTAB(0,0)FNangle(FNtalk_adc(a_channel%,no_avs%) - dirn%*hyst);
VDU 28,0,30,7,29
CLS
PRINTTAB(0,0)-10*FNpower(FNtalk_adc(s_channel%,no_avs%));
@%=&01000505
ENDPROC
:
:
DEF PROCnormalize
VDU 28,0,5,79,0
COLOUR 7
CLS
PRINT TAB(0,4)"Align two scans or shift one scan [a/s]";
ans$=GET$
IF ans$="A" OR ans$="a" THEN
    CLS
    PRINTTAB(0,4)"Select two scans for aligning";
    TIME=0
    REPEAT UNTIL TIME>150
    PROCview_scans
    first_scan%=this_scan%
    PROCview_scans
    second_scan%=this_scan%
    PROCalign_scans(first_scan%,second_scan%)
    GCOL 7
    PROCbox
    PROCmemory(first_scan%)
    PROCmemory(second_scan%)
ELSE
    PROCshift(this_scan%)
    GCOL 7
    PROCbox
    PROCmemory(this_scan%)
ENDIF
ENDPROC
:
:
DEF PROCshift(a_scan%)
PROCe_width(a_scan%)
FOR a%=1 TO points(a_scan%,0,0)
points(a_scan%,1,a%)=points(a_scan%,1,a%)-max
points(a_scan%,0,a%)=points(a_scan%,0,a%)-(epsilon1 + epsilon2)/2
NEXT a%
ENDPROC
:
:
DEF PROCcoverage
VDU 28,0,5,79,0
COLOUR 7
old_av%=no_avs%
INPUT TAB(0,4)"Number of Averages = "no_avs%
IF no_avs% <1 THEN no_avs%=1

```

```

IF no_avs% > 1000 THEN no_avs%=1000
ENDPROC
:
:
DEF PROCfit(a_scan%,the_offset,posn%,range%)
x1=0:x2=0:x3=0:x4=0:yx2=0:yx=0:y=0 : N%=0
FOR d%=posn%-range% TO posn%+range%
xi=TAN(RAD(points(a_scan%,0,d%)))
yi=points(a_scan%,1,d%)
x1=x1+xi : x2=x2+(xi*xi) : x3=x3+(xi*xi*xi) : x4=x4+(xi*xi*xi*xi)
yx2=yx2+(yi*xi*xi) : yx=yx+(yi*xi) : y=y+yi : N%=N%+1
NEXT d%
determ=x4*(x2*N%-x1*x1) -x3*(x3*N% - x1*x2) +x2*(x3*x1 - x2*x2)
determ=1/determ
a_fit=determ*(yx2*(x2*N% - x1*x1) +yx*(x2*x1 -N%*x3) +y*(x3*x1 -x2*x2))
b_fit=determ*(yx2*(x1*x2 -N%*x3) +yx*(x4*N% -x2*x2) +y*(x2*x3 -x4*x1))
c_fit=determ*(yx2*(x3*x1 -x2*x2) +yx*(x3*x2 -x4*x1) +y*(x4*x2 -x3*x3))
x_min=-b_fit/(2*a_fit)
y_min=a_fit*x_min*x_min +b_fit*x_min +c_fit
c_3=c_fit - the_offset - 0.869
REM the power at 1/e field is 8.69dB down on the offset value
IF (b_fit*b_fit > 4*a_fit*c_3) THEN
x_3p=(-b_fit + SQR(b_fit*b_fit - 4*a_fit*c_3))/(2*a_fit)
x_3m=(-b_fit - SQR(b_fit*b_fit - 4*a_fit*c_3))/(2*a_fit)
x_min=DEG(ATN(x_min))
x_fit=0
IF (points(a_scan%,0,posn%)>0) AND (x_3p>0) THEN x_fit=x_3p
IF (points(a_scan%,0,posn%)<0) AND (x_3m<0) THEN x_fit=x_3m
IF x_fit=0 THEN COLOUR 15 : PRINTTAB(0,0)"Bollocks"; : a=GET
ELSE
PRINTTAB(0,0)"Bollocks"; : a=GET
ENDIF
ENDIF
ENDPROC
:
:
DEF PROCscan_width(a_scan%)
PROCe_width(a_scan%)
scan_width(a_scan%)=wideness
VDU 28,0,5,79,0
@%=&01020307
CLS
PRINTTAB(0,0)"Central angle = ":points(a_scan%,0,maxpos%)
PRINTTAB(35,0)"Fit angles = ";epsilon1;" "epsilon2
INPUTTAB(0,2)"Wavelength [mm] =" ,lambda
waist_size=lambda/(PI*TAN(RAD(0.5*wideness)))
PRINTTAB(0,2)"Waist size calculated from beam = "waist_size
INPUTTAB(0,4)"Aperture diameter [mm] =" ,a_diameter
w_w0=0.6435*a_diameter/(2*waist_size)
IF w_w0<1 THEN
PRINTTAB(0,4)"Waist size larger than 0.6435*aperture radius"
ELSE
t_length=SQR(w_w0*w_w0 - 1)*waist_size*waist_size*PI/lambda
PRINTTAB(0,4)"Calculated position of waist behind aperture = ";t_length
ENDIF
PRINTTAB(0,5)"Hit a key to continue";
go_on%=GET
ENDPROC

```



```

:
:
DEF PROCe_width(scan_no%)
max=10
maxpos%=0
FOR e%=1 TO points(scan_no%,0,0)
IF points(scan_no%,1,e%)<=max THEN max=points(scan_no%,1,e%): maxpos%=e%
NEXT e%
REM fit curve around 1/e width
d%=0
REPEAT : d%=d%+1 : UNTIL points(scan_no%,1,maxpos%-d%)>(max+0.869)
lower%=d%
d%=0
REPEAT : d%=d%+1 : UNTIL points(scan_no%,1,maxpos%+d%)>(max+0.869)
upper%=d%
PROCfit(scan_no%,max,maxpos%-lower%,5)
REM find root that corresponds to maxpos%-lower%
epsilon1=DEG(ATN(x_fit))
PROCfit(scan_no%,max,maxpos%+upper%,5)
epsilon2=DEG(ATN(x_fit))
wideness=ABS(epsilon1 - epsilon2)
scan_width(scan_no%)=wideness
REM epsilon2 is always positive
IF epsilon2<epsilon1 THEN
    temporary=epsilon1
    epsilon1=epsilon2
    epsilon2=temporary
ENDIF
ENDPROC
:
:
DEF PROCalign_scans(scan_1%,scan_2%)
PROCe_width(scan_1%)
y_top1=max : x_top1=(epsilon1+epsilon2)/2
PROCe_width(scan_2%)
y_top2=max : x_top2=(epsilon1+epsilon2)/2
shift_angle=(x_top1 - x_top2)/2
FOR d%=1 TO points(scan_1%,0,0)
    points(scan_1%,0,d%)=points(scan_1%,0,d%)-shift_angle
    points(scan_1%,1,d%)=points(scan_1%,1,d%)-y_top1
NEXT d%
FOR d%=1 TO points(scan_2%,0,0)
    points(scan_2%,0,d%)=points(scan_2%,0,d%)+shift_angle
    points(scan_2%,1,d%)=points(scan_2%,1,d%)-y_top2
NEXT d%
ENDPROC
:
:
DEF PROCcup_scan
VDU 28,2,23,7,17
COLOUR 6
PRINTTAB(0,this_scan%)scan_ID$(this_scan%)
IF this_scan%>=4 THEN
    this_scan%=0
ELSE
    this_scan%=this_scan%+1
ENDIF

```

```

VDU 28,2,23,7,17
COLOUR 12
PRINTTAB(0,this_scan%)scan_ID$(this_scan%)
ENDPROC
:
:
DEF PROCadcread
REM This procedure was written entirely by Andy Harvey, and contains
REM some code that is not actually used within this program.
FRED%=&03000000 :REM base address of FRED in slot
ROM_address%=&33C0000 :REM base address of podule ROM in slot 0
int_status_address%=&3000 :REM IRQ and FIQ status bits within ROM
bus_VIA%=FRED%
podule_VIA%=&33C2000
REM ***** assign VIA register addresses *****
port_B%=0
port_A%=4*&01 :REM port A
B_dir%=4*&02 :REM port B dirn. reg.
A_dir%=4*&03 :REM port A dirn. reg.
timer2_low%=4*8
timer2_high%=4*9
ACR%=4*&0B :REM Aux Control Reg
PCR%=4*&0C :REM Peripheral Control Reg
IntFR%=4*&0D :REM interrupt Flag Register
IntER%=4*&0E :REM Interrupt Enable Register
counter_base%=4*&20
DAC%=4*&30
ADC_base%=4*&40
Pcol=7:Lcol=7:Rcol=7:Bcol=7:Ccol=7:gain=-1
array_size%=600
DIM result%(array_size%)
resultH%=0:resultL%=0
status%=0
DIM program% &1000 :REM Unsure of required size here.
FOR opt%=8 TO 10 STEP 2 :REM range check, then range check and report errors
P%=program%
L%=P% + &1000
REM The following that is enclosed within '[ .. ]' is assembly code.
[
OPT opt%
.start_adc \entry;R0=ADC No.,R1=channel number,R11=FRED%
\ensure select_flag is set to >7 after crate power up
STMFD R13!,[R2-R4,R11,R14] \exit;nothing
ADD R11,R11,#ADC_base% \modification '\ 12-04-91
ADD R11,R11,R0, ASL #3 \ADC addresses are at increments of 8
ADR R3,select_flag \get selected channel
LDR R4,[R3] \and
CMP R4,R1 \if different from new one
STRNEB R1,[R11,#4] \write channel No. to ADC
STRNE R1,[R3] \store new channel
STRB R1,[R11] \start conversion
LDMFD R13!,[R2-R4,R11,R14]
MOVS PC,R14
.select_flag \flag for channel number
EQUd &FF
\
.read_adc \entry;R0=adcNo;R11=FRED%

```

```

STMFD R13!,{R1,R2,R11,R14}    \exit;R0=conversion
ADD R11,R11,#ADC_base%
ADD R11,R11,R0, ASL #3
.read_adc_status
LDRB R0,[R11,#4]              \read status bit - only bit 0 is valid
TST R0,#1                     \status bit goes low when conversion complete
BNE read_adc_status
LDRB R0,[R11]                 \get hi byte
LDRB R1,[R11]                 \get lo byte
STRB R0,[R11]                 \start_adc
ADD R0,R1,R0, ASL #8          \
TST R0,#&8000                 \is it -ve
ORRNE R0,R0,#&FF0000
ORRNE R0,R0,#&FF000000        \if so convert to 32 bit 2's complement int.
RSB R0,R0,#0                  \make answer -ve because adc input is inverted
\ now check to see if these are the biggest or smallest readings so far
\ ADR R1,min_adc
\ LDR R2,[R1]                  \get previous min value
\ CMP R0,R2
\ STRLT R0,[R1]                \replace it if new one is smaller
\ LDR R2,[R1,#4]               \get previous max value
\ CMP R0,R2
\ STRGT R0,[R1,#4]             \replace it if new one is larger
LDMFD R13!,{R1,R2,R11,R14}
MOVS PC,R14
.min_adc
EQU 0                          \address for min reading
.max_adc
EQU 0                          \address for max reading
\
\selects channel, starts and reads the adc from USR mode R2 times and returns
\the sum of R2 reads in R0
\ a min and max value are updated at each adc_read
.read_adc_USR                  \entry;R0=adc No.,R1=channel No.,R2=number
STMFD R13!,{R2-R12}           \exit;R0=32 bit 2's compliment result
MOV R11,#FRED%                 \enter SVC mode so can talk to FRED
MOV R3,#0                      \zero accumulator register
MOV R4,R0                      \save channel number
SWI "OS_EnterOS"
BL start_adc
.read_adc_USR_loop
MOV R0,R4                      \get channel number back for read_adc
SWI "OS_IntOff"
\ BL start_adc
BL read_adc
SWI "OS_IntOn"
ADD R3,R3,R0
SUBS R2,R2,#1                  \decrement no of samples counter
BGT read_adc_USR_loop         \if not finished then loop
MOV R0,R3                      \stick accumulated result in R3
TEQP PC,#0                    \return to user mode
MOVNV R0,R0
LDMFD R13!,{R2-R12}
MOVS PC,R14                    \return from subroutine
]
NEXT opt%
ENDPROC

```

```

:
:
DEF PROCset_adc
COLOUR 7
INPUT "adc module number?      "A%
INPUT "angle voltage channel?   "a_channel% : B%=angle_ch%
INPUT "detector voltage channel? "s_channel% : CLS
ENDPROC

:
:
DEF FNTalk_adc(chan%,averages%)
LOCAL l_offset
REM The delay here is to allow the adc channel switching, time to
REM settle down before reading begins at the new channel. Ideally
REM this should be taken care of within the assembly language
REM routine, and thus be transparent to the user of this routine.
REM This however is a workable fix.
B%=chan%
C%=averages%
adc_val=USR(read_adc_USR) : REM The result from this first read is
:                          : REM ignored. It switches channel if B%
:                          : REM has changed since last called.
REM wait$=INKEY$(delay%) : REM Delay mechanism provides 'delay' centi-seconds.
adc_val=(USR(read_adc_USR))/C%
IF chan%=s_channel% THEN
  l_offset=power_offset
ELSE
  l_offset=angle_offset
ENDIF
=adc_val - l_offset

```